SIMULATION OF AN INTEGRATED SOLAR ABSORPTION SYSTEM WITH ORGANIC RANKINE CYCLE FOR SOIL COOLING APPLICATION

OLABOMI RASAQ ADEKUNLE

A thesis submitted in fulfilment of the
requirements for the award of the degree of
Doctor of Philosophy

Razak School of UTM in Engineering and Advanced Technology
Universiti Teknologi Malaysia

NOVEMBER 2017

I declare that this thesis entitled *"Simulation of an Integrated Solar Absorption System with Organic Rankine Cycle for Soil Cooling Application"* is the result of my own research except as cited in the references. The thesis has not been accepted for any degree and is not concurrently submitted in candidature of any other degree.

Signature	:	
Name	:	OLABOMI RASAQ ADEKUNLE
Date	:	NOVEMBER, 2017

To my beloved (late) Parents; Alhaji Ahmad-Tijani Oladokun Olabomi and Hajia Wulemat Aibinuola Olabomi,(فَرَوحٌ وَرَيحانٌ وَجَنَّتُ نَعيمٍ), and my very wonderful family

ACKNOWLEDGEMENT

All thanks to Allah, who made it possible for me to complete this study at HIS appointed time. Many thanks to Dr. Saad Abbas who accepted my proposal and introduced me to Prof. Dato' Ir. Dr. A Bakar Jaafar, who then became my main supervisor, gave me the supports to achieve my goal and the opportunity to work with him as a Research Assistant under "***eScience"*** Project. I thank my co-supervisors; Emeritus Prof. Dr. Md Nor Musa, and Dr Shamsul Sarip for their unconditional support all through. I appreciate the supports from management of Razak School, and from staff of Ocean Thermal Energy Centre (Shaffiq Bin Rahmat, Azrin Bin Ariffin, and Ayuni Binti Romainodin).

I really appreciate the untiring support from my mentor, H.R.M Oba Abdul-Rasheed Ayotunde Olabomi, and my entire family members. I can't quantify the efforts of my brothers and sisters; Alhaji T.A Olabomi, Sherifat Agboola, Dhikrullah Olawale Olabomi, Muftau Kola Olabomi, Alhaja Jumoke Adeyemi, Alhaji Dele Alamu, Alhaji R.A Lawal, and their wives and husbands. Special thanks to my friends; Yunus Adegboye, Sunday Adeoye, Ademola Oladipo, Yakubu A. Momohjimoh, and others, who were always on visit to my family at home during these periods. Dr. Umar, Dr Abubakar Sulaiman, Dr Ali Gambo, Dr Obaji, Dr Yusuf Mohammed, and others can rarely be thanked enough.

I thank the management of *"Prototype Engineering Development Institute of NASENI, Nigeria"* for approving my study leave. Special thanks to the Muslim community of the Institute, and to Mr. Hamzat H. Olaoye, whose personal efforts are unimaginable.

To my darling wife and children (Kafayat Omolola Olabomi, Faridah Omolade Olabomi, and Sultan Adewole Olabomi), I really appreciate your patience, hopes, and prayers at all times, without which this achievement might not be possible.

Ultimately, acknowledgement goes to Ministry of Science, Technology and Innovation (MOSTI) Malaysia, for giving full financial support to this research under **eScience Fund** (Project number: **06-01-06-SF1393**) for "*Integration of Rankine Power and Absorption Refrigeration Cycles for Low Load Optimized Solar Thermal Chilled Water Soil Cooling System",* from 1st of May 2015 to 31st of October 2017.

ABSTRACT

In hot tropical countries like Malaysia, high-value temperate crops are mainly grown on slopes of cool mountain resorts. These crops do not grow well on lowland soil that is subjected to high thermal load due to high solar irradiation. There is always great demand for these temperate crops and as such, highland farming business is now so lucrative that the farming activities become out of control. Over-farming exposes the neighboring settlers and tourist spots to severe soil erosion, leading to numerous incidents of landslide. Research on greenhouse temperate farming activities have been attempted in lowland areas. However, only the interior air volume of planting zone is thermally conditioned on an assumption that it will simulate that of temperate-like climate. Studies have revealed that rather than controlling the greenhouse interior air, it is the soil that requires cooling to encourage the growth of the right micro-organisms for temperate crops to grow well. In this project, a new and non-conventional solar thermal chilled water cooling system was developed and operated to condition the agricultural soil where roots of planted crops take up all the essentials from, with optimum performance at about 18 ºC soil temperature. The proposed cooling system was made up of two components: the combined absorption refrigeration and organic Rankine cycle subsystem, and soil cooling subsystem. The study included modelling of soil cooling load and area of soil bed to determine the average cooling plant capacity required to overcome the load as well as the chilled water pipe dimensions and configurations. Mass and energy balance analyses of the combined cooling and power plant components were carried out to assess its performance and energy input for its operation, while the soil bed analysis was done to determine the chilled water flow rates suitable to keep the soil temperature within the set range. Independent studies were conducted on experimental rig consisting of laboratory scale soil bed of 0.25 m^2 and an absorption chiller of 50 W cooling capacity to analyse the performance of the modelled plant to offset the soil cooling load. Chilled water production rate from the chiller was found to be within the required rate to achieve the set soil bed temperature. Validation of theoretical soil cooling model with the experimental results gave a mean error of 14 %, while that of the coefficient of performance of the experimental and modelled chiller gave error of 8 %. Hence, showing reasonable agreements between the modelled and experimental results. Parametric analyses of the soil cooling and combined plant were carried out to optimize their performances, and economic analysis of the combined system showed that its financial viability increases with system capacity. The proposed system of cooling is technically feasible, economically viable and environmentally beneficial with annual greenhouse gas emission reduction potentials equivalent to 6.7 tCO_2 per kW of cooling capacity.

ABSTRAK

Di negara-negara beriklim tropika panas seperti Malaysia, tanaman berkepadatan tinggi ditanam terutamanya di resort dilereng gunung yang sejuk. Tanaman ini tidak mengalami pertumbuhan yang baik di kawasan tanah rendah disebabkan beban terma yang tinggi akibat penyinaran solar yang tinggi. Terdapat permintaan yang tinggi untuk tanaman beriklim sederhana dan oleh itu, perniagaan berasaskan tanaman ladang di kawasan tanah tinggi memberi keuntungan yang begitu menguntungkan di mana aktiviti yang tidak terkawal menjadikan penanaman di kawasan lereng yang berdekatan dan tempat-tempat pelancongan menghadapi hakisan tanah yang teruk, yang membawa kepada banyak insiden tanah runtuh. Kajian tentang aktiviti perladangan di kawasan tanah rendah sederhana rumah hijau telah dilaksanakan namun hanya jumlah udara dalaman zon penanaman termal diandaikan dengan anggapan bahawa ia akan mensimulasikan iklim sederhana. Walau bagaimanapun, kajian telah menjelaskan bahawa tanah tinggi memerlukan proses penyejukan untuk menggalakkan pertumbuhan mikroorganisma yang tepat untuk tanaman sederhana berkembang dengan baik, bukannya menyejukkan udara dalaman rumah hijau. Dalam kajian ini, sistem penyejukan air dingin dan panas bukan konvensional dibangunkan telah dan dikendalikan untuk mengkaji keadaan tanah pertanian di mana akar tanaman yang ditanam terbentuk dengan prestasi optimum pada suhu tanah sekitar 18 ºC. Sistem penyejukan yang dicadangkan terdiri daripada dua komponen: penyejukan penyerapan gabungan dan subsistem kitaran Rankine organik, dan subsistem penyejukan tanah. Kajian ini merangkumi model beban penyejukan tanah dan kawasan dasar tanah bagi menentukan kapasiti loji penyejukan purata yang diperlukan untuk mengatasi beban serta dimensi dan konfigurasi paip air sejuk. Analisis terhadap keseimbangan massa dan tenaga gabungan dari komponen penyejukan dan pencetus kuasa telah dijalankan untuk menilai prestasi dan input tenaga yang beroperasi, manakala analisis dasar tanah dilakukan untuk menentukan kadar aliran air sejuk yang sesuai untuk menjaga suhu tanah dalam pelbagai set. Kajian bebas dijalankan pada rig eksperimen yang terdiri daripada dasar tanah berskala 0.25 m^2 dan penyerapan berkapasiti penyejukan 50 W untuk menganalisis model prestasi loji bagi mengimbangi beban penyejukan tanah. Kadar pengeluaran air sejuk dari tabung penyejuk didapati berada dalam kadar yang diperlukan untuk mencapai suhu dasar tanah yang ditetapkan. Secara teori pengesahan model penyejukan tanah menunjukkan ralat 14 % dari keputusan kajian, manakala pekali prestasi kajian tabung penyejuk menunjukkan kesilapan sebanyak 8 %, membuktikan bahawa terdapat hubungan antara keputusan dari model dan kajian. Analisis parametrik gabungan penyejukan tanah dan tumbuhan telah dijalankan untuk mengoptimumkan prestasi tersebut dan analisis ekonomi sistem gabungan menunjukkan bahawa terdapat peningkatan dalam kapasiti sistem. Secara teknikalnya sistem penyejukan yang dicadangkan adalah bersesuaian, berdaya maju dari segi ekonomi dan bersesuaian dengan potensi pengurangan pelepasan gas rumah hijau tahunan bersamaan dengan 6.7 tCO_2 per kW kapasiti penyejukan.

TABLE OF CONTENTS

LIST OF TABLES

LIST OF FIGURES

LIST OF ABBREVIATIONS

ANOVA	-	Analysis of Variance
B-C	-	Benefit-to-Cost
CCHP	-	Combined Cooling Heating and Power
COP	-	Coefficient of Performance
CPF	-	Constant Primary Flow
DOE	-	Design of Experiment
GHG	-	Greenhouse Gas
GSHP	-	Ground Source Heat Pump
HDPE	-	High Density Polyethylene
HHV	-	High Heating Value
HTF	-	Hot Thermal Fluid
HVAC	-	Heating Ventilation and Air Conditioning
IRR	-	Internal Rate of Return
LHV	-	Low Heating Value
NI	-	National Instrument
NIST	-	National Institute of Standard Technology
NPV	-	Net Present Value
OFAT	-	One Factor At a Time
ORC	-	Organic Rankine Cycle
RET	-	Renewable Energy Technology
RSM	-	Response Surface Methodology
VAR	-	Vapour Absorption Refrigeration

LIST OF SYMBOLS

Q_{inc}	-	Incident radiation
ρ_a	-	Air density
C_{pa}	-	Air heat capacity
T_0	-	Soil temperature
T_0^1	-	Soil temperature in K
T_a^1	-	Air temperature in K
k_s	-	Soil thermal conductivity
ρ_{vo}	-	Soil surface vapour density
ρ_{va}	-	Surface vapour density
$e_{a(t)}$	-	Water vapour pressure
M_w	-	Molar mass of water
r_p	-	Inner pipe radius
t_p	-	Pipe thickness
h_c	-	Convective heat transfer coefficient
σ	-	Boltzmann constant
r_a	-	Soil-air boundary resistance
K	-	Von Karman constant
ρ_w	-	Water density
N_u	-	Nusselt number
C_{pw}	-	Heat capacity of water
ε_s	-	Soil emissivity
ε_a	-	Emissivity of air
k_w	-	Water thermal conductivity
R	-	Ideal gas constant
U	-	Wind speed

LIST OF APPENDICES

CHAPTER 1

INTRODUCTION

1.1 Background

Radiant cooling with chilled water is found suitable for a number of applications (such as building comfort cooling, and agricultural soil cooling) in the tropical climate countries. This is partly due to better thermal capacity of water, its less pumping power requirement than the chilled air (Seo. *et al.*, 2014), and most importantly its effective removal of sensible heat either from living zone, or from the agricultural soil. This is because human activity leading to heat generation is closer to the floor than the ceiling, and microbial activities of planted crops mostly take place in the soil. Meanwhile, high soil temperature affects the performance of crops (Sattelmacher *et al.*, 1990). Figure 1.1 shows the general effects of soil temperature difference on root and shoot development of a planted crop. In addition, the operative temperature of a room for instance, is greatly influenced by the radiant cooling as it becomes the dominant process of heat transfer (Mikeska. and Svendsen, 2015). This is therefore increasing the implementation of radiant soil (floor) cooling in the tropical climate region as a way of reducing the air conditioning loads (Seo. *et al.*, 2014).

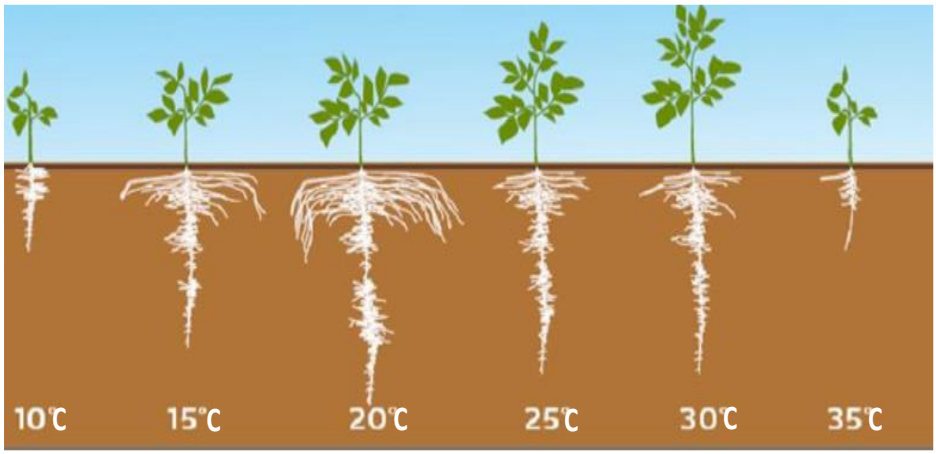

Figure 1.1: Effects of soil temperature on development of planted crop (Yara, 2015)

Furthermore, implementation of soil cooling process towards the cultivation of high-value temperate crops in the tropics is observed to be a more energy saving process than air-cooled greenhouse systems, more importantly it has been established that most of the physiological processes of planted crops are controlled by soil temperature which if higher than optimal, will alter the root growth and functionalities (Nabi and Mullins, 2008). However, soil temperature control requires energy expenditure which if alternatively provided will make the system to be both economically viable and environmentally benign. Applying solar thermal technology to tackle solar radiation imposed load is one of the interesting research areas in the tropics where there is high solar potential that is available in phase with the load. Meanwhile, absorption cooling system and organic Rankine power cycle are typical thermally activated technologies that are found suitable for utilization of low-grade thermal energy such as geothermal and solar energy (Tchanche *et al.*, 2011; Khamooshi *et al.*, 2013; Kim *et al.*, 2012) through solar collector. Besides utilizing low-grade thermal energy, the two cycles use organic working fluids, making their combination for power and cooling an interesting research area in the recent time. This study takes the advantage of the thermally activated technologies to overcome the thermally imposed cooling load through the combined cooling and power plant cycle. However, unlike previous studies on combined plant systems, cooling is the primary goal in this study.

1.1.1 Energy Demand and Cooling Systems

In the recent time, research on the application of renewable energy (such as Solar, Wind, Geothermal, and Ocean thermal) is gaining more attention as a result of the need to meet ever-growing energy demand (mostly for cooling), and environmental issues. Solar thermal energy has been popular in the research field as a decentralized renewable source of energy with higher application potentials in the tropical and sub-tropical regions (Agyenim *et al.*, 2010; Chua and Oh, 2012). Solar energy is a clean and abundantly free source of energy which can be found anywhere on the surface of the earth where day and night exist, and it is easily tapped at the point of use. A major constraining factor for solar energy application is its seasonal nature resulting from its availability that is directly tied to day and night cycle, and earth's orbit around the sun as well as the local weather condition of a place (such as rainfall, haze, typhoon and cloud cover). Additionally, solar energy is generally a diffuse energy source (Hlbauer, 1986) and for it to be technologically useful, it must be captured using solar collector which must be properly sized to avoid unnecessarily increased cost (Bajpai, 2012). However, series of studies have been conducted on the use of thermal storage (Vadiee and Martin, 2013; Nizami *et al.*, 2013; Qu *et al.*, 2010) as well as battery bank (Sanaye and Sarrafi, 2015) to absorb the variation in solar energy supply.

Solar thermal energy has application potentials in diverse areas such as heating, ventilation, and air-conditioning (HVAC) system as well as in electrical power generating systems in domestic, industrial, commercial, and agricultural sectors. Solar thermal applications for cooling systems have received increased research interest in the recent time (Leavell, 2010; Lu *et al.*, 2013; Agyenim *et al.*, 2010; He *et al.*, 2015), likewise for Rankine systems to generate electrical power (Luzzi *et al.*, 1999; Stodola and Modi, 2009; Saitoh *et al.*, 2007; Sanaye and Sarrafi, 2015). Regarded as low-grade heat energy (Tchanche *et al.*, 2011; Mikeska. and Svendsen, 2015), solar thermal energy is found suitable for absorption cooling system and organic Rankine power cycle because the two systems utilize working fluids that change phase at temperatures below the boiling point of water and at low pressure (Arvay. *et al.*, 2011). The common features in the thermodynamic properties of the working fluids for the two cycles have triggered more research interests in the combined power and cooling

system using organic Rankine cycle, and absorption refrigeration systems (Saitoh *et al.*, 2007; Datla, 2012; Abed *et al.*, 2013; Ziviani *et al.*, 2014; Padilla *et al.*, 2010; Feng *et al.*, 2000; Tamm *et al.*, 2004) and utilizing low-grade heat sources like solar, geothermal, biomass and industrial waste heat.

1.1.2 Radiant Soil Cooling

For economic reasons and maintenance of sustainable environment, more energy efficient measures are being analysed by researchers, mostly to meet the cooling demands; during summer in the temperate regions, and year-round in the hot and humid tropical regions. This has become imperative as the building energy consumption accounts for about 40 % of the global energy consumption (Dong, 2010; Khan *et al.*, 2016). Heating ventilation and air-conditioning (HVAC) system accounts for a larger percentage of this building energy consumption, amount of which depends on the climatic region. In Oman, 54.7 % electricity in 2008 was consumed by building, and air-conditioning took the larger percentage (Gastli and Charabi, 2011). More than 60 % of building electricity consumption the Kingdom of Saudi Arabia is taken by air-conditioning and refrigeration systems (Said *et al.*, 2012), most of which are vapour compression types. About 33 % of the total Hong Kong electricity is consumed by refrigeration and air conditioning system (Fong *et al.*, 2010a). Furthermore, about 15 % of the global total electricity produced is consumed by refrigeration and air-conditioning systems (Hong *et al.*, 2011). However, radiant floor cooling methods provide better indoor comfort in building with lower energy requirement relative to conventional air cooling systems (Zarrella. *et al.*, 2014; Zhao *et al.*, 2016). The result of the experimental field study on radiant cooling of a tropical residential building by (Wongkee. *et al.*, 2014a) shows 70 % energy saving compared to conventional air conditioning system.

A major relative advantage of radiant cooling system over the traditional HVAC system is its ability to be coupled with renewable energy sources, allowing high efficiency and more energy savings thereby contributing to reduction in building

energy demand and total energy consumption (De Carli and Tonon, 2011; Wu. *et al.*, 2015; Yu. and Yao, 2015).

1.1.3 Planted Crops and Soil Temperature

The biochemical and physical activities taking place in the soil are effected by soil temperature; influencing soil water movement and soil microbial activities (Nik. *et al.*, 1986), with the resultant effect on overall development of roots and shoots of the planted crops (Nabi and Mullins, 2008). The effects of soil cooling and supplemental lighting on five selected cultivars were investigated by (Labeke. and Dambre, 1993) in which soil cooling contributed to increase in flower production of the tested cultivars and extended the flowering production beyond winter to summer periods.

Low soil temperature generally favours temperate crops. This is evident in the cultivation of high-values temperate crops in some high altitudes in the tropics (such as Cameron highland in Malaysia) where ambient air and soil temperatures are low. As such, many research studies have been carried out on the cultivation of temperate crops in the tropics (Mongkon *et al.*, 2014; Mekhilef *et al.*, 2013) but mostly based on greenhouse farming systems.

Temperate crops can also thrive well on the tropical lowlands by cooling the soil through hydronic/radiant cooling system. This is considered more energy efficient than air cooling of the greenhouse currently in practice (Zhao. *et al.*, 2014). With the huge solar thermal potential in the tropics, the energy efficient soil cooling can be achieved with innovative chilled water production from a combined plant of vapour absorption refrigeration and organic Rankine power system, and its application for the cooling process via network of buried pipes in a dimensioned soil bed.

1.2 Problem Statement

Tropical climate countries are mostly characterized with high ambient air temperature and relative humidity. These have always constituted heavy cooling loads and resultant increased energy demand for cooling in all sectors. Specifically, only high temperature adaptive crops thrive well in the hot tropical region because, the year round high air temperature and relative humidity are beyond the optimal level for most high-value temperate crops making their cultivation in the tropics a serious challenge due to heat stress (Peet *et al.*, 2003; Max *et al.*, 2009) that results from the heavy cooling load. On the other hand, temperate regions are found to be generally cold with temperature range between 10 ℃ and 20 ºC. Meanwhile, low soil temperature, with average values between 14 ºC and 22 ºC favours the cultivation of most of the high-value crops (Yara, 2015). High-value crops are non-staple agricultural crops (such as fruits, vegetables, spices, condiments ornamentals and flowers,) that are known to have higher return per hectare of land than other widely cultivated crops, presenting an opportunity for farmers to increase their income (Othman *et al.*, 2015). Some of these crops are also cultivated in the tropics but with very low quality and at high cost of cultivation except on some few highlands (hill/upland agriculture). Meanwhile this at times results in erosion (Jim and Charles, 2009) and devastation of mountain ecosystems and adjourning communities.

Besides highland farming, growing of temperate crops on lowlands in the Tropics has mostly been through greenhouse farming system that involves air-conditioning of entire volume of the planting zone with the intent to create temperate-like thermal condition for the planted crops. However, most of the greenhouses farming systems use conventional cooling that consumes huge amount of power, thereby contributing to increase in energy demands. Sorption cooling systems could be applied in this case but also require some amount of energy to operate the pumps and other parasitic loads.

Thus, in this study, integration of vapour absorption refrigeration cycle with organic Rankine cycle for simultaneous chilled water production and power generation, using solar energy is proposed. The proposed system is based on the

hypothesis that, chilled water output from the integrated cycle is suitable for radiant cooling of a dimensioned soil bed to a range of temperature suitable for optimum development of some temperate crops and the proposed system is sustainable. Figure 1.2 shows the schematic diagram of the proposed system.

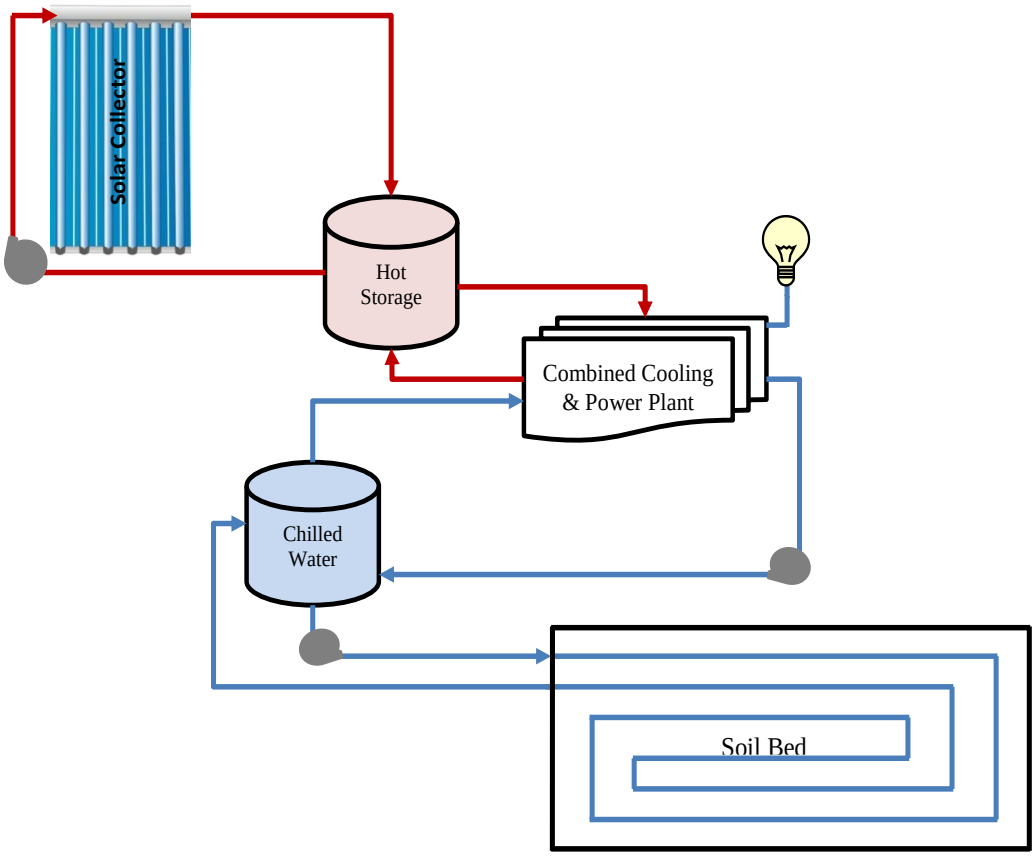

Figure 1.2: Conceptual solar VAR-ORC soil cooling system

1.3 Research Objectives

The main objective of this work is to investigate an integrated plant of vapour absorption refrigeration and organic Rankine power cycle (VAR-ORC) for soil cooling to overcome the cooling load caused by the radiant effects of the hot environment.

The research objectives are:

i. To develop mathematical models of soil cooling load, and of the combined plant cooling system performance.
ii. To develop a physical model to optimize the chilled water flow rate that produces soil temperature distribution suitable for small scale temperate crop farming.
iii. To develop test rig for the validation of the mathematical model.
iv. To analyse the economics of the developed system in comparison with that of a conventional system of a similar cooling capacity.

1.4 Scope of the Research

Insulated box has been used for the experimental soil bed in this study and heat transfer across the walls is assumed negligible. Similarly, since the experimental chiller is small in capacity, requiring less than 0.5 m^2 of solar collector to capture the needed heat, activation of the chiller was achieved through an electric heater instead. The study considered only the daytime application of chilled water for soil cooling, and only the estimation of solar collector size required to capture the needed amount of heat for running the system based on daily available solar radiation. Furthermore, the soil used in this study is the local soil obtained from Kuala Lumpur. However, with the idea of the soil characteristics, the developed model is suitable to estimate the cooling load elsewhere. Other assumption to reduce the complexity of the model equations include; (i) temperature profile in the pipe vicinity is not affected by the presence of the pipe, as such, pipe surface temperature is uniform in the axial direction, (ii) soil surrounding the pipe is homogeneous and has a constant thermal conductivity, (iii) chilled water pipe has a uniform cross sectional area in the axial direction, (iv) consideration is given to vertical heat conduction in the soil bed (Qin *et al.*, 2002), (v) undisturbed soil temperature is uniform around the chilled water pipe surface (Moncef and Kreider, 1996) and equal to the external temperature of the pipe (Mongkon *et al.*, 2014), (vi) there exists a perfect contact between the earth tube (pipe) and the soil (Niu

et al., 2015), (vii) heat losses through the heat exchangers of the combined plant are negligible (Rasih and Ani, 2012), (viii) pressure losses in piping and equipment are considered negligibly small. The study is focused on cooling of agricultural soil to a temperature range of 18 ºC ± 2, which is considered to be suitable for most high value temperate crops.

1.5 Significance of the Study

The main focus of this research is to develop the concept of chilled water production and power generation using low-grade solar energy, and application of the chilled water for radiant soil cooling process. The expected result of the study is significant but not limited to the following;

i. The result of this study intends to contribute to the better utilization of the free energy source for simultaneous supply of power and cooling system.
ii. This study intends to serve as a tool for research focus on the application of solar thermal chilled water for soil cooling as well as for comfort cooling in agriculture and domestic building respectively. This is a less energy consuming application.
iii. To also aid domestication of high-value temperate crops in the lowland areas of the Tropics. This can be practiced on a small scale, and can collectively contribute to the national economy by reducing the importation of the so called temperate crops.
v. This combined plant is virtually a stand-alone system which can be applied to radiant floor cooling system in domestic and public places with advantages of reducing pressure on the energy demand and reducing the environmental issues associated with the current cooling and primary energy production systems.

1.6 Research Questions

Based on the objectives and scope of this study, the following questions are intended to be answered;

i. With reference to the location and weather condition, what is the average cooling load imposed on a meter-square of soil bed?
ii. What size of the soil bed (A_s) can a certain plant capacity optimally cool, and vice versa?
iii. What effective solar field area (A_c) will optimally give the thermal energy (Q_b) needed to vaporize the refrigerant to produce the desired cooling (Q_{evp}) and power (W_t)?
iv. For a particular chilled water temperature, what is the optimized flow rate to keep the soil temperature within the set range?
v. What is the overall performance of the combined plant and the soil cooling system?
vi. Is the developed system economically impressive, and under what conditions?

1.7 Thesis Organization

The thesis is majorly divided into five chapters; Chapter 1 (Introduction), Chapter 2 (Literature Review), Chapter 3 (Methodology), Chapter 4 (Results and Discussions), and Chapter 5 (Conclusions and Recommendations).

The introductory part of the thesis is focused on the background of the study as it relates to the need for the cooling and the relative advantages of hydronic radiant cooling against the traditional air cooling system as well as the application of renewable energy for combined cooling and power systems. It also highlighted the problems of the traditional systems of cooling and power and the available alternatives

to both cooling and power. Objectives of the study were set as well as the scope, and significance of the study.

Chapter 2 is on the thorough review of the previous studies on both the combined power and cooling systems, and the radiant cooling system but with focus on agricultural soil cooling. It was discovered that these two areas of applications are rarely combined: application chilled water from any source for radiant soil cooling, and chilled water production from the combined plant have been individually reported in the literature. However, in the reported combined plants, chilled water production has always been a secondary goal to improve the efficiency of power generation.

Chapter 3 started with the modelling of the soil cooling load that is to be overcome by the plant. This was done by taking the soil thermal properties and location weather conditions into consideration. This was followed by modelling of the chilled water piping network with reference to the pipe properties and expected performance. Modelling of the combined plant capacity involves the components sizing as well as performance optimization. For the implementation of the mathematical models, software programming codes were developed for models calculations. The experimental rig, consisting of ammonia based absorption chiller and a dimensioned soil bed has been used to validate the modelled system. This was followed by the parametric study of the soil cooling, and of the combined plant, using *RSM*. The system economic analysis was carried out using RETScreen analysis software.

Chapter 4 is on analysis of the analytical and experimental results, and validation of the models. The results of the parametric analysis and optimization of the combined plant are presented and discussed. The economic analyses, with the financial viability and emission reduction resulting from implementing the developed system, compared with a base case of similar capacity are also presented and discussed.

Chapter 5 is the conclusive summary of the thesis but with the emphasis on the results and new discovery from the present study. Recommendations are also given on the future areas of study.

CHAPTER 2

LITERATURE REVIEW

2.1 Introduction

This section of the study is focused on the issues surrounding the present energy production and utilization, and applications of solar, as a free and safe energy source for radiant soil cooling systems. The section covers the state of art review on;

i. Solar energy potentials, its harvesting and its contributions to the utilization of HVAC in the tropical climate countries as well as its possible advantages of reducing peak energy demand;
ii. The combined power and cooling cycles (utilizing low-grade thermal energy) with focus on the combination of organic Rankine cycle and vapour absorption refrigeration cycle (using NH_3-H_2O and other working fluids);
iii. Radiant soil cooling system, with more emphases on agricultural soil cooling through the network of chilled water piping and pumping systems;
vii. Heat transfer and soil thermal properties as well as the influence of solar radiation heat on the development of planted crops;

Review of various related theoretical and experimental studies on the subject are presented so as to examine the outcome of this study with reference to other published literatures. The summary of the review is presented in Figure 2.1.

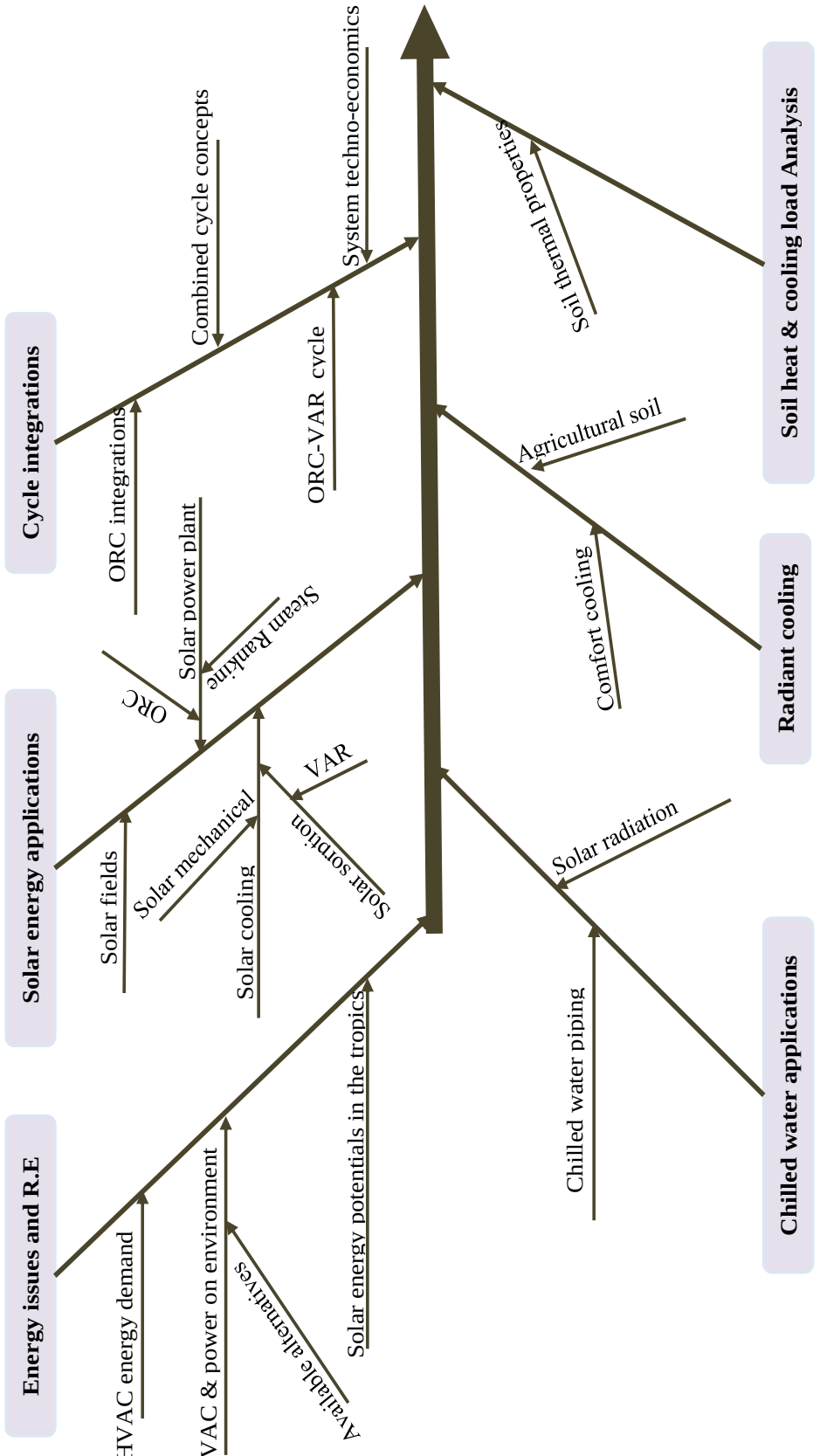

Figure 2.2: Review process summary

2.2 Energy Issues and Renewable Energy Option

Energy is considered as the pivot of technology and modern day development and as a result, it can be seen as the additional factor of production: after man, machine, capital and entrepreneurship (Bajpai, 2012). At the same time the demand for energy, particularly for cooling and heating is ever increasing (Deng *et al.*, 2011). Conversely, the larger proportion of the present global energy mix is non-renewable (Kaygusuz, 2012) and environmental unfriendly, necessitating the quest for alternative energy sources. To achieve all-round development, it is paramount to secure a constant, reliable, affordable and environmental friendly energy supply that must be efficiently utilized for the required task, and in the long term, should constitute no threat to the society.

Research interests have been focused on utilization of alternative and renewable energy sources (such as solar, wind, biomass, geothermal, ocean thermal, and tidal) due partly to the overwhelming awareness on issues of the current energy supply, ranging from its imminent and fast depletion to environmental problems such as ozone layer depletion, global warming and other pollutions resulting from their production and/or application. Renewable energy sources are seen as green (Oh *et al.*, 2010), abundantly free (Marc *et al.*, 2012), and with very little or no harmful effect on environment either from their usage or their process of production (Chen, 2012).

To support the use of renewable energy, countries around the world have been coming up with renewable energy policies that are targeted at mitigating the environmental impacts occasioned by conventional energy sources and also to have affordable and sustainable energy supplies, by providing motivation (in the form of feed-in-tariff, subsidies and Renewable Portfolio Standard) towards the development of renewable energy technologies (Solangi *et al.*, 2011) and to be less reliant on fossil fuel.

Malaysia ‘Renewable Energy Act (2011)’, is aimed at enhancing the utilization of indigenous renewable energy sources for national electricity supply security and

sustainable socio-economic development through implementation of special tariff and motivational incentives (Chen, 2012). This is expected to improve the renewable energy proportion of the national power generation mix, enhance development of renewable energy industries as well as conserving the environment (Solangi *et al.*, 2011). This implementation is with the involvement of a number of key Malaysian government ministries and agencies in energy efficiency improvement (Mekhilef *et al.*, 2012). Pakistan Council of Renewable Energy Technology (PCRET) and Alternative Energy Development Board (AEDB) were saddled with the responsibility of implementation and actualization of renewable energy policy in Pakistan (Khan and Pervaiz, 2013). Energy Performance Building Directive (EPBD) was established by the European Parliament in 2002 and was modified in 2009 to mandate each of the member states to set up minimum energy performance as well as to develop and implement Energy Performance Certificate (EPC) for the building energy performance rating (Boyano *et al.*, 2013). In addition, in response to energy crisis witnessed in the 1973 between the Arab nations and the western world, Nigerian government established the Energy Commission of Nigeria (ECN) in 1979 with the mandate to conduct research and development (R&D) on renewable energy technologies and to popularize its applications all over the country (Ilenikhena and Ezemonye, 2010). To support the utilization of renewable energy, the Chinese National Development and Reform Committee (NDRC) developed policies to support renewable electricity generation, heating and cooling as well as RE research to replace oil in many applications (Wang *et al.*, 2009). Leading examples are found in Denmark, United States of America, Canada, France, Spain, and Australia where favourable policies were made to enhance renewable energy technologies (Mendonça *et al.*, 2009; Solangi *et al.*, 2011).

Of all the renewable energy sources, solar energy is found to be the most promising source (as shown in Figure 2.2); it is in-exhaustive in supply and available all over the world where day and night exist, and under no monopoly. It is estimated that about 1.8×10^{11}MW of solar energy falls on the earth surface daily which if properly utilized, could be more than the world energy consumption (Bajpai, 2012). This is confirming the potential of solar energy as a promising source of alternative

energy. Another reason for increasing research interest has to do with free supply of solar energy in replacement of the conventional energy that must be paid for.

Theoretical and experimental researches have been carried out on solar energy particularly on its application for cooling system as the need for cooling is always in phase with the peak solar energy availability (Martínez *et al.*, 2012). It can rightly be said that peak cooling demand and peak solar radiation are naturally correlated. As such, many research efforts have been devoted to harnessing solar energy for cooling, heating and power generations (Masson. *et al.*, 2006; Treberspurg. *et al.*, 2011); mostly for low-grade thermal energy applications like organic Rankine system, and sorption cooling systems (Saitoh *et al.*, 2007; Delgado-Torres and García-Rodríguez, 2010).

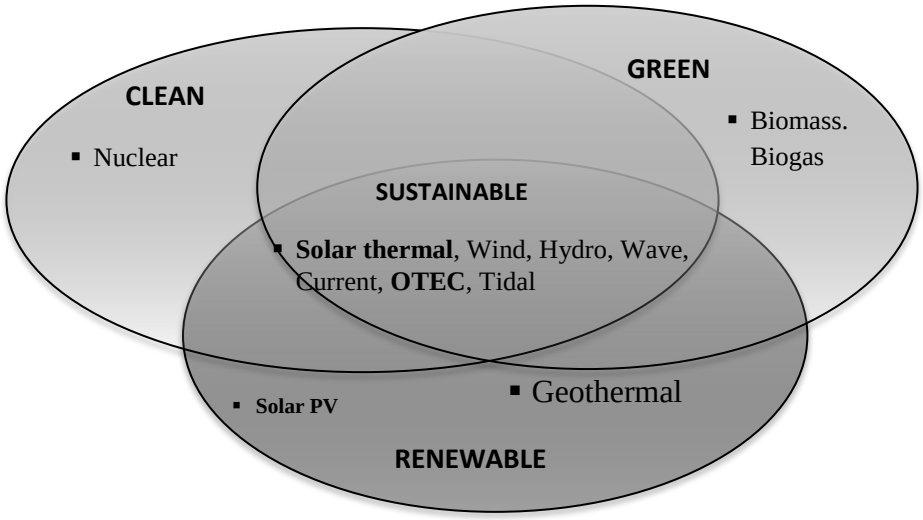

Figure 2.2: Forms and classifications of energy (Jaafar, 2014)

2.3 Solar Energy Potentials in the Tropics

Solar energy is a form of electromagnetic radiation having wavelengths between 0.3μm to over 3μm, most of which is concentrated in the visible and the near-infrared wavelength range (Daut *et al.*, 2012). The concept of purposeful concentration of solar energy was first witnessed in 212 BC when the Greek Scientist (Archimedes)

devised a method to burn Roman war fleet using concave metallic mirrors (shinning shield) to concentrate the sun's rays to burn the Roman fleet (Kalogirou, 2004).

Solar thermal energy (Figure 2.3) has been very popular in the research field in recent times as a decentralized energy source for power generation most importantly in tropical and sub-tropical regions where the potential is relatively higher (Agyenim *et al.*, 2010; Chua and Oh, 2012). However, a major constraint is that it is a diffuse energy source (Hlbauer, 1986), thus a solar collector is required to capture it in technologically useful quantity: the collector must be properly sized to avoid unnecessarily increased cost (Bajpai, 2012). Another constraining factor is the seasonal nature of solar energy which results from its availability that is directly tied to day and night cycle and earth's orbit round the sun as well as the local weather condition of a place such as haze, cloud cover, rainfall and typhoon (Mongkon *et al.*, 2013; Ssembatya. *et al.*, 2014). However, this is usually taken care of by thermal storage to bridge the demand gap (Ibrahim *et al.*, 2017).

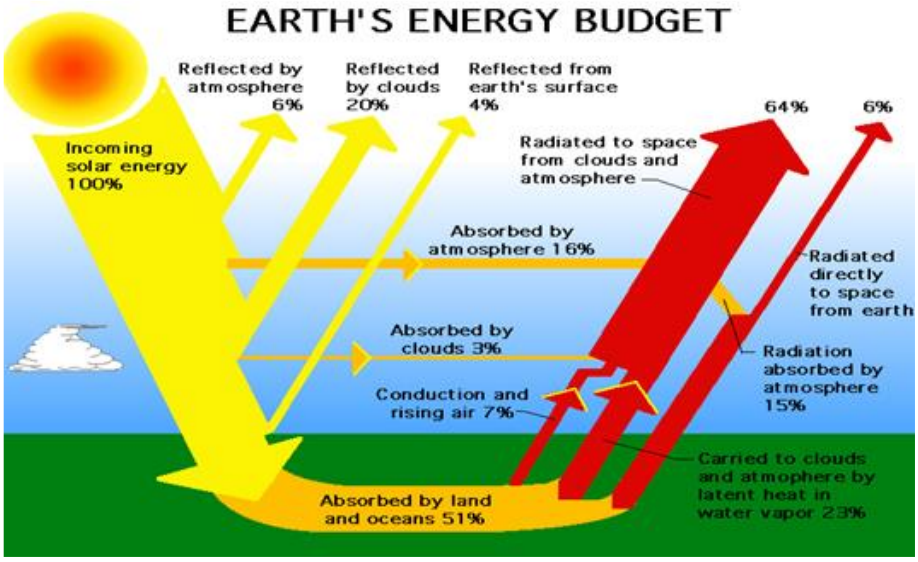

Figure 2.3: Daily solar radiations proportion on ground surface (NASA, 2017)

Generally, the Tropics is a region defined by the Tropic of Cancer in the northern hemisphere with latitude of 23.5 ºN and the Tropic of Capricorn in the southern hemisphere with latitude of 23.5 ºS (as shown in Figure 2.4). This region, known as tropical zone is mostly found to be torrid. Most countries found in this region

are characterized with hot and humid climate (Parameshwaran *et al.*, 2012; Chang *et al.*, 2009; Mekhilef *et al.*, 2012).

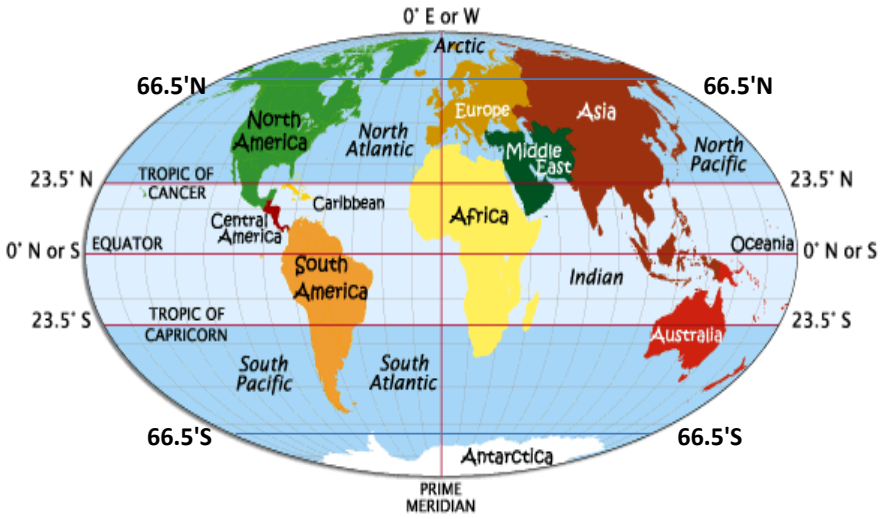

Figure 2.4: Global latitudes of regions (worldatlas, 2017)

To make the better use of the tropical climate solar characteristics, a number of theoretical and experimental research studies have been carried out towards the utilization of the ample solar energy resources in the region. Experimental analysis was conducted by Yin on the performance of absorption solar cooling in China and it was found out that system performance is positively affected by solar radiation availability (Yin *et al.*, 2013). Solar hybrid (adsorption and desiccant) air conditioning system was proposed by Fong for high temperature cooling in sub-tropical cities (Fong *et al.*, 2010b): their study confirmed the technical feasibility of the system. In the study conducted by Marc on solar cooling system for buildings in tropical climate, it was concluded a major advantage for solar cooling (especially in the tropics) is the availability of free thermal source mostly when building thermal load demand is maximum (Marc *et al.*, 2012). Comprehensive analysis of renewable energy in Malaysia is shown in Table 2.1 (Oh *et al.*, 2010), while the survey of solar energy at different parts of Malaysia by Mekhilef is, presented in Table 2.2 (Mekhilef *et al.*, 2012). These show the vast potentials of Malaysia solar energy utilization. Furthermore, the analysis of Malaysia weather data by (Tang, 2012), using data from Subang Meteorological Station, showed that average daily temperature is between 24 ^{o}C and 32 ^{o}C (as shown in Figure 2.5) with daily radiation mostly between 8:00hrs and

18:00hrs clock time per day (as shown in Figure 2.6) but with usually high relative humidity; between 66 % and 95 % (Tang, 2012).

Table 2.1: Renewable energy potential in Malaysia (Oh *et al.*, 2010)

Renewable Energy	**Potential (MW)**
Mini-hydro	500
Biomass/biogas (oil palm mill waste)	1,300
Municipal solid waste	400
Solar PV	6,500
Wind	Low wind speed (less than 2.0 m/sec)

Table 2.2: Average annual solar radiation in Malaysia (Mekhilef *et al.*, 2012)

Irradiance	Yearly average value (kWh/m^2)
Kuching	1470
Bandar Baru Bangi	1487
Kuala Lumpur	1571
Petaling Jaya	1571
Seremban	1572
Kuantan	1601
Johor Bahru	1625
Senai	1629
Kota Baru	1705
Kuala Terengganu	1714
Ipoh	1739
Taiping	1768
George Town	1785
Bayan Lepas	1809
Kota Kinabalu	1900

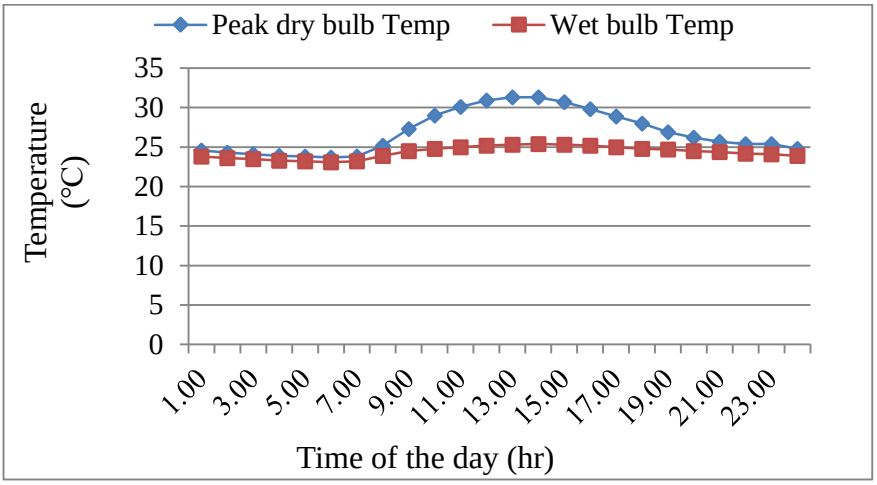

Figure 2.5: Malaysia's peak dry bulb and wet bulb temperatures (Tang, 2012)

Utilization of solar energy offers numerous advantages that include but not limited to the following;

i. Aiding of decentralized energy supply and energy security;
ii. Environmental safety, as it involves no emission of greenhouse gases;
iii. Rural integration, especially in the developing countries of the world;
iv. Its application for water desalination helps in improving water quality and quality of lives; and
v. Non-reliance on the gradually depleting fossil fuel.

Meanwhile some of the limitations/constraints include the high initial cost, infancy of the technology (which can be addressed through continuous R&Ds), and lack of proper awareness especially in the remote areas where it is most needed.

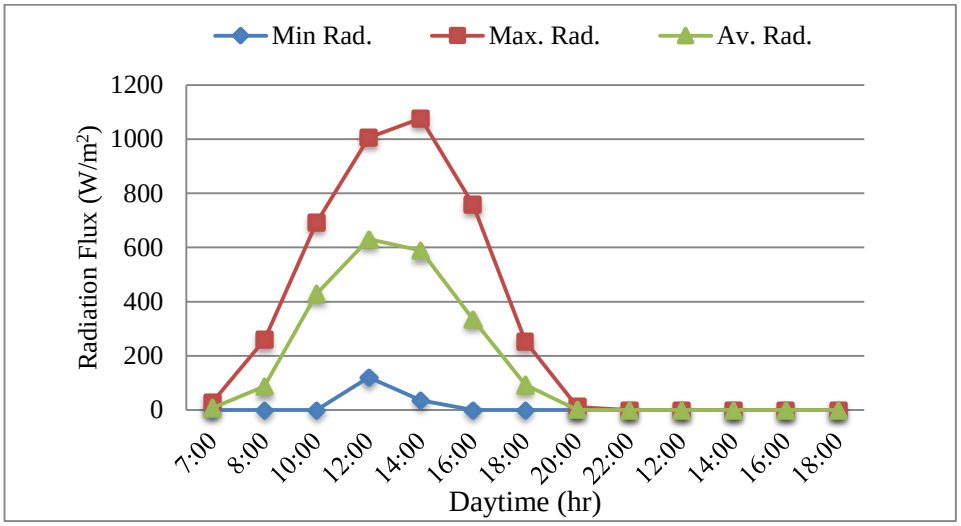

Figure 2.6: Daytime horizontal solar radiation in Malaysia (Tang, 2012).

2.4 Solar Field

Solar energy is harvested through the solar photovoltaic (PV) cell, solar thermal collector or their hybrid, referred to as PV/T (Khan and Pervaiz, 2013; Zhang *et al.*, 2012). Solar PV cells allow direct conversion of solar energy to electrical energy as direct current (DC) or inverted to alternating current (AC) for appliance usage. Meanwhile the obtainable efficiency from PV cells is usually between 9 % and 15 % (Daut *et al.*, 2012; Kalogirou, 2004; Gaglia *et al.*, 2017), depending on the material making up the PV cell. However, advances in solar PV technologies has actually caused improvement from what it used to be in the last two decades (Kalogirou, 2004).

Solar thermal collectors do not directly convert solar energy to electrical energy but it is used majorly to capture solar heat and supply it through thermal fluid for the activation of HVAC systems (Duan *et al.*, 2012; Tsoutsos. *et al.*, 2009). The coefficient of performance (*COP*) of solar collector is however between 0.7 and 2.0 (Fong *et al.*, 2010b; Mokhtar *et al.*, 2010), depending the type of the collector. Review of solar thermal refrigeration systems was carried out by (Ullah *et al.*, 2013) and it was concluded that "the solar photovoltaic system can provide electricity as well as refrigeration but solar thermal refrigeration is more efficient". Based on the scope of

this work, only solar thermal application is considered and solar energy is harvested through the solar collector.

2.4.1 Solar Collectors

Basically solar collector constitutes an important part of solar thermal energy utilization for heating (in form of domestic hot water and space heating), cooling (air-conditioning/refrigeration), or for power generating system. Solar collector is a heat exchanger containing absorber pipe with high absorptivity (~ 0.96) for short wave length radiation and low emissivity (~ 0.04) for long wave radiation (Qu, 2008; Kalogirou, 2004), making it able to absorb incoming solar radiation which is then converted to heat energy of the transport fluid (such as air, water and oil) and transferred through the fluid to the point of use. Solar collectors are broadly categorized into concentrating and non-concentrating types which can be further sub-divided to various types as shown in Table 2.3. Concentrating types are sun tracking and consist of a wider parabolic shaped dish with reflecting mirrors that converge the solar radiation to its vocal point called 'hot spot' (Kadir and Rafeeu, 2010). Parabolic dishes, parabolic through, and solar tower are major types of solar collector under concentrating type and are more appropriate for industrial power cycles (Quoilin. and Lemort, 2009; Price *et al.*, 2002). Flat plate and evacuated tube are the most common non-concentrating solar collectors (Chidambaram *et al.*, 2011) and are most suitable for low-grade temperature applications. These are also referred to as stationary collectors. Non-concentrating collector is considered in this work.

Table 2.3: Common features of collectors (Mokhtar *et al.*, 2010; Deng *et al.*, 2011; Bajpai, 2012)

Solar Collector		**Temp Range (°C)**	***COP* (average)**	**Application**
Class	Type			
Non-concentrating	Flat Plate	85	0.7 – 0.85	Single effect Absorption
	Evacuated tube	85	0.7 – 0. 85	Single effect absorption
Concentrating	Parabolic trough	180	1.4	Double effect Absorption
	Linear Fresnel	180	1.9	Triple effect Absorption
Solar thermal large scale	Parabolic trough	250	2.0	Triple effect absorption
		>350		Power block
	Central receiver	250	2.0	Triple effect absorption
		>350		Power block

2.4.2 Performance Indicators

Most often, the performance indicators of interest in solar cooling systems are the solar fraction ($S_{fraction}$), solar thermal gain ($G_{thermal}$), and coefficient of performance (COP) (Fong *et al.*, 2009).

Solar fraction ($S_{fraction}$) is a measure of proportion of solar energy contribution to the total energy required by solar cooling system to drive its refrigeration unit. This is usually applicable when an auxiliary heat supply is involved (Kadir and Rafeeu, 2010). Solar fraction of value close to 1 is an indication that the system is more energy efficient. Thus the value of solar fraction will be zero if no solar energy is involved and 1.0 if the system is totally driven by solar energy.

$$S_{fraction} = \frac{Q_{solar}}{Q_{solar}+Q_{aux}} \tag{2.1}$$

Where Q_{solar} and Q_{aux} are the respective solar energy and auxiliary heat supplied to activate the system.

Solar thermal gain ($G_{thermal}$) is the amount of useful solar energy that can be obtained through the collector. This is however tied to the type of collector and the intensity of solar radiation available (Fong *et al.*, 2010b). The useful energy gained is theoretically given as;

$$Q_u = A_c Q_{inc} \eta_c \tag{2.2}$$

Where A_c is the effective area of the collector, Q_{inc} is the solar radiation intensity and η_c is the thermal efficiency of the collector array.

Thus, the theoretical efficiency of the collector is given as;

$$\eta_c = \frac{Q_u}{Q_{inc} \times A_c} \tag{2.3}$$

Q_u can also be expressed in terms of the energy transfer to the thermal fluid, that is;

$$Q_u = \acute{m} C_p (T_h - T_l) \tag{2.4}$$

Where $\acute{m}$ and C_p are the respective mass flow rate and specific heat capacity of the thermal fluid, and T_h & T_l are outlet and inlet temperatures of the thermal fluid, respectively.

Coefficient of performance (COP) is the performance indicator that measures the amount of heat energy consumed by a refrigerating unit to net refrigeration effect of the cooling system. It is otherwise defined as the quotient between the heat absorbed by the evaporator (Q_{evp}) and the heat gained by the working fluid from the generator (Q_{gen}). For a sorption refrigeration system, the *COP* is given as;

$$COP = \frac{Q_{evp}}{Q_{gen}} \quad (2.5)$$

Where Q_{evp} the refrigeration is effect and Q_{gen} is the heat supplied by the generator.

2.5 Solar Cooling Systems

Solar cooling majorly comprises of solar electric compression cooling, solar mechanical compression cooling, solar desiccant cooling, solar absorption cooling and solar adsorption cooling (Fong *et al.*, 2009; Baniyounes *et al.*, 2013). However, based on the scope of this research, only solar absorption cooling system is discussed in detail.

2.5.1 Solar Absorption Cooling System

Solar absorption cooling/refrigeration system involves pumping of binary mixture as working fluid (refrigerant and absorber) through a solution heat exchanger, to the generator for vaporization of the refrigerant. The refrigerant causes the cooling effect (in the evaporator) after being subjected to a pressure differential through the expansion valve. The cooled refrigerant is used for cooling process, or to cool another (heat transport) fluid for further cooling processes. Most common refrigerant-absorbent (working fluid) pairs are Ammonia-water NH_3-H_2O), and Lithium bromide-water (LiBr-H_2O). Absorption cooling can be single, double or multiple effects system (Kalkan *et al.*, 2012). This is discussed in more detail in the following sections.

2.5.2 Absorption Chiller System

Historically, the idea of absorption refrigeration started in the 1700s when it was discovered that 'ice' could be produced by evaporating water within an evacuated

container in the presence of sulfuric acid (Ullah *et al.*, 2013). Ferdinand Carré (A French Engineer/Scientist) in 1859 designed the first machine that used ammonia-water working fluid pair to produce ice that was used for food store (Srikhirin. *et al.*, 2001; Kalkan *et al.*, 2012) and got the first US patent for his absorption unit in 1860 (Deng *et al.*, 2011). The new system (with water-lithium bromide working fluid) was later introduced in 1950 (Ullah *et al.*, 2013) for commercial purposes.

Absorption refrigeration is considered a closed cycle system that can be driven by low-grade heat sources like waste heat, geothermal heat, and solar energy to achieve cooling or refrigeration. Solar absorption cooling system is gaining research attention in recent times as a result of increase interest in the quests for alternative energy especially for HVAC systems. Meanwhile, one of the challenges with absorption cooling system is its relatively low coefficient of performance (between 0.5 and 1.5) compared with the compression type with *COP* in excess of 3.0 (Somers *et al.*, 2011; Agyenim *et al.*, 2010; Kalogirou. *et al.*, 2001). This *COP* also depends on the working fluid and the number of stage/effect of the system. As a result, there are many theoretical and experimental studies on absorption refrigeration system that aimed at achieving better performance of the system. Studies were conducted by (Abdulateef. *et al.*, 2007; Abdulateef. *et al.*, 2008) on the comparison of solar driven absorption refrigerator, based on some selected working fluids to improve the system performance. In another study, (Khamooshi *et al.*, 2013) did the review of thermodynamic properties of Ionic liquids as working fluids to overcome some common challenges associated with the common absorption refrigeration working fluids like LiBr-H_2O and NH_3-H_2O. Furthermore, the design analysis of solar powered absorption cooling system was carried out by (Bajpai, 2012), for a definite system to determine the system optimum parameter. For better improvement on the efficiency of absorption refrigeration system, an experimental study was conducted by (Sözen *et al.*, 2012) on a diffusion absorption refrigeration system (DARS) and they came up with a low energy/cost design for the system. Review of absorption refrigeration technologies was carried out by (Srikhirin. *et al.*, 2001), considering single, double and multiple effects and various working fluids to improve absorber performance and to increase the technological interest in the field of absorption refrigeration systems. Some of the observed advantages of absorption refrigeration system include;

i. Highly economical as it involves low or no maintenance because it has no moving part;
ii. High reliability and long service life;
iii. Quiet (silent) operation and does not contribute to environmental pollution;
vi. Helps in efficient energy utilization and more useful in remote places where grid-tied electricity is a problem;

2.5.3 Basic Absorption Refrigeration Principles

The basic absorption refrigeration cycle is presented in Figure 2.7 with the main components as; absorber, generator, condenser, and evaporator (Khamooshi *et al.*, 2013). Starting from the absorber, low pressure aqua-ammonia solution (containing refrigerant and absorbent) is pumped to the generator at elevated pressure. The solution passes through a heat exchanger where it is preheated by the return stream from the generator. Heat is supplied to the generator from the heat source which can be solar collector, biomass, gas or electric heater, to drives off the refrigerant (in vapour form) from the mixture of the weak solution. This is also referred to as desorption (Somers *et al.*, 2011; Kasperski and Eichler, 2012; Garimella, 2012). The liquid absorbent returns to the absorber through the expansion valve that reduces its pressure. The refrigerant (strong solution) vapour leaving the generator enters the condenser and condenses into liquid, where it loses most of its heat (Cloutier, 2002). It then flows through an expansion valve that causes reduction in its pressure. This pressure reduction also causes reduction in saturation temperature of the refrigerant; making it extremely cold (Gupta, 2011; Cai *et al.*, 2014) saturated liquid which then evaporates and extracts heat from the evaporator space before flowing into absorber tank where it is absorbed to become weak, low-pressure saturated liquid to repeat the cycle again. The heat extraction from the evaporator is referred to as refrigeration/cooling effect of the system

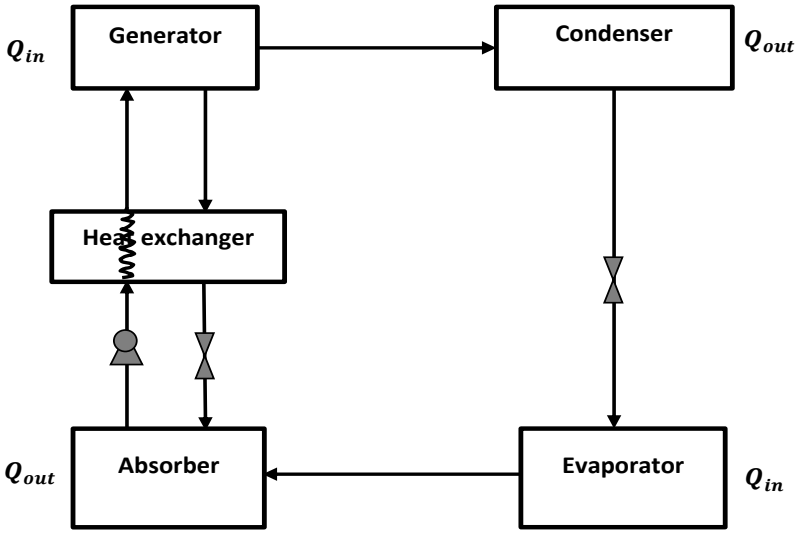

Figure 2.7: Basic single-effect absorption refrigeration cycle

2.5.4 Single, Double, and Multi-Effects Systems

Absorption refrigeration system is also grouped (base on the number of refrigerant vapour generation) into single-effect, double-effect, triple-effect or multiple-effect (Deng *et al.*, 2011; Garimella, 2012; Hong *et al.*, 2011; Sharizal, 2006) as shown in Table 2.4. The single effect type (Figure 2.7) operates at lower temperature than double/triple/multi-effects types. Double-effect types (Figure 2.8), is characterized with two generators and two solution heat exchangers (Sharizal, 2006). Low pressure binary solution is pumped through HX_1 to HX_2 then to the generators 1 and 2 from where it flows to the condenser in which it is condensed and cooled before flowing through the expansion valve to the evaporator and back to the absorption tank to repeat the cycle. HX_2 can also pass the solution to generator 2 which can as well pass it to HX_1. Literatures showed that two single-effects cycles can form a double-effect cycle as the *COP* of double effect is relatively equal to two of the single-effects *COP* (Srikhirin. *et al.*, 2001; Ullah *et al.*, 2013). The coefficient of performance of an absorption refrigeration system is expressed as;

$$COP = \frac{Cooling\ capacity\ achieved}{Generator\ heat\ input + work\ done\ on\ the\ pump} \tag{2.6}$$

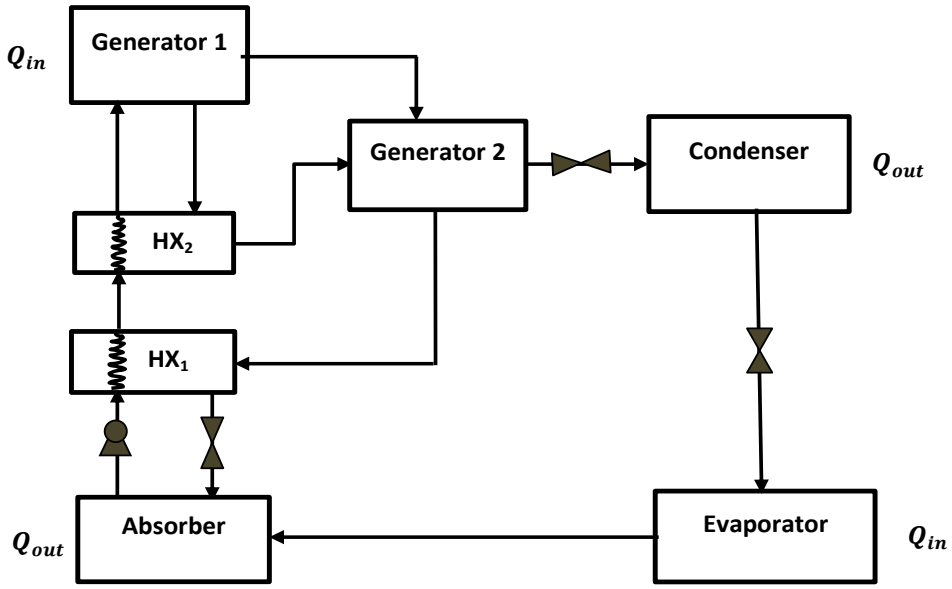

Figure 2.8: Double-effect absorption refrigeration cycle (Ullah *et al.*, 2013; Srikhirin. *et al.*, 2001)

Table 2.4: Features of single and double effect absorption chiller (Deng *et al.*, 2011; Srikhirin. *et al.*, 2001)

Properties	**Single-effect**		**Double-effect**	
Working fluids	$LiBr\text{-}H_2O$	$NH_3\text{-}H_2O$	$LiBr\text{-}H_2O$	$NH_3\text{-}H_2O$
Operating pressure and temperature	2 – 3 bar, 70 – 100 ℃ hot water or direct fired	2 – 16 bar, steam or 70 – 110 ℃ hot water	4 – 8 bar, steam or 120 – 170 ℃ hot water	8 – 16 bar, steam or 170 – 220 ℃ hot water
Refrig. output	5 – 10 ℃ chilled water		5 – 10 ℃ chilled water	
Capacity range	5 – 7,000 kW	4.5 – 90 kW	20 – 11,630 kW	<110kW
Cooling method	Water-cooled or air-cooled (small unit)		Water-cooled or air-cooled	
COP range	0.5 – 0.7	0.5 – 0.75	0.7 – 1.2	0.7 – 1.2

2.5.5 Working Fluids and their Properties

Working fluid is vital to both the absorption cooling system and organic Rankine system, because the performance of both cycles depends on the

thermodynamic properties of the working fluids used (Khamooshi *et al.*, 2013). Working fluids serve as the heat transport medium through which series of heat exchange processes take place to either lose or gain energy or work, to or from the heat exchange medium. This process is accomplished through the mass flow and enthalpy exchange across the heat exchange medium. In absorption process, the ultimate goal is cooling while power generation is the main target in Rankine cycle process. To achieve better system performance, various studies have been conducted in search of best performing working fluid for individuals of absorption cooling and organic Rankine cycle as well as their combination for power and cooling (Sanjay, 2003; Li *et al.*, 2013; He *et al.*, 2010). Ammonia-water (NH_3-H_2O) mixture and Lithium bromide-water (LiBr-H_2O) mixture are found to be the most common working fluids used as refrigerant-absorber mixtures for vapour absorption cooling system (Somers *et al.*, 2011). Although alternative working fluids (such as Ionic working fluids) are being studied to replace these popular fluids due to perceived issues with them (Khamooshi *et al.*, 2013; Weith *et al.*, 2014; Abdulateef. *et al.*, 2007) and to further improve the absorption cooling performance. Meanwhile, these working fluids are mainly for absorption refrigeration system. For Rankine cycle, water (H_2O), carbon dioxide (CO_2), Ammonia (NH_3) or other organic fluids can be used as working fluid, but for ORC, organic fluids are the preferred options for low-grade thermal energy utilization (Li *et al.*, 2013). Research has shown that binary mixture of working fluid results in better overall performance in Rankine cycle (Abed *et al.*, 2013). The result of "thermodynamic studies of working fluid combination" by (Sanjay, 2003) for combined power and cooling gave lower thermodynamic efficiency with hydrocarbon working fluids than ammonia-water pair. Ammonia-water working fluid was proposed by (Xu. *et al.*, 2000) for combined power and cooling. Because ORC uses refrigerant, its combination with VAR is possible, yet selection of refrigerant must be based on some factors; the overall efficiency, cost, safety and impact on environment must be taken into consideration. Generally working fluid should;

i. Have remarkable difference between the boiling points of pure refrigerant and the working fluid mixture under the same condition;
ii. Possess favourable transport properties (thermal conductivity, viscosity, diffusion coefficient etc.) for better heat and mass transfer;

iii. Be thermally stable, non-flammable, non-corrosive, non-toxic and non-fouling;
iv. Be regularly available at reasonable cost;
v. Have low operating temperature and pressure;

In reality, all the desirable properties may be difficult to achieve from a particular working fluid for a particular purpose. Some of the refrigerants with their properties are shown in Table 2.5.

Table 2.5: Properties of common refrigerant (Khennich and Galanis, 2012; Kim *et al.*, 2012; NIST; McQuay, 2002)

Refrigerant	**Common Application**	T_{crit} (°C)	T_{boil} (°C)	P_{crit} (Bar)	ODP	GWP
R-114 ($C_2F_4Cl_2$)	Sorption cooling	145.7	32.5	14.8	1	3.9
R-245fa ($C_3H_3F_5$)	ORC	154	14.4	36.34	0	820
R-290 Propane ($CH_3CH_2CH_3$)	ORC	96.7	-42.1	42.5	0	0
R-124 (C_2HF_4Cl)	Sorption cooling	122.5	-12.1	36.4	0.02	620
R-125 (CHF_2CF_3)	Sorption cooling	66.1	-54.6	36.3	0	2800
R-134a (CH_2FCF_3)	Sorption cooling, ORC Power	101.1	-26.1	4.6	0	1300
R-143a ($C_2H_3F_3$)	Sorption cooling	73.1		38.1	0	4300
R-152a ($C_2H_4F_2$)	Sorption cooling	113.6	-24.0	44.9	0	120
R-32 (CH_2F_2)	Sorption cooling	7 8.1	-51.7	57.8	0	650
R-718 (H_2O)	Sorption cooling, RC	373.9	100	220.6	0	< 1
R-717 (NH_3)	Sorption, ORC	132.2	-33.3	42.5	0	0

2.6 Rankine Cycle and Organic Rankine Cycle

Traditional steam Rankine cycle has been applied in the past to generate power but with very high operating temperature and pressure (Kalogirou, 2004). The power

range is usually quite large and generally in the range of 10MWe and above with relatively low efficiency; around 10 % (Arvay. *et al.*, 2011). Basically, Rankine cycle (Figure 2.9) involves four main steps (Sanjay, 2003; Arvay. *et al.*, 2011), which are;

i. Pumping of working fluid from low pressure to the boiler, at high pressure;
ii. Heating/superheating of the working fluid at constant pressure in the boiler to vaporise the working fluid;
iii. Expansion of the vaporized working fluid through the turbine from which the mechanical work is converted to electrical energy;
iv. Condensation of the working fluid through the condenser before it is pumped back to repeat the cycle;

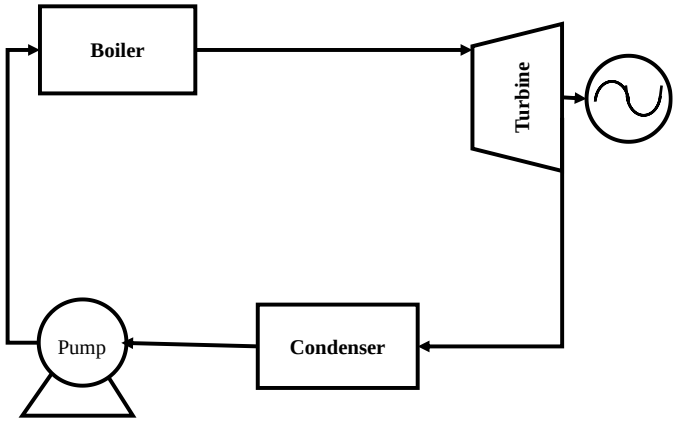

Figure 2.9: Schematic representation of Rankine cycle

2.6.1 Organic Rankine Cycle (ORC)

The growing interest in the application of low-to-moderate grade heat energy has made organic Rankine cycle (ORC) popular in the recent times (Ziviani *et al.*, 2014). Organic Rankine cycle is similar in configuration and principle to the traditional steam Rankine cycle (Leslie. *et al.*, 2009) except that;

i. It uses organic working fluid with favourable thermodynamic properties.

ii. It is possible in smaller installation in the range of few kWe (Quoilin *et al.*, 2013), or less.

iii. It can operate at lower temperature and pressure therefore can be powered with solar energy, geothermal energy and biomass heat energy (Quoilin. and Lemort, 2009) which are considered low-grade heat energy, and with improved efficiency (Arvay. *et al.*, 2011).

iv. Smaller sizes of the turbine and piping systems are required and this leads to reduced cost. Its low condensing pressure also leads to elimination of the need for vacuum and gas purging equipment that is commonly used in steam condensing cycle (Borunda. *et al.*, 2016).

The lower operating conditions are possible because the working fluids are mostly refrigerants that can change phase at normal pressure and at temperature that is well below the boiling point of water (< 100 ℃), making them suitable for low-grade heat applications. The heat regarded as moderate-to-low-grade fall just below 370 ℃ (Ziviani *et al.*, 2014) and are usually rejected to the atmosphere especially as waste heat in the industries. Since ORC conveniently utilizes temperature in this range, many studies have been carried out to increase the overall efficiency of most industrial processes by generating additional power through the integration of ORC to make use of the waste heat (Yamada *et al.*, 2009; Wei *et al.*, 2007) that would have been thrown into the atmosphere. Table 2.6 shows the possible energy sources that can be utilized by ORC.

Table 2.6: Different energy sources for ORC application (Ziviani *et al.*, 2014)

Energy source	**Application scale (kW)**		
	Large	**Middle/small**	**Micro**
Waste heat recovery	√	√	√
Geothermal	√	√	
Biomass	√	√	
Solar thermal		√	√

Some of the relative advantages of ORC power plant as highlighted by (Sotomonte. *et al.*, 2011; Quoilin. and Lemort, 2009) are;

i. Higher cycle and turbine efficiencies;
ii. Low mechanical stress as a result of low tangential velocity;
iii. With organic liquid, risk of turbine blade erosion (due to moisture in the vapour flow) is reduced;
iv. Equipment longer life span;
v. Requires no water treatment;

2.6.2 Rankine Efficiency

Generally, for thermal power plant, cycle efficiency is defined as the ratio of power output to the heat input into the system; this efficiency is defined in terms of the gross or net power output.

$$\eta_{gross} = \frac{P_{gross}}{\dot{Q}_b} \tag{2.7}$$

$$\eta_{net} = \frac{P_{net}}{Q_b}$$

$$P_{net} = P_{gross} - \sum W_{pi} \tag{2.8}$$

Where P_g and P_{net} are turbine gross and net power outputs, respectively, W_{pi} is the power consumed to pump the working fluid, $\dot{Q}_b$ is boiler heat input to vaporize the working fluid.

Working fluid plays an important role in the cycle efficiency of Rankine power system, therefore one of the main challenges in ORC power system is the choice of appropriate working fluid that can both give maximum efficiency (Karellas. and Schuster, 2008) and be environmental friendly. The mathematical model by (Sotomonte. *et al.*, 2011) to find better organic working fluid for ORC in biomass cogeneration reveals that the cycle efficiency depends more on the thermodynamic properties of the working fluid than the system configuration.

2.6.3 Organic Working Fluids

Primary working fluid conveys the thermal energy from the solar collector to the boiler where this thermal laden fluid is used to vaporize the organic fluid, which in turn flows with high pressure to the turbine to perform useful work. Various organic working fluids have been proposed and used for ORC. R113 ($C_2Cl_3F_3$) was used by (Saitoh *et al.*, 2007) in the development and testing of solar organic Rankine cycle, using scroll expander in the turbine. They then suggested the use of solar organic Rankine system for future power generation and distribution on small scale. Pentane was used by (Leslie. *et al.*, 2009) as working fluid in ORC for capturing of 5.5MW of electricity from 27MW output gas fired steam turbine. The additional energy was achieved with no fuel addition and almost no emission. The result of mathematical analysis by (Sotomonte. *et al.*, 2011) confirmed that the efficiency of ORC is a function of the thermodynamic properties of the organic working fluid. Studies by (Delgado-Torres and García-Rodríguez, 2010) considered various working fluids (Propane, R134a, R227ea, R152a, NH_3, Isobutane, Butane, R245fa, Neopentane, R245ca, Isopentane and Pentane) while working on the low-temperature (solar) application for ORC. The consideration was based on their thermodynamic properties and effects on the environment.

2.7 ORC Integrations

The possibility of integrating ORC with other cycles and its ability to utilize heat energy from various low-grade heat sources had made it to become more popular in recent times. Studies were conducted on optimization of ORC using low-grade heat recovery (Ziviani *et al.*, 2014), to evaluate the system ability to deliver the electricity, heating and cooling (using electric air-conditioner) demands of a living apartment. Combination of ORC with desalination technology was analysed (Delgado-Torres and García-Rodríguez, 2010); their system was powered by solar energy through the solar collector to produce fresh water in some areas with problem of rising water scarcity. Ocean thermal energy conversion (OTEC) is an alternative energy extraction process

that uses the natural temperature gradient (15–25K) between the warm ocean surface and the cold deep ocean. Due to the low temperature application of ORC, series theoretical and experimental studies have been carried out on application of ORC for OTEC to improve energy generation efficiency (Yamada. *et al.*, 2006; Yamada *et al.*, 2009; Ziviani *et al.*, 2014). ORC has reportedly been applied with fuel cell; in this process, solid oxide fuel cell (SOFC), regarded as topping cycle produces electricity by conversion of fuel chemical energy to electrical energy (Dincer *et al.*, 2009), while ORC (bottoming cycle) recovers the waste heat from the topping cycle to generate additional electricity (Ziviani *et al.*, 2014).

2.8 Absorption Refrigeration–Organic Rankine Combined Cycles

2.8.1 Combined Cooling, Heating and Power System driven by Solar Energy

This system was designed by (Jiangfeng *et al.*, 2009) and powered by solar energy, making it different from the conventional high temperature combined cooling, heating and power (CCHP) systems that use gas turbine. In this system (shown in Figure 2.10), Rankine cycle is combined with an ejector refrigeration cycle to produce cooling, heating and power simultaneously. The system was theoretically proven to be feasible through thermodynamic simulation. However, the experimental validation was not done, necessitating further studies on the system.

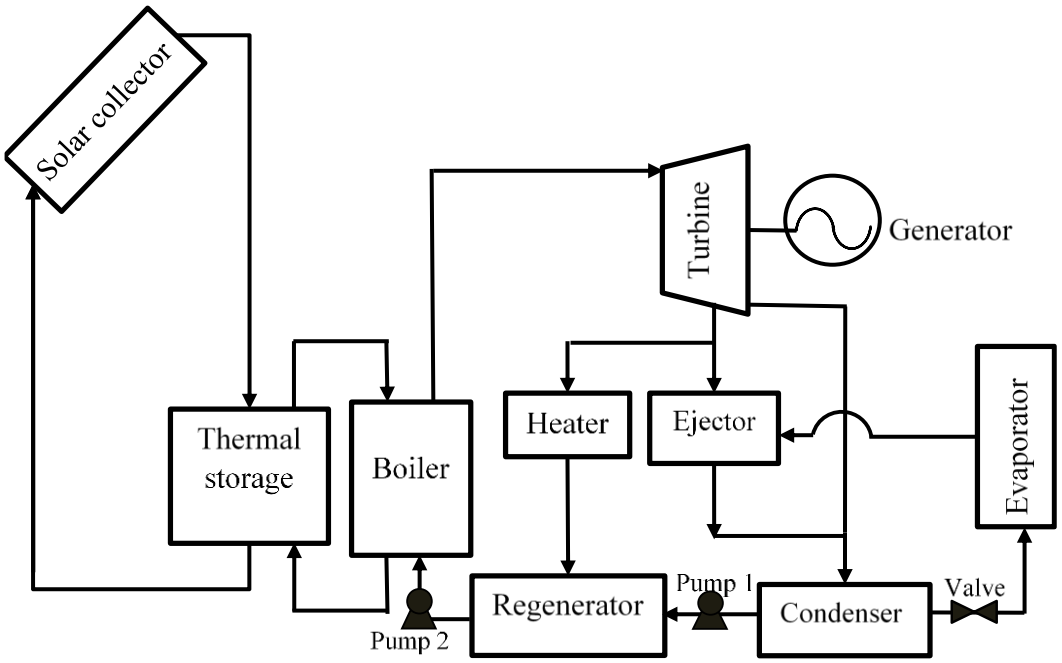

Figure 2.10: Block representation of CCHP with ejector system (Jiangfeng *et al.*, 2009)

2.8.2 Rankine Cycle with Absorption Chiller

A combined ORC and absorption cooling system was designed and patented by (Freund, 2012), and used to generate power and cooling by integrating Rankine cycle with an Absorption chiller. The system is powered by waste heat recovery. Its major components include, waste heat recovery boiler, turbine, generator, boiler/desorber, recuperator, condenser and condenser/evaporator (Figure 2.11). In this arrangement, the condenser of the Rankine cycle is combined with the evaporator of the absorption chiller cycle. The working fluids are Lithium chloride/water and liquid CO_2; with water and CO_2 as the refrigerant of the absorption chiller and Rankine system respectively. Meanwhile this is only applicable in the areas with heavy industrial activities where large amount of waste heat being generated and ejected to the atmosphere can be efficiently utilized. In addition, water as a working is definitely not suitable for low-grade temperature application of ORC, necessitating the use of two working fluids and cycles which may make the system a bit complicated.

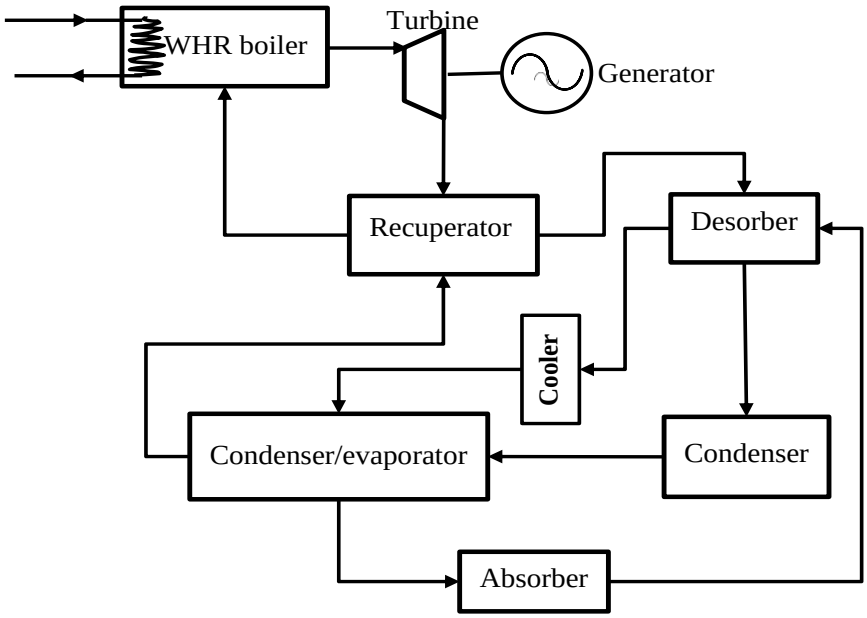

Figure 2.11: Rankine cycle with absorption chiller using WHR (Freund, 2012)

2.8.3 Goswami Cycle

The development of power cycle that makes use of working fluid mixture was made by (Kalina, 1984), mainly for OTEC power plant, using low grade heat source. The cycle makes use of working fluid with very small temperature difference between the working fluid and the heat source (Tamm *et al.*, 2004). A novel combined cycle (based on ammonia-water working fluid) was later proposed by Goswami in 1999 (Feng *et al.*, 2000; Goswami and Xu, 1999) for power and refrigeration (Figure 2.12), taking the advantages of the thermodynamic properties of ammonia-water mixture, but with the power generation as the primary goal of the cycle. The working principle of the cycle is summarized below;

i. Ammonia-rich saturated, low-pressure working fluid mixture is pumped from the absorber to high-pressure boiler.
ii. The solution is preheated by the recovery heat of the weak solution returning from the boiler to absorber.
iii. The solution mixture is partially boiled in the boiler leading to increased concentration of ammonia in the working fluid vapour.

iv. Passing through the rectifier, ammonia vapour becomes purified by condensing out the remaining water.

v. The pure ammonia is then superheated and expanded through the turbine to produce work.

vi. The expansion in the turbine leads to reduction in ammonia temperature thereby making it suitable for heat extraction (refrigeration) before being absorbed by the water in the absorber tank.

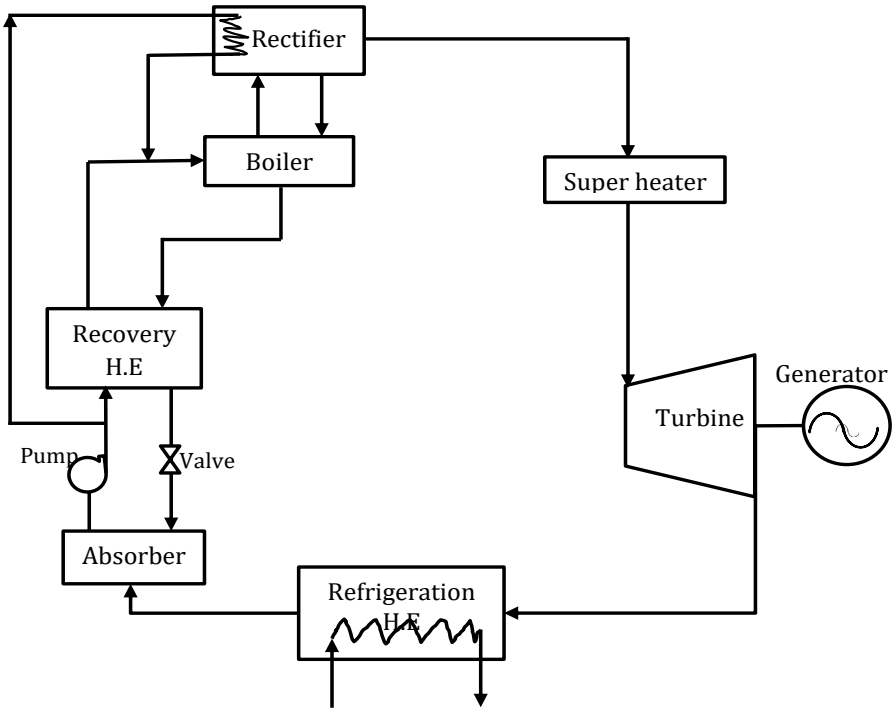

Figure 2.12: Goswami combined power and refrigeration cycle (Wang *et al.*, 2016)

Goswami cycle has been investigated by researchers (Xu. and Goswami, 1999), using low-grade solar collector and geothermal energy respectively to drive the cycle. Parametric analysis of the cycle had been carried out to improve both the turbine efficiency and cooling performance of the cycle (Padilla *et al.*, 2010). Experimental investigations were carried out by (Tamm *et al.*, 2004) for the validation of Goswami cycle and it was found out that the results of the test data were in agreement with the theoretical simulations results. Meanwhile, Goswami cycle is reported to produce low cooling effect (Padilla *et al.*, 2010; Wang *et al.*, 2016) because refrigeration effect

relies only on the pressure reduction caused by turbine expansion. It is most desirable when the chilled water temperature around (or just below) ambient temperature is needed. It is also observed that chilled water production is not the primary target/goal in the Goswami cycle in which case, the inclusion of the refrigeration cycle is also primarily to improve the efficiency of the power cycle (Xu. *et al.*, 2000). Therefore to have better cooling effects (where chilled water is primary and power is additional goal), there is need for further expansion of the exhaust refrigerant vapour from the turbine. This study did not only introduce further ammonia expansion, but also reduced the complexity in the design, by non-inclusion of the superheater (since power generation is a complementary requirement).

2.8.4 Chilled Water Piping and Flow Rates

In HVAC system, and specifically cooling system, chilled water network plays an important role. Cooling is achieved by distribution of chilled water throughout the conditioned space via the network of pipes connecting the HVAC equipment with the space being conditioned. Therefore, efficient use of chilled water through pipe design and optimal flow rate are important in chilled water application for cooling system. Optimization of design and synthesis of chilled water network was proposed by (Lee *et al.*, 2013) which was also demonstrated with two case studies conducted on "a Malaysian wafer fabrication foundry" and "a Taiwanese wafer fabrication facility". Future study was suggested on the investigation of interaction between the chiller unit and chilled water network systems. There are a number of studies on the chilled water network design for cooling system (Miyazaki and Akisawa, 2009; Chen and Xu, 2012; Liu *et al.*, 2012).

Chilled water pumping has always been considered on three main configurations (Hubbard, 2011), although these may not be given a detailed explanation in this research. The configurations include;

i. Constant primary flow (CPF) system,

ii. Constant primary flow/variable secondary flow (P/S) system, and

iii. Variable primary flow (VPF) system.

Regarded as the most basic of the three piping configurations, CPF system (as shown in Figure 2.13) employs constant speed chilled water pumps and mostly useful for smaller plants (Hubbard, 2011). The flow of chilled water is controlled (varied) by turning-off the pump based on capacity requirements. Constant primary flow/variable secondary flow (P/S) system involves primary and secondary loops and 2-ways valve. Constant flow pumping is employed in the primary loop while the secondary loop uses variable flow pumping. The primary loop is connected to the chiller (or chilled water tank in any case) and the secondary loop is connected to the load while the two loops are interconnected to each other (McQuay, 2001). Variable primary flow (VPF) system makes use of 2-ways valve and variable speed drives (which is on the main chilled water pumps). This arrangement allows varying the flow rate of the chilled water circuit. The design is less than P/S system but the control may be complex due to the newness of the system (Hubbard, 2011). The common attributes of the three systems are shown in Table 2.7. The load requirement is given as the product of flow rate and change in temperature, that is;

$$Q_{load} = \acute{m}_w C_{pw} \Delta T \tag{2.9}$$

Where $\acute{m}_w$ is the chilled water flow rate (kgs^{-1}), C_{pw} is the heat capacity of water ($kJkg^{-1}K^{-1}$) and ΔT is the chilled water temperature range.

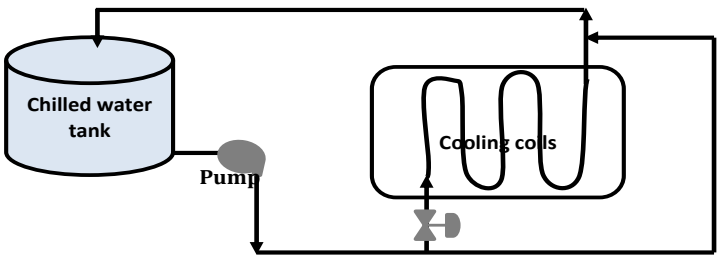

Figure 2.13: Constant primary flow configurations for chilled water distribution

Table 2.7: Piping system attributes (Hubbard, 2011)

Configuration	CPF	P/S	VPF
Pump energy	Base load	50-60 % lower	60-70 % lower
Delta-T mitigation	Not applicable	Higher energy	Less energy
Control valve	3-ways	2-ways	2-ways
Installed cost	Base case	10 % higher	5 % higher
Control complexity	Simple	Simple	Sometimes complex
Plant space	Based case	Larger	Base case

2.9 Radiant Cooling System

As a result of the superior heat transfer properties and lower transport energy consumption of water than that of air, hydronic/radiant heating system has become popular in the cold regions in the recent past. This system is observed to provide superior comfort than conventional air heating (Seo. *et al.*, 2014; Siegenthaler, 2014) and is now being combined with cooling systems, to be used during the summer periods. Hydronic/Radiant cooling is mainly an alternative air conditioning process of lowering the indoor surface temperature to remove the sensible heat by pumping of chilled water though the network of pipes buried underneath the conditioned surface. Radiant heat mostly accounts for the heat emitted from the floor to the surface, (Olesen, 2008), and it is obvious that occupants are closer to the floor than the ceiling, making radiant floor cooling a more efficient choice of cooling systems. Studies have also revealed that "angle factor" of person in radiant floor cooling/heating is 2.5 times as that in ceiling cooling" (Han and Zhang, 2011; Olesen, 1997; Olesen, 2008), meaning that, a unit degree change in floor temperature has 2.5 times effects on mean radiant temperature than similar change in ceiling temperature. Radiant cooling systems have been well researched in the tropical and sub-tropical regions and found to be more suitable for large spaces (Zhao. *et al.*, 2014). From the numerical and experimental analysis done by (Han and Zhang, 2011) on radiant floor cooling of office apartment in China, it was concluded that the system performance is more affected by low pipe thermal conductivity than water velocity, suggesting that pumping velocity can be reduced to save power consumption due to pumping, meanwhile according to (De Carli

and Tonon, 2011) the radiant floor cooling performance depends more on the thickness and thermal conductivity of the material in which the cooling pipe (tube) is embedded.

Furthermore, ground-source heat pump (GSHP) has been extensively applied for soil cooling process where heat removal is achieved through the embedded heat exchanger pipe (earth tube) that transfers heat between the soil and GSHP (Moncef and Kreider, 1996; Demir *et al.*, 2009). Design of solar thermal cooling system was done by (Kalkan *et al.*, 2012), which is to be integrated into present and future residential apartments. Further study on their work was suggested to include integration of GSHP system with the building so that soil can act as heat sink for cooling the building. Various studies have been focused on radiant cooling systems especially in large spaces with moderate-to-high occupancy density (Mikeska. and Svendsen, 2015). Zhao, in (Zhao. *et al.*, 2015) studied the prediction of radiant floor cooling capacity of large spaces, using Xi'an Xianyang international airport in China as a case study to find out the extent of transient solar radiation effect on the cooling capacity of radiant floor cooling system. In the earlier study, they (Zhao. *et al.*, 2014) did analysis of solar radiation effects on the capacity of radiant floor cooling in the same airport, based on 'on-site performance measurement'. Experimental field study and comfort assessment of radiant cooling of residential building in tropical Thailand was done by (Wattanakit. *et al.*, 2014; Wongkee. *et al.*, 2014b). The study revealed that radiant cooling together with dehumidification is able to improve the thermal comfort of the studied space, with the achievement of about 70 % energy savings compared with the conventional air conditioning system. However, dehumidification was suggested to avoid surface condensation of the cooled inner wall, or alternatively the cooled surface temperature could be kept above the dew point (Ahmed and Medhat, 2012). All these studies and applications point to the better performance of chilled water for cooling application than chilled air systems and most importantly for soil/floor cooling systems.

2.10 Agricultural Soil Cooling

Most high-value crops (such as strawberry, cabbage, tulip and sunflower) are preferred crops worldwide but their cultivation is usually limited to temperate climate regions because their cultivation normally requires low soil and air temperatures (Marie-Christine 1993). This has actually made the hot and humid tropical climate countries the net-importers of these crops. Meanwhile, the effect of temperature on agricultural crops has triggered more studies on the control of soil temperature especially to reduce variation in soil temperature for optimum plant development (Hasson and Hussain, 1987). The results of an experimental investigation by (Labeke. and Dambre, 1993) on the effects of soil cooling and supplementary lighting on some selected cultivars showed that, even though, plants responses may be cultivars dependent, soil cooling and supplementary lighting resulted in marginal improvement on the overall development of the tested crops (Table 2.8).

Table 2.8: Effects of soil cooling and lighting cultivars (Labeke. and Dambre, 1993)

Plant	**Flowering period**	**Treatment and effects**	
		Soil cooling	**Supplemental lighting**
Red sunset	Spring	Flower production started 1 month earlier in 1st year	Early flower production by 2 months
		Combined treatment resulted in 3 months earlier flower production in the 2nd year	
Yellow king	Spring	Negative effect	No effect
Mona lisa	Periodic	Improvement in Autumn flower production (in 2nd year)	Remarkable increase in stem yield (2nd year)
Libelle	Periodic	Year round flower production	Year round flower production
Annabel	Year round	Extension of peak flower production beyond autumn/winter	Higher flower production in Jan and Feb of the 2nd year

In the analysis of the effects of mulch applications on soil temperature by (Hasson and Hussain, 1987), it was found out that the temperature of the mulched soil varied slowly between 17 ℃ and 20 ℃ while that of un-mulched soil varied rapidly

between 17 ℃ and 24 ℃ which may result in physiological disturbance and low productivity in planted crops. Investigations of the effects of covering maize ridges with straw in China by (Rong *et al.*, 2013), to reduce solar radiation heat effects, showed that it is efficient for improving the yield of maize in rain-fed field. A number of researcher (Mihalakakou, 2002; Ramos and Martínez-Casasnovas, 2010; Lee and Strand, 2008) have studied the effects of soil temperature on crop growth, and yield.

Because of the economic nature of the temperate crops, several attempts have been made to condition the planting zone in the Tropics to make it suitable for growing high-value temperate crops. Experimental studies were conducted by (Max *et al.*, 2009), on the effects of greenhouse cooling methods on growth, fruit yield and quality of tomato in a tropical climate (Thailand) using fan and pad cooling system to condition the planting zone. An experimental study was conducted by (Jain. and Tiwari, 2002) on a 24 m^2 greenhouse using evaporating cooling with cooling pad in order to determine the optimal temperature in the greenhouse planting. Literatures from (Morille *et al.*, 2013; Lychnos and Davies, 2012; Marı *et al.*, 2007) showed that the protected planting zones in the Tropics are always conditioned to lower temperature suitable for growing of protected and high-value crops (mostly temperate crops).

"To find the best way to harness the power of cold water", the temperate crop farming was demonstrated by Deep Sea Water Research Institute, Kumejima Japan, by pumping of very cold deep sea water through the network of pipes buried under soil to cool the soil to low temperature suitable enough for growing some winter crops (Figure 2.14). Meanwhile, the use of deep sea water is only feasible within the reasonable range of distance from the sea.

Figure 2.14: Deep seawater cold season vegetable bed (KumeGuide, 2014)

Malaysia Agricultural Research and Development Institute (MARDI) gave the account of current cultivation area of vegetable in the country as 44000 hectares and proposed research programs on varieties of vegetables to include some temperate vegetables (such as cabbage, cauliflower, broccoli and lettuce). This can be efficiently achieved through the implementation of solar thermal chilled radiant soil cooling system.

2.10.1 Heat Transfer and Soil Thermal Properties

Soil surface heat energy balance as it relates to agricultural soil has many applications, which include the heat flux and evaporations estimation for irrigation purposes (Qin *et al.*, 2002). Meanwhile, energy balance between the soil and ambient air is complex in nature. As a result of the soil surface-to-ambient air heat transfer complexity, simplification assumptions are usually employed (Puri, 1987; Liu *et al.*, 2005; Wu. *et al.*, 2015), which are usually based on the intended application.

The degree of evaporation, the existence of mulch (natural or artificial), and effect of soil thermal regime all influence the near surface soil temperature (Novak, 1981). Therefore, soil temperature is basically a function of its thermal properties such as; soil thermal conductivity, thermal diffusivity and the volumetric heat capacity of

the soil as well as amount of heat transfer to the soil (majorly from solar radiation). Soil thermal conductivity (K_s), in a simpler form, is the heat flux through the soil divided by the change in temperature along the heat flux. The thermal conductivity of soil ($Wm^{-1}K^{-1}$) is influenced by compactness of the soil and its moisture contents (Demir *et al.*, 2009; De Carli and Tonon, 2011). Thermal diffusivity on the other hand is the temperature change resulting from flow of a unit quantity of heat through a unit volume per unit time (m^2s^{-1}). Volumetric heat capacity ($kJm^{-3}K^{-1}$) of soil is its ability to store heat energy during change in temperature. The three properties are related as;

$$\propto = \frac{k}{\rho C_p} \tag{2.10}$$

Where $\propto$ is the diffusivity (m^2s^{-1}), k is the thermal conductivity ($Wm^{-1}K^{-1}$), ρ is the soil density (Kgm^{-3}) and C_p is the specific heat capacity of the soil. The term ρC_p is the volumetric heat capacity of the soil.

However, this study is not intended to go into more details on the soil heat transfer but only as it relates to soil heat exchange due solar radiation absorbed by the soil and the transfer of such heat between the soil surface and the buried chilled water pipe.

2.11 Economic Analysis

Decision making on systems design requires more than just the thermodynamic analysis and optimization of the system, as such more attention is being paid to the system economic analysis (Wang *et al.*, 2016). Particularly, decision making on Renewable Energy Technology (RET) projects is a complex task that requires the determination of the technically feasible technology, the energy efficiency index, as well as the economic efficiency of the potential project. Meanwhile, the decision must be made at the initial stages of the project which in most cases are new or unfamiliar projects. RETScreen® software is a unique decision support tool, designed to address

this kind of problems. It is a tool that can quickly analyse and evaluate the viability of one or more renewable energy technology options at the initial stage of the project (Ackom, 2005). RETScreen® was developed by the Natural Resources Canada (NRC) with contributions from about 85 experts and organizations including the United Nations Environment Program (UNEP) and the National Aeronautics & Space Management (NASA) to provide international weather data base (RETScreen, 2005). The software runs on Microsoft excel and it is suitably useful for evaluation of energy production and savings, costs, emissions reductions, financial viability, life cycle cost, and risk assessment of different types of Energy efficient and Renewable Energy Technologies. RETScreen has been used by researchers (Lee *et al.*, 2012; Tarigan *et al.*, 2015; Duggirala, 2010; Ackom, 2005) for feasibility and viability studies of renewable energy projects and energy efficient technologies. The software is a stepwise modelling tool (as shown in Figure 2.15), in which each of the steps is associated with Excel worksheet. The software usually analyses renewable energy project by comparing its financial and emission details with a base case (using other energy sources).

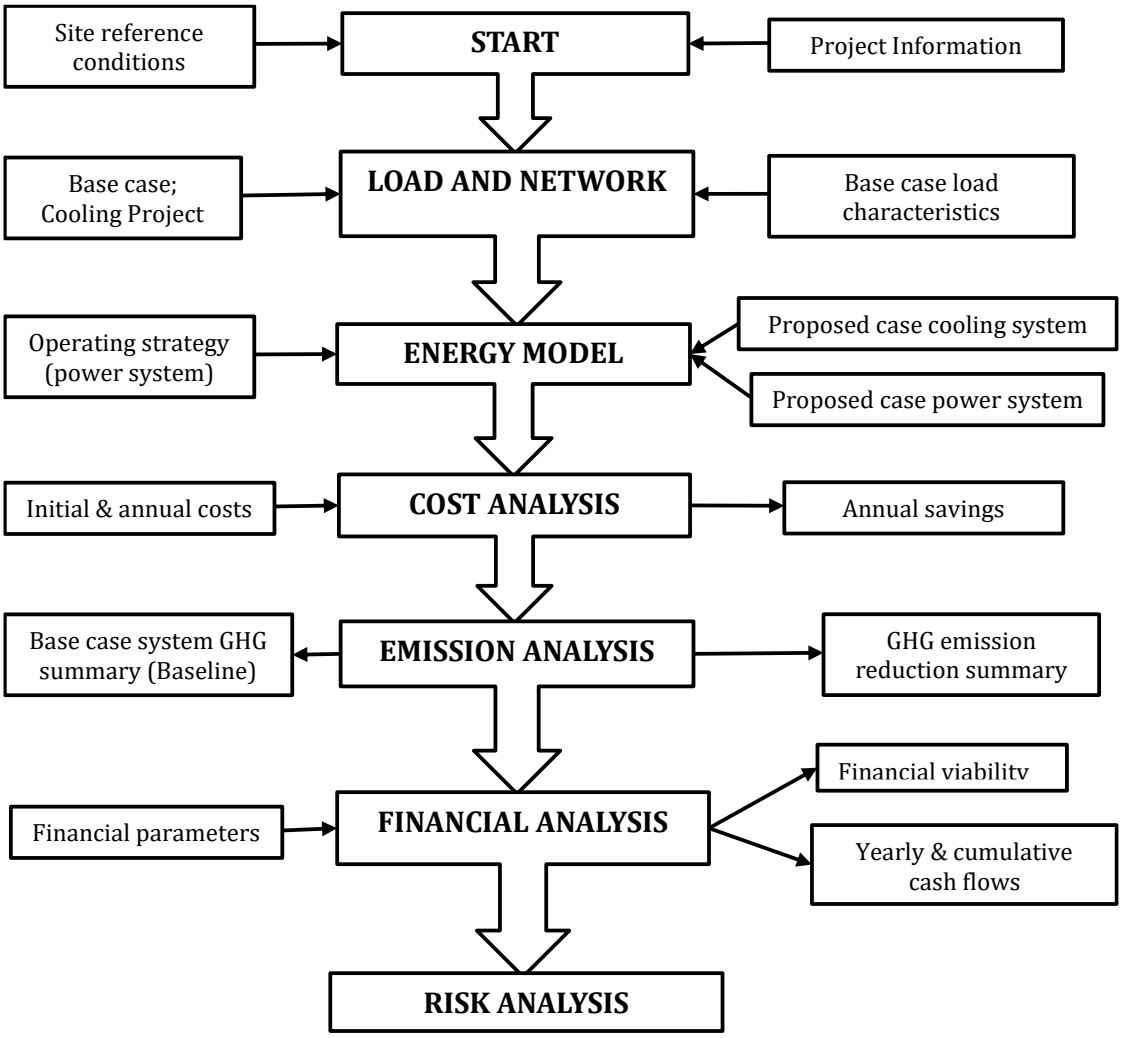

Figure 2.15: RETScreen® application paths

2.12 Summary

Based on the reviewed literature, it is no doubt that the critical issues regarding the energy supply and utilization, food security as well as environmental safety in the tropical lowlands can rightly be addressed by employing the solar potentials in the Tropics via solar thermal technologies. A number of research efforts have been devoted to solar thermal applications across the globe for HVAC, for power plant, and for combined cycle systems as applicable to domestic, industrial, commercial, and agricultural sectors. However the following observations seem to necessitate further research efforts in the direction of this study;

i. Most of the soil or floor cooling applications reviewed were achieved through circulation of chilled air; a more energy consuming process than chilled water. However, few of that chilled water applications for radiant cooling were mainly obtained from the grid-electricity powered cooling system.

ii. Most combined power and cooling plants in the literature operating on low-to-medium grade heat use separate cycles and separate sets of working fluid for the power and cooling therefore making the plant design a little bit complex.

iii. For the combined power and cooling cycles that operated on one cycle and one set of working fluid, power generation formed the primary goal and cooling was secondary; as such, the temperatures of chilled water obtainable from such cycles were just a bit below the ambient temperature and might not be suitable in cases where higher ‘cooling effect’ is required.

CHAPTER 3

RESEARCH METHODOLOGY

3.1 Introduction

This study is on an integrated system of a combined power and refrigeration plant, and on a radiant soil cooling systems. The combined plant is modelled to meet the specific requirement to overcome a radiant soil cooling load, therefore the methodology part of this study starts with the soil heat transfer modelling to determine the "soil cooling load". This is done to have an idea of the cooling load which the modelled combined plant must optimally provide. For the soil cooling process, thermal properties of the soil at the project location are considered. While the heat transfers across the "soil–pipe–chilled water" section is modelled using properties of soil, pipe, and chilled water, respectively. For a specified load, the equivalent combined plant component parts are modelled to determine its overall capacity (including the required energy input, and the effective size of the solar collector). The thermodynamic properties of the working fluid are employed in the plant components modelling. The modelling methodology, equations, and assumptions used are described in details in the following parts of this chapter.

Relating the soil cooling load to the area of soil bed, gives the idea of the approximate plant cooling capacity needed to overcome the load (and vice versa), and the length of the chilled water pipe required to circulate the cooling effect.

Computer programming algorithm and codes are developed for the implementation of the calculations involved in the models. The modelled system is

further validated with laboratory scale experimental rig put together at the Ocean Thermal Energy Centre, Universiti Teknologi Malaysia, Kuala Lumpur campus. The modelled system is suitable for a number of hydronic cooling systems. The structure of the chapter and the methodology approach are represented in Figure 3.1. Parametric analysis conducted on the modelled plant is used to optimize its performance so as to assess its technical feasibility, while economic analysis conducted on the complete system is to assess its financial viability.

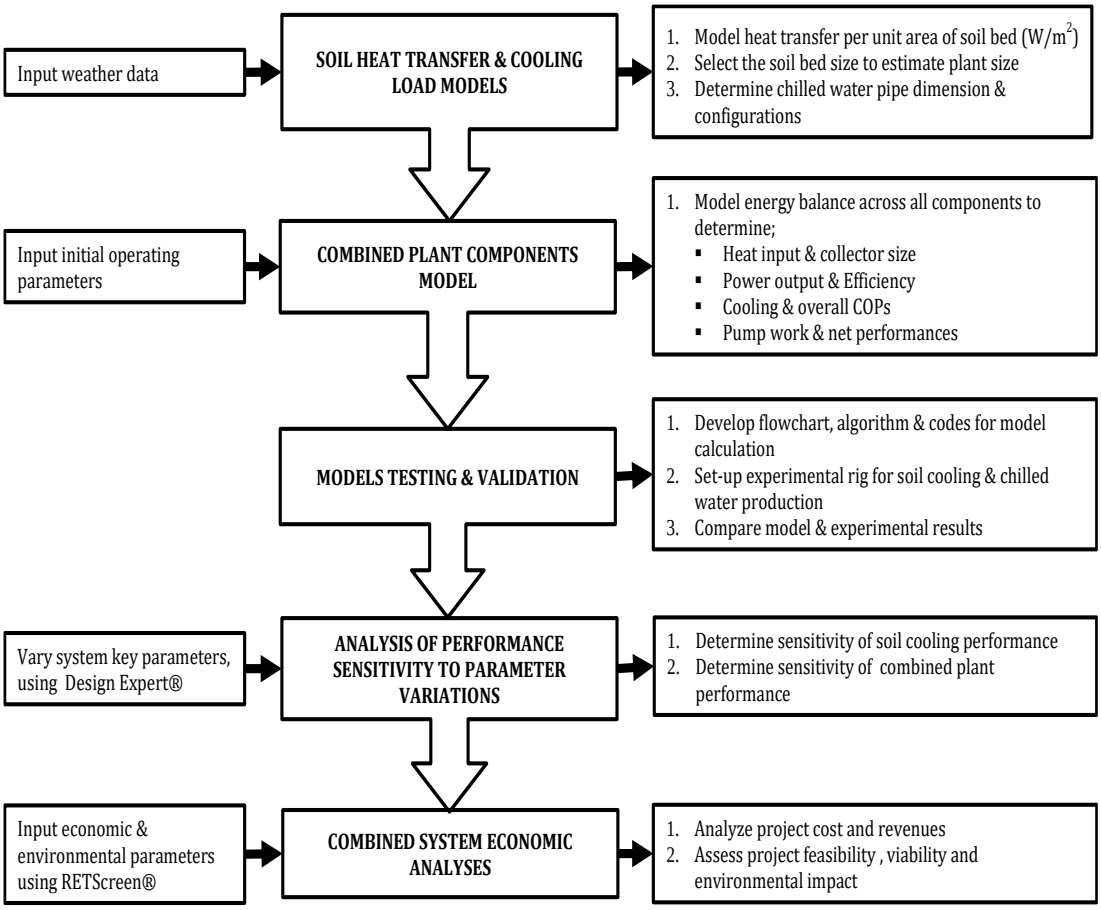

Figure 3.1: Methodology summary

3.2 Cooling Load and Combined Plant Models

An integration of a power cycle with a refrigeration cycle to produce chilled water is proposed. The primary aim is to model a system of combined cooling and power plant that is capable of cooling a dimensioned bed of soil to a set temperature range. This involves determining a certain plant chilling capacity that can overcome the cooling load corresponding to a certain size of soil bed to be cooled (the exercise can be reversely carried out). This also involves determining the heat transfer area hence the length of pipe that will be required to distribute the chilled water for the cooling. Thus, the approach employed in this section of the study involves three main steps (Figure 3.2) that are further interrelated to determine the soil bed size *(A_s)* and chilled water pipe length *(l)* with a known plant capacity. Each of the steps is further analysed and discussed in the following sections.

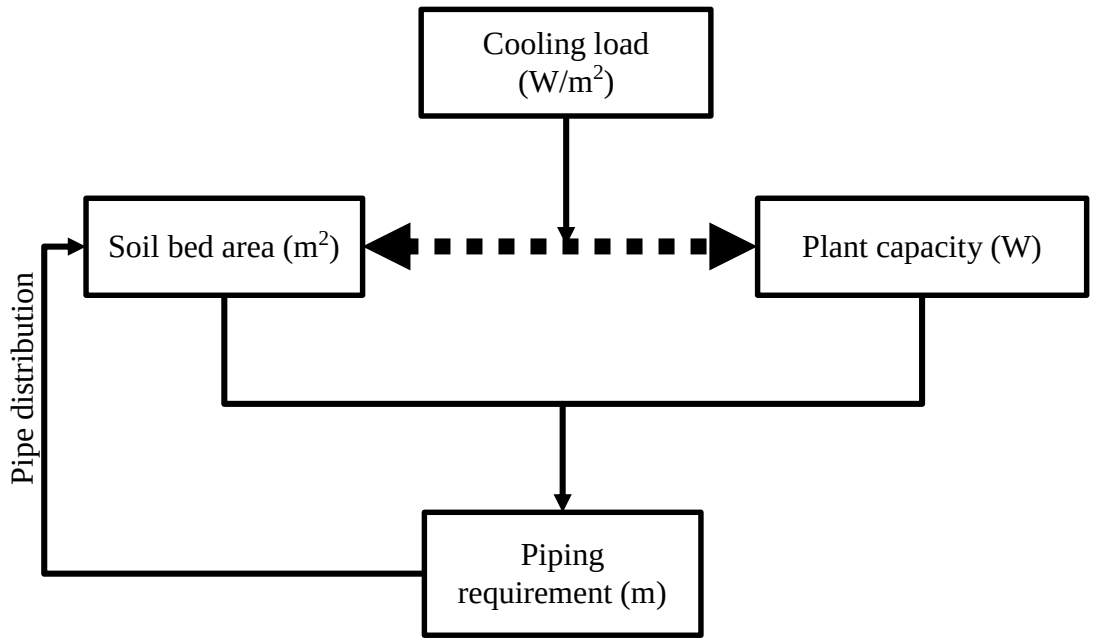

Figure 3.2: Summarized chart for combined system modelling

3.2.1 Soil Heat Transfer and Cooling Load Models

In this section, the heat transfer between the homogeneous soil structure and the ambient environment (under the influence of solar radiation) is considered together with the net transfer occurring as a result of the temperature difference between bulk soil and the chilled water in the pipe (buried under the soil). The summaries of the soil heat transfer processes are listed in a stepwise approach below, with illustration in Figure 3.3.

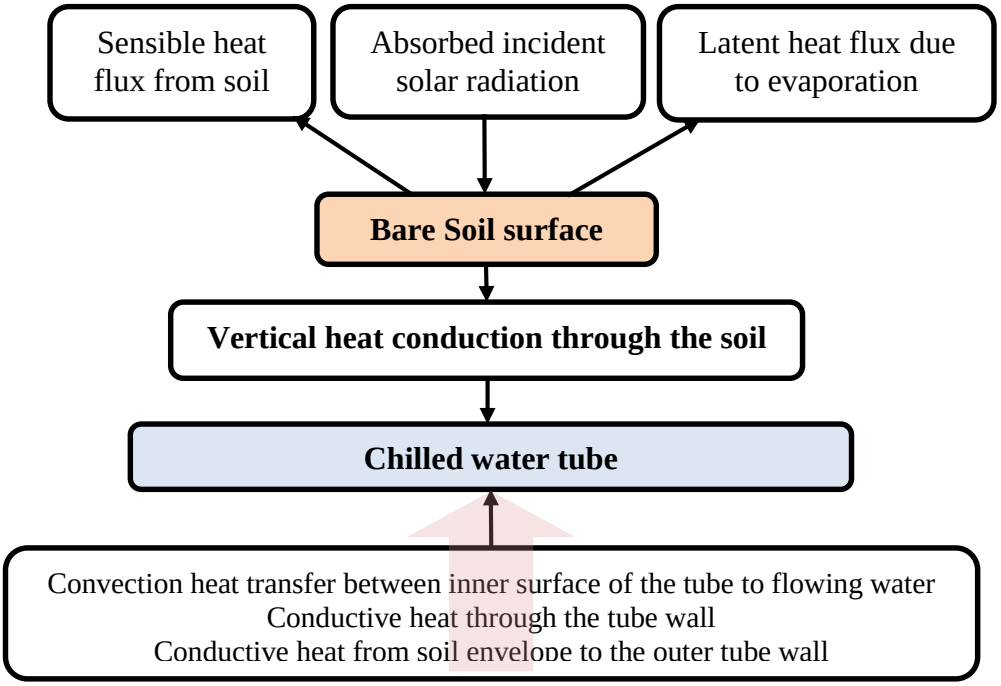

Figure 3.3: Heat transfer model

i. Modelling of ground (soil) surface heat transfer: that is, heat transfer resulting from the temperature difference between the bare soil surface and the ambient environment under the influence of solar radiation;

ii. Modelling of the vertical heat conduction from the soil surface down to the buried chilled water pipe;

iii. Modelling of heat gained by the chilled water by conduction through the pipe wall followed by convection from pipe inner surface of the pipe to the flowing water.

3.2.1.1 Soil Surface Heat Transfer

The temperature at the upper layer of the soil is usually affected by;

i. Evaporation rate, which is the degree to which the soil surface dries out.
ii. Availability of surface cover in the form of vegetation (for cultivated soil) or mulch (for bare soil).
iii. Thermal regime effect, which is a function of the duration and intensity of solar heat on the soil.

However, many of the crop and root development processes (such as soil carbon cycle, efflux of CO_2 via root respiration and microbial decomposition of organic soil matters) are mainly controlled by soil temperature (Muerth and Mauser, 2012). Hence, soil temperature is a major focus point in dealing with crop development especially in the tropical climate where the soil temperature is always high and most importantly as it relates to cultivation of temperate climate crops in the Tropics. To accurately predict the soil-surface heat transfer, different models have been proposed by various researchers.

i. Two – layer model was developed by (Shuttleworth and Wallace, 1985) comprising of plant layer and soil layer or two types of plants.
ii. Three – layer model was developed by (Brenner *et al.*, 1999) comprising of plant, soil under the plant and bare soil or three types of plants.
iii. Bare soil and three types of plant was developed by (Huntingford *et al.*, 2000).

The study in this thesis is not limited to the prediction of soil heat flux, therefore to avoid complications in modelling, only bare soil model (Figure 3.4) is considered. It is also assumed that there is no heating source from the soil, and as such, only solar radiation is the heat source that plays important role in the micro-meteorological activities of the soil-surface interaction (Qin *et al.*, 2002).

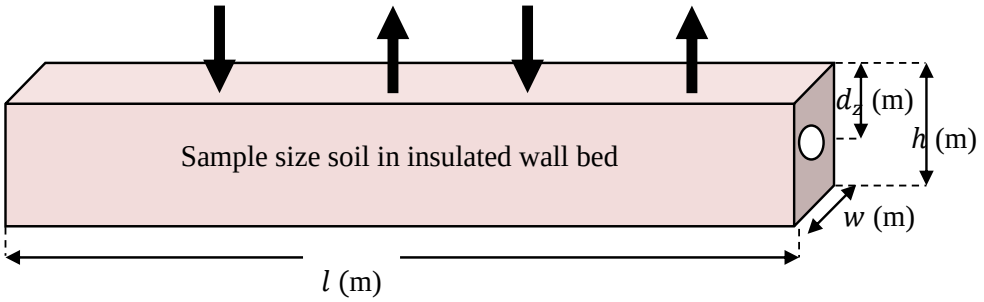

Figure 3.4: Block representation of bare soil bed

3.2.1.2 Soil Surface Heat Balance

Considering a bare soil with no energy storage, the heat energy balance between the soil surface and the ambient atmosphere is expressed as;

$$\bar{Q}_s = R_n - (\bar{Q}_h + \bar{Q}_L) \tag{3.1}$$

Where R_n is net solar radiation flux, $\bar{Q}_h$ is sensible convective heat flux from the soil to the atmosphere, and $\bar{Q}_L$ is the latent heat flux due to vaporization or condensation.

The short wave solar radiation received by the upper part of the atmosphere is about 1395 W/m^2 (Qin *et al.*, 2002). Only a percentage of this amount finally gets to the ground surface; the radiation encounters scattering, reflection, and absorption in the atmosphere. The percentage of the radiation that finally reaches the soil surface and absorbed by the soil is also a function of the soil albedo (Figure 3.5). This amount is referred to as **net radiation**, expressed by (Yunus, 2003) as;

$$R_n = (1-\propto)Q_{inc} \tag{3.2}$$

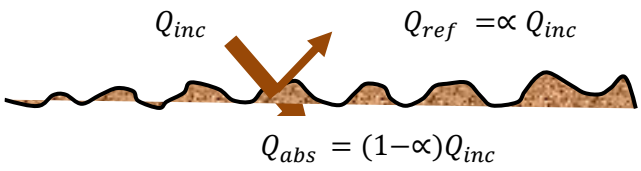

Figure 3.5: Solar radiations on bare soil surface

With respect to Stefan-Boltzmann law, the net radiation absorbed by bare soil is expressed as;

$$R_n = (1-\propto)Q_{inc} + \sigma\mathcal{E}_s(\mathcal{E}_a T_a^4 - T_s^4) \quad (3.3)$$

Where Q_{inc} is incident solar radiation on the soil (W/m^2), $\propto$ is the soil surface albedo, σ is the Boltzmann constant, $\mathcal{E}_s$ & $\mathcal{E}_a$ are soil and air emissivities, and T_s & T_a are the respective temperatures at the soil surface and air.

The ground surface–ambient air temperature difference always results in **sensible heat transfer ($\bar{Q}_h$)** between the two sides. This is also affected by the resistance of the surface to heat transfer (r_a). The sensible heat flux from the soil to the atmosphere (or vice versa) is given by (Novak, 2010; Qin *et al.*, 2002) as;

$$\bar{Q}_h = \frac{\rho_a C_{pa}(T_0 - T_a)}{r_a} \quad (3.4)$$

And the surface resistance to the heat flux (r_a) is expressed as;

$$r_a = \frac{\ln(Z_r - \frac{d}{Z_0})^2}{K^2 U_r} \quad \text{(Liu } \textit{et al.}\text{, 2007; Villagarcía } \textit{et al.}\text{, 2007; Qin } \textit{et al.}\text{, 2002)} \quad (3.5)$$

Where $\rho_a$is density of air above the soil, C_{pa} is specific heat of air (at constant pressure), r_a is boundary layer resistance (sm^{-1}), Z_r is the reference height, d is 0 for

bare soil (Liu *et al.*, 2007; Novak, 2010), U_r is the wind speed, K is Van Karman constant.

Energy exchange due to evaporation or condensation between the ground surface and the atmosphere is a function of moisture availability in the atmosphere (Muerth and Mauser, 2012). The energy required for the evaporation is regarded as **latent heat flux** $\bar{Q}_L$ and is given as;

$$\bar{Q}_L = \rho_w q_l E \tag{3.6}$$

$$E = \frac{\rho_{v_0} - \rho_{v_a}}{r_a \rho_w} \text{ (Novak, 2010)} \tag{3.7}$$

$\rho_{v_{0(t)}} = \rho_v^*(T) h_r = [\frac{1.323}{T} e^{\left(\frac{17.27T - 4717.3}{T - 35.85}\right)}] h_r$ (Tetëns, 1930) modified by (Novak, 2010).

$$\rho_{v_{a(t)}} = \frac{e_a(t) M_w}{R T_a(t)} \text{ (Novak 1981)}$$

Therefore, the net heat energy absorbed at the surface of dimensioned soil bed in this case, is expressed as;

$$\bar{Q}_s = R_n - (\bar{Q}_h + \bar{Q}_L) A_s \tag{3.8}$$

Where ρ_{v_0} is soil surface vapour density, ρ_{v_a} water vapour density at reference height, h_r is height of soil surface roughness, $e_a(t)$ is water vapour pressure at reference height, M_w is molar mass of water, and R is the ideal gas constant, A_s is the surface area of the soil bed.

3.2.1.3 Soil Cooling Load

With reference to (ASHRAE, 2009), cooling load calculation helps to determine the total sensible cooling load resulting from heat gained through;

i. Opaque surfaces such as walls, floors, ceilings, and doors;
ii. Transparent fenestration surfaces such as windows, skylights, and glazed doors;
iii. Infiltration and ventilation;
iv. Occupancy effects;

Opaque body in the above refers to heat gained resulting from the temperature difference across surfaces or solar gain incident on the surface. In this study, the cooling load of interest falls in the first category (solar gain incident on the surface) since a bare soil is being considered in the model. Meanwhile, it is a common practice in load design to always consider uncertainties that may arise from service conditions or load variations (Moser and Folkman, 2008). This is usually taken care of by ***'factor of safety'*** which is used either to allow future growth in loads so that the equipment can operate within the safe range (Sharizal, 2006) , or to reduce the possibility of oversizing or under-sizing of HVAC equipment (Parameshwaran *et al.*, 2012). Therefore the cooling load in this study is calculated as the product of the net heat flux on the soil and a safety factor, given as;

$$\bar{Q}_{load} = \bar{Q}_s \times \gamma \tag{3.9}$$

Where γ is the factor of safety, and $\bar{Q}_s$ is the net heat flux on the soil.

3.2.1.4 Vertical Heat Conduction

Conductive heat transfer in soil is considered as the net exchange of kinetic energy by the soil molecules. This usually occurs from a higher temperature (hot)

region to the lower temperature (cold) region (Muerth and Mauser, 2012; Rose, 1969). In this study, the soil surface is the hot region while the external surface of the chilled water pipe is the cold region. However, researches by (Moncef and Kreider, 1996) and (Novak, 1981) have shown that at any given depth (z) below the surface, the undisturbed ground (soil) temperature (T_s^u) follows a periodical/harmonic variation with time and the expression can simply be put as;

$$T_s^u(z,t) = T_m + T_{am}R_e(e^{iwt}) \tag{3.10}$$

This is in consonance with the earlier study conducted by (Kusuda and Archenbach, 1965) as reported by (Moncef and Kreider, 1996) with reference to undisturbed soil temperature around chilled water tube.

The heat conduction from the top soil to the chilled water tube can be expressed using the Fourier heat conduction equation. The vertical heat flux due to conduction depends largely on the temperature gradient through the conducting depth, and the thermal conductivity of the soil through which the conduction is taking place (Muerth and Mauser, 2012). Thus, in the absence of temperature gradient, conduction process decays.

$$\bar{Q}_{cond} = -k_s \frac{\Delta T}{\Delta Z} A_s \tag{3.11}$$

However, heat conduction through a homogeneous layer ($z_i \; and \; z_{i+1}$) is a function of the depth and time (Muerth and Mauser, 2012). Therefore;

$$\bar{Q}_{cond(i,i+1)} = -k_{s(i)} \frac{\Delta T_{i(t)}}{\Delta Z_i} A_s$$

In this study, conduction heat transfer analysis is limited to the vertical distance between the soil surface and chilled water tube, therefore our ΔZ_i is fixed as Z, and the transfer considered with respect to time is given as;

$$\bar{Q}_{cond}(t) = -k_s \frac{\Delta T_s^u(t)}{Z} A_s \quad (3.12)$$

Where k_s is the soil thermal conductivity, A_s is the surface area of the soil bed and ΔZ is the vertical depth between the top soil and the chilled water pipe, $T_s^u$is the undisturbed soil temperature, T_m & T_{am} are mean and amplitude of the ground surface temperature variations, w is the angular frequency of the periodic variation ($w = 2\pi/day$).

3.2.1.5 Chilled Water–Soil Heat Transfer

Soil cooling process is achieved through the heat transfer from the soil bed, across the chilled water pipe network (earth tube), to the chilled water flowing through the pipe. This heat transfer equals to the amount of heat gained by the chilled water as it flows along the earth tube. Figure 3.6 shows the modelling sequence for the heat transfer processes. However, the processes occurring around the earth tube is usually complex (Lee. and Strand, 2006), hence some assumptions made to reduce the complexities include;

i. The soil surrounding the earth tube is assumed homogeneous with constant thermal conductivity.
ii. The temperatures of the soil in contact with the earth tube and that of earth tube external wall are assumed equal.
iii. The presence of the earth tube has no effect on the temperature profile of the immediate surrounding soil, hence, the temperature at the surface of the earth tube is uniform along the axial direction (Lee and Strand, 2008).
iv. The earth tube has uniform cross sectional area in axial direction.

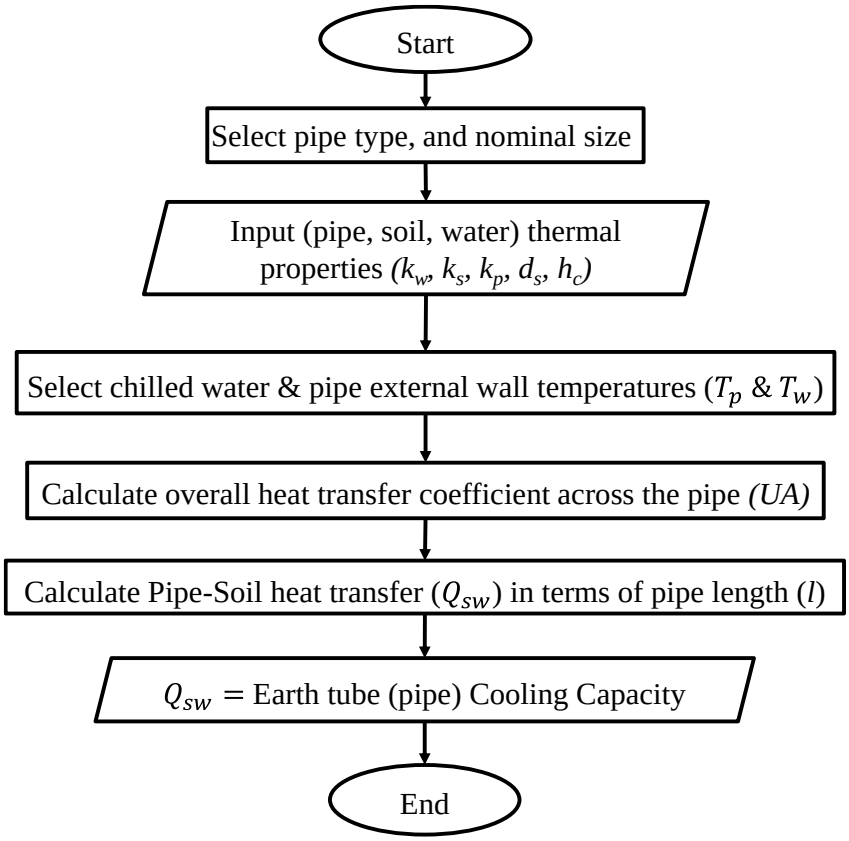

Figure 3.6: Summarized flow for calculating pipe-soil heat transfer

The heat transfer between the chilled water and the surrounding soil is determined using the 'total heat transfer coefficient' (UA) across the wall of the chilled water tube to the surrounding soil (Figure 3.7).

$$Q = UA(T_p - T_w) \tag{3.13}$$

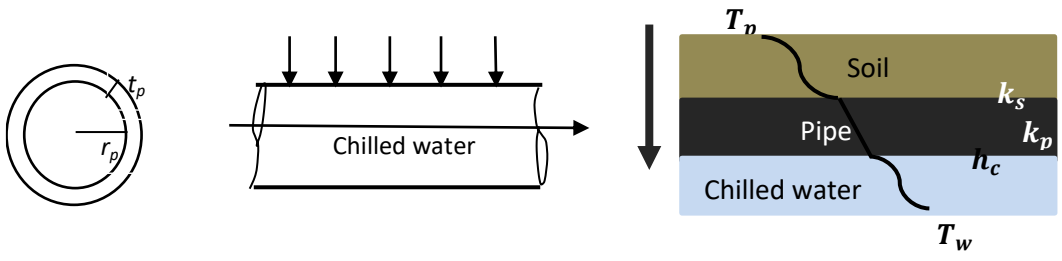

Figure 3.7: Chilled water tube cross section and heat flows

The overall heat transfer coefficient (UA) is expressed in terms of the resistance to heat transfer across the earth tube (Lee and Strand, 2008). The resistance against the flow of heat across the chilled water tube (to the chilled water) from the surrounding soil (analogous to electrical resistance) is represented in Figure 3.8, followed by the stepwise analysis of the resistance across each of the boundary layers.

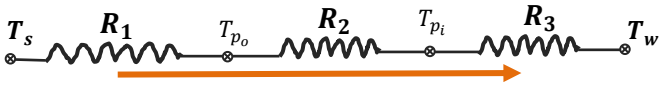

Figure 3.8: Schematics of resistances to heat transfer across chilled water tube

Resistance R_1 to convective heat transfer between the chilled water and the inner surface of the tube is expressed as;

$$R_1 = \frac{1}{hA} = \frac{1}{2\pi r_t l h_c} \tag{3.14}$$

$$h_c = \frac{N_u k_w}{2r_t} \text{ (Subramanian, 2008)}$$

Resistance R_2 to conductive heat transfer from the outer surface of the tube to its inner surface is given as;

$$R_2 = \frac{1}{2\pi l k_p} \ln\left(\frac{r_t + t_p}{r_t}\right) \tag{3.15}$$

Resistance R_3 to conductive heat transfer between surrounding soil and the external wall of the tube is expressed as;

$$R_3 = \frac{1}{2\pi l k_s} \ln\left(\frac{r_t + t_p + d_s}{r_t + t_p}\right) \tag{3.16}$$

Total resistance R_t is given as;

$$R_t = R_1 + R_2 + R_3 \tag{3.17}$$

Total heat transfer coefficient is expressed as;

$$U_t = UA = \frac{1}{R_t} \tag{3.18}$$

Assuming steady flow in the system, the heat transfer between the surrounding soil (outside the tube) and chilled water (in the tube), the net heat transfer is given as;

$$\bar{Q}_{sw} = UA[T_s - T_w] \tag{3.19}$$

Where h_c is convective heat transfer coefficient, *l* is the tube length, r_t inner radius of the chilled water tube, $t_p$is the tube thickness, d_s is the distance between the tube external wall and the surrounding soil, k_w is the thermal conductivity of water, T_s& T_w are the temperatures of the surrounding soil and chilled water, respectively, and N_u is Nusselt number. However, T_s is assumed equal to T_p.

3.2.1.6 Earth Tube Material

In the HVAC system applications, radiant floor/soil cooling with chilled water/chilled air is usually achieved through the network of pipes between the HVAC system and the conditioned space. However, horizontal earth tube system (HETS) is popular in radiant heat transfer between soil and buried tube with the application of a working fluid (Mongkon *et al.*, 2014; Lee and Strand, 2008), which is in most cases air or water. In this study, chilled water is the working fluid through which the heat transfer takes place.

Furthermore, the exchange off heat between the chilled water and the cooled surface is usually determined with reference to construction parameters as well as the difference between the temperatures of the chilled water and the cooled surface (Zhao. *et al.*, 2015; Zhao *et al.*, 2013). These are also taken into consideration in this study. Meanwhile, it is observed that material type is not the only determining factor on the

thermal performance of earth tubes, as tubes (earth tube) made of aluminium, plastic, and other materials have previously been used in this application, whereas the main consideration in material selection (in this case) are; cost, durability, strength, and resistance to corrosion. With regards to the nature of the present application, High Density Polyethylene (HDPE) tube (with properties shown in Table 3.1) that has been used in similar applications by Akbulut. *et al.*, 2016 and Cui *et al.*, 2008, is considered because;

i. It is easier to install than metal pipes.
ii. It has better resistance to corrosion.
iii. It is cheaper and easier to get.
iv. Less prone to cracks and breaks due to gravitational load.

Table 3.1: Properties of HDPE

Property	**Numerical value**	**Unit**
Melting Temperature (℃)	100-150 (Zalba. *et al.*, 2003)	℃
Thermal conductivity	0.49 (INEOS)	(W/m-K)
Heat of fusion	245 (INEOS)	kJ/kg
Corrosion resistance	Virtually inert (INEOS)	-
Specific weight	955	Kg/m^3
Tensile strength	22.44 (Hamid *et al.*, 2013)	MPa
Specific heat (23 ℃)	2.25 (INEOS)	kJ/kg-K

3.2.2 Combined Plant Components Modelling and Sizing

As against previous studies on combined power and cooling systems, in which the main goal has always been power generation while cooling is usually to improve the power cycle efficiency, the primary goal in this section of the study is the achievement of cooling; therefore the modelling of combined plant in this study is majorly on vapour absorption refrigeration cycle, with inclusion of ORC turbine (within the same cycle) that is able to make use of absorption cycle refrigerant (NH_3) as its working fluid.

The modelling presented here is carried out based on mass and energy balances across each of the subsystem of the combined plant (Figure 3.9), with reference to the thermodynamic properties of the working fluid. The thermodynamic properties of the working fluid are obtained from the National Institute of Standard Technology (NIST) database. The database is known as REFPROP from which the thermodynamic properties of most refrigerants (working fluids) are calculated, using the equation of state (Schimpf and Span, 2015).

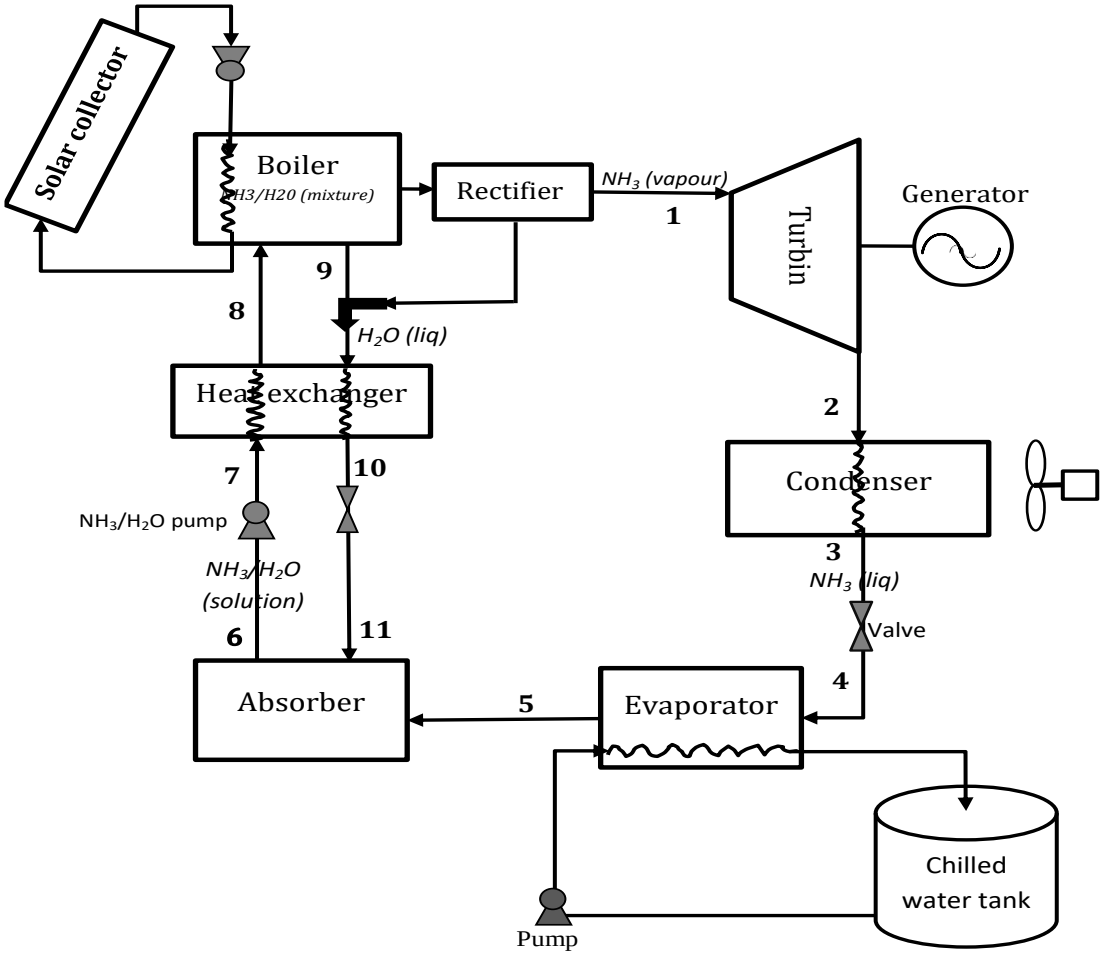

Figure 3.9: Integrated model of combined VAR–ORC system

With respect to the laws of conservation of mass and energy; the total material and energy into a system component equals the total material and energy out of the system component.

$$\sum_{in}(\dot{m}) = \sum_{out}(\dot{m}) \tag{3.20}$$

$$\sum_{in}(\rho_1 V_1 A_1) = \sum_{out}(\rho_2 V_2 A_2) \tag{3.21}$$

Furthermore, rate of change of internal energy (kinetic and potential) within a system equals net energy transferred by heat, work and mass within the system.

$$\frac{d\acute{E}_{system}}{dt} = \acute{E}_{in} - \acute{E}_{out} \tag{3.22}$$

But at steady state;

$$\frac{d\acute{E}_{system}}{dt} = 0$$

Therefore, $\acute{E}_{in} = \acute{E}_{out}$

$$\bar{Q}_{in} + \acute{W}_{in} + \sum_{in} \dot{m}\left(h + \frac{V^2}{2} + \text{ƃ}z\right) = \bar{Q}_{out} + \acute{W}_{in} + \sum_{out} \dot{m}\left(h + \frac{V^2}{2} + \text{ƃ}z\right) \tag{3.23}$$

Considering the energy balance with respect to sign convention, that is;

$$\left.\begin{matrix} Energy\ input \\ and \\ Work\ output \end{matrix}\right\} \Rightarrow Positive \quad \& \quad \left.\begin{matrix} Energy\ output \\ and \\ Work\ input \end{matrix}\right\} \Rightarrow Negative$$

$$\bar{Q} - \acute{W} = \sum_{out} \dot{m}\left(h + \frac{V^2}{2} + \text{ƃ}z\right) - \sum_{in} \dot{m}\left(h + \frac{V^2}{2} + \text{ƃ}z\right) \tag{3.24}$$

It is also assumed that the changes in potential and kinetic energy are negligible, therefore;

$$\bar{Q} - \acute{W} = \dot{m}(h_2 - h_1) \tag{3.25}$$

Meanwhile, for component sizing, the size of each of the components is expressed in terms of the component heat transfer area (A_{ht}) in m^2. This is given as;

$$A_{ht} = \frac{\dot{Q}}{U.\Delta T_{lm}} = \frac{\dot{m}(h_2 - h_1)}{U.\Delta T_{lm}} \quad (3.26)$$

Where U is the component heat transfer coefficient, ṁ is the fluid mass flow rate, h_2& h_1 are the inlet and outlet enthalpies of the fluid across the component, and ΔT_{lm} is the logarithmic temperature difference between the inlet and outlet fluid.

3.2.2.1 VAR–ORC Combined Plant Components Modelling

The present system is designed to overcome a particular load size. Therefore, the modelled plant size is equivalent to the load requirement of interest. The modelling is done with respect to the mass and energy balance across the plant's component parts. To determine the energy and mass balance, each of the plant components is treated as a separate entity (as represented in Figure 3.10) over which the energy and mass balances are carried out. The major components of the combined plant include; boiler, turbine, condenser, evaporator, absorption tank, and solution heat exchanger. Mass and energy balances have always been the focal point in component modelling of ORC and sorption cooling systems. Dynamic model for a 30kW LiBr-H_2O (single-effect) absorption chiller was developed by (Marc *et al.*, 2012), considering steady and transient states based on mass and energy balances of each of the system components, together with the equations of state and heat transfer. Series of modelling with mass and energy balances have been carried out by various researchers (Hong *et al.*, 2011; Borunda. *et al.*, 2016; Pratihar *et al.*, 2010; Sanjay, 2003). To simplify the mathematical modelling of the combined plant, the following assumptions were made.

1. The plant operates at steady state and the fluids are incompressible.
2. Heat transfer between the system and environment is negligible
3. Expansion through the throttling valve is isentropic ($h_3 = h_4$), so zero work done is assumed across the valve.

Figure 3.10: Component energy balance model

Heat is supplied to the boiler from the solar collector via the hot collector fluid (water) to indirectly heat up and vaporize the refrigerant (NH_3) from the working fluid solution (NH_3-H_2O). The working fluid is a solution mixture of Ammonia (NH_3) and water (H_2O), originally in 35 % and 65 % composition respectively. The total heat gained by the working fluid in the boiler (Q_{boiler}), is modelled as the product of mass flow, and the enthalpy difference of the working fluid stream between the inlet and outlet of the boiler (Abed *et al.*, 2013). From the boiler, the superheated vapour ammonia exits with high pressure to the turbine. The energy balance across the boiler is given as;

$$\dot{Q}_{boiler} = \dot{m}_1 h_1 + \dot{m}_9 h_9 - \dot{m}_8 h_8 \tag{3.27}$$

The mass fraction of the working fluid mixture components is expressed in equation 3.28 as;

$$\dot{m}_8 = \dot{m}_1 + \dot{m}_9 \rightarrow \dot{m}_8 X_8 = \dot{m}_1 X_1 + \dot{m}_9 X_9 \tag{3.28}$$

$$\dot{m}_8 = \frac{1 - X_9}{X_8 - X_9} \dot{m}_1$$

$$\dot{m}_9 = \frac{1 - X_8}{X_8 - X_9} \dot{m}_1$$

The material size of the boiler is determined by considering the heat transfer area (A_b) of the boiler, as expressed in equation 3.29. However, the material type and properties play a major role in the component sizing.

$$A_b = \frac{\dot{Q}_{boiler}}{U.\Delta T_{lm}} \tag{3.29}$$

Where X represents the NH_3 mass fraction in the working fluid, $\dot{m}_r$, $\dot{m}_w$, and $\dot{m}_{sol}$ are the mass flow rates of ammonia, water, and NH_3-H_2O solution respectively, h is the enthalpy of the fluids, ΔT_{lm} is the logarithmic temperature difference between the inlet and outlet fluids, U is the component heat transfer coefficient and a function of the boiler material type and thermal properties.

The superheated ammonia refrigerant vapour expands through the turbine to produce useful work, which is converted to electrical power by the turbine generator. The ammonia vapour pressure exit from the turbine is set to be equal to saturation pressure at the condenser inlet and the condensation is assumed to be isobaric. That is;

$$P_2 = P_{3(sat)} \tag{3.30}$$

The gross power output (W_t) from the turbine-generator is given as;

$$\dot{W}_t = \dot{m}_r(h_1 - h_2)\eta_t \tag{3.31}$$

Where η_t = isentropic efficiency of the turbine; usually between 80 and 95 %, (Quoilin *et al.*, 2013).

However, it should be noted that turbine efficiency values in power generation systems largely depends on the fuel (heat source) type, and conversion technology employed.

The NH_3 vapour exiting the turbine is cooled and condensed in the condenser, loosing most of its heat to become saturated liquid. For the modelled plant in this study, condenser pressure is kept at 10bar and the corresponding (saturated) ammonia temperature at this point is 25 ℃. Heat removed from the condenser ($\dot{Q}_c$) is given as;

$$\dot{Q}_c = \dot{m}_r(h_2 - h_3) \tag{3.32}$$

Passing through the throttling (expansion) valve, the liquid refrigerant undergoes a pressure reduction, making its temperature to drastically reduce. The extremely cold refrigerant flows into the evaporator where it evaporates and exchanges heat with chilled water in the evaporator. The heat removed from the evaporator ($\dot{Q}_{evp}$) is known as the refrigeration effect (cooling effect) of the cooling system. This is given as;

$$\dot{Q}_{evp} = \dot{m}_r(h_5 - h_4) \tag{3.33}$$

$$h_3 = h_4 \tag{3.34}$$

The chilled water flow rate at the evaporator is determined using the heat transfer relations between the chilled water and the chilled evaporator tube, with respect to the heat transfer coefficient between them.

$$\acute{m}_{cw} = \frac{U_c A_{evp}(\Delta T_{evp})}{Cp_{cw}(\Delta T_{cw})} \tag{3.35}$$

Where ΔT_w & ΔT_{evp} are the respective changes in temperatures of the chilled water and working fluid, Cp_{cw} is the chilled water heat capacity, and A_{evp} are the area of the evaporator which can be determined using equation 3.26.

Leaving the evaporator, the refrigerant then exits as saturated vapour, and flows to the absorption tank where it is absorbed by the low pressure absorbent (H_2O) to again form the solution mixture. From the absorption tank, the solution mixture is pumped back (through the solution heat exchanger) to the boiler to repeat the cycle. The energy balance at the absorption tank is given as;

$$\dot{Q}_{abs} = m_5 h_5 + m_{11} h_{11} - m_6 h_6 \tag{3.36}$$

This is also expressed as;

$$\dot{Q}_{abs} = m_r h_5 + m_w h_{11} - m_{sol} h_6$$

The solution heat exchanger (sometimes called pre-heater) is used to maximize the heat energy recovery process (internal energy recovery) by exchanging heat between the hot fluid (absorbent) coming from the boiler and the cold high-pressure working fluid from the absorber. The heat transfer between the two streams is modelled by considering the energy transfer by the streams across the component at their different temperatures. The amount of heat exchanged is given as;

$$\dot{Q}_{Hx} = \acute{m}_7 h_7 + \acute{m}_9 h_9 - \acute{m}_8 h_8 - \acute{m}_{10} h_{10} \quad (3.37)$$

This is also expressed as;

$$\dot{Q}_{Hx} = \acute{m}_{sol}(h_7 - h_8) + \acute{m}_w(h_9 - h_{10})$$

Energy is consumed by the solution pump to raise the pressure of working fluid mixture. The energy consumed by the pump is given as;

$$\dot{Q}_p = \frac{\acute{m}_{sol} V_7 (p_7 - p_6)}{\eta_p} \quad (3.38)$$

Where $\acute{m}_{sol}$ and V are the mass flow rate and specific volume of H_2O-NH_3 solution through the pump, η_p is the efficiency of the solution pump, p_6 & p_7 are the inlet and exit pressure through the pump.

Effective solar collector size required for the system activation is determined using (Bajpai, 2012; Yeh. *et al.*, 2002)relation, expressed as;

$$Q_u = Q_{inc} \times A_c \quad (3.39)$$

$$Q_b = kQ_u \tag{3.40}$$

Where k is the efficiency of the solar collector, Q_u is the solar energy (W) absorbed by the collector, Q_{inc} is the available solar heat (per square metre) on the earth (W/m^2), A_c is the effective area of the collector.

3.2.3 Combined Plant–Cooling Load–Piping Systems Integrations

The modelled cooling load (Q_{load}) is expressed as the product of the net heat gained by the soil and a safety factor (γ). Safety factor is commonly added to accommodate possible variation in design values so that the system can optimally cope with variations in load (Flueckiger *et al.*, 2013) This has been applied by previous researchers in similar areas of study by adding 10–25 % of the designed values (Liu. *et al.*, 2014; Sharizal, 2006) depending on the complexity of the design.

$$Q_{load} = Q_s \times \gamma \tag{3.41}$$

The equivalent chiller capacity (Q_{evp}) is expressed as the product of the cooling load and the area of the soil bed to be cooled.

$$Q_{evp} = Q_{load} \times A_s \tag{3.42}$$

$$A_s = \frac{Q_{evp}}{Q_{load}} \tag{3.43}$$

Relating the chilled water tube cooling capacity (with respect to soil bed area) with the plant cooling capacity gives the approximate length of the chilled water pipe (earth tube). With all specifications appropriately selected, the calculated length is equivalent to the length of the earth tube that is evenly networked through the soil bed for even temperature distribution within the soil bed.

3.2.4 Chilled Water Flow Rate Optimization

To determine the chilled water flow rate for optimum soil temperature distribution, conductive heat flow between the soil surface and earth tube plays an important role. Temperature difference between the undisturbed soil (surrounding the earth tube) and soil surface causes difference in heat content between soil load (Q_{load}) and chilled water cooling capacity (Q_{sw}). The temperature difference is responsible for the conductive heat (Q_{cond}) between the soil surface and the chilled water pipe. This is mathematically expressed as;

$$Q_{cond}(t) = Q_{load}(t) - Q_{sw} \tag{3.44}$$

Therefore, soil temperature corresponding to the optimized chilled water flow rate is expressed in the following equation as;

$$T_s^t = \frac{d_z}{k_s A_s}\tau\left\{Q_{load}(t) - \dot{m}_w(i)C_{pw}\Delta T\right\} + T_p \tag{3.45}$$

Where $Q_{load}(t)$ is the time value of the cooling load imposed on the soil over the analysis period, T_s^t is the soil temperature during the measurement period, T_p is the undisturbed soil temperature along the chilled water tube, τ is correction factor due to earth tube depth.

3.3 Energy Balance across the System Boundary

3.3.1 Steady State Energy Balance

Based on law of conservation of energy and mass (as expressed in equations 3.20 – 3.25), the steady state energy balance of the modelled plant is presented with respect to the system boundary in Figure 3.11.

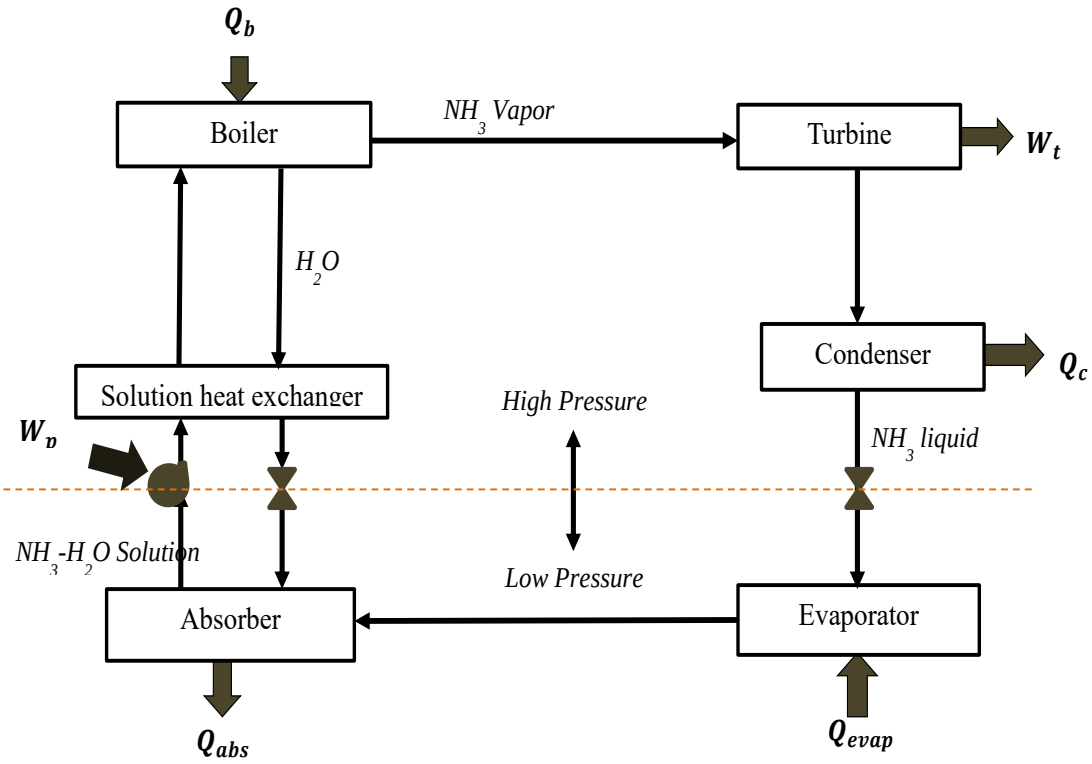

Figure 3.11: ORC-VAR system boundary

The system energy balance implies that;

Heat gained by the system + Work done on the system = Heat rejected to the surrounding + Heat loss to produce work + System loss

$$Q_b + Q_{evap} + W_p = Q_c + Q_{abs} + Q_t + Q_{loss} \quad (3.46)$$

The energy inputs are from the boiler, the cooling effect, and from the solution pump (Q_b, Q_{evap}, $and\ W_p$, respectively) while the energy outputs are from the condenser, from the absorber, loss due to expansion in the turbine (to produce power), and the system heat loss (Q_c, Q_{abs}, Q_t, $and\ Q_{loss}$, respectively).

3.3.2 Transient Energy Balance

Absorption cooling systems commonly have high mass of the internal components and accumulation of fluids inside the vessels; making the transient phase a bit longer than in mechanical compression chillers, therefore transient energy modelling is also considered important. Although not intended to be included in this study, the objectives of transient performance analysis in sorption cooling systems include;

i. To determine the energy input & output at each section of the plant at different time of operation; and

ii. To present (with good accuracy) the plant performance (daily, weekly, or seasonally).

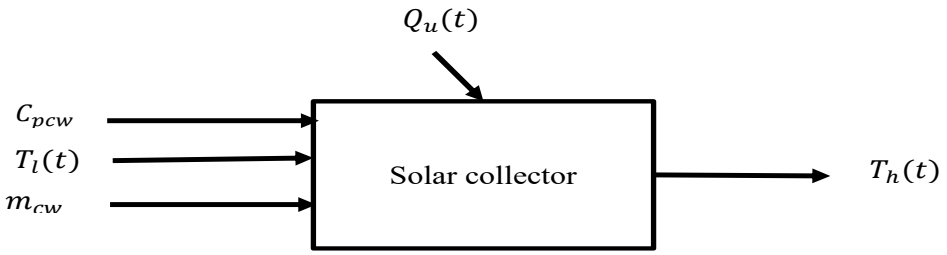

Figure 3.12: System transient energy flow

The heat energy required to drive the system is a function of solar radiation received by the collector. Meanwhile, the collector thermal fluid output varies with time of the day (Figure 3.12). However, the dynamic modelling of the solar is not intended in the present study but the estimation of effective solar collector size.

$$Q_u(t) = m_{cw}C_{pcw}(T_h - T_l)(t) \tag{3.47}$$

$$Q_u(t) = m_{cw}C_{pcw}\frac{\partial T}{\partial t} \tag{3.48}$$

Where $Q_u(t)$ is the solar collector energy potential from solar radiation (which is also a function of time and collector area), $m_{cw}\ and\ C_{pcw}$ are mass flow rate and heat

capacity of the collector thermal fluid, and $T_h \; and \; T_l$ are the respective outlet and inlet temperatures of the thermal fluid from (and to) the collector.

3.4 Performance Evaluation

Performance analysis of the present system is mainly based on steady state. The steady state performance evaluation is done to assess the coefficient of performance and the organic Rankine efficiency of the combined plant. Further performance analysis is carried out through the parametric analysis and optimization of the plant by varying the key parameters and studying their effects on the plant performance. The key parameters of interest in this study are the working fluid vaporizing temperature and pressure, and the mass fraction of NH_3 in the NH_3-H_2O working fluid mixture. The parametric analysis is done using *RSM* of the Design Expert®. The details are contained in section 3.8.

3.4.1 Power Cycle Efficiency

Power cycle efficiency is defined based on its output of interest. This depends on whether is it gross power or net power output. The gross power output can be determined by the turbine shaft power as presented in Equation 3.31. However, the net power output is affected by the energy consumed by other components (such as the working fluid pump) during the operation (Schröder *et al.*, 2014). Gross and net power efficiencies are represented by Equations (3.49) and (3.50), respectively.

$$\eta_{gross} = \frac{W_t}{Q_{in}} \tag{3.49}$$

$$\eta_{net} = \left\{\frac{[W_t - \sum W_{pi}]}{Q_{in}}\right\} \tag{3.50}$$

Where W_{pi} represents the power consuming components, Q_{in} is the energy required to vaporize the working fluid.

3.4.2 Cooling Coefficient of Performance

The performance of HVAC system is usually measured in terms of the Coefficient of Performance (*COP*), which relates the cooling output to the energy input for driving the system. This is represented as;

$$COP = \frac{\dot{Q}_{evp}}{\dot{Q}_{boiler}} \tag{3.51}$$

3.4.3 Combined Plant Performance

Measuring the performance of power and cooling combined cycle, based on first law of efficiency by adding the power and refrigeration output then dividing them by the heat input may result in power cycle exceeding the Carnot efficiency (Demirkaya *et al.*, 2013); this is just like adding "oranges to apples" according to (Vijayaraghavan and Goswami, 2003). However, in this study, with cooling as the primary goal, the performance of the combined plant is expressed as modified COP, given as;

$$COP = \left\{\frac{[\acute{m}_r(h_5 - h_3)] + [(\acute{m}_r(h_1 - h_2) - \acute{m}_{sol}V_7(P_7 - P_6)]}{\dot{Q}_{boiler}}\right\} \tag{3.52}$$

$$COP = \frac{\dot{Q}_{evap} + W_{net}}{\dot{Q}_{boiler}} \tag{3.53}$$

$$W_{net} = W_t - \sum \dot{Q}_{pi}$$

It is also to be noted that the relative newness of power and refrigeration systems on a single cycle in the literature (Tamm *et al.*, 2004), resulted in the modification of the performance calculation expressions.

However, to consider individuals of the two output performances (η_{ORC} and $COP_{cooling}$) in relation to the same energy source, their performances can be represented in equations 3.54 and 3.55, respectively as;

$$\eta_{ORC} = \frac{W_t}{Q_b - Q_{evp}} \tag{3.54}$$

$$COP_{cooling} = \frac{Q_{evp}}{Q_b - W_t} \tag{3.55}$$

When the system performance is based on the overall solar energy received by the collector, equations 3.50 and 3.53 can be modified as;

$$\eta_{thermal} = \left\{\frac{[W_t - \sum W_{pi}]}{Q_u}\right\} \tag{3.56}$$

$$COP_{thermal} = \frac{\bar{Q}_{evap} + W_{net}}{\bar{Q}_u} \tag{3.57}$$

Where $\sum \bar{Q}_{pi}$ indicates the situation where more than one pumps are considered in the performance measurement, $\bar{Q}_u$ is the total heat supplied by the collector (through the thermal fluid).

3.4.4 Soil Cooling Efficiency

The efficiency of soil cooling process considered in this study refers to the percentage of the soil cooling load that the chilled water is able to overcome. This is

a time dependent measure of the system performance. The soil cooling efficiency is expressed as;

$$\eta_{soil\ cooling} = 1 - \frac{Q_{load}(t) - Q_{sw}}{Q_{load}(t)} \times 100 \quad (3.58)$$

3.5 Model Calculation with C#

The overall system capacity, comprising the soil cooling load, the combined cooling and power plant, and the chilled water tube cooling capacities have been mathematically modelled, and the mathematical equations for the system performance and parametric analysis have also been developed. The required data for the modelled plant to produce the desired results have been defined through the thermodynamics of the working fluid (Appendix B). However, to make the calculations in the model easier, programming codes have been developed, using a computer programming language. The model calculation is implemented in an objected oriented programming language, C# (pronounced C-sharp). Just like C++, Java, COBOL, etc, C# is a modern computer programming language that can be used to build any kind of applications that operate with **".Net Framework"**. It is object oriented language, safe and reliable (Zheng. *et al.*, 2012; Qela. and Mouftah, 2008), and most importantly with syntax simplifications. Some of the favourable features of C# include;

i. It is user friendly and good to use for non-programmer.
ii. It has better programmer's productivity because it has flexibility of reduced number of code-lines compared with other programming languages.
iii. It is developed and managed by Microsoft, so it is just an add-in to the MS word.

C# has been used in various similar applications. Implementation of the simulation of house heating system was carried out by (Qela. and Mouftah, 2008), using C#, to find out about the efficiency of the heating system, its energy

consumption, and cost associated to the system when operated under different situations. In their review and case study, (Carrasco. and Girty, 2015) utilized C# in the implementation of reference frame identification for the calculation of change in mass occurring during weathering process. The implantation was carried out by following the general mathematical and statistical steps involved in the calculations. "A* algorithm" was developed by (Nordin. *et al.*, 2012), and implemented in C# for finding the shortest ambulance routing path in Shah Alam. They utilized C# programming purposely to reduce the calculation time required for finding the shortest routing distance.

3.5.1 Solution Algorithm Development

Solution algorithms were developed for each of the processes. However, because C#, as an object-oriented programming, has an important concept like inheritance (Bishop. and Horspool, 2008) that allows the reuse of code functionality, once such code has been defined in the previous class (derived class inheriting from a base class). The succeeding processes become less cumbersome once the first related process has been properly defined. This also ensures the speeding up of implementation time. The algorithm also shows the stepwise model calculation implementation in the developed C# programming.

3.6 Experimental Investigation

3.6.1 Test Site Description

The experimental rig was set up at the Ocean Thermal Energy Centre of the Universiti Teknologi Malaysia, Kuala Lumpur campus, with the climatic location shown in Table 3.2.

Table 3.2: Site reference conditions and project location

Climate data location	Kuala Lumpur/Subang
Latitude	3.1 ºN
Longitude	101.6 ºE
Elevation	22 m
Heating design temperature	16.5 ℃
Cooling design temperature	19.5 ℃
Earth temperature amplitude	7.3 ℃

The day-time solar radiation availability at the test site is usually between 7:00hr and 19:00hr clock time. However, the soil bed was positioned in a place where it was exposed to about 85 % of the available daytime solar radiation. Thus, it is expected to exhibit real planting field characteristics.

3.6.2 Experimental Set up

The test rig developed in this study consists of the chilled water production plant and the soil bed. Thus, the experimental study was conducted in two phases; (i) chilled water production subsystem and (ii) soil cooling subsystem, as shown in Figure 3.13. Data collected from the set-up include chilled water flow rates and temperatures from the chiller, the soil bed and the chilled water pipes, using T-type thermocouples. Each of the subsystems was independently studies and their results were analysed and compared with those obtained from the mathematical models. The temperatures recorded during the experimental study were logged to the computer hard disk through the National instrument data logger.

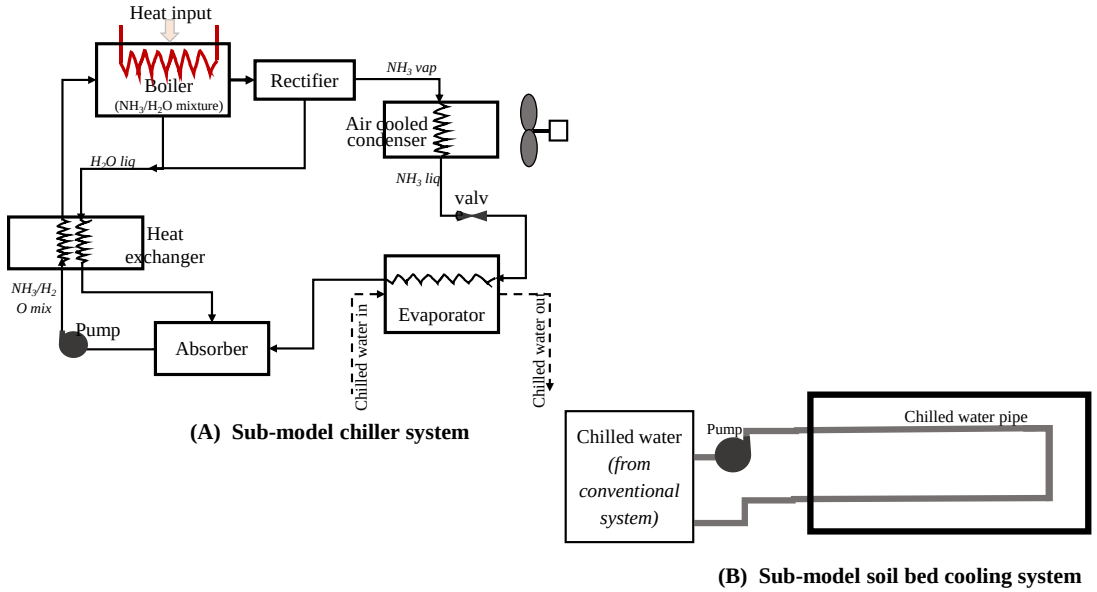

Figure 3.13: Skematic representation of sub-model of absorption chiller (A), and sub-model of soil bed cooling (B) experimental set-up

With reference to Figure 3.2, the subsystems are interrelated since the plant was designed to meet the load requirements of the soil bed. The capacity of the plant is a function of the imposed load per unit area of the soil bed.

3.6.2.1 Soil Cooling Subsystem

The soil cooling subsystem contains two soil beds (cooled soil bed and control soil bed). Each of the soil bed was filled with loamy soil obtained at the experimental site (Kuala Lumpur Malaysia). The chilled water tube was buried at 0.15 m depth below the soil bed surface. The properties of the soil and that of the soil bed, and chilled water pipe are shown in Table 3.3. Type-T thermocouples were used to measure the temperatures at 8 points on the set up; four on the cooled soil bed, one on the control soil bed, one each on chilled water inlet and return, and one to measure the ambient air temperature. Average of the temperature readings by the thermocouples on the cooled soil bed was used as the cooled soil temperature. The selected chilled water pipe and soil bed have the following specifications as shown in Table 3.3.

Table 3.3: Soil bed and chilled water pipe specifications

Soil bed container		**Soil**			**Chilled water pipe**				
Material	Top Surface area	Type	Thermal cond.	pH	Material	Length	OD	Thickness	Thermal cond.
Polystyrene box	0.25 m^2	Loamy	1.5 W/m-K	4.85-5.0	HDPE	1.0 m	0.02m	0.0025m	0.42W/m-K

High-density polyethylene pipe (HDPE) of 1.0 m length was evenly networked through the soil bed for the temperature distribution. Chilled water was then pumped through the buried chilled water pipe to cool the dimensioned soil bed as shown in Figure 3.14.

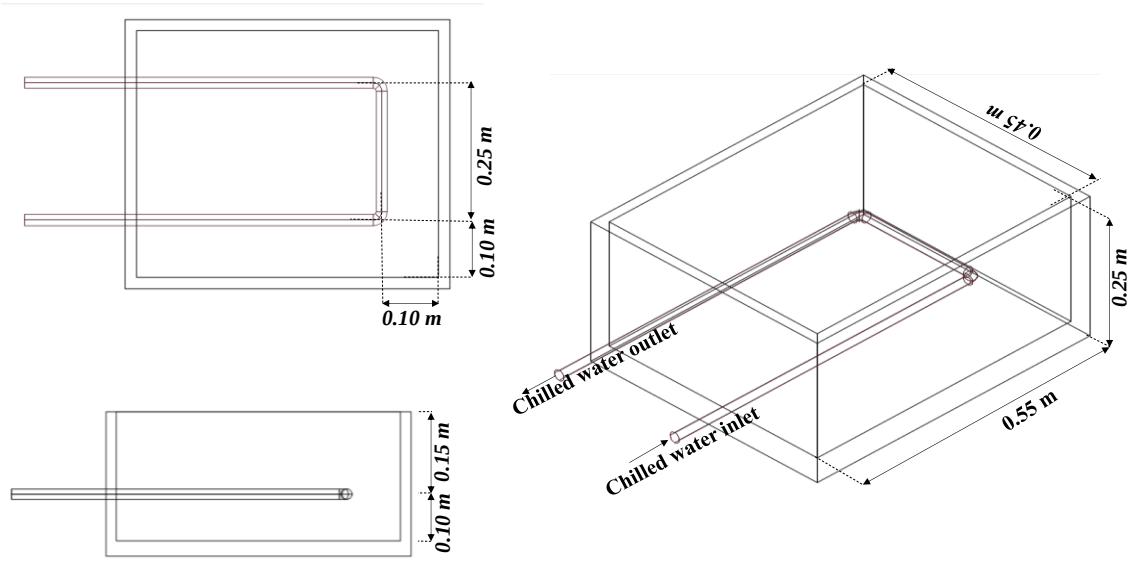

Figure 3.14: Experimental soil bed and piping configuration

3.6.2.2 Chilled Water Production Subsystem

The experimental investigation of the chilled water production subsystem had been done through the study of a mini absorption cooling unit (in Figure 3.15), taking

its operational parameters at steady state to determine its performance characteristics. The chiller was manufactured by Shandong XINGKE intelligent technology company limited. It is a thermally activated system, operating on ammonia-water mixture with 0.35/0.65 of NH_3/H_2O mass fraction, and suitable for chilling a 0.04 m^3 space volume (40 litre) capacity. Table 3.4 gives the basic specification of the chiller, while other operating details taken during the experimental study are presented in Chapter 4.

Table 3.4: Experimental chiller's design specification

Model	**Cooling capacity**	**Boiler Pressure**	**NH_3/H_2O Mass Fraction**	**Total effective cooling volume**
XC-40	50 W	16 bar	0.35/0.65	40 litre

Prior to the experimental study, sections of the evaporator, solution heat exchanger, and boiler pipes were insulated against the ambient environment to reduce the interference and losses to as low as possible. The condenser and absorber are air-cooled and were allowed to be fully exposed to the ambient air; the air-cooling of the components was aided by a mini fan with 2.5 W capacity. The activation of the chiller was achieved through an electric heater, and energy delivered by the heater was quantified in terms of the collector deliverable energy. Chiller's required energy was regulated through its thermostat. T-Type thermocouples were used to measure the operating temperatures and details of the data points are shown in Table 3.5.

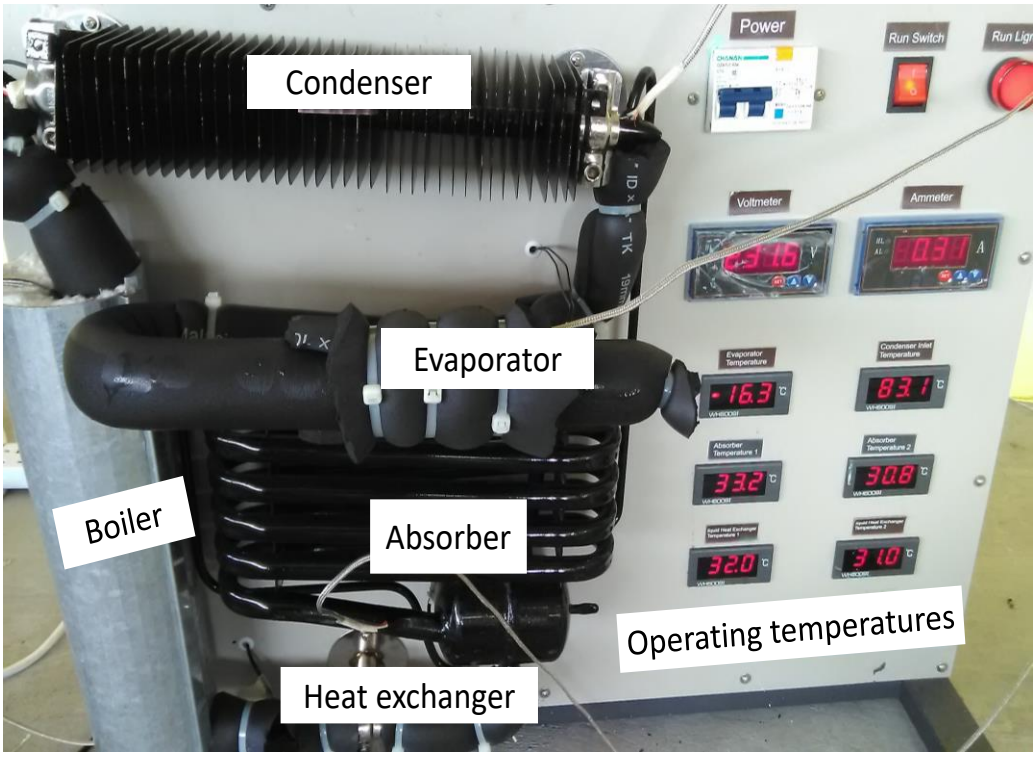

Figure 3.15: Experimental absorption refrigeration system

3.6.3 Data Collection Methods

The overall set up contained 14 numbers of data collection points; five point on the chiller, eight on the soil beds and one for the ambient air temperature. Chiller's operating temperatures at the boiler, condenser, evaporator, absorber and solution heat exchanger were measure via the T-type thermocouples as shown in Figure 3.16).

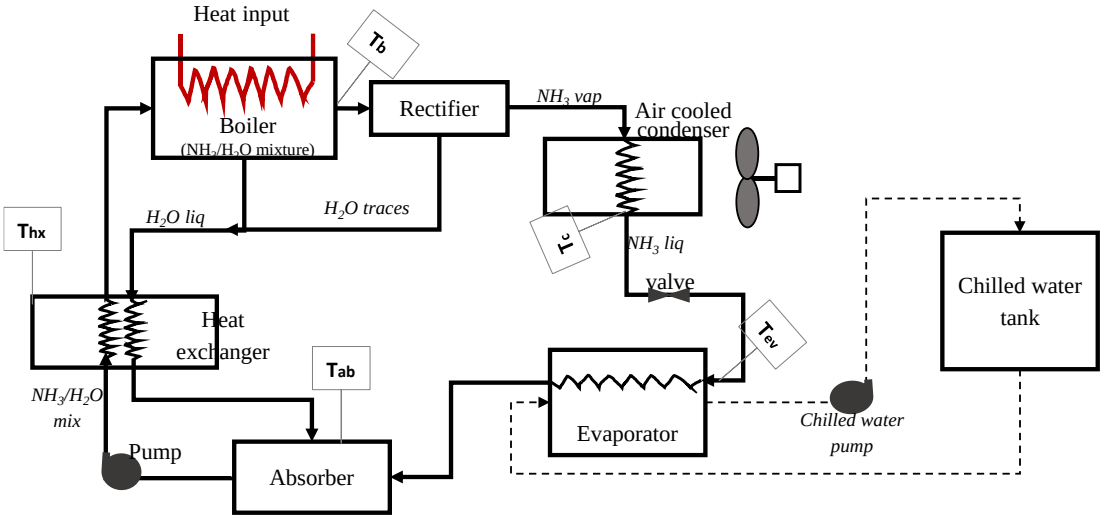

Figure 3.16: Components of the experimental (HN_3/H_2O) chiller with chilled water storage

Soil bed subsystem contained nine data point; one flow sensor for measuring the chilled water flow rate to the soil bed, four thermocouples on the cooled soil bed, one thermocouple each on the inlet and outlet of the chilled water to the soil bed as shown in Figure **3.17**. Control soil bed and ambient air temperatures were also measured using the thermocouples. Table 3.5 contains the list of data points for the experimental set up.

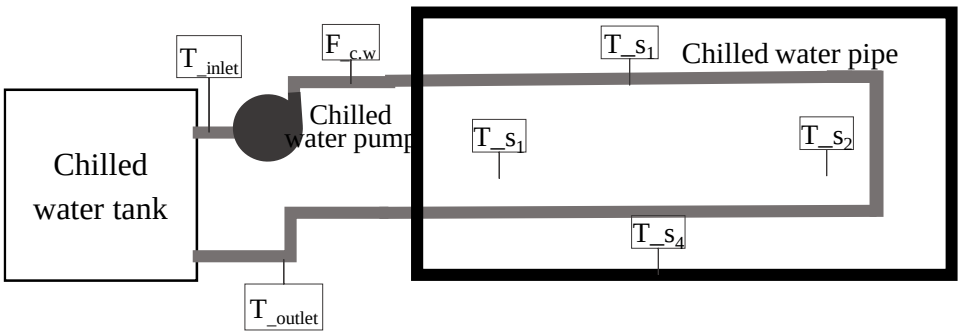

Figure 3.17: Schematic diagram of cooled experimental soil bed with temperature and flowrate measurement

Table 3.5: Instrumentation for the experimental data collection

Data Point	Data Label	Medium	Measuring Tool	Capacity Range
Temperature				
Cooled Soil bed	T_s_1 T_s_2 T_s_3 T_s_4	Soil	T – Type Thermocouple	-250 to +400
Control Soil bed	$T\__{control\ soil}$			
Ambient air (for soil cooling & chiller)	$T\__{air}$	Air		
Soil bed Chilled Water Inlet	$T\__{inlet}$	Water		
Soil bed Chilled Water outlet	$T\__{out}$			
Boiler Exit Temperature	T_b	NH_3		
Condenser Exit Temperature	T_c			
Evaporator Temperature	T_{ev}			
Absorber Temperature	T_{ab}	NH_3-H_2O		
Solution Heat Exchanger	T_{hx}			
Flow Rates				
Chilled water-to-Soil bed	$F\__{c.w}$	H_2O	Flow control LCD display Water sensor	0.01 to 9999 lit/m

National Instrument (NI) data logger was used for the experimental data acquisition. This required the installation, configuration, and calibration of the test panel and data measuring tools. Prior to data reading, acquisition and logging, the NI data logger was installed together with the LabVIEW. This helps in the online visualization of the acquired data during the experimental campaign. Other data collection details are contained in Appendix D.

3.6.4 Experimental Methods

The experimental rig consists of; (i) the soil cooling subsystem, and (ii) the chilled water production subsystem.

The chilled water tube was buried in the soil at a depth of 150 mm below the soil bed surface. The tubes were at 200 mm apart, and 100 mm from the wall of the soil bed. To achieve the desired soil temperature (18 ℃$\pm$2) on the soil bed, four sets of chilled water flow rate were used and their cooling effects on the soil were observed at different prevailing weather conditions during the day for the chilled water temperature between 3 ℃ and 10 ℃. The soil cooling experiment took place between 6:00am to 10:00pm (clock time) within which solar radiation was available. This is done to observe the effect of chilled water temperature and its flow rates in the presence and absence of solar radiation heat.

The chilled water production rate was determined by the cooling rate of the chiller's evaporator. The chiller unit runs on known operating pressure and working fluid mass fraction. However, the mass flow rates of the working fluids were determined, based on its capacity, and operating temperatures and pressures. Working fluids temperatures at each of the system components were measured from external surface of the pipes with T-type thermocouples. The true values were however calculated using Gorman equation (Gorman *et al.*, 2013);

$$T_{fluid} - Tmeasured = (T_{measured} - T_{amb-air})\left[\frac{1-\theta_{crit}}{\theta_{crit}}\right] \qquad (3.59)$$

Where; $T_{measured}$, T_{air} and T_{fluid} are measured temperature, air temperature, and the actual temperature of the fluid respectively, θ_{crit} is a dimensionless parameter relating the temperature in x,y,z directions.

The Coefficient of Performance of absorption refrigeration, based on temperature, has been developed by (Stanish and Perlmutter, 1981), and modified and

used for absorption chiller performance verifications by (Kaushik *et al.*, 1983; Mazouz *et al.*, 2014). However, the theoretically achievable *COP* based on the ideal cycle operating on NH_3-H_2O was reported to be 1.5 (Mazouz *et al.*, 2014) from which only around 0.5 is actually achievable in the reality (El May et al 2011) from the commercial absorption chiller cycles.

Further modifications have been made to (Stanish and Perlmutter, 1981) equation by (Gordon and Ng, 1995) to include the cooling capacity of the chiller in the analysis of the *COP*. The modified form of the (Gordon and Ng, 1995) equation (equation 3.60) is used in this study to analyse the *COP* of the studied chiller.

$$\frac{1}{COP_{cooling}} = \left[\frac{T_{cond}-T_{evp}}{T_{evp}}\right]\left[\frac{T_{boiler}}{T_{boiler}-T_{abs}}\right] + \left[\frac{1}{Q_{evp}}\right]\left[\frac{T_{boiler}}{T_{boiler}-T_{cond}}\right] \times Q_{loss} \quad (3.60)$$

Where; Q_{loss} is the system loss (due to the irreversibility) from the components of the chiller.

$$Q_{loss} = \left[q_{cond}^{loss} + q_{abs}^{loss}\right] - \left[\frac{T_{cond}}{T_{evp}} \times q_{evp}^{loss}\right] - \left[\frac{T_{cond}}{T_{boiler}} \times q_{boiler}^{loss}\right] \quad (3.61)$$

3.6.5 Modified Cooling and Power System

Upon the exhaustive study of the mini absorption cooling unit, its operational parameters at steady state were taken to determine its performance characteristics, and its adaptability with an organic Rankine turbine was investigated. The adaptability is however a simulated based, referred to as "modified cooling and power plant". The analysis of the modified plant was carried out based on the operational characteristics of the experimental absorption chiller unit.

It was reported by (Rice, 1965) that nearly all the pressure drops due to expansion in ORC turbine occurs in the nozzle. This is caused by reduction in the nozzle diameter that increases the fluid speed. Therefore the predicted pressure drop

could be used to determine the equivalent nozzle diameter for the selected turbine. If the working fluid pressure differential along the turbine is known, the properties along this region are used to determine the gross power produced by the turbine; taking the possible losses into consideration. In the (Rice, 1965) experimental studies on similar system, the flow of working fluid through the turbine nozzle is considered choked and nearly all the pressure drop in the turbine occurs at the nozzle with only a negligible expansion occurring along the rotor. Experimental analysis of Tesla turbine by (Romanin, 2012) also revealed that at the inlet temperature of similar choked system, the pressure ratio across the nozzle should be at critical pressure ratio. However, irrespective of the outlet (downstream) flow condition, the mass flow rate of chocked flow is constant (Park. *et al.*, 2001). With reference to Figure 3.10, this is simply expressed in equation as;

$$\frac{P_2}{P_1} \approx \frac{P_{n.t}}{P_1} \tag{3.61}$$

Where P_1, P_2, and $P_{n.t}$ are the turbine inlet, outlet, and throat pressures, respectively.

However, (Munson. *et al.*, 2009), cited by (Romanin, 2012) gave the critical pressure ratio of turbine with air as working fluid at 350K to be about 0.53. It should be noted that the experimental machines in the references used different working fluids and this may not make the results obtained from this study to be a perfect match with them. However, this gives an approximate ranges of expected performance from the chosen turbine and also displays how the turbine performance correlates with the its geometries and operational parameters (Rice, 1965).

This approach is also helpful because the experimental rig in this study is miniature in size, making it a bit difficult to secure a suitable turbine size. Moreover, it is reported that the knowledge of the turbine nozzle geometries and/or fluid characteristic can help in predicting the power and efficiency deliverable from the turbine (Neckel and Godinho, 2015). The conceptual turbine nozzle diameter is determined using Bernoulli equation;

$$P_1 + {}^1\!/_2\,\rho V_1^2 + \rho g h_1 = P_2 + {}^1\!/_2\,\rho V_2^2 + \rho g h_2 \tag{3.63}$$

The passage of the working fluid through the nozzle (with reduced diameter) results in occurrence of "choke" along the flow in the tube, leading to decrease in pressure of the fluid, and increase in its velocity but with no effect on the mass flow rate at the downstream (Javidmand and Hoffmann, 2016). However, height is not considered in this study, which is a closed system. Therefore, the equation 3.63 is rewritten in relation to the present study as;

$$P_i + \frac{1}{2}\rho v_i^2 = P_o + \frac{1}{2}\rho v_0^2 \tag{3.64}$$

Based on the continuity equation, the fluid mass flow ($\acute{m}_r$) through the turbine nozzle is constant and determined as;

$$\acute{m}_r = \rho_r A_i v_i = \rho_r A_o v_0 \tag{3.65}$$

Substituting the fluid velocity term in equation 3.63 with$\left(\frac{\acute{m}_r}{\rho A}\right)$, the pressure change of the working fluid in the nozzle is expressed as;

$$\Delta P = \frac{1}{2}\left(\frac{\acute{m}_r^2}{\rho}\right)\left[\frac{1}{A_o^2} - \frac{1}{A_i^2}\right] \tag{3.66}$$

Where ρ *and* A are the density of the working fluid, and the cross sectional area of the nozzle, and can be written as;

$$\Delta P = \frac{1}{2}\left(\frac{m_r^2}{\rho}\right)\left[\frac{1}{\frac{1}{4}(\pi d_o^2)} - \frac{1}{\frac{1}{4}(\pi d_i^2)}\right] \tag{3.67}$$

The thermodynamic properties of the working fluid together with the prevailing operating conditions were analysed to assess the performance of the turbine for its applicability in this system of combined cooling and power. The expansion of the

working fluid through the nozzle (due to diameter reduction) leads to the transfer of the working fluid momentum into kinetic energy that causes the rotation of the turbine discs.

Changes in working fluid properties at the nozzle diameter were observed and used for calculating the equivalent work done across the section, using equation 3.68 which is analogous to the one-dimensional model by (Song *et al*., 2017) in equation 3.69 for calculating the turbine output power.

$$W_t = \acute{m}_r(h_i - h_o)\eta_t \tag{3.68}$$

$$W_t = \acute{m}_r(v_i U_i - v_o U_o) \tag{3.69}$$

Experimental analysis of Tesla turbine was first conducted by (Rice, 1965) and it was concluded that the turbine efficiency could be improved up to 90 %. Similarly, the experimental studies by (Ho-Yan, 2011) on Tesla turbine indicated the possibility of more than 70 % efficiency. The studies conducted by (Deam *et al.*, 2008) on mini scale Tesla turbines (with sub centimetre diameter) using viscous working fluid showed that the efficiency can be up to 40 % while the experimental and computational analyses of Tesla turbines by (Hoya and Guha, 2009) gave efficiency of 25 %. However, the turbine nozzle designed by same authors was able to improve the efficiency beyond 25 %. These series of previous research give an excellent basis for the verification of the present micro-scale turbine to be suitable in this application.

3.7 Model Validation

To establish the reliability of the method used in research and the consistency of the results obtained from such method, model validation is utmost required and this has always been considered the final stage in the application of system analysis (Sakellari, 2005). The model developed by (Ayompe. *et al.*, 2011) on forced circulation of solar water heating using evacuated tube and flat plate collectors was

validated with experimental data under different operating and weather conditions. Cooling and heating performance models for embedded pipe and ground source heat exchangers have been developed by (Safa. *et al.*, 2015; Liu *et al.*, 2016) and were both validated with experimental data to access possible improvement in the system. The model validation path in this study is shown in Figure 3.18. This is followed by parametric analysis and optimization of the modelled system performance with respect to variations in its key operating parameters.

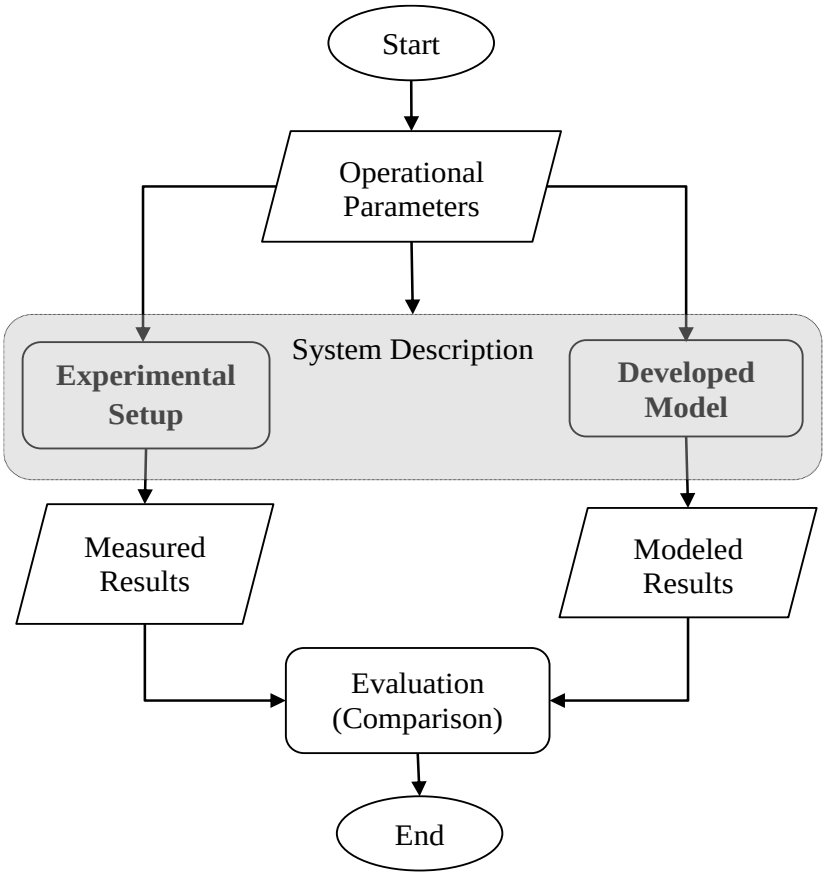

Figure 3.18: Validation path

3.8 Models Parametric Analysis

The performance of thermodynamic systems (such as thermally activated cooling and power) is largely dependent on the suitable selection of the operational parameters. Therefore, assessment of the system performance and its optimization

have always been based on investigation of the influence of each of the system's key parameters (Lee and Strand, 2008). The effects of air flow rates, pipe dimension (length, diameter, and thickness) on heat transfer between the ground buried pipes were investigated by (Moncef and Kreider, 1996; Ahmed *et al.*, 2016) through the parametric analysis.

In this study, the modelled and experimental soil cooling had majorly taken into consideration, the effects of chilled water flow rates. The chilled water temperature had been kept within a range, while the climatic effect (in the form of ambient air temperature due to solar radiation) could not be controlled. Parametric study is further conducted on the cooling process using the response surface methodology (*RSM*) of the Design Expert® software version 10, for further analysis. Response surface methodology (*RSM*) comprises of mathematical and statistical analysis tools, suitable for defining effects of independent parameters (either separately or in combination) on the output (Hariharan *et al.*, 2013). With *RSM*, performance evaluation can be made at intermediate levels that might not have been experimentally studied (Hariharan *et al.*, 2013; Rout *et al.*, 2014). Central composite design (Custom) of the *RSM* was used in this study with 20, and 23 number of (totally randomized) runs to analyse the parameters for the soil cooling and combined plant models, respectively. The key parameters (regarded as factors) and their effects (regarded responses), as well as their types and levels are shown in Table 3.6. Further results of the parametric analysis are presented in Chapter 4.

Table 3.6: Factors and responses for system parametric analysis

Process	Factors				Responses
	Name	**Type**	**Level**	**Range**	
Soil Cooling	Ambient air Temperature	Continuous	N/A	(25–35) ℃	Soil Temp (T_s)
	Chilled water Temperature	Continuous	N/A	(1.5–8.5) ℃	
	Flow rates	Discrete	4	(0.24–0.6) kg/min	
Combined Plant	Boiler's Temperature	Discrete	8	(65–65) ℃	W_t, W_{sp}, Q_{loss}, $COP_{cooling}$, ORC_{eff}, $COP_{overall}$,
	Boiler's pressure	Discrete	4	(21–21) bar	
	Working fluid mass fraction	Continuous	N/A	0.3–0.7	

The analysis of variance (ANOVA) was performed to assess the interaction between the factors and responses of the system. Probability (p-value) and Fisher variation ratio (F-value) were used to determine the significance of the models, and specifically, a p-value not more than 0.05 is desirable (Rout *et al.*, 2014; Puri *et al.*, 2002; Hariharan *et al.*, 2013; Gontard *et al.*, 1992), which indicates 95 % confidence interval. The qualities of fit of the models (F-values and P-values) were however checked to determine the model significance. Furthermore, the diagnostic plots of the models interaction were observed to check if the model responses are within the set boundary; for this, LAMBDA values within the required minimum and maximum values are desirable. Additional results of the parametric analysis are contained in Appendix G.

3.8.1 Soil Cooling Analysis

In the soil cooling experiments (as described in the previous sections), the effects of selected chilled water flow rates over a range of temperatures were studied. However, ambient air temperature also plays an important role on soil temperature and

affects the performance of chilled water application on the cooled soil temperature. The effects of variation in values of these chilled water flow rates and temperature, and that of ambient air temperature are further studied on the performance of the chilled water application for soil cooling. Using the developed model, the effects of variation in experimental values of the chilled water temperature and flow rates, as well as the temperature of the ambient air were examined on the soil temperature. This was done to determine the most relevant factor that affects the cooled soil temperature and the level of significance of the effect.

3.8.2 Combined Plant Analysis

Parametric analysis plays an important role in the performance enhancement of Rankine cycle and sorption cooling systems and has been applied for such in various studies (Tamm, 2003; Tamm *et al.*, 2004; Padilla *et al.*, 2010; Yang *et al.*, 2017; Sukri *et al.*, 2016). The performance investigation through the parametric analysis in this study is presented in the following sections (3.8.2.1 – 3.8.2.3) using the "Response Surface Methodology" of the Design Expert that allows simultaneous analysis of more than one factors and responses; unlike the conventional *"One-Factor-At-Time"* (OFAT).

3.8.2.1 Working Fluid Boiling Temperature

The performance of a thermally activated system is highly dependent on the temperature available for its activation. This influences the performance of the sorption cooling system, the Rankine power cycle as well as the combined cycle systems. In this study, investigation is carried out on the sensitivity of the system to change in working fluid boiling temperature from the design value.

3.8.2.2 Turbine Inlet Pressure

The effect of pressure differential due to expansion through the turbine is normally felt on the Rankine power efficiency. However, since the plant in this study is a combined cycle of Rankine and absorption cooling, the resultant effect of system sensitivity to turbine inlet pressure is investigated on the combined cycle.

3.8.2.3 Working Fluid Mass Fraction

The cycle makes use of multicomponent working fluid (refrigerant and absorbent) for which the composition is very sensitive to its thermodynamic properties at each stage of the cycle, and ultimately on the general performance of both the power and the cooling systems. The study investigated the sensitivity of the combined cycle performance with respect to a range of NH_3 proportion in NH_3-H_2O mixture.

3.9 Project Analysis with RETScreen®

Decision making on Renewable Energy Technologies (RETs) remains critical to implementation of clean energy projects because, the prove that a similar technology is cost-effective and reliable in some locations may not be enough to establish same in other locations (Ackom, 2005). Although not intended to be a detailed engineering design tool (Ackom, 2005), RETScreen software is purposely developed for pre-feasibility and feasibility studies of RETs projects at the initial stage. The software is a stepwise program (as shown in Figure 3.19) and contains data tools that run on Microsoft Excel spread-sheet with various inbuilt project models that include; (i) Energy efficiency measures, (ii) Power, (iii) Power-multiple technologies, (iv) Heating, (v) Cooling, (vi) Combined heating and power, (vii) Combined cooling and power, (viii) Combined heating and cooling, (ix) Combined cooling, heating and power, and (x) User defined models.

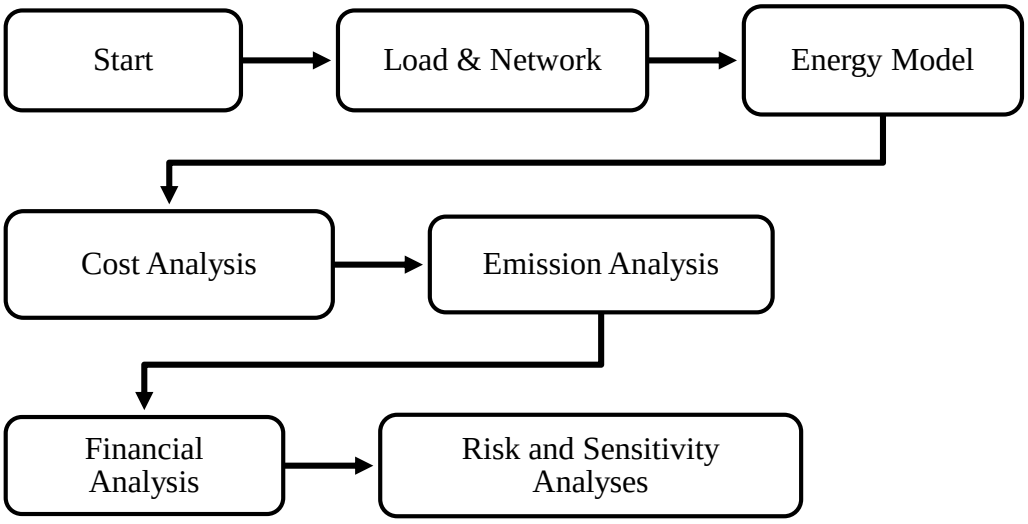

Figure 3.19: RETScreen® application paths

Each of the project models can be implemented on a number technologies or grid options, depending on the type of project being analysed. Methods of analysis can also be basic or detailed, depending on the intended objectives of the analysis. The stepwise approach used in the project economic analysis in this study is contained in the following sections (3.9.1–3.9.6).

3.9.1 Project Information and Site Reference Conditions

RETScreen contains global data; therefore the first stage of the project analysis is usually the project information and site conditions. These include project name and location, project type and analysis method (method 1 or 2), language, currency and measurement units (metric or imperial), climate data location, and the site heating value. The heating value can be higher or lower value (HHV or LHV). However, HHV is used only in Canada and USA while LHV is recommended for the rest of the world (RETScreen, 2005). As such, in this project, LHV is used while method 2 and Ringgit Malaysia (MYR) were used for the full analysis of the project with respect to its location. Heating value refers to the amount of heat that available from complete

combustion of fuel; measured as a unit of energy per unit mass (kJ/kg) or volume of substance (J/mol).

3.9.2 Base Case Load and Network

The load and network section of the analysis looks into the base case cooling load (base load and peak load) with respect to the floor/soil bed area (m^2) to be cooled as well as fuel consumption (kWh) and rate (RM/kWh). Also considered at this stage is the power source and technology required for the power generation as well as the costs of generating the power to be used for the cooling system under the base case. The proposed system characteristics were also analysed with further details in Appendices H.

3.9.3 Energy Model

This is the part of the analysis containing the 'Solar Resource and Heating Load calculation worksheets that is used for calculating the passive solar design annual energy production with respect to system specifications, and site location and conditions.

3.9.4 Cost Analysis

The cost contents of the project economic analysis include the initial costs and annual costs. The initial cost which is also referred to as capital cost (Abdullah and Hieng, 2010) or total investment cost takes the major share of the total project cost in this study. It usually comprises of the costs associated with; project feasibility study, project development, engineering design, procurement of components and spare parts, and miscellaneous expenses.

On the other hand, the annual cost (annual operating cost) refers to the cost incurred during the service life of the project. This is expressed by (Abdullah and Hieng, 2010) as;

$$C_{op} = C_{fc} + C_m \tag{3.70}$$

Where C_{op} is the annual operating cost, C_{fc} is the annual fuel cost and C_m is the annual maintenance cost of the project.

In this project, the initial cost is based on the quotation obtained from the supplier. Meanwhile, procurement of parts and engineering design form the major parts of the initial cost. This is because of the project is a mini type and falls under those for which feasibility and development costs can be ignored (RETScreen, 2005). It is recommended that the feasibility should be between 1 % and 5 % of the total project cost, and for smaller project, the proponent can go directly to engineering stage as the development and feasibility costs may not be justified due to the size of the project. Further details of the project cost are shown in Appendix H.

3.9.5 Emission Analysis

International Energy Agency (IEA) statistics showed that about 42 % of the total global CO_2 emission came from burning of fossil fuels purposely for electricity and heat supply in the year 2011 (Mansouri Majoumerd and Assadi, 2014). Meanwhile, one of the objectives of the application of RETs systems is to reduce the carbon footprints in the atmosphere for safe and healthy environment (Leavell, 2010; Kalkan *et al.*, 2012; Khan and Pervaiz, 2013). Therefore, in dealing with economic analysis of RETs systems, the impact on environment is always considered and compared with a base case that uses non-renewable energy systems (Smith *et al.*, 2013). In this study, the emission analysis is done based on the fuel type used to power the cooling system and on the GHG emission reduction from the system implementation.

The model gives the emission reduction summary for both power and cooling systems of the proposed case in tons of carbon dioxide (tCO_2) equivalence and net annual GHG emission is calculated and quantified in terms of number of barrels of crude oil (not consumed) for implementing this project instead of the base case. More details are contained in appendices H.

3.9.6 Financial Analysis

This section of the economic analysis is concerned with the selection of operating financial parameters that allow the calculation of; project cost and savings, annual income, financial viability, yearly cash flows, and cumulative cash flows graph. The financial parameters include but not limited to fuel/electricity cost escalation and general inflation rates, with common values between 2 and 3 % (RETScreen, 2005), discount rate (that is used to calculate annual-life-cost savings), incentives and grants, debt ratio (0–90 %), interest rate on debt (%), term of debt (year), debt payment plan, effective income tax (%), depreciation method, rate (%) and period (year), and the proposed project life that depends on the prevailing circumstances.

In this study, the project cost and savings contained in the financial analysis worksheets were calculated based on inputs from the cost analysis which are mainly the engineering design, procurement of parts and miscellaneous expenses. Annual income basically contains income accrued from electricity cost savings and export, sales of proceeds from the cooled soil, and GHG reduction resulting from using this RETs applications. Financial feasibility of the project focuses on the pre and after tax on equity and assets, simple and equity payback, annual life cycle saving, and benefit-to-cost (B-C) ratio, that also gives indication of the project viability. Yearly and cumulative cash flows are net cash flows (pre & after tax) over the life of the project in tabular and graphical representation respectively.

3.10 Summary

In this chapter, models had been developed for; (1) the calculation of soil cooling load, (2) the component model and sizing of the combined cooling and power plant to optimally deliver the cooling required to overcome the load of a particular size of the soil bed, and (3) the piping requirement and chilled water flow rates. Computer programming codes (in C#) had been developed for implementation of the model calculations. Based on the developed models, an experimental rig were developed and tested to validate the modelled systems. The parametric analyses of the modelled plant have been carried out for its performance assessment, using Design Expert®.

After the technical analysis of the modelled system, the economic analysis had been carried out with RETScreen® Software to assess the financial viability of the developed system for cooling application. This analysis is normally done in comparison of any proposed model with a base case. The results of both the technical and economic analysis are presented in the following chapter.

CHAPTER 4

RESULTS AND DISCUSSION

4.1 Introduction

As highlighted in the previous chapter, the modelled system is made up of soil cooling subsystem and combined plant (for power and cooling) subsystem. The modelling of the plant was preceded by soil cooling load model. The soil cooling model was used to predict the cooling load, which in turn helped in estimating the optimum plant size required to offset the predicted loads (Sharizal, 2006). Based on the model specifications, test rigs, comprising of laboratory-scale soil bed, and an absorption chiller of equivalent capacity were used for the experimental verification of the model. The chilled water application for soil cooling during daytime and the cooling production from the chiller were experimentally studied and their performances were analysed. Results from the experimental rigs were then compared with those obtained from the mathematical analysis for the validation of the developed models. Parametric analyses were carried out on the soil cooling and the combined plant using "Response Surface Methodology (*RSM*)" of the Design of Expert®.

The economic analyses of system, based on the balance of all expenses and income from the developed system have been carried out not only to assess the feasibility of the system, but also its financial viability and emission reductions: this is basically done in comparison with a base case (Sabetia. and Boyaghchi, 2016; Stevanovic, 2016; Boyano *et al.*, 2013). Thus; the base case that in this study is electricity powered system of the same capacity for the same amount of load, and operated under the same condition for the same length of time.

4.2 Modelled Systems Characteristics

With details in section 3.6.2.1 of Chapter 3, the modelled soil cooling load has been analysed with reference to the solar insolation for Kuala Lumpur–Subang Station, obtained from the National Aeronautic and Space Administration (NASA); as contained in the Appendix A. Other parameter values involved in the analytical models calculations were obtained from published literatures.

Sorption cooling systems are usually rated based on the nominal cooling capacity (Tozer *et al.*, 2005; Wang *et al.*, 2011; Yin *et al.*, 2013; Thongtip and Aphornratana, 2017), also referred to as refrigeration capacity. This is used in most cases to determine the working fluid mass flow rate of the system with known operating temperatures and pressures. The present cooling subsystem consists of a 50 W rated cooling capacity vapour absorption chilling plant. In modelling the plant, the thermodynamic properties of the working fluids (from REFPROP) were made use of. The working fluid is Ammonia-water mixture with 0.35/0.65 (NH_3/H_2O) initial composition. Soil cooling analysis was based on the effects of chilled water flow rates and temperatures on the soil during the daytime, using four sets of chilled water flow rates.

4.3 Analytical Results

In modelling of combined power and cooling plant, using the mixture of NH_3/H_2O working fluid, it is suggested by (Xu. *et al.*, 2000; Lu. and Goswami, 2002) that; for cycle performance, there exist some optimum operating conditions. In this study of the combined cooling and power cycle, optimum conditions were selected based on similar cycles (published in the literature) for the combined cycle and/or individuals of the ORC and VAR cycles. Based on the selected conditions, the thermodynamic properties of the working fluid at the major stages of the modelled cycle plant were used in the model calculations. Modelling of the combined plant was carried out with respect to operating pressures, temperatures, and working fluid

composition (Appendix B) to determine the key parameters of the combined plant. These parameters were fixed (with some factors of safety) and used to develop experimental rig for both the soil cooling and the chilled water production subsystems (Table 4.1).

Table 4.1: Initial parameters

Parameter	Designed Value
Working fluid vaporizing temperature (T_{-r})	80 ℃
Pressure at the boiler	16 bar
Turbine outlet/condenser inlet pressure	10 bar
Evaporator inlet pressure	2 bar
Working fluid (HN_3/H_2O) mass fraction	0.35/0.65
Soil bed geometry	$0.55\ m \times 0.45\ m \times 0.35\ m$
Pipe (earth tube) dimension	l(*1.0 m*), Θ(*0.02 m*), and t*(0.0016 m*)

4.3.1 Mass and Energy Balance across the System Components

C# programming codes were developed for the implementation of the modelled systems calculations. The calculated parameters for the model system include the mass and energy balance across all the major components at the designed temperatures and pressures across such components. However, it should be noted that the system is considered at steady state, so the results presented here are at steady state condition. Energy balance analysis for the combined plant was carried out with respect to the thermodynamic properties of the fluid at each state of the modelled plant with 50W cooling capacity, operating within the specified stages. Using REFPROP software developed by the National Institute for Standard Technology (NIST) the calculated values of the energy balance for the combined system are shown in Table 4.2.

Table 4.2: Calculated properties of combined system

System property	Calculated values
Boiler heat (Q_b)	94.6 W
Heat lost to Turbine shaft (Q_t)	4.16 W
Turbine gross work (W_t)	3.56 W
Condenser's heat rejection (Q_c)	51.6 W
Absorber heat rejection (Q_{abs})	80.8 W
Heat exchanger (Q_{hx})	7.97 W
Working fluid pump (W_{sp})	0.13 W
NH_3-H_2O flow rate $(\acute{m}_{sol})$	1.21×10^{-4}kg/sec
NH_3 flow rate $(\acute{m}_r)$	4.26×10^{-5} kg/sec
H_2O flow rate $(\acute{m}_w)$	7.91×10^{-5} kg/sec
$COP\_{cooling}$	0.549
Heat source (Q_u)	99.5 W
Effective collector size (A_c)	0.3 m^2
Soil load (Q_{load})	201 W/m^2
Area of Soil bed	0.25 m^2
Soil cooling efficiency	86 %

The performance of the modelled plant is centred around; the turbine gross power and efficiency (W_t and η_{ORC}), the cooling coefficient of performance ($COP_{cooling}$), the work done on solution pump (W_{sp}), the overall *COP*, and the heat loss (Q_{loss}) from the system, with reference to the system boundary in Figure 3.11.

Based on plant nominal capacity and initial parameters, 95 W of heat energy would be required to vaporize the working fluid; requiring an evacuated tube collector of about 0.3 m^2 effective area for solar energy collection. This is optimally required for running the plant to offset the cooling load of a 0.25 m^2 area of soil bed with reference to the project location and climatic conditions.

Analytical values from NIST software, for the energy balance with reference to equation 3.46 shows that the system heat loss accounts for 8.6 % of the total energy input to vaporize the working fluid. A gross power of 3.56 W could be obtained from the turbine, which is equivalent to an efficiency of 7.98 %. Cooling and overall *COPs*

of 0.549 and 0.566, respectively, are achievable from the modelled system based on the initial specifications and operating parameters.

4.3.2 Cooling Production

The evaporation taking place at condition 4–5 of the Figure 3.9 is caused by exchange of heat between the working fluid (NH_3) and the chilled water flowing through the evaporator space (Baniyounes *et al.*, 2013) before the absorption of the working fluid by the low-pressure absorbent in section 5–6 of the same Figure. Temperature of the chilled water is designed to vary between 5 ºC and 10 ºC, with the minimum temperature corresponding to the maximum temperature of the refrigerant at the exit from the evaporator space. Flow rate of the chilled water obtainable from the evaporator is determined using equation (3.35). An average flow rate of 0.282 kg/min of chilled water could be obtained from the evaporator if inlet chilled water temperature is maintained at 10 ºC.

4.3.3 Daytime Soil Cooling

Since the modelled systems (soil load and plant capacity) are based on the nominal values of load and plant cooling capacity, the performance of the modelled cooling system is affected by variations in the peak cooling load during the daytime. It is also considered that in the absence of external heat source (solar radiation heat) on the soil, its temperature gradient decays over time, leading to a thermal equilibrium within the soil bed ($\Delta T = 0$, thus; $Q_{cond} \approx 0$); bringing the conductive heat flux close to zero. Thus the soil cooling analysis presented in this study is basically focused on the daytime, during which the thermal load affects the soil temperature. Soil cooling efficiency is calculated as;

$$\eta_{Soil\ Cooling} = \left[1 - \frac{(Peak\ Load) - (Cooling\ Capacity)}{(Peak\ load)}\right] \times 100 \qquad (4.1)$$

Furthermore, using the solar radiation data from NASA (as contained in Appendix A, soil temperature was studied for the period of 7:00hr and 19:00hr of the day within which the solar radiation heat affects the soil. The key factor affecting soil temperature is the soil solar radiation imposed load which also varies with the time of the day. Therefore, with respect to the soil bed size in this study, chilled water flow rates between 0.06 kg/min to 0.6 kg/min were selected to for the cooling process and their effects were observed for optimal performance in offsetting the load, using equation 3.45. The cooled soil temperature profile, shown in Figure 4.1 indicates the effects of the mid-day peak load on the cooling performance based on the selected chilled water flow rates. It however shows that the performance of the soil cooling with the selected chilled water flow rates is affected by daytime peak load.

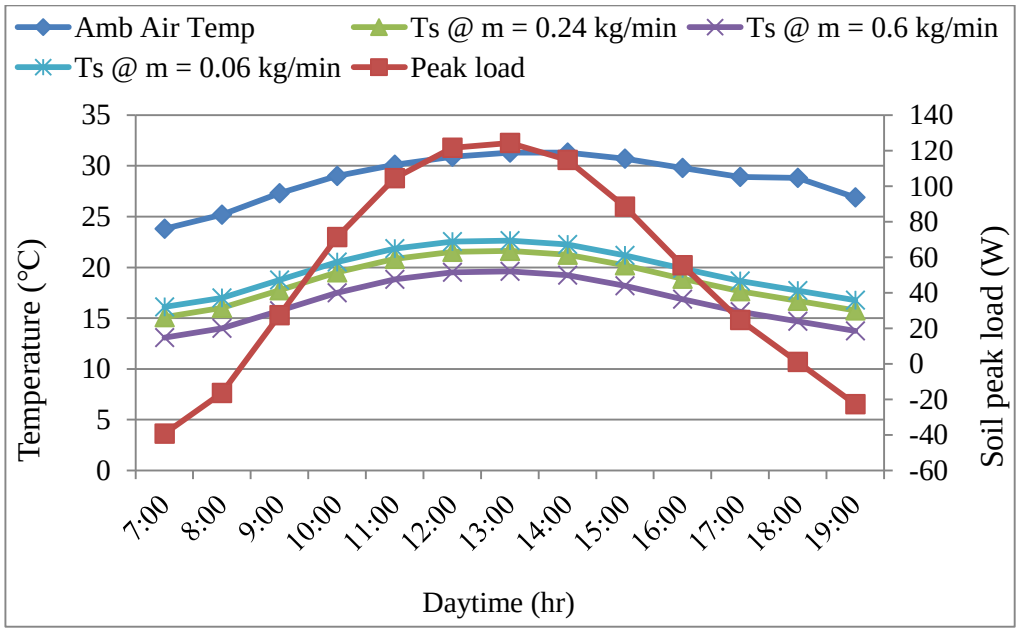

Figure 4.1: Modelled soil temperatures profile during daytime at different chilled water flowrates

4.4 Experimental Results

4.4.1 Cooling Production

Experimental runs were carried out on the investigated chiller by taking the temperature profiles of its working fluid across its components to determine its steady state energy balance and performance characteristics. Chilled water production was achieved from the chiller's evaporator, whose cooling rates were used to determine the chilled water production rates as shown Figure 4.2.

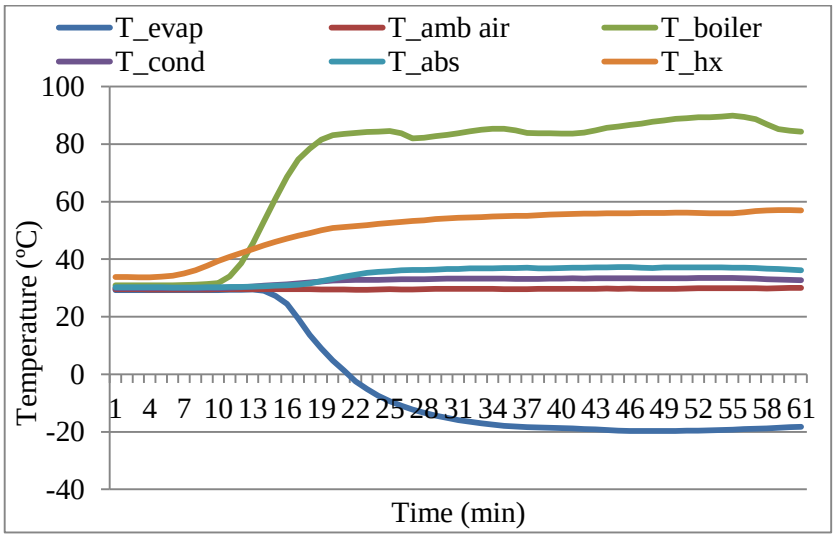

Figure 4.2: Absorption chiller's operating temperature profile

In all the experimental runs, condenser temperature varied between 30 ºC and 35 ºC whereas the evaporator temperature was observed to range between -10 ºC and -24 ºC with the average steady state value of about -18 ºC (Appendix F); corresponding to working fluid saturated vapour of 2 bar.

It was observed that the cooling effects in the evaporator commenced when the working fluid temperature reached about 61 ºC in the boiler. At this point, the evaporator temperature reduced from ambient value of 29.44 ºC to 27.28 ºC. With continuous heating, the steady state was reached at about 85 ºC of the working fluid

temperature; corresponding to evaporator, ambient air, condenser, absorber, and solution heat exchanger temperatures of -19.8 ºC, 29.7 ºC, 33.3 ºC, 37.1 ºC, and 56 ºC, respectively. The cycle thermodynamic properties at these stages were used for the analysis of the system.

To determine the chilled water production rate, the evaporator operating characteristics was analysed. By integrating (conceptual) chilled water tank (with sets of inlet and outlet chilled water temperatures) with the evaporator, the mass flow rates of the chilled water were determined through the heat exchange between the chilled water and the evaporator. Chilled water flow rates were determined using equation 4.2, given as;

$$\acute{m}_w = \frac{\acute{m}_r C_{pr} \Delta T_r}{C_{pw} \Delta T_w} \tag{4.2}$$

Where $\acute{m}_r$ and $\acute{m}_w$are the respective flow rates of refrigerant and chilled water, C_{pr} and C_{pw} are the respective heat capacities of refrigerant and water, and ΔT_r and ΔT_w are the respective change in refrigerant and water temperatures due to heat exchange in the evaporator

From Figure 4.3, the experimental chiller gave an average chilled water flow rate of 0.3 kg/min (18 kg/hr.), keeping the chilled water temperatures at the exit and inlet of the chiller are at an average of 5 ºC and 10 ºC, respectively. The chilled water and refrigerant exit temperatures from the evaporator were assumed equal.

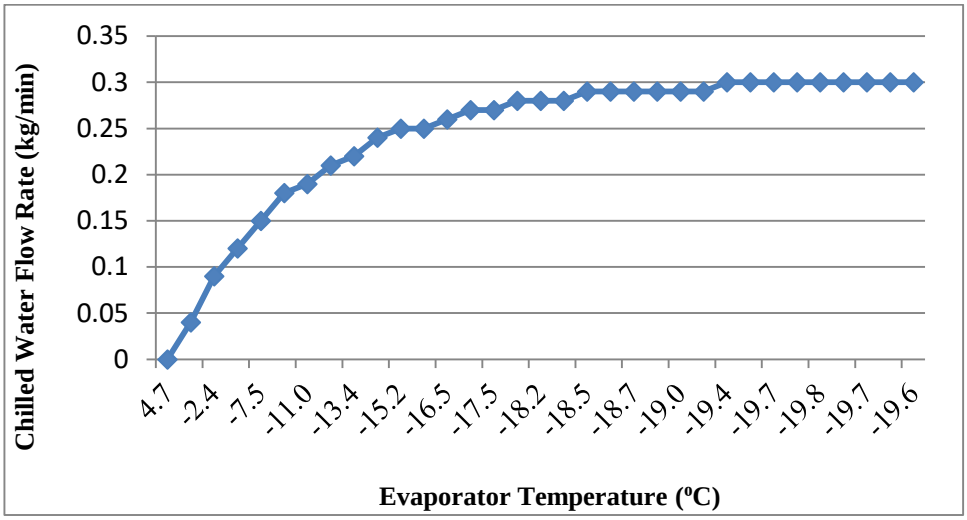

Figure 4.3: Calculated chilled water flow rate set at 5 ºC

However, at its steady state when the boiler temperature was 85 ºC, the energy balances across each of the components were determined as shown in Table 4.3. This gave chiller's coefficient of performance of 0.56. The mass flow rates of the working fluids were determined based on the chiller's nominal capacity and working fluid mass fraction.

Table 4.3: Calculated chiller energy balance at steady state

Components	Temperature	Energy Balance
Boiler	85	90.06
Condenser	33	55.62
Evaporator	-19	50.0
Absorber	34	85.0
Bubble pump	85	0.24

4.4.2 Soil Temperature Profile

To cool the soil to the set range of temperatures, chilled water temperatures to the soil bed were maintained between 2.5 ºC and 10 ºC, while the flow rates were varied from 0.24 kg/min to 0.6 kg/min. The effects of the chilled water flow rates were observed on the cooled soil and compared with that of the control soil bed. For

offsetting the cooling load of the soil bed in this study, Figure 4.4 (A – D) show that the selected flow rates fall within the required rate. While the chilled water flow rate of 0.24 kg/min (Figure 4.4 A) was only sufficient in the morning and evening periods (during minimum load), 0.36 kg/min and 0.48 kg/min were observed to be optimally sufficient during the whole study periods. However, higher chilled water flow rate (0.6 kg/min) was only be required during the mid-day peak load, which corresponds to 10:00hr and 16:30hr clock time of the day as shown in Figure 4.4 D. During this period, the cooling system may be required to operate at maximum capacity.

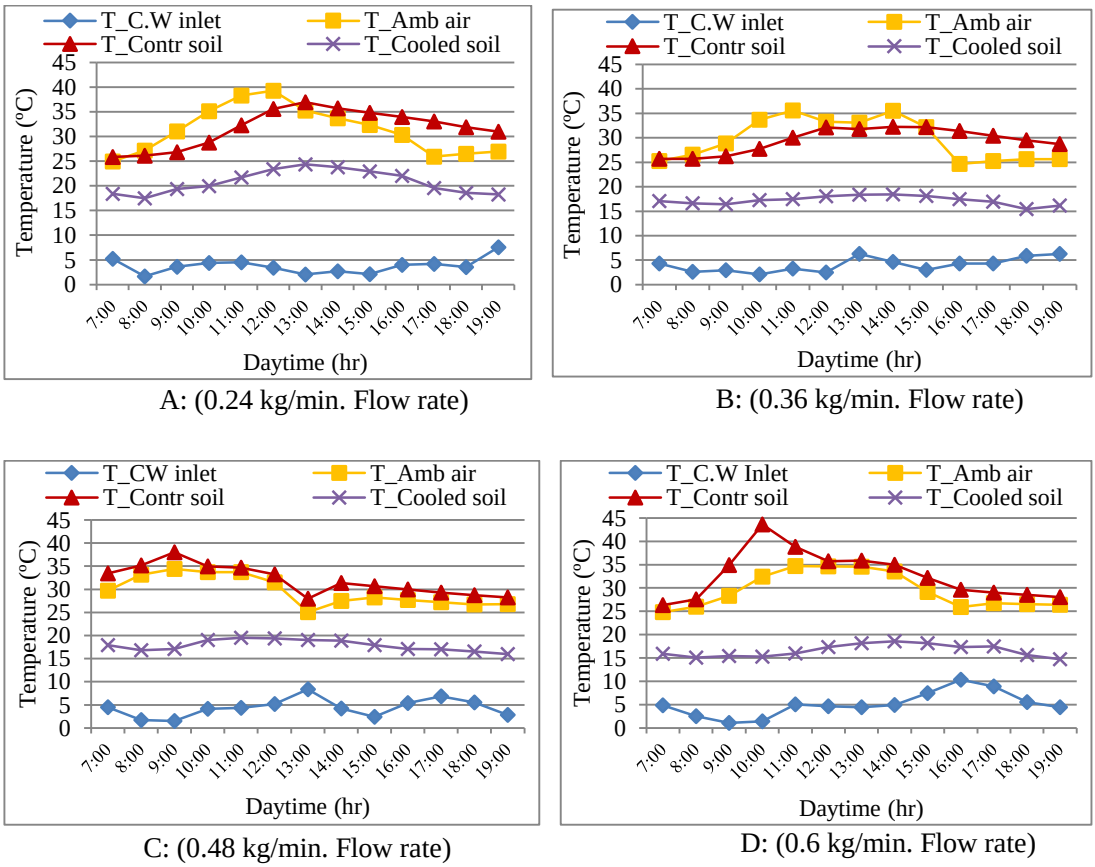

Figure 4.4: Experimental soil temperature profiles at different chilled water flow rates

However, besides the chilled water flow rates and temperatures, the effects of daytime weather condition were observed on the soil temperature profile during the mid-day, when the air temperature and solar radiation were at the peak. For this, analyses of factors and responses were conducted, using *RMS* of the "Design Expert®,

to study the extent of the effects of chilled water and ambient air temperatures, and the sets of chilled water flow rates.

It was also observed that chilled water pumping may not be required at night-time: all the T_s in Figure 4.4 (A-D) were at lower temperature values, irrespective of the chilled water temperature. This is due to the lack of additional load at night-time. Depending on the daily climatic condition, the set of flow rates selected for the cooling process were found to be suitable to achieve the set soil temperature if appropriately optimized with respect to the daytime ambient conditions. Furthermore, analysis of the heat removal capabilities of the selected flow rates (as shown in Figure 4.5) indicated that; to achieve the soil temperature of 18 ºC±2, the optimum chilled water flow rate falls between 0.36 kg/min and 0.48 kg/min. These flow rates would be sufficient to keep the temperature of the soil bed in this study at the set range during the peak load. It also indicated that flow rates beyond 0.48 kg/min may be is not required during the peak load or at any time of the day.

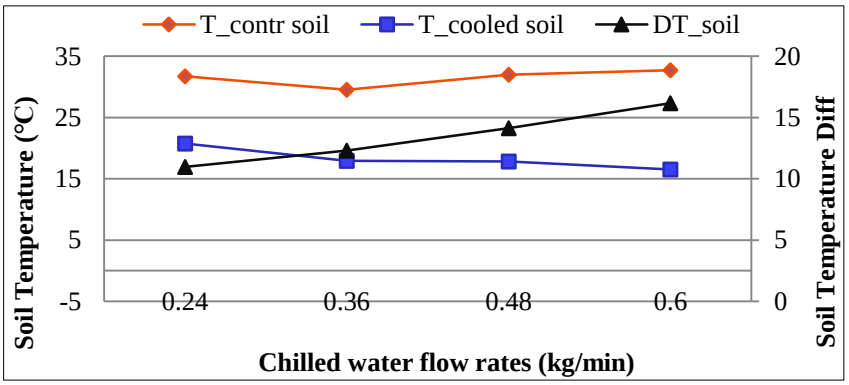

Figure 4.5: Chilled water flow rate heat removal capacity

4.5 Models Comparison and Validation

To check the reliability of the model, variations between the analytical results and measured values from the experiment have been quantified using the percentage errors and standard deviation under the same conditions.

4.5.1 Modelled and Experimental Soil Cooling Rates

This section of the thesis is focused on the comparison of the daytime soil temperature profiles. The comparison is based on the results of the analytical and experimental models soil cooling processes, using the same chilled water inlet temperatures and flow rates. Figure 4.6 (A–D) show the comparison of experimental and modelled soil cooling temperature profiles with different chilled water flow rates and temperatures, and at different ambient air temperatures.

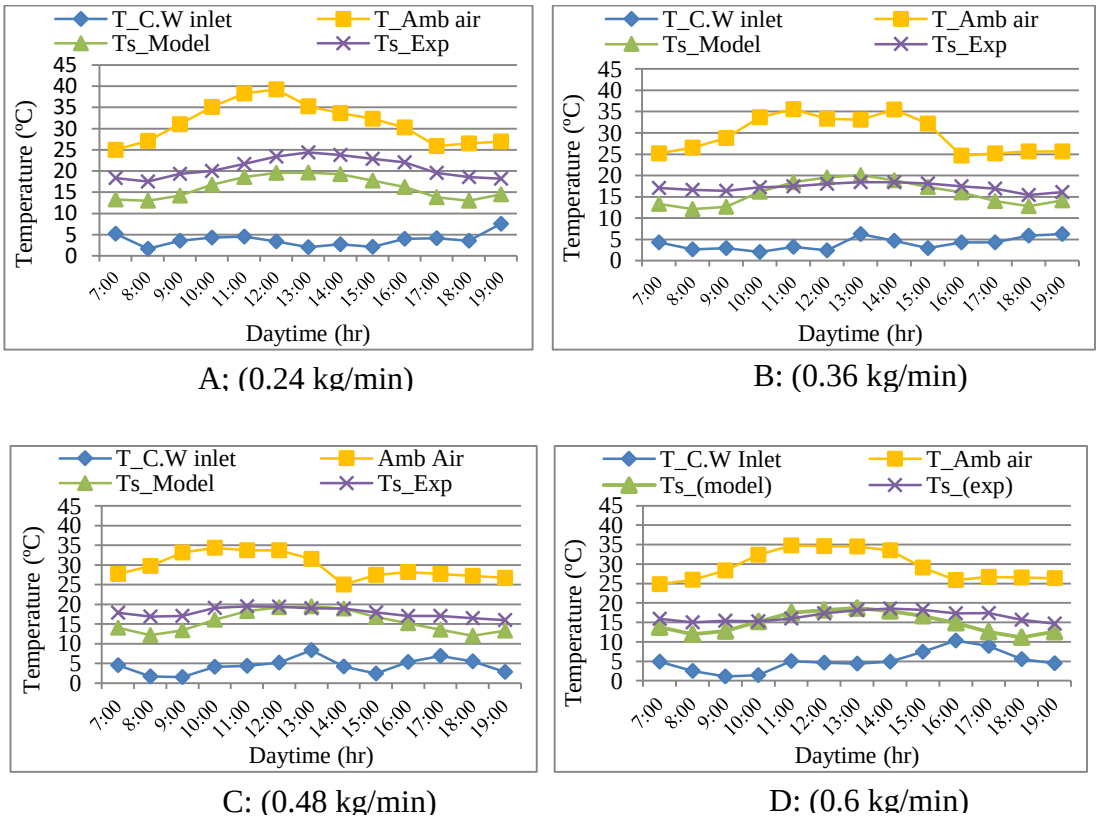

Figure 4.6: Experimental and modelled soil temperature profiles for different chilled water flow rates

Both the experimental and modelled soil temperatures were observed to respond to chilled water flow rates and temperatures, and the ambient conditions of each of the experimental days. The modelled soil temperatures in Figure 4.6 D were however lower than the experimental values. This is due partly to some simplification assumptions in the modelling and the use of historical climatic data for the peak load

analysis, while the ambient air temperature during the experimental day was very high. However, Figure 4.7, which contains the average values of all data shows that cooled soil temperatures, based on the model equations and experimental test, are reasonably close with an average values of the standard deviation and percentage error of 1.75 and 14.24 %, respectively (Table 4.4).

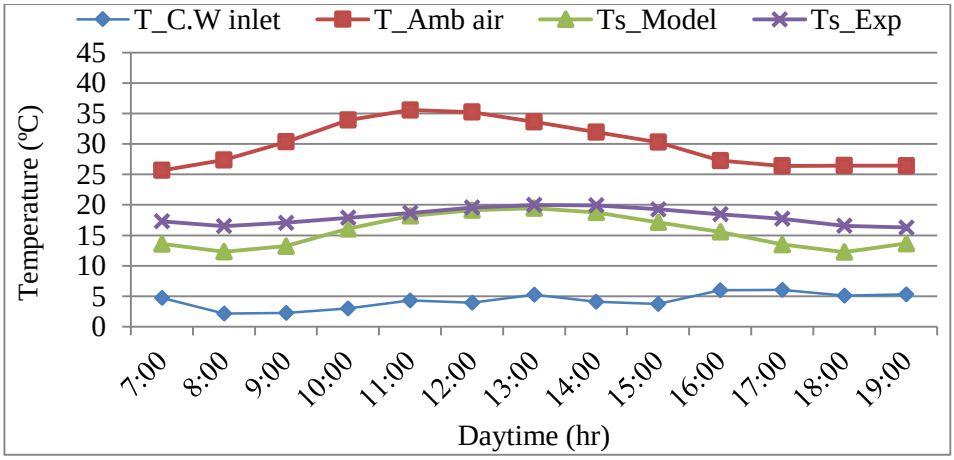

Figure 4.7: Average values of experimental and modelled soil temperature profile

An important observation from Figures 4.4 to 4.6 is that, soil temperatures in soil beds were not only affected by the chilled water flow rate but also by the chilled water inlet temperature and daytime ambient air temperature. As such, following section (4.7.1) is concerned with analysis of the sensitivity of soil temperature to variation in each of these factors (chilled water temperatures and flow rates, and ambient air temperatures).

Table 4.4: Experimental and model soil temperature comparison

Time (hr)	C.W Inlet Temp (°C)	Soil Temp (°C)		% Error	STDev
		Exp.	Model		
7:00	4.74	17.31	13.61	21.39	2.62
8:00	2.13	16.50	12.32	17.53	2.96
9:00	2.28	17.05	13.24	27.76	2.69
10:00	3.00	17.88	16.06	25.97	1.29
11:00	4.29	18.65	18.18	13.89	0.33
12:00	3.92	19.55	19.15	6.98	0.28
13:00	5.27	19.98	19.47	4.18	0.36
14:00	4.12	19.92	18.76	2.27	0.82
15:00	3.74	19.28	17.14	2.69	1.51
16:00	6.01	18.47	15.58	7.17	2.04
17:00	6.06	17.72	13.49	12.10	2.30
18:00	5.12	16.55	12.26	18.53	3.04
19:00	5.28	16.26	13.66	24.62	1.84
Average	4.30	18.09	15.61	14.24	1.75

4.5.2 Modelled and Experimental Chilled Water System

The modelled plant and the experimental chiller were compared with respect to their coefficient of performance, using an ideal absorption cooling cycle *COP,* and comparing with the present model using REFPROP. The assessment of the experimental chiller is based on its temperature profile during operation, thus coefficient of performance has been analysed based on system operating temperature using the relation in equation 3.61 (Gordon and Ng, 1995).

Some approximations were made to give room for the analysis of the *COP* of the studied chiller: these include;

i. Once the steady state is reached, absorption chillers normally operate within a close range of boiler temperatures (Gordon and Ng, 1995; Miles *et al.*, 1993), as such, analysis in this study only considered the boiler's

operation between 82ºC and 90 ºC within which the steady state has been established.

ii. Since the chiller was insulated against the ambient environment, losses in the system (from Equation 3.62) that occurred from the air-cooled condenser and absorber have been approximated to 5 % of the heat input.

Meanwhile, it is required that same operating conditions be set for both simulated/analytical and experimental setup for them to be reasonably compared (Massaguer. *et al.*, 2014). Thus the cooling *COP* for the experimental chiller, based on measured data and modelled equation has been considered under the same operating temperature, pressure and working fluid flow rates and mass fraction.

Table 4.5: Experimental & modelled chiller's *COP* comparison

$T_{\_boiler}$ (ºC)	$COP_{\_cooling}$		% Error	STDev
	Exp.	Model		
82	0.528	0.561	5.882	0.023
83	0.507	0.560	9.464	0.037
84	0.500	0.558	10.394	0.041
85	0.493	0.555	11.171	0.044
86	0.489	0.553	11.573	0.045
87	0.497	0.549	9.472	0.037
88	0.506	0.547	7.495	0.029
89	0.513	0.544	5.698	0.022
90	0.520	0.539	3.525	0.013
Averages	0.506	0.552	8.297	0.032

The comparison of the *COP* of the chiller, based on the measured data and model equations using REFPROP, is presented in Table 4.5 with average percentage error of 8.30 and standard deviation of 0.03; showing strong agreement in performances between measured data and modelled data. This shows that the modelled equation with the thermodynamic properties of the working fluid, using REFPROP is suitable to reasonably predict the performances of the system.

4.5.3 Component Analysis of the Experimental Chiller

The analysis of the experimental chiller was done, using the temperature data obtained during its steady state operation. The data were combined with its capacity and other nominal details and used to determine other thermodynamic properties of the chiller. The thermodynamic properties calculated with REFPROP are presented in Table 4.6.

Table 4.6: Calculated working fluid thermodynamic properties of experimental chiller

Components	**Temp (°C)**	**Press (bar)**	**h (KJ/Kg)**	**Internal Energy (kJ/kg)**	**S (KJ/Kg-K)**	**V (m^3/kg)**
Boiler	85	16	1766.60	1607.10	6.0139	0.09969
Condenser	33	16	499.57	496.86	2.0054	0.00169
Evaporator	-19	2	256.23	255.93	1.1431	0.00151
Absorber	34	2	41.40	41.17	0.8446	0.00115
Heat Exchanger	54	16	132.50	130.62	1.1267	0.00117
	P inlet = 16 bar		NH_3:H_2O Ratio = 35:65			

At the selected stages of the chiller, mass and energy balances across the major components showed that the heat gained by the working for vaporization is 90.1 W, while the heat rejection of 55.6 W and 85 W occurred from the condenser and absorber, respectively. Only 0.2 W of energy was expended on the bubble pump to create pressure increase at the boiler section. However, the condenser and absorber are air-cooled; requiring the application of 2.5 W (USB) mini-fan to improve their cooling performances: this increased the electrical energy requirement of the system to 2.7 W. The amount of heat to vaporize the working fluid required an evacuated solar collector (with 95 % thermal efficiency) size of 0.29 m^2, with reference to the available solar radiation at the experimental location.

4.5.4 Combined Plant Analysis

The combined plant is the modified chiller with the integration of organic Rankine turbine, as shown in Figure 3.9. Under the same operating conditions at the boiler with the experimental chiller, the inclusion of the ORC turbine reduced the temperature and pressure of the condenser, thus, the working fluid characteristics at the condenser results in the few observable changes between the experimental chiller and the combined plant. The coefficient of performance of the chiller and the efficiency of the ORC were also determined differently from the conventional approaches. Table 4.7 shows the thermodynamic properties of the combined plant and its working fluid.

Table 4.7: Working fluid thermodynamic properties of combined plant

Stage	**Temp (°C)**	**Pressure (bar)**	**h (KJ/Kg)**	**Internal Energy (kJ/kg)**	**S (KJ/Kg-K)**	**V (m^3/kg)**
Boiler	85	16	1766.6	1607.1	6.0139	0.09969
Turbine	40	10	1671.3	1532.7	5.9383	0.13866
Condenser	25	10	460.82	1498.1	1.8804	0.1286
Evaporator	-19	2	256.23	255.93	1.1431	0.00151
Absorber	34	2	41.402	41.172	0.84457	0.00115
Heat Exchanger	54	16	132.5	130.62	1.1267	0.00117
	P inlet = 16 bar		NH_3:H_2O = 35:65			

Energy expended due to expansion through the ORC turbine is equivalent to 3.535 W of gross power output. As shown in Table 4.8, about 7.52 % reduction in the heat rejection by the condenser (from 55.6 W in the experimental chiller to 51.44 W in the combined plant) was also observed. However, since the working fluid is the same, in type and composition, and the two systems use the same process path, energy balance at other components remain the same.

Table 4.8: Experimental chiller and combined plant energy balance

Components Energy Balance	**Symbol**	**Energy Balance Values**		
		Experimental Chiller	**Combined Plant**	**% Variation**
Boiler heat	Q_b	90.06 W	90.06 W	0
Turbine work	W_t	-	3.54 W	-
Condenser's heat	Q_c	55.62 W	51.44 W	7.52⬇
Absorber heat	Q_{abs}	85.0 W	85.0 W	0
Working fluid pump	W_{sp}	0.24 W	0.24 W	0
System Loss	Q_{loss}	0.3 W	0.32 W	6.25⬆
Cooling Performance	*COP*	0.555	0.578	3.98⬆
ORC Efficiency	η_{ORC}	-	8.825	-
Collector Size	(A_c)	0.3 m^2		

The heat energy losses as well as the coefficient of performance were observed to increase by 6.25 % and 3.98 % respectively. The percentage increase in the *COP* of the combined plant is expected to add to the technical feasibilities of combining the two cycles. The efficiency of the ORC cycle is low, however, power generation is not the main goal of this study. Furthermore, the gross power obtainable from the ORC part of the combined cycle exceeded the chiller's requirements (for pumping and for condenser and absorber air-cooling) by 0.84 W, which is expected to be available for export to the grid.

4.6 Parametric Analysis of Soil Cooling System

Observations of the soil temperatures against the chilled water flow rates in section 4.5.2 indicated that soil temperature is not only effected by the variation in chilled water flow rates but also by the variations in chilled water temperatures and ambient environment. Further analysis of the results of the experimental soil cooling was carried out, using Design Expert® version 10, to assess the extent of the effects of variation of all the three parameters on the cooling performance. Table 4.9 shows the results of the analysis.

Table 4.9: Factors and response on soil cooling analysis

Run	Factors			Response
	Amb Air Temp (°C)	**Chilled water Temp (°C)**	**Chilled water Flow Rates (kg/min)**	**T_s (°C)**
1	31.5	8.5	0.48	19.05
2	25.5	2.5	0.36	17.60
3	31.5	8.5	0.36	19.98
4	31.0	3.5	0.24	19.29
5	25.0	5.5	0.36	18.57
6	35.0	5.0	0.60	17.27
7	31.0	3.5	0.24	19.29
8	25.0	4.5	0.48	17.29
9	27.0	8.5	0.60	17.77
10	31.5	8.5	0.36	19.98
11	35.5	4.5	0.48	18.06
12	31.5	7.5	0.48	18.72
13	35.0	4.5	0.24	19.89
14	29.0	7.5	0.60	17.61
15	25.0	5.5	0.36	18.55
16	25.0	4.8	0.60	16.46
17	26.5	4.5	0.36	18.34
18	35.5	4.5	0.60	17.13
19	29.0	7.5	0.36	19.47
20	25.0	4.5	0.36	18.23

As contained in Appendix G1-1, the overview of the factors-responses correlations of 0.210, 0.256, and 0.572 for ambient air temperature, chilled water temperature, and chilled water flow rate respectively, indicated that the effects of chilled water flow rates is the most significant on cooled soil temperature (T_s), while those of the ambient air and chilled water temperatures are fairly similar in significance. The analysis of variance (ANOVA) performed to find out the interactions of the factors and responses showed that the model is significant. The model has F and p values of 7.09 and 0.0030, respectively, and "*Lack of Fit*" with p and F values of 2.14 and 0.299. The *Lack of Fit* is not significant; indicating that the model is good. The regression equation developed from the ANOVA for the soil temperature (T_s) is given in equation 4.3 as;

$$T_s = 17.777 + 0.073\ (A) + 0.318(B) - 466.693(C) \qquad (4.3)$$

Where A, B, and C are the values of ambient air temperature, chilled water temperature, and chilled water flow rates, respectively.

Model diagnostic plot (Figure 4.8) shows the "Lambda value" of 1.61, regarded as the best, with respect to Lambda's low and high values. However, with 0.42 kg/min flow rate, the cooled soil temperature can be kept below 19.5 ℃, even when the ambient and chilled water temperatures are observably high. Indicating that flow rate beyond 0.42 kg/min may not be required at any time of the cooling process in this particular case (Figure 4.9).

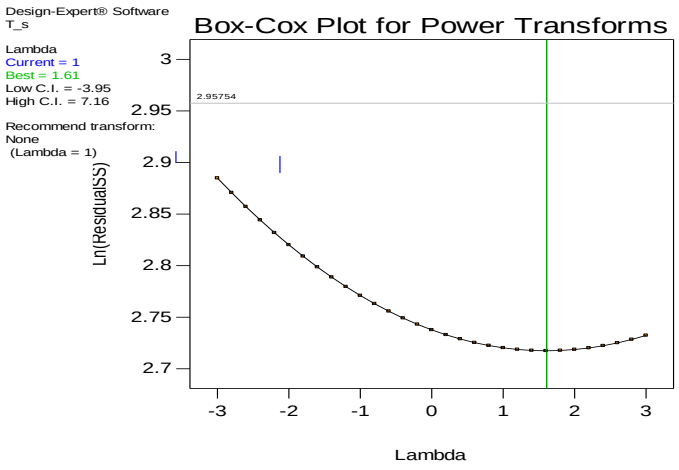

Figure 4.8: Model diagnostics plots for soil cooling analysis

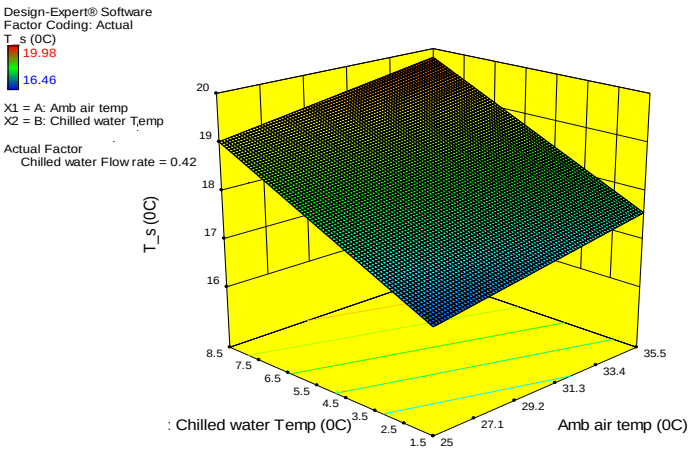

Figure 4.9: 3-D plots of chilled water and ambient air on cooled soil

4.7 Parametric Analysis of Combined Plant

The analysed system in section 4.6.4 was based on the selected parameters of the combined plant. However, the performance of the plant (gross power output, pumping power, heat loss, cooling *COP*, ORC efficiency, and the overall *COP*) can be improved by careful selection of the key operation parameters (Yang. *et al.*, 2015). Furthermore, it has also been reported that, in designing combined systems (such as CHP, CCHP and CCP), determining the best configuration with respect to the thermodynamics of all subsystems and overall energy efficiency is considered very critical (Maraver *et al.*, 2013) right from the initial stage of the project.

In this study, improvement of the plant performance has been carried out through the parametric analysis, using *RSM*. Table 4.10 shows the results of analysis of the key parameters of interest (working fluid mass fraction, boiler's pressure, and working fluid vaporizing temperature). Effects of these parameters on the plant performance are presented in the following sections of the thesis.

Table 4.10: Factors and response on combined plant analysis

Run	Factors			Responses					
	W/F Temp (°C)	**Boiler Press (bar)**	**W/F C.R**	**$W_{\_t}$ (kW)**	**$W_{\_sp}$ (kW)**	**$Q_{\_loss}$ (kW)**	**$COP_{\_cooling}$**	**$ORC_{\_eff}$**	**$COP_{\_overall}$**
1	65	12	0.65	0.00213	0.00008	0.00042	0.677	8.551	0.721
2	85	21	0.45	0.00403	0.00023	0.00644	0.590	10.398	0.628
3	65	15	0.45	0.00212	0.00016	0.00167	0.624	6.578	0.657
4	80	21	0.6	0.00356	0.00018	0.00208	0.649	11.628	0.687
5	90	15	0.35	0.00450	0.00021	0.01227	0.529	9.183	0.566
6	100	12	0.5	0.00542	0.00011	0.00779	0.589	13.466	0.635
7	100	21	0.65	0.00542	0.00016	0.00358	0.643	16.338	0.688
8	85	15	0.65	0.00403	0.00011	0.00185	0.657	13.386	0.698
9	100	12	0.5	0.00542	0.00011	0.00779	0.589	13.466	0.635
10	100	18	0.3	0.00542	0.00029	0.02023	0.475	8.936	0.516
11	80	12	0.3	0.00356	0.00018	0.01145	0.518	7.095	0.553
12	70	12	0.4	0.00260	0.00014	0.00388	0.595	7.118	0.629
13	65	21	0.3	0.00212	0.00035	0.00512	0.555	4.856	0.583
14	90	18	0.55	0.00450	0.00016	0.00455	0.621	12.868	0.663
15	90	18	0.55	0.00450	0.00016	0.00185	0.628	13.386	0.665
16	85	21	0.45	0.00403	0.00023	0.00644	0.590	10.398	0.629
17	100	18	0.3	0.00542	0.00029	0.02023	0.475	8.936	0.516
18	65	15	0.45	0.00212	0.00016	0.00167	0.625	6.578	0.657
19	65	15	0.45	0.00212	0.00018	0.00512	0.623	6.126	0.656
20	65	21	0.65	0.00212	0.00016	0.00034	0.677	8.151	0.710
21	80	15	0.5	0.00356	0.00014	0.00392	0.618	10.310	0.666
22	80	15	0.45	0.00356	0.00016	0.00167	0.625	9.659	0.657
23	85	15	0.65	0.00403	0.00011	0.00185	0.657	13.385	0.688

Factors-responses correlations gave the general overview of the sensitivity of each of the factors on the performances of the plant (as shown in Table 4.11). The model generally showed that, increasing the working fluid vaporizing temperature only favours the ORC part at the expense of the cooling performances. Meanwhile, in this study, cooling is the primary goal, requiring some trade-offs to achieve overall system optimal performance.

Table 4.11: Factors-responses correlations for combined plant

Factor	Response	Correlation
Working fluid vaporizing temperature (W/F Temp)	Gross Power ($W_{\_t}$)	1.000
	Pump Power ($W_{\_sp}$)	0.072
	Heat Loss ($Q_{\_loss}$)	0.579
	$COP_{\_cooling}$	-0.429
	$ORC_{\_eff}$	0.728
	$COP_{\_overall}$	-0.357
Boiler's pressure (Boiler Press)	Gross Power ($W_{\_t}$)	0.066
	Pump Power ($W_{\_sp}$)	0.586
	Heat Loss ($Q_{\_loss}$)	0.005
	$COP_{\_cooling}$	0.017
	$ORC_{\_eff}$	0.102
	$COP_{\_overall}$	0.015
Working fluid mass fraction (C.R)	Gross Power ($W_{\_t}$)	-0.055
	Pump Power ($W_{\_sp}$)	-0.723
	Heat Loss ($Q_{\_loss}$)	-0.738
	$COP_{\_cooling}$	0.904
	$ORC_{\_eff}$	0.606
	$COP_{\_overall}$	0.929

Variations in boiler pressure only significantly affected the pumping power requirements, with no significant effects on other outputs of the plant. This correlates with the studies by (Al-Sulaiman. *et al.*, 2012) in which the effects of variation in turbine inlet pressure was insignificant and it was concluded that ORC turbine could be run on low pressure to save cost.

Variation in the working fluid mass fraction significantly and positively correlated with the cooling performance. It however correlated negatively with heat loss and pumping power, and insignificantly, negatively correlated with the gross power output.

4.7.1 Gross Power ($W_{\_t}$) Sensitivity to Parameter Variation

The model is significant with the p-value of < 0.0001 and a corresponding F-value of 2.2×10^7(as shown in Appendix G2-3); indicating that there is only 0.01 % chance that an F-value of the model could be large due to noise. It also has an insignificant "*Lack of Fit"* of 1.29, and R^2 of 1.00. The regression equation obtained from the ANOVA, for the gross power output is expressed in equation 4.4 as;

$$W_t = -4.525 \times 10^{-3} + 1.080 \times 10^{-4}(A) - 6.276 \times 10^{-6}(B) + 7.830 \times 10^{-5}(C) + 2.587 \times 10^{-8}(AB) - 4.430 \times 10^{-7}(AC) - 2.723 \times 10^{-6}(BC) - 8.369 \times 10^{-8}(A^2) + 1.595 \times 10^{-7}(B^2) + 8.046 \times 10^{-6}(C^2) \quad (4.4)$$

From Figure 4.10, gross power ($W_{\_t}$) is observed to be significantly improved with increase in working fluid temperature alone, and a maximum of 5.5 W could be achieved from the turbine if the working fluid temperature at the boiler is increased to 100 ℃. Since increase in pressure had less significant effect on the power output, it would be more energy efficient to operate this ORC cycle under reasonably low pressure to save cost.

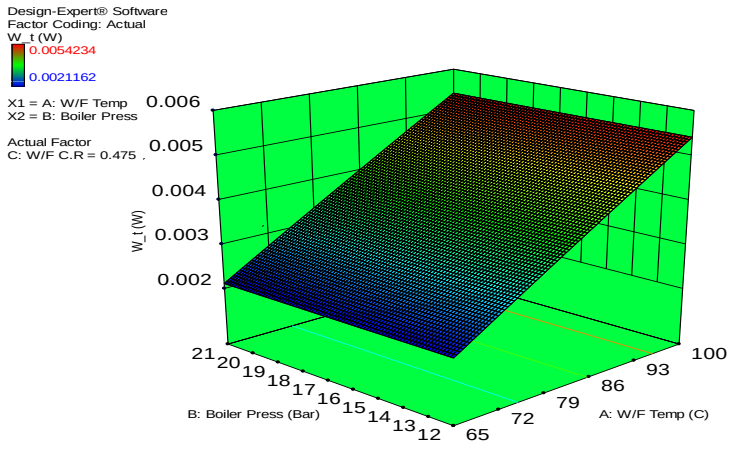

Figure 4.10: Effects of parameters variations on gross power output

4.7.2 Pumping Power ($W_{\_sp}$) Sensitivity to Parameter Variation

The model is significant with the p-value of < 0.0001 and a corresponding F-value of 190.57, meaning that there is less than 0.01 % chance that an F-value of the model could be large due to noise. The mode has a non-significant *"Lack of Fit"* of 0.76, and R^2 of 0.992, indicating that the model term is good. Similarly, the regression equation obtained from the ANOVA for the pump energy consumption ($W_{\_sp}$) is expressed in equation 4.5 as;

$$W_{sp} = 1.702 \times 10^{-4} - 2.848 \times 10^{-6}(A) + 3.563 \times 10^{-5}(B) - 7.567 \times 10^{-4}(C) - 2.972 \times 10^{-8}(AB) + 6.189 \times 10^{-7}(AC) - 2.56 \times 10^{-5}(BC) + 1.806 \times 10^{-8}(A^2) - 2.576 \times 10^{-7}(B^2) + 7.631 \times 10^{-4}(C^2) \quad (4.5)$$

However from Figure 4.11, effect of boiler pressure variation is observed to be more significant on the energy required to pump working fluid, with the least significant effect form the working fluid temperature. Thus, to minimize the pumping power, lower boiler pressure is equally recommended in this case. This will also save cost associated with high pressure operation.

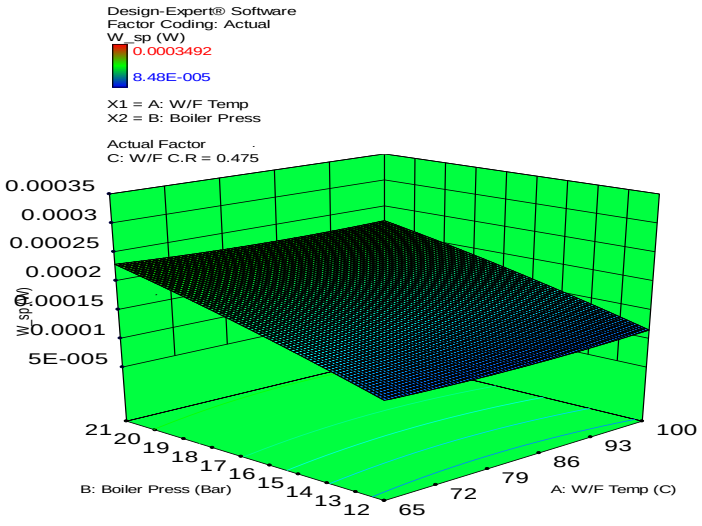

Figure 4.11: Effects of parameters variations on solution pump

4.7.3 Heat Loss ($Q_{\_loss}$) Sensitivity to Parameter Variation

The model is significant, having the p-value of < 0.0001 with a corresponding F-value of 46.86, which also means that there is only less than 0.01 % chance that an F-value of the model could be large due to noise. The model has an insignificant "*Lack of Fit*" of 0.75 and R^2 of 0.970. The regression equation obtained from ANOVA for predicting the plant heat loss ($Q_{\_loss}$) is expressed in equation 4.6 as;

$$Q_{loss} = 8.901 \times 10^{-3} + 3.081 \times 10^{-5}(A) - 1.863 \times 10^{-4}(B) - 0.02432(C) + 6.769 \times 10^{-6}(AB) - 8.915 \times 10^{-4}(AC) + 1.825 \times 10^{-4}(BC) + 3.081 \times 10^{-6}(A^2) - 1.371 \times 10^{-5}(B^2) + 0.06605(C^2) \quad (4.6)$$

The goal here is to reduce the heat loss to as low as reasonably practicable in order to improve energy efficiency. Figure 4.12 shows that operating the plant at elevated working fluid temperature significantly increased the heat loss. In Table 4.12, it was observed that high NH_3 mass fraction contributes to reduction in losses. However, there is always a limit to NH_3 fraction of the working fluid to achieve absorption and for safety requirement.

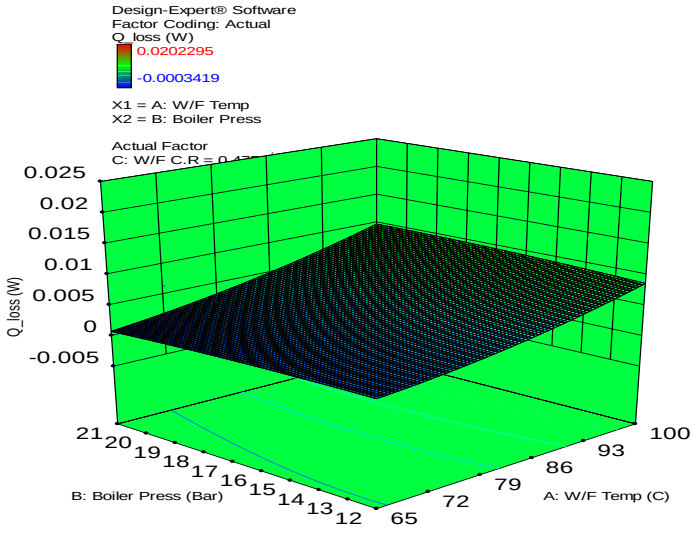

Figure 4.12: Effects of parameters variations on heat loss

4.7.4 Sensitivity on Cooling *COP*

The model is significant with the p-value of < 0.0001 and a corresponding F-value of 1559.41, indicating that, there is only about 0.01 % chance that an F-value of the model could be large due to noise. It also has an insignificant "*Lack of Fit*" of 0.61 and R^2 of 0.999. For the cooling *COP*, equation 4.7 expresses the regression equation obtained from the ANOVA, which can be used to predict the cooling *COP* of the plant.

$$COP_{cooling} = 0.53197 - 3.379 \times 10^{-3}(A) + 1.426 \times 10^{-3}(B) + 0.709(C) - 2.918 \times 10^{-6}(AB) + 3.708 \times 10^{-3}(AC) - 8.232 \times 10^{-4}(BC) + 4.066 \times 10^{-7}(A^2) - 2.349 \times 10^{-5}(B^2) - 0.61498(C^2) \quad (4.7)$$

From Figure 4.13, both of the working fluid temperature and boiler's pressure are observed to have negative effects on the cooling *COP* of the combined plant. Thus it is recommended that plant be operated at moderate temperature and pressure for optimal cooling *COP*.

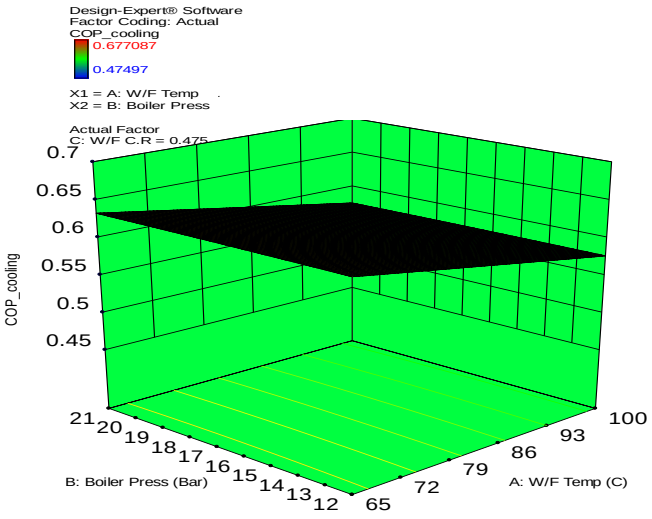

Figure 4.13: Effects of parameters variations on cooling *COP*

4.7.5 ORC Efficiency Sensitivity to Parameter Variation

The model is significant with the p-value of < 0.0001 and an F-value of 359.87. It also has non-significant "*Lack of Fit*' of 1.05, and R^2 of 0.993 which all indicated that the model is good. The ANOVA regression equation for efficiency of the organic Rankine cycle is expressed in equation 4.8 as;

$$ORC_{eff} = -10.228 + +0.290(A) - 0.226(B) - 2.529(C) + 8.321 \times 10^{-4}(AB) + 0.3241(AC) - 0.108(BC) - 1.70110^{-3}(A^2) + 6.246 \times 10^{-3}(B^2) - 7.1142(C^2) \quad (4.8)$$

Figure 4.14 shows that the working fluid temperature significantly affects the ORC efficiency. This could also be observed in Table 4.11 where the response of *ORC* efficiency to factors is highest with the working fluid temperature, with a value of 0.728.

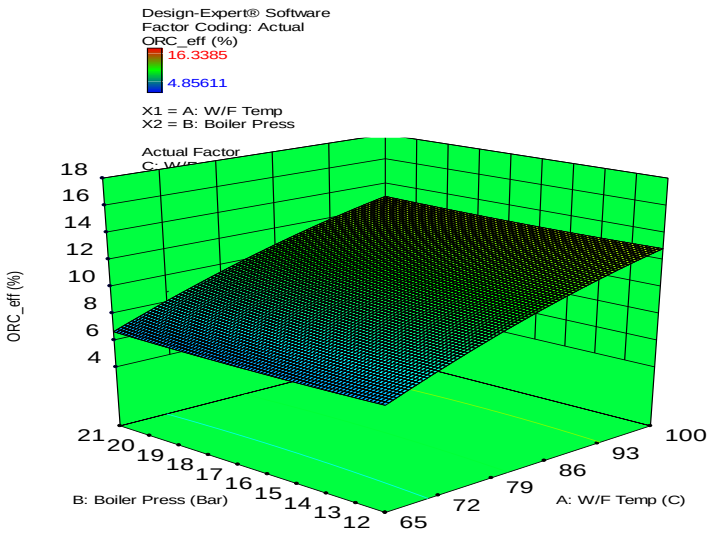

Figure 4.14: Effects of parameters variations on ORC efficiency

4.7.6 Overall *COP* Sensitivity to Parameter Variation

The model is significant, having the p-value of < 0.0001 with a corresponding F-value of 579.26. It also has an insignificant "*Lack of Fit*" of 1.51 and R^2 of 0.996.

The regression equation obtained from the ANOVA for the overall *COP* of the combined plant is expressed in equation 4.9 as;

$$COP_{overall} = 0.5955 - 3.921 \times 10^{-3}(A) - 5.879 \times 10^{-3}(B) + 0.885(C) + 2.358 \times 10^{-5}(AB) + 3.013 \times 10^{-3}(AC) - 2.453 \times 10^{-3}(BC) + 4.862 \times 10^{-6}(A^2) + 1.480 \times 10^{-4}(B^2) - 0.696(C^2) \quad (4.9)$$

For the overall *COP* of the combined plant, boiler pressure was found to non-significant with linear, 2FI, and quadratic relations. Ignoring the non-significant relations in the model, equation 4.8 can be reduced to equation 4.10 as;

$$COP_{overall} = 0.5955 - 3.921 \times 10^{-3}(A) + 0.885(C) + 3.013 \times 10^{-3}(AC) + 4.862 \times 10^{-6}(A^2) - 0.696(C^2) \quad (4.10)$$

Where A, B and C are the working fluid temperature, boiler pressure, and working fluid mass fraction, respectively.

Figure 4.15 shows that overall *COP* generally diminished with increase in working fluid temperature and pressure. However, the F-value of the model ANOVA showed that temperature variation significantly affects the *COP* more than the pressure; suggesting that the plant would be better operated at the minimum temperature and pressure to improve its performance.

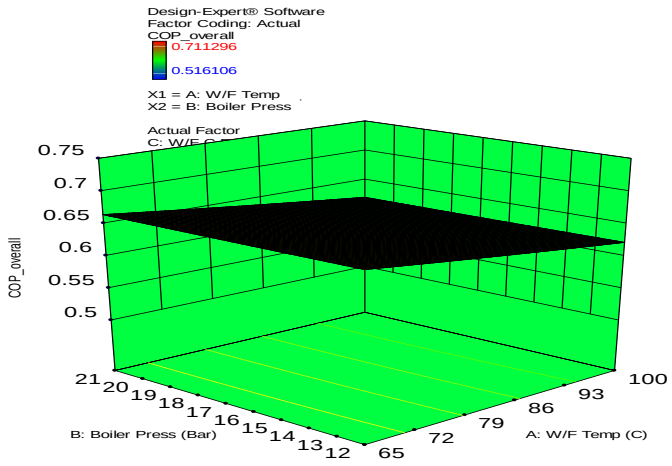

Figure 4.15: Effects of parameter variation on overall *COP*

4.8 Plant Economic Analysis

The 4th objective of this study is to analyse the economics of the developed system in comparison with a conventional system of similar cooling capacity, under the same service conditions.

Economic analysis is carried out not only to assess the financial viability but also to analyse environmental impact of the project in terms of the emission reduction in comparison with the selected base case of a same capacity but using different energy source.

However, since the developed project is less than mini/micro scale, the results of the analyses may not be impressively significant to conclude on its economic performance. As such, 3 additional scenarios were analysed under the same operating conditions so as to observe the developed project in a near practicable sense. The scenarios analysed with their capacities as; (i) 1.76 kW (or 0.5TR) capacity, (ii) 3.5 kW (or 1TR) capacity, and (iii) 7 kW (or 2TR) capacity.

Analyses of all the four scenarios were carried out based on the projects financial (internal rate of return, payback time, net present value, and benefit-to-cost ratio), and environmental (emission analysis) parameters, as contained in Table 4.12 and Table 4.13, respectively. Further details of the techno-economics of the 4 scenarios are contained in appendix H (1-4).

Table 4.12 shows the financial parameters (tax rate, inflation and fuel escalation rate, project life, and discount rates for each of the considered scenarios. The inflation rate applies to both the operating and maintenance costs, and the revenues. An average of RM 2000.00 was used as labour and other inputs costs per hectare (10,000 m^2) of agricultural soil bed per month. Annual vegetable output from one hectare of land, according to MARDI report by Yahya, was estimated to 18.7 tons (18,700 kg) (Yahya, 2001), and 1kg of vegetable had been valued at RM 2.5: this is observed to be reasonably not too optimistic.

Table 4.12: Projects financial summary

Economic Parameter	Items	Plant Cooling Capacity		
		1.76 kW	**3.5 kW**	**7.0 kW**
	1. Soil bed size (m^2)	9.00	18.00	36.00
Fixed Cost (RM)	1. Initial investment	49,350.00	64,525.00	97,650.00
Annual cost (RM)	1. Maintenance & Repair	350.00	525.00	787.50
	2. Labour	21.60	43.20	86.40
	3. Tax	0.00	0.00	0.00
Total annual costs (RM)		**371.60**	**568.20**	**873.90**
Annual Income/Revenue (RM)	1. Fuel cost saving	3,531.00	7,018.00	13,897.00
	2. Electricity export	0.0051	0.0187	0.0505
	3. Vegetables sales	60.75	121.50	243.00
Total annual income (RM)		**3591.75**	**7139.52**	**14140.05**
Inflation & Fuel escalation rate (2.5 %)		80.50	164.28	331.65
Expected Annual Cash flow (RM)		3220.15	6571.32	13266.15
IRR		5 %	10 %	14 %
NPV (RM)		(1,229.57)	32,902.98	30,607.39
Discount rate		5 %	5 %	10 %
Project life (year)		20	20	20
Payback (year)		12	8	6
Benefits to Cost Ratio		1.34	2.11	1.75

From Table 4.12, the financial viabilities of projects with capacities less than 3.5 kW (1 TR) is observed to be less impressive, considering the NPV and payback period. This is a laboratory size project which contains nearly all the components of the bigger capacity sizes; thus, it would be a bit difficult to breakthrough, comparing the initial cost with the income. Plants with 3.5 kW and 7.0 kW capacities were observed to be more financially viable with positive NPV, equity payback of 8 years and 6 years, respectively, and IRR of 10 % and 14 %, respectively. The benefit-to-cost ratio is better in the 3.5 kW capacity than that of 7.0 kW capacity only because lower discount rate applied in the former than the later. However, each of the projects contributed to GHG emission reduction (as shown in Table 4.13), quantified in terms of the barrels of crude oil not used. The combined yearly cash flows of the projects over their projected lives in Figure 4.16, also shows that developed project is more financially viable with bigger capacity.

Table 4.13: Projects emission reduction summary

	Plant cooling capacity			
Net annual GHG emission reduction	**0.05kW**	**1.76kW**	**3.5kW**	**7kW**
	0.3 tCO_2; Equivalent to 0.7 barrels of crude oil not consumed.	11.8 tCO_2; Equivalent to 27.4 Barrels of crude oil not consumed.	23.4 tCO_2; Equivalent to 54.4 Barrels of crude oil not consumed.	46.4 tCO_2; Equivalent to 108 Barrels of crude oil not consumed.

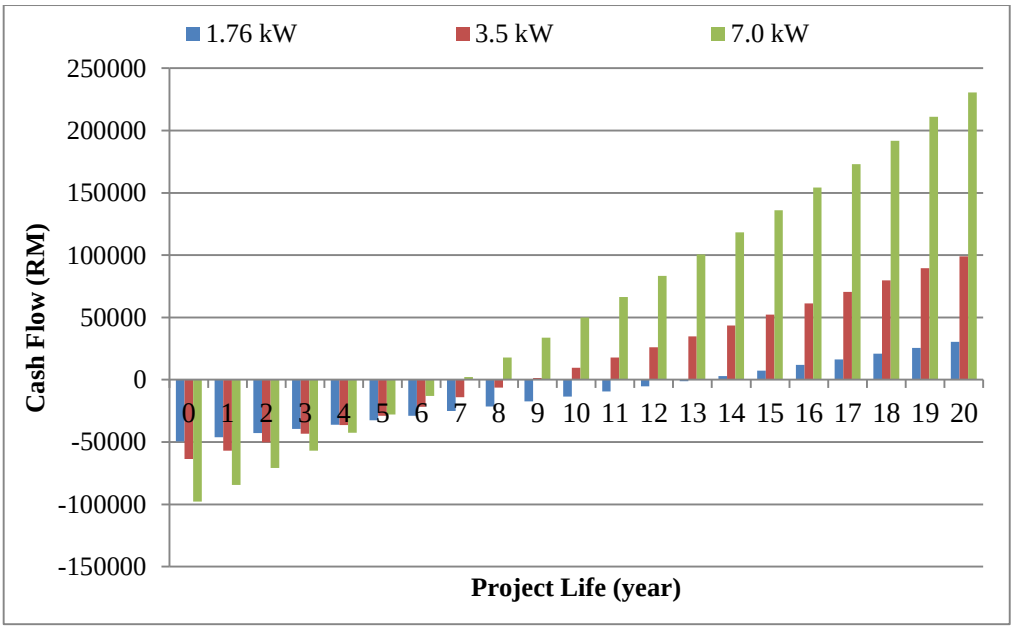

Figure 4.16: Project annual cash flow

4.9 Summary

In this chapter of the thesis, the results had been presented and analysed. The results presented include the modelling and experimental analyses of the soil cooling, the chilled water production from absorption chiller, the combined plant and its parametric analyses, as well as the economic analyses of the developed system for cooling application.

Analytical models results have been validated with the results obtained from the experimental setups and good agreements were found between the analyses of the results obtained from both the experimental rig and the model.

The parametric analyses (through *RSM*) had been carried out, and the effects of each of the key parameters had been analysed and discussed for the soil cooling system, and for combined plant system.

The economic analysis of the combined plant in comparison with a similar plant for the same application and under the same service condition and environment, had been studied and discussed. This had shown the viability of the project and its environmental impacts. The environmental impacts in form of the GHG emission reduction had also been quantified in terms of the unused barrels of crude oil.

CHAPTER 5

CONCLUSIONS AND RECOMMENDATIONS

5.1 Conclusion

The energy, in the form of solar heat contained within any given land surface area, could be harnessed with vapour absorption refrigeration–organic Rankine cycle (VAR–ORC) combined plant to lower soil temperature. The combined plant makes use of low-grade solar energy for the production of chilled water in any soil or space cooling application. However, due to the diffused nature of this source of energy, solar thermal collector could be installed to capture the required amount of solar energy to produce a higher rate of chilled water. The cooling load required to lower the soil temperature could be supplied by an absorption chiller; however, an organic Rankine cycle would be required to generate the necessary amount of electrical energy to operate pumps and other ancillary loads of the system.

The cooling load requirement of a particular size of soil bed could only be optimally offset by a certain capacity of the combined plant. A set of mathematical models had been successfully developed in this study in order to design a combined VAR–ORC plant with the right sizing of the required solar thermal collectors for a given size of a land area. The models would also help in specifying cooling system requirements as well as the expected system performance.

The physical model developed in this study was suitable for selecting the chilled water flow rates required to achieve a set of soil temperatures that would be needed for a particular type of high-value temperate crop. This model had been

developed in relation to the soil cooling load, soil bed size and chilled water pipe dimension; thus, it could be concluded that the application of this physical model could be extended beyond the experimental size of soil bed in this study with acceptable range of variations.

The results of the mathematical models in this study had been validated with those obtained from the experimental rig as presented in Chapter 4, with good agreement. Variations between the experimental and modelled results were considered acceptable due to some approximations and simplification assumptions in the models development. It could be concluded that the developed models could be used to predict the soil cooling and combined plant performances with reasonable accuracy.

Further analysis of the effects of relevant factors on the performance of the proposed system using response surface methodology (*RSM*) showed that chilled water flow rate had the most significant effect on the temperature of the cooled soil. A maximum chilled water flow rate of 0.42 kg/min would be sufficient during the peak load to achieve the set soil temperature (18 ºC ± 2) for 0.25 m^2 area of soil bed in this study.

The effects of the variations in key operating parameters (temperature, pressure, and working fluid mass fraction) on the combined plant performance showed that the plant optimum performance would require some trade-offs between the coefficient of performance and the organic Rankine cycle efficiency. The overall plant performance diminished at elevated temperature and pressure; thus, operating the plant at low temperature and pressure would ensure its optimal performance and save the cost. This is in consonance with the earlier study by (Al-Sulaiman *et al.*, 2012).

The proposed system has higher potential for financial viability with bigger capacity. As presented in Chapter 4, the economic viability of the proposed system starts from 3.5 kW capacity upwards. This is based on the financial parameters, including inflation rate, fuel escalation rates, electricity rate, and selling price of vegetables.

Implementing a project such as in this study has the potential to contribute to the GHG emission reduction that is equivalent to 6.7 tCO_2 per kW of cooling capacity in a year. It could, therefore, be concluded that the proposed system of soil cooling would be economically viable and environmentally beneficial.

5.2 Recommendations

This area of study is generally wide in scope and cuts across a number of technologies and their applications. However, the work reported in this thesis has been completed within the spate of time and resource, and within the limit of the scope of this research. As such, the following areas are suggested for future research to gain more insight into the applications of solar thermal energy for general cooling and power generation, and for radiant soil or floor cooling systems:

i. Since a complete system, consisting of a large size of soil bed and bigger capacity of the combined plant, could hardly be explored in a laboratory and within the stipulated period of this research, any integration of an absorption chiller with organic Rankine cycle in the future, for a bigger capacity, for simultaneous cooling and power generation, would give further insight into the economic viability of the system;

ii. The study only investigated the sensitivity of soil temperature to the ambient environment. However, in upgrading the systems to a bigger size, the dynamic analysis of ambient air and the daytime conditions on the chilled water plant performance, and its resultant effects on the cooled soil, should be looked into; and

iii. Since the study had focused only on the agricultural soil cooling, that is a hydronic radiant cooling system, the application of solar thermal chilled water from a combined cooling and power could be extended to a number of radiant cooling systems, including comfort cooling in

buildings and other process cooling systems. For such purposes, much improved programming codes for cooling load and combined plant capacity estimation should be developed.

REFERENCES

Abdulateef., J. M., Sopian., K. and Alghoul, M. A. (2008). Optimum Design for Solar Absorption Refrigerarion Systems and Comparison of the Performances using Ammonia-Water, Ammonia-Lithium Nitrate and Ammonia-Sodium Thiocyanate Solutions. *International Journal of Mechanical and Materials Engineering*. 3(1)**,** 17-24.

Abdulateef., J. M., Sopian., K., Alghoul., M. A., Sulaiman., M. Y., Zaharim., A. and Ahmad, I. (2007). Solar Absorption Refrigeration System Using New Working Fluid Pairs. *International Journal of Energy*. 3(1)**,** 1-6.

Abdullah, M. O. and Hieng, T. C. (2010). Comparative analysis of performance and techno-economics for a $H_2O–NH_3–H_2$ absorption refrigerator driven by different energy sources. *Applied Energy*. 87(5)**,** 1535-1545.

Abed, H., Atashkari, K., Niazmehr, A. and Jamali, A. (2013). Thermodynamic optimization of combined power and refrigeration cycle using binary organic working fluid. *International Journal of Refrigeration*. 36(8)**,** 2160-2168.

Ackom, E. K. (2005). *Technical & Economic Viability Analysis of Renewable Energy Technologies in Ghana.* PhD, Brandenburg University of Technology.

Agyenim, F., Knight, I. and Rhodes, M. (2010). Design and experimental testing of the performance of an outdoor LiBr/H2O solar thermal absorption cooling system with a cold store. *Solar Energy*. 84(5)**,** 735-744.

Ahmed, A. and Medhat, A. F. (2012). Tropical Modeling of Concrete-Core-Radiant Cooling System "Application on Alexandria, Egypt". *9th International Conference on Heat Transfer, Fluid Mechanics and Thermodynamics.* Malta, Egypt.

Ahmed, S. F., Amanullah, M. T. O., Khan, M. M. K., Rasul, M. G. and Hassan, N. M. S. (2016). Parametric study on thermal performance of horizontal earth pipe cooling system in summer. *Energy Conversion and Management*. 114**,** 324-337.

Akbulut., U., Kıncay., O. and Utlu, Z. (2016). Analysis of a wall cooling system using a heat pump. *Renewable Energy*. 85**,** 540-553.

Al-Sulaiman., F. A., Hamdullahpur., F. and Dincer, I. (2012). Performance assessment of a novel system using parabolic trough solar collectors for combined cooling, heating, and power production. *Renewable Energy*. 48**,** 161-172.

Arvay., P., Muller., M. R., Ramdeen., V. and Cunningham, G. (2011). Economic Implementation of the Organic Rankine Cycle in Industry. ACEEE Summer Study on Energy Efficiency in Industry Rutgers University. 1-11.

ASHRAE (2009). Residential cooling and heating load calculations. *2009 American Society of Heating, Refrigerating and Air-Conditioning Engineers*. (pp. 1-16). ASHRAE.

Ayompe., L. M., Duffy., A., McCormack., S. J. and Conlon, M. (2011). Validated TRNSYS model for forced circulation solar water heating systems with flat plate and heat pipe evacuated tube collectors. *Applied Thermal Engineering*. 31**,** 1536-1542.

Bajpai, V. K. (2012). Design of Solar Powered Vapour Absorption System. Proceedings of the World Congress on Engineering WCE 2012 London, U.K., 1-5.

Baniyounes, A. M., Liu, G., Rasul, M. G. and Khan, M. M. K. (2013). Comparison study of solar cooling technologies for an institutional building in subtropical Queensland, Australia. *Renewable and Sustainable Energy Reviews*. 23**,** 421-430.

Bishop., J. and Horspool, R. N. (2008). On the Efficiency of Design Patterns Implemented in C# 3.0. *TOOLS EUROPE*. 11**,** 356-371.

Borunda., M., Jaramillo., O. A., Dorantes., R. and Reyes, A. (2016). Organic Rankine Cycle coupling with a Parabolic Trough Solar Power Plant for cogeneration and industrial processes. *Renewable Energy*. 86**,** 651-663.

Boyano, A., Hernandez, P. and Wolf, O. (2013). Energy demands and potential savings in European office buildings: Case studies based on EnergyPlus simulations. *Energy and Buildings*. 65**,** 19-28.

Brenner, A. J., Puigdefa, J., Domingo, F. and Villagarcõ, L. (1999). Evapotranspiration model for semi-arid shrub-lands tested against data from SE Spain. *Agricultural and Forest Meteorology*. 95**,** 67-84.

Cai, D., He, G., Tian, Q. and Tang, W. (2014). Thermodynamic analysis of a novel air-cooled non-adiabatic absorption refrigeration cycle driven by low grade energy. *Energy Conversion and Management*. 86**,** 537-547.

Carrasco., T. L. and Girty, G. H. (2015). Identifying a reference frame for calculating mass change during weathering: A review and case study utilizing the C# program assessing element immobility and critical ratio methodology. *Catena*. 125**,** 146-161.

Chang, W. S., Wang, C. C. and Shieh, C. C. (2009). Design and performance of a solar-powered heating and cooling system using silica gel/water adsorption chiller. *Applied Thermal Engineering*. 29(10)**,** 2100-2105.

Chen, Q. and Xu, Y.-C. (2012). An entransy dissipation-based optimization principle for building central chilled water systems. *Energy*. 37(1)**,** 571-579.

Chen, W.-n. (2012). Renewable Energy Status in Malaysia. *In:* Malaysia, S. E. D. A. (ed.).

Chidambaram, L. A., Ramana, A. S., Kamaraj, G. and Velraj, R. (2011). Review of solar cooling methods and thermal storage options. *Renewable and Sustainable Energy Reviews*. 15(6)**,** 3220-3228.

Chua, S. C. and Oh, T. H. (2012). Solar energy outlook in Malaysia. *Renewable and Sustainable Energy Reviews*. 16(1)**,** 564-574.

Cloutier, M. (2002). Refrigeration Cycles. (pp. 1-17).

Cui, P., Yang, H. and Fang, Z. (2008). Numerical analysis and experimental validation of heat transfer in ground heat exchangers in alternative operation modes. *Energy and Buildings*. 40(6)**,** 1060-1066.

Datla, B. V. (2012). Organic Rankine Cycle System Analysis for Low GWP Working Fluids. *International Refrigeration and Air Conditioning Conference.* Purdue University: Purdue e-Pubs.

Daut, I., Zainuddin, F., Irwan, Y. M. and Razliana, A. R. N. (2012). Analysis of Solar Irradiance and Solar Energy in Perlis, Northern of Peninsular Malaysia. *Energy Procedia*. 18**,** 1421-1427.

De Carli, M. and Tonon, M. (2011). Effect of modelling solar radiation on the cooling performance of radiant floors. *Solar Energy*. 85(5)**,** 689-712.

Deam, R. T., Lemma, E., Mace, B. and Collins, R. (2008). On Scaling Down Turbines to Millimeter Size. *Journal of Engineering for Gas Turbines and Power*. 130(5)**,** 261-277.

Delgado-Torres, A. M. and García-Rodríguez, L. (2010). Analysis and optimization of the low-temperature solar organic Rankine cycle (ORC). *Energy Conversion and Management*. 51(12)**,** 2846-2856.

Demir, H., Koyun, A. and Temir, G. (2009). Heat transfer of horizontal parallel pipe ground heat exchanger and experimental verification. *Applied Thermal Engineering*. 29(2-3)**,** 224-233.

Demirkaya, G., Padilla, R. V. and Goswami, D. Y. (2013). A review of combined power and cooling cycles. *Wiley Interdisciplinary Reviews: Energy and Environment*. 2(5)**,** 534-547.

Deng, J., Wang, R. Z. and Han, G. Y. (2011). A review of thermally activated cooling technologies for combined cooling, heating and power systems. *Progress in Energy and Combustion Science*. 37(2)**,** 172-203.

Dincer, I., Rosen, M. A. and Zamfirescu, C. (2009). Exergetic Performance Analysis of a Gas Turbine Cycle Integrated With Solid Oxide Fuel Cells. *Journal of Energy Resources Technology*. 131(3)**,** 032001.

Dong, B. (2010). *Integrated Building Heating, Cooling and Ventilation Control.* PhD, Carnegie Mellon University.

Duan, Z., Zhan, C., Zhang, X., Mustafa, M., Zhao, X., Alimohammadisagvand, B. and Hasan, A. (2012). Indirect evaporative cooling: Past, present and future potentials. *Renewable and Sustainable Energy Reviews*. 16(9)**,** 6823-6850.

Duggirala, B. (2010). *Analyzing Sustainable Energy Opportunities for a Small Scale Off-Grid Facility: A Case Study at Experimental Lakes Area (ELA), Ontario.* Master, University of Manitoba.

Feng, X., Goswami., D. Y. and Bhagwat, S. S. (2000). A combined power/cooling cycle. *Energy*. 25**,** 233-246.

Flueckiger, S. M., Yang, Z. and Garimella, S. V. (2013). Review of Molten-Salt Thermocline Tank Modeling for Solar Thermal Energy Storage. *Heat Transfer Engineering*. 34(10)**,** 787-800.

Fong, K. F., Chow, T. T., Lee, C. K., Lin, Z. and Chan, L. S. (2009). Comparative study of different solar cooling systems for buildings in subtropical city. *Solar Energy*. 84(2)**,** 227-244.

Fong, K. F., Chow, T. T., Lee, C. K., Lin, Z. and Chan, L. S. (2010a). Advancement of solar desiccant cooling system for building use in subtropical Hong Kong. *Energy and Buildings*. 42(12)**,** 2386-2399.

Fong, K. F., Lee, C. K., Chow, T. T., Lin, Z. and Chan, L. S. (2010b). Solar hybrid air-conditioning system for high temperature cooling in subtropical city. *Renewable Energy*. 35(11)**,** 2439-2451.

Freund, S. W. 2012. *Rankine Cycle Integrated with Absorption Chiller*. NY, United States patent application 12/916,191.

Gaglia, A. G., Lykoudis, S., Argiriou, A. A., Balaras, C. A. and Dialynas, E. (2017). Energy efficiency of PV panels under real outdoor conditions–An experimental assessment in Athens, Greece. *Renewable Energy*. 101**,** 236-243.

Garimella, S. (2012). Low-grade waste heat recovery for simultaneous chilled and hot water generation. *Applied Thermal Engineering*. 42**,** 191-198.

Gastli, A. and Charabi, Y. (2011). Solar water heating initiative in Oman energy saving and carbon credits. *Renewable and Sustainable Energy Reviews*. 15(4)**,** 1851-1856.

Gontard, N., Guilbert, S. and Cuq, J.-L. (1992). Edible Wheat Gluten Films: Influence of the Main Process Variables on Film Properties using Response Surface Methodology. *Journal of Food Science*. 57(1)**,** 190-199.

Gordon, J. M. and Ng, K. C. (1995). A General Thermodynamic Model for Absorption Chillers: Theory and Experiment. *Heat Recovery Systems & CHP*. 15(1)**,** 73-83.

Gorman, J. M., Sparrow, E. M. and Abraham, J. P. (2013). Differences between measured pipe wall surface temperatures and internal fluid temperatures. *Case Studies in Thermal Engineering*. 1(1)**,** 13-16.

Goswami, D. Y. and Xu, F. (1999). Analysis of a New Thermodynamic Cycle for Combined Power and Cooling Using Low and Mid Temperature Solar Collectors *Journal of Solar Energy Engineering*. 121**,** 91-97.

Gupta, Y. (2011). *Research and Development of a Small - Scale Adsorption Cooling System.* PhD, Arizona State University.

Hamid, F., Akhbar, S. and Halim, K. H. K. (2013). Mechanical and Thermal Properties of Polyamide 6/HDPE-g- MAH/High Density Polyethylene. *Procedia Engineering*. 68**,** 418-424.

Han, X. and Zhang, X. (2011). Experimental study on a residential temperature–humidity separate control air-conditioner. *Energy and Buildings*. 43(12)**,** 3584-3591.

Hariharan, N. M., Sivashanmugam, P. and Kasthurirengan, S. (2013). Optimization of thermoacoustic refrigerator using response surface methodo- logy*. *Journal of Hydynamics*. 25(1)**,** 72-82.

Hasson, A. M. and Hussain, R. (1987). Effect of Polyethylene Mulch on Soil Temperature Variation under Planted Greenhouse in Aridic Region. *Solar & Wind Technology*. 4(4)**,** 459-465.

He, T., Zhang, X., Wang, C., Wang, M., Li, B., Xue, N., Shimizu, K., Takahashi, K. and Wu, Y. (2015). Application of Solar Thermal Cooling System Driven by Low Temperature Heat Source in China. *Energy Procedia*. 70**,** 454-461.

He, Z., Zhao, Z., Zhang, X. and Feng, H. (2010). Thermodynamic properties of new heat pump working pairs: 1,3-Dimethylimidazolium dimethylphosphate and water, ethanol and methanol. *Fluid Phase Equilibria*. 298(1)**,** 83-91.

Hlbauer, W. M. I. (1986). Performance of solar crop dryers. 5**,** 121-137.

Ho-Yan, B. P. (2011). Tesla Turbine for Pico Hydro Applications. *Guelph Engineering Journal*. 4**,** 1-8.

Hong, D., Chen, G., Tang, L. and He, Y. (2011). A novel ejector-absorption combined refrigeration cycle. *International Journal of Refrigeration*. 34(7)**,** 1596-1603.

Hoya, G. A. and Guha, A. (2009). The design of a test rig and study of the performance and efficiency of a Tesla disc turbine. Proceedings of the Institution of Mechanical Engineers. Part A: Journal of Power and Energy, 451-465.

Hubbard, R. S. (2011). Energy Impacts of Chilled-Water-Piping Configuration. *In:* Inc, J. C. (ed.). HPAC Engineering.

Huntingford, C., Verhoef, A., Stewart, J. and Huntingfors, C. (2000). Dual versus single source models for estiamting surface temperature of African Savannah. *Hydrology and Earth System Sciences*. 4(1)**,** 185–191.

Ibrahim, N. I., Al-Sulaiman, F. A. and Ani, F. N. (2017). Solar absorption systems with integrated absorption energy storage–A review. *Renewable and Sustainable Energy Reviews*. Article in press**,** 10.

Ilenikhena, P. A. and Ezemonye, L. N. (2010). Solar Energy Applications in Nigeria. *WEC MONTREAL*.

INEOS Typical Engineering Properties of High Density Polyethylene. *In:* Polymers, I. O. (ed.). USA: INEOS Olefins & Polymers.

Jaafar, A. B. (2014). Ocean Thermal Energy-driven Development in Malaysia. Ocean Thermal Energy Conversion Center, Universiti Teknologi Malaysia.

Jain., D. and Tiwari, G. N. (2002). Modeling and optimal design of evaporative cooling system in controlled environment greenhouse. *Energy Conversion and Management*. 43**,** 2235-2250.

Javidmand, P. and Hoffmann, K. A. (2016). A comprehensive modeling of choked two-phase flow through short-tube orifices with application to alternative refrigerants HFO-1234yf and HFO-1234ze. *International Journal of Refrigeration*. 69**,** 114-135.

Jiangfeng, W., Dai, Y., Gao, L. and Ma, S. (2009). A new combined cooling, heating and power system driven by solar energy. *Renewable Energy*. 34(12)**,** 2780-2788.

Jim, F. P. G. and Charles, D. J. (2009). Tropical agriculture. *The weather and climate of the tropics*. (pp. 6). Royal Meteorological Society: Royal Meteorological Society.

Kadir, M. Z. A. A. and Rafeeu, Y. (2010). A review on factors for maximizing solar fraction under wet climate environment in Malaysia. *Renewable and Sustainable Energy Reviews*. 14(8)**,** 2243-2248.

Kalina, A. I. (1984). Combined-Cycle System With Novel Bottoming Cycle. *Journal of Engineering for Gas Turbines and Power*. 106**,** 737-742.

Kalkan, N., Young, E. A. and Celiktas, A. (2012). Solar thermal air conditioning technology reducing the footprint of solar thermal air conditioning. *Renewable and Sustainable Energy Reviews*. 16(8)**,** 6352-6383.

Kalogirou, S. A. (2004). Solar thermal collectors and applications. *Progress in Energy and Combustion Science*. 30(3)**,** 231-295.

Kalogirou., S., Florides., G., Tassou., S. and Wrobel, L. (2001). Design and Construction of a Lithium Bromide Water Absorption Refrigerator. *CLIMA 2000/Napoli 2001 World Congress.* Napoli: CLIMA.

Karellas., S. and Schuster, A. (2008). Supercritical Fluid Parameters in Organic Rankine Cycle Applications. *International Journal of Thermodynamics*. 11(3)**,** 101-108.

Kasperski, J. and Eichler, J. (2012). Ammonia–water absorption cycle on three-dimensional graphs – The Absorption 3D tool software. *International Journal of Refrigeration*. 35(7)**,** 1958-1966.

Kaushik, S. C., Tomar, C. S. and Chandra, S. (1983). Coefficient of Performance of an Ideal Absorption Cycle. *Applied Energy*. 14**,** 115-121.

Kaygusuz, K. (2012). Energy for sustainable development: A case of developing countries. *Renewable and Sustainable Energy Reviews*. 16(2)**,** 1116-1126.

Khamooshi, M., Parham, K. and Atikol, U. (2013). Overview of Ionic Liquids Used as Working Fluids in Absorption Cycles. *Advances in Mechanical Engineering*. 2013**,** 1-7.

Khan, H. A. and Pervaiz, S. (2013). Technological review on solar PV in Pakistan: Scope, practices and recommendations for optimized system design. *Renewable and Sustainable Energy Reviews*. 23**,** 147-154.

Khan, M. M. A., Ibrahim, N. I., Saidur, R., Mahbubul, I. M. and Al-Sulaiman, F. A. (2016). Performance assessment of a solar powered ammonia–water absorption refrigeration system with storage units. *Energy Conversion and Management*. 126**,** 316-328.

Khennich, M. and Galanis, N. (2012). Optimal Design of ORC Systems with a Low-Temperature Heat Source. *Entropy*. 14(12)**,** 370-389.

Kim, Y. J., Kim, S., Joshi, Y. K., Fedorov, A. G. and Kohl, P. A. (2012). Thermodynamic analysis of an absorption refrigeration system with ionic-liquid/refrigerant mixture as a working fluid. *Energy*. 44(1)**,** 1005-1016.

KumeGuide (2014). Deep Sea Water Research Institute.

Kusuda, T. and Archenbach, P. R. (1965). Earth temperature and thermal diffusivity at selected stations in the United States. *ASHRAE Transaction*. 71(1)**,** 61-75.

Labeke., M.-C. v. and Dambre, P. (1993). Response of five Alstroemeria cultivars to soil cooling and supplementary lighting. *Scientia Horticulturae*. 56**,** 135-145.

Leavell, K. A. B. (2010). Practical Solar Thermal Chilled Water. Proceedings from the Thirty-second Industrial Energy Technology Conference New Orleans, Los Angeles. ESL-IE-10-05-03, 1-15.

Lee, J.-Y., Chen, C.-L., Wen, T.-L., Ng, D. K. S., Foo, D. C. Y. and Wang, T.-C. (2013). Synthesis and design of chilled water networks using mathematical optimization. *Applied Thermal Engineering*. 58(1-2)**,** 638-649.

Lee, K.-H., Lee, D.-W., Baek, N.-C., Kwon, H.-M. and Lee, C.-J. (2012). Preliminary determination of optimal size for renewable energy resources in buildings using RETScreen. *Energy*. 47(1)**,** 83-96.

Lee, K. H. and Strand, R. K. (2008). The cooling and heating potential of an earth tube system in buildings. *Energy and Buildings*. 40(4)**,** 486-494.

Lee., K. H. and Strand, R. K. (2006). Implementation of an Earth tube System into Energyplus Program. *In:* Illinois, U. o. (ed.).

Leslie., N. P., Sweetser., R. S., Stovall., T. K. and Zimron, O. (2009). Recovered Energy Generation Using an Organic Rankine Cycle System. *In:* ASHRAE (ed.).

Li, H., Bu, X., Wang, L., Long, Z. and Lian, Y. (2013). Hydrocarbon working fluids for a Rankine cycle powered vapor compression refrigeration system using low-grade thermal energy. *Energy and Buildings*. 65**,** 167-172.

Liu, B. C., Liu, W. and Peng, S. W. (2005). Study of heat and moisture transfer in soil with a dry surface layer. *international Journal of Heat and Mass Transfer*. 48**,** 4579-4589.

Liu, S., Lu, L., Mao, D. and Jia, L. (2007). Evaluating parameterizations of aerodynamic resistance to heat transfer using field measurements. *Hydrology and Earth System Sciences*. 11(1)**,** 769-783.

Liu, X.-f., Liu, J.-p., Lu, J.-d., Liu, L. and Zou, W. (2012). Research on operating characteristics of direct-return chilled water system controlled by variable temperature difference. *Energy*. 40(1)**,** 236-249.

Liu, X., Zhang, Y., Shen, J., Yao, S. and Zhang, Z. (2016). Characteristics of air cooling for cold storage and power recovery of compressed air energy storage (CAES) with inter-cooling. *Applied Thermal Engineering*. 107**,** 1-9.

Liu., M., Saman., W. and Bruno, F. (2014). Computer simulation with TRNSYS for a mobile refrigeration system incorporating a phase change thermal storage unit. *Applied Energy*. 132**,** 226-235.

Lu, Z. S., Wang, R. Z., Xia, Z. Z., Lu, X. R., Yang, C. B., Ma, Y. C. and Ma, G. B. (2013). Study of a novel solar adsorption cooling system and a solar absorption cooling system with new CPC collectors. *Renewable Energy*. 50**,** 299-306.

Lu., S. and Goswami, D. Y. (2002). Theoretical Analysis of Ammonia-Based Combined Power/Refrigeration Cycle at Low Refrigeration Temperatures. International Solar Energy Conference Reno, Nevada, USA. ASME, 117-125.

Luzzi, A., Lovegrove., K., Filippi., E., Fricker., H., Schmitz-Goeb., M., Chandapillai., M. and Kaneff, S. (1999). Techno-Economic Analysis of a 10 Mwe Solar Thermal Power Plant using Ammonia-Based Thermochemical Energy Storage. *Solar Energy*. 66(2)**,** 91-101.

Lychnos, G. and Davies, P. A. (2012). Modelling and experimental verification of a solar-powered liquid desiccant cooling system for greenhouse food production in hot climates. *Energy*. 40(1)**,** 116-130.

Mansouri Majoumerd, M. and Assadi, M. (2014). Techno-economic assessment of fossil fuel power plants with CO2 capture – Results of EU H2-IGCC project. *International Journal of Hydrogen Energy*. 39(30)**,** 16771-16784.

Maraver, D., Sin, A., Royo, J. and Sebastián, F. (2013). Assessment of CCHP systems based on biomass combustion for small-scale applications through a review of the technology and analysis of energy efficiency parameters. *Applied Energy*. 102**,** 1303-1313.

Marc, O., Sinama, F. and Lucas, F. (2012). Decision making tool to design solar cooling system coupled with building under tropical climate. *Energy and Buildings*. 49**,** 28-36.

MARDI. Malaysian Agriculture Research and Development Institute.

Marı, E. G., Colomer, R. P. G. and Blaise-Ombrecht, C. A. (2007). Performance analysis of a solar still integrated in a greenhouse. *Desalination*. 203(1-3)**,** 435-443.

Martínez, P. J., Martínez, J. C. and Lucas, M. (2012). Design and test results of a low-capacity solar cooling system in Alicante (Spain). *Solar Energy*. 86(10)**,** 2950-2960.

Massaguer., E., Massaguer., A., Montoro., L. and Gonzalez, J. R. (2014). Development and validation of a new TRNSYS type for the simulation of thermoelectric generators. *Applied Energy*. 134**,** 65-74.

Masson., S. V., Qu., M. and H.Archer, D. (2006). Performance Modeling of a Solar Driven Absorption Cooling System for Carnegie Mellon University's Intelligent Workplace. *ICEBO2006, Shenzhen, China.* China: Renewable Energy Resources and a Greener Future.

Max, J. F. J., Horst, W. J., Mutwiwa, U. N. and Tantau, H.-J. (2009). Effects of greenhouse cooling method on growth, fruit yield and quality of tomato (Solanum lycopersicum L.) in a tropical climate. *Scientia Horticulturae*. 122(2)**,** 179-186.

Mazouz, S., Mansouri, R. and Bellagi, A. (2014). Experimental and thermodynamic investigation of an ammonia/water diffusion absorption machine. *International Journal of Refrigeration*. 45**,** 83-91.

McQuay (2001). Chiller Plant Design. *In:* International, M. (ed.). McQuay International.

McQuay (2002). Application Guide: Refrigerants. *In:* International, M. (ed.). McQuay International.

Mekhilef, S., Faramarzi, S. Z., Saidur, R. and Salam, Z. (2013). The application of solar technologies for sustainable development of agricultural sector. *Renewable and Sustainable Energy Reviews*. 18**,** 583-594.

Mekhilef, S., Safari, A., Mustaffa, W. E. S., Saidur, R., Omar, R. and Younis, M. A. A. (2012). Solar energy in Malaysia: Current state and prospects. *Renewable and Sustainable Energy Reviews*. 16(1)**,** 386-396.

Mendonça, M., Lacey, S. and Hvelplund, F. (2009). Stability, participation and transparency in renewable energy policy: Lessons from Denmark and the United States. *Policy and Society*. 27(4)**,** 379-398.

Mihalakakou, G. (2002). On estimating soil surface temperature profiles. *Energy and Buildings*. 34**,** 251-259.

Mikeska., T. and Svendsen, S. (2015). Dynamic behavior of radiant cooling system based on capillary tubes in walls made of high performance concrete. *Energy and Buildings*. 108**,** 92-100.

Miles, D. J., Sannors, D. M., Nowakowski, G. A. and Shelton, S. V. (1993). Gas Fired Sorption Heat Pump Development. *Heat Recovery Systems & CHP*. 13(4)**,** 347-351.

Miyazaki, T. and Akisawa, A. (2009). The influence of heat exchanger parameters on the optimum cycle time of adsorption chillers. *Applied Thermal Engineering*. 29(13)**,** 2708-2717.

Mokhtar, M., Ali, M. T., Bräuniger, S., Afshari, A., Sgouridis, S., Armstrong, P. and Chiesa, M. (2010). Systematic comprehensive techno-economic assessment of solar cooling technologies using location-specific climate data. *Applied Energy*. 87(12)**,** 3766-3778.

Moncef, K. and Kreider, J. F. (1996). Analytical Model for Heat Transfer in an Underground Air Tunnel. *Energy Conversion Management*. 17(10)**,** 1561-1574.

Mongkon, S., Thepa, S., Namprakai, P. and Pratinthong, N. (2013). Cooling performance and condensation evaluation of horizontal earth tube system for the tropical greenhouse. *Energy and Buildings*. 66**,** 104-111.

Mongkon, S., Thepa, S., Namprakai, P. and Pratinthong, N. (2014). Cooling performance assessment of horizontal earth tube system and effect on planting in tropical greenhouse. *Energy Conversion and Management*. 78**,** 225-236.

Morille, B., Migeon, C. and Bournet, P. E. (2013). Is the Penman–Monteith model adapted to predict crop transpiration under greenhouse conditions? Application to a New Guinea Impatiens crop. *Scientia Horticulturae*. 152**,** 80-91.

Moser, A. P. and Folkman, S. (2008). *Buried Pipe Design*. Third Edition. edition. New York, Chicago, San Francisco, Lisbon, London, Madrid, Mexico City, Milan, New Delhi, San Juan, Seoul, Singapore, Sydney, Toronto: Mc Graw Hill.

Muerth, M. and Mauser, W. (2012). Environmental Modelling & Software Rigorous evaluation of a soil heat transfer model for mesoscale climate change impact studies. *Environmental Modelling and Software*. 35**,** 149-162.

Munson., B. R., Young., D. F., Okiishi., T. H. and Huebsch, W. W. (2009). *Fundamentals of Fluid Mechanics*. United States of America: John Wiley & Sons, Inc.

Nabi, G. and Mullins, C. E. (2008). Soil Temperature Dependent Growth of Cotton Seedlings Before Emergence. *Pedosphere*. 18(1)**,** 54-59.

NASA , National Aeronautic and Space Administration. Global Energy Budget. Accessed 2017. Cited 2017

Neckel, A. L. and Godinho, M. (2015). nfluence of geometry on the efficiency of convergent–divergent nozzles applied to Tesla turbines. *Experimental Thermal and Fluid Science*. 62**,** 131-140.

Nik., A. R., Kasran., B. and Hassan, A. (1986). Soil Temperature Regimes under Mixed Dipterocarp Forests of Peninsular Malaysia. *Pertanika*. 9(3)**,** 277-284.

NIST, N. I. o. S. a. T. *Reference Fluid Thermodynamic and Transport Properties - REFPROP*. U.S Department of Commerce.

Niu, F., Yu, Y., Yu, D. and Li, H. (2015). Heat and mass transfer performance analysis and cooling capacity prediction of earth to air heat exchanger. *Applied Energy*. 137**,** 211-221.

Nizami, D. J., Lightstone, M. F., Harrison, S. J. and Cruickshank, C. A. (2013). Negative buoyant plume model for solar domestic hot water tank systems incorporating a vertical inlet. *Solar Energy*. 87**,** 53-63.

Nordin., N. A. M., Zaharudin., Z. A., Maasar., M. A. and Nordin, N. A. (2012). Finding Shortest Path of the Ambulance Routing: Interface of A* Algorithm using C#

Programming. *IEEE Symposium on Humanities, Science and Engineering Researc*. Malaysia.

Novak, M. D. (1981). *The Moisture and Thermal Regimes od a Bare Soil in the Lower Fraser Valley During Spring.* PhD, The University of British Columbia.

Novak, M. D. (2010). Dynamics of the near-surface evaporation zone and corresponding effects on the surface energy balance of a drying bare soil. *Agricultural and Forest Meteorology*. 150(10)**,** 1358-1365.

Oh, T. H., Pang, S. Y. and Chua, S. C. (2010). Energy policy and alternative energy in Malaysia: Issues and challenges for sustainable growth. *Renewable and Sustainable Energy Reviews*. 14(4)**,** 1241-1252.

Olesen, B. (2008). Radiant Floor Cooling Systems. *ASHRAE Journal*. 50(9)**,** 16-22.

Olesen, B. W. (1997). *Possibilities and limitations of radiant floor cooling*.

Othman, N. F., Ya'acob, M. E., Abdul-Rahim, A. S., Othman, M. S., Radzi, M. A. M., Hizam, H., Wang, Y. D., Ya'acob, A. M. and Jaafar, H. Z. E. (2015). Embracing new agriculture commodity through integration of Java Tea as high Value Herbal crops in solar PV farms. *journal of Cleaner Production*. 91**,** 71-77.

Padilla, R. V., Demirkaya, G., Goswami, D. Y., Stefanakos, E. and Rahman, M. M. (2010). Analysis of power and cooling cogeneration using ammonia-water mixture. *Energy*. 35(12)**,** 4649-4657.

Parameshwaran, R., Kalaiselvam, S., Harikrishnan, S. and Elayaperumal, A. (2012). Sustainable thermal energy storage technologies for buildings: A review. *Renewable and Sustainable Energy Reviews*. 16(5)**,** 2394-2433.

Park., K. A., Choi., Y. M., Choi., H. M., Cha., T. S. and Yoon, B. H. (2001). The evaluation of critical pressure ratios of sonic nozzles at low Reynolds numbers. *Flow Measurement and Instrumentation*. 12**,** 37-41.

Peet, M., Sato, S., Clément, C. and Pressman, E. (2003). Heat Stress Increases Sensitivity of Pollen, Fruit and Seed Production in Tomatoes (Lycopersicon Esculentum Mill.) to Non-Optimal Vapor Pressure Deficits. *Acta Hortic*. 618**,** 209-215.

Pratihar, A. K., Kaushik, S. C. and Agarwal, R. S. (2010). Simulation of an ammonia–water compression–absorption refrigeration system for water chilling application. *International Journal of Refrigeration*. 33(7)**,** 1386-1394.

Price, H., Lüpfert, E., Kearney, D., Zarza, E., Cohen, G., Gee, R. and Mahoney, R. (2002). Advances in Parabolic Trough Solar Power Technology. *Journal of Solar Energy Engineering*. 124(2)**,** 109.

Puri, S., Beg, Q. K. and Gupta, R. (2002). Optimization of Alkaline Protease Production from Bacillus sp. by Response Surface Methodology. *Current Microbiology*. 44**,** 286-290.

Puri, V. M. (1987). Heat and Mass Transfer Analysis and Modeling in Unsaturated Ground Soils for Buried Tube Systems. *Energy in Agriculture*. 6**,** 179-193.

Qela., B. and Mouftah, H. (2008). Simulation of a House Heating System using C# - an Energy Conservation Perspective. *In:* University of Ottawa, O., ON Canada (ed.). School of Information Technology and Engineering, University of Ottawa, Ottawa, ON Canada.

Qin, Z., Berliner, P. and Karnieli, A. (2002). Numerical solution of a complete surface energy balance model for simulation of heat fluxes and surface temperature under bare soil environment. *Applied Mathematics and Computation*. 130(1)**,** 171-200.

Qu, M. (2008). *Model Based Design and Performance Analysis of Solar Absorption Cooling and Heating System.* PhD, Carnegie Mellon University.

Qu, M., Yin, H. and Archer, D. H. (2010). A solar thermal cooling and heating system for a building: Experimental and model based performance analysis and design. *Solar Energy*. 84(2)**,** 166-182.

Quoilin, S., Broek, M. V. D., Declaye, S., Dewallef, P. and Lemort, V. (2013). Techno-economic survey of Organic Rankine Cycle (ORC) systems. *Renewable and Sustainable Energy Reviews*. 22**,** 168-186.

Quoilin., S. and Lemort, V. (2009). Technological and Economical Survey of Organic Rankine Cycle Systems. *5th Eyropean Conference on Economics and Management of Energy Industry.* Algarve, Portugal.

Ramos, M. C. and Martínez-Casasnovas, J. A. (2010). Effects of precipitation patterns and temperature trends on soil water available for vineyards in a Mediterranean climate area. *Agricultural Water Management*. 97(10)**,** 1495-1505.

Rasih, R. A. and Ani, F. N. (2012). Double-Effect Solar Absorption Thermal Energy Storage. *Jurnal Mekanikal*. (35)**,** 38-53.

RETScreen (2005). RETScreen® software. 2007 ed. RETScreen International Clean Energy Decision Support Centre: RETScreen International Clean Energy Decision Support Centre.

Rice, W. (1965). An Analytical and Experimental Investigation of Multiple-Disk Turbines *Journal of Engineering for Power*. 29-33.

Romanin, V. D. (2012). *Theory and Performance of Tesla Turbines.* PhD, University of California, Berkeley.

Rong, L., Hou, X., Jia, Z., Han, Q., Ren, X. and Yang, B. (2013). Effects on soil temperature, moisture, and maize yield of cultivation with ridge and furrow mulching in the rainfed area of the Loess Plateau, China. *Agricultural Water Management*. 116**,** 101-109.

Rose, C. W. (1969). *Agricultural Physics*. 2nd. edition. Oxford, London, Edinburgh, New York, Toronto, Sydney, Paris, Braunschweig: Pergamon Press, Oxford.

Rout, S. K., Choudhury, B. K., Sahoo, R. K. and Sarangi, S. K. (2014). Multi-objective parametric optimization of Inertance type pulse tube refrigerator using response surface methodology and non-dominated sorting genetic algorithm. *Cryogenics*. 62**,** 71-83.

Sabetia., V. and Boyaghchi, F. A. (2016). Multi-objective Optimization of a Solar Driven Combined Power and Refrigeration System Using Two Evolutionary Algorithms Based on Exergoeconomic Concept. *Journal of Renewable Energy and Environment*. 3(1)**,** 43-51.

Safa., A. A., Fung., A. S. and Kumar, R. (2015). Heating and cooling performance characterisation of ground source heat pump system by testing and TRNSYS simulation. *Renewable Energy*. 84**,** 565-575.

Said, S. A. M., El-Shaarawi, M. A. I. and Siddiqui, M. U. (2012). Alternative designs for a 24-h operating solar-powered absorption refrigeration technology. *International Journal of Refrigeration*. 35(7)**,** 1967-1977.

Saitoh, T., Yamada, N. and Wakashima, S.-i. (2007). Solar Rankine Cycle System Using Scroll Expander. *Journal of Environment and Engineering*. 2(4)**,** 708-719.

Sakellari, D. (2005). *Modelling the Dynamics of Domestic Low-Temperature Heat Pump Heating Systems for Improved Performance and Thermal Comfort - A Systems Approach.* Doctor of Philosophy Thesis, Royal Institute of Technology Stockholm, Sweden.

Sanaye, S. and Sarrafi, A. (2015). Optimization of combined cooling, heating and power generation by a solar system. *Renewable Energy*. 80**,** 699-712.

Sanjay, V. (2003). *Thermodynamics Studies on Alternative Binary Working Fluids Combinations and Configurations for a Combined Power and Cooling Cycle.* University of Florida.

Sattelmacher, B., Marschner, H. and Kuhne, R. (1990). Effects of Root Zone Temperature on Root Activity of Two Potato {Sohnum tuberosum L.) Clones with Different Adaptation to High Temperature. *Journal of Agronnomy and Crop Science*. 165**,** 131-137.

Schimpf, S. and Span, R. (2015). Simulation of a solar assisted combined heat pump – Organic rankine cycle system. *Energy Conversion and Management*. 102**,** 151-160.

Schröder, E., Neumaier, K., Nagel, F. and Vetter, C. (2014). Study on Heat Transfer in Heat Exchangers for a New Supercritical Organic Rankine Cycle. *Heat Transfer Engineering*. 35(18)**,** 1505-1519.

Seo., J.-M., Song., D. and Lee, K. H. (2014). Possibility of coupling outdoor air cooling and radiant floor cooling under hot and humid climate conditions. *Energy and Buildings*. 81**,** 219-226.

Sharizal, S. A. (2006). *Integrated Solar Energy and Absorption Cooling Model for HVAC (Heating, Ventilating, and Air Onditioning) Applications in Buildings.* PhD, Michigan Technological University.

Shuttleworth, W. J. and Wallace, J. S. (1985). Evaporation from sparse crops-an energy combination theory. *Quarterly Journal of the Royal Meteorological Society*. 111(469)**,** 839-855.

Siegenthaler, J. 2014. Hydronic Radiant Ceiling Cooling for Smaller Buildings. *Hydronics Zones*, p.22.

Smith, A. D., Mago, P. J. and Fumo, N. (2013). Benefits of thermal energy storage option combined with CHP system for different commercial building types. *Sustainable Energy Technologies and Assessments*. 1**,** 3-12.

Solangi, K. H., Islam, M. R., Saidur, R., Rahim, N. A. and Fayaz, H. (2011). A review on global solar energy policy. *Renewable and Sustainable Energy Reviews*. 15(4)**,** 2149-2163.

Somers, C., Mortazavi, A., Hwang, Y., Radermacher, R., Rodgers, P. and Al-Hashimi, S. (2011). Modeling water/lithium bromide absorption chillers in ASPEN Plus. *Applied Energy*. 88(11)**,** 4197-4205.

Sotomonte., C. A. R., Ribeiro., S., Oliveira., E., Lora., E. E. S. and Venturini, O. J. (2011). Organic Rankine Cycle Associated with an Absorption Chiller for Biomass Applications. *Engenharia Térmica*. 10(01-02)**,** 11-22.

Sözen, A., Menlik, T. and Özbaş, E. (2012). The effect of ejector on the performance of diffusion absorption refrigeration systems: An experimental study. *Applied Thermal Engineering*. 33-34**,** 44-53.

Srikhirin., P., Aphornratana., S. and Chungpaibulpatana, S. (2001). A review of absorption refrigeration technologies. *Renewable and Sustainable Energy Reviews*. 5**,** 343-372.

Ssembatya., M., Pokhrel., M. K. and Reddy, R. (2014). Simulation studies on performance of solar cooling system in UAE conditions. *Energy Procedia*. 48**,** 1007-1016.

Stanish, M. A. and Perlmutter, D. D. (1981). Salt Hydrates as Absorbents in Heat Pump Cycles. *Solar Energy*. 26**,** 333-339.

Stevanovic, S. (2016). Parametric study of a cost-optimal, energy efficient office building in Serbia. *Energy*. 117(2016)**,** 492-505.

Stodola, N. and Modi, V. (2009). Penetration of solar power without storage. *Energy Policy*. 37(11)**,** 4730-4736.

Subramanian, R. S. (2008). Heat transfer in Flow Through Conduits. *In:* University, D. o. C. a. B. E. C. (ed.) *Department of Chemical and Biomolecular Engineering Clarkson University*.

Sukri, M. F., Musa, M. N., Senawi, M. Y. and Nasution, H. (2016). Modeling and Parametric Study of Cooling Loads Characteristics for Automotive AirConditioning System. *Applied Mechanics & Materials*. 819**,** 189-201.

Tamm, G., Goswami, D. Y., Lu, S. and Hasan, A. A. (2004). Theoretical and experimental investigation of an ammonia–water power and refrigeration thermodynamic cycle. *Solar Energy*. 76(1-3)**,** 217-228.

Tamm, G. O. (2003). *Experimental Investigation of an Ammonia-Based Combined Power and Cooling Cycle.* PhD, University of Florida.

Tang, C. K. (2012). Chapter 2 – Malaysia's Weather Data. *Building Energy Efficiency Technical Guideline for Passive Design*. (pp. 1-30). Malaysia.

Tarigan, E., Djuwari and Kartikasari, F. D. (2015). Techno-economic Simulation of a Grid-connected PV System Design as Specifically Applied to Residential in Surabaya, Indonesia. *Energy Procedia*. 65**,** 90-99.

Tchanche, B. F., Lambrinos, G., Frangoudakis, A. and Papadakis, G. (2011). Low-grade heat conversion into power using organic Rankine cycles – A review of various applications. *Renewable and Sustainable Energy Reviews*. 15(8)**,** 3963-3979.

Tetëns, O. (1930). Über einige meteorologische begriffe. *Z. Geophys*. 6**,** 297–309.

Thongtip, T. and Aphornratana, S. (2017). An experimental analysis of the impact of primary nozzle geometries on the ejector performance used in R141b ejector refrigerator. *Applied Thermal Engineering*. 110**,** 89-101.

Tozer, R., Syed, A. and Maidment, G. (2005). Extended temperature–entropy (T–s) diagrams for aqueous lithium bromide absorption refrigeration cycles. *International Journal of Refrigeration*. 28(5)**,** 689-697.

Treberspurg., M., Djalili., M., Staller., B. H. and IFZ (2011). New technical solutions for energy efficient buildings. *In:* SCI-Network (ed.).

Tsoutsos., T., Karagiorgas., M., Zidianakis., G., Drosou., V., Aidonis., A., Gouskos., Z. and Moeses, C. (2009). Development of the Application of Solar Thermal Cooling Systems in Greece and Cyprus. *Fresenius Environmental Bulletin*. 8(7b)**,** 1-15.

Ullah, K. R., Saidur, R., Ping, H. W., Akikur, R. K. and Shuvo, N. H. (2013). A review of solar thermal refrigeration and cooling methods. *Renewable and Sustainable Energy Reviews*. 24**,** 499-513.

Vadiee, A. and Martin, V. (2013). Thermal energy storage strategies for effective closed greenhouse design. *Applied Energy*. 109**,** 337-343.

Vijayaraghavan, S. and Goswami, D. Y. (2003). On Evaluating Efficiency of a Combined Power and Cooling Cycle. *Journal of Energy Resources Technology*. 125(3)**,** 221.

Villagarcía, L., Were, A., Domingo, F., García, M. and Alados-Arboledas, L. (2007). Estimation of soil boundary-layer resistance in sparse semiarid stands for evapotranspiration modelling. *Journal of Hydrology*. 342(1-2)**,** 173-183.

Wang, H., Peterson, R. and Herron, T. (2011). Design study of configurations on system COP for a combined ORC (organic Rankine cycle) and VCC (vapor compression cycle). *Energy*. 36(8)**,** 4809-4820.

Wang, J., Wang, J., Zhao, P. and Dai, Y. (2016). Thermodynamic analysis of a new combined cooling and power system using ammonia–water mixture. *Energy Conversion and Management*. 117**,** 335-342.

Wang, R. Z., Ge, T. S., Chen, C. J., Ma, Q. and Xiong, Z. Q. (2009). Solar sorption cooling systems for residential applications: Options and guidelines. *International Journal of Refrigeration*. 32(4)**,** 638-660.

Wattanakit., S., Chirarattananon., S. and Chaiwiwatworakul, P. (2014). Comfort Assessment of Radiant Cooling in Building in Tropical Climate. *5th International Conference on Sustainable Energy and Environment (SEE 2014).* Bangkok, Thailand: Science, Technology and Innovation foe ASEAN Green Growth.

Wei, D., Lu, X., Lu, Z. and Gu, J. (2007). Performance analysis and optimization of organic Rankine cycle (ORC) for waste heat recovery. *Energy Conversion and Management*. 48(4)**,** 1113-1119.

Weith, T., Preißinger, M., Pöllinger, S. and Brüggemann, D. (2014). Multi-Effect Plants and Ionic Liquids for Improved Absorption Chillers. *Heat Transfer Engineering*. 35(16-17)**,** 1462-1472.

Wongkee., S., Chirarattananon., S. and Chaiwiwatworakul, P. (2014a). A Field Study of Experimental of Radiant Cooling for Residential Building in a Tropical Climate. *Journal of Automation and Control Engineering*. 2(1)**,** 67-70.

Wongkee., S., Chirarattananon., S. and Chaiwiwatworakul, P. (2014b). A study of radiant cooling for a room with daytime application in tropical climate. *International Journal of Smart Grid and Clean Energy*. 3(3)**,** 347-352.

worldatlas Equator Map, Tropic of Cancer Map, Tropic of Capricorn Map, Prime Meridian. Accessed 2017. Cited 2017.

Wu., X., Zhao., J., Olesen., B. W., Fang., L. and Wanga, F. (2015). A new simplified model to calculate surface temperature and heat transfer of radiant floor heating and cooling systems. *Energy and Buildings*. 105**,** 285-293.

Xu., F. and Goswami, D. Y. (1999). Thermodynamic properties of ammonia–water mixtures for power-cycle applications. *Energy*. 24**,** 525-536.

Xu., F., Goswami., D. Y. and Bhagwat, S. S. (2000). A combined power/cooling cycle. *Energy*. 25**,** 233-246.

Yahya, T. M. B. T. (2001). Crop Diviersification in Malaysia. Crop Diversification in the Asia-Pacific Region Bangkok, Thailand. RAP PUBLICATION.

Yamada, N., Hoshi, A. and Ikegami, Y. (2009). Performance simulation of solar-boosted ocean thermal energy conversion plant. *Renewable Energy*. 34(7)**,** 1752-1758.

Yamada., N., Hoshi., A. and Ikegami, Y. (2006). Thermal Efficiency Enhancement of Ocean Thermal Energy Conversion (OTEC) Using Solar Thermal Energy. *4th International Energy Conversion Engineering Conference and Exhibit (IECEC).* San Diego, California.

Yang, F., Zhang, H., Yu, Z., Wang, E., Meng, F., Liu, H. and Wang, J. (2017). Parametric optimization and heat transfer analysis of a dual loop ORC (organic Rankine cycle) system for CNG engine waste heat recovery. *Energy*. 118**,** 753-775.

Yang., F., Zhang., H., Bei., C., Song., S. and Wang, E. (2015). Parametric optimization and performance analysis of ORC (organic Rankine cycle) for diesel engine waste heat recovery with a fin-andtube evaporator. *Energy*. 91**,** 128-141.

Yara (2015). Crop Nutrition: Effect of Soil Temperature on Root Development.

Yeh., H.-M., Ho., C.-D. and Hou, J.-Z. (2002). Collector efficiency of double-flow solar air heaters with fins attached. *Energy*. 27**,** 715-727.

Yin, Y. L., Zhai, X. Q. and Wang, R. Z. (2013). Experimental investigation and performance analysis of a mini-type solar absorption cooling system. *Applied Thermal Engineering*. 59(1-2)**,** 267-277.

Yu., G. and Yao, Y. (2015). The Experimental Research on the Heating and Cooling Performance of Light Floor Radiant Panels. *9th International Symposium on Heating, Ventilation and Air Conditioning (ISHVAC) and the 3rd International Conference on Building Energy and Environment (COBEE).* Procedia Engineering.

Yunus, A. C. (2003). *Heat Transfer: A Practical Approach*. Second. edition.: McGraw-Hill.

Zalba., B., Marin., J. M. M., Cabeza., L. F. and Mehling, H. (2003). Review on thermal energy storage with phase change: materials, heat transfer analysis and applications. *Applied Thermal Engineering*. 23**,** 251-283.

Zarrella., A., Carli., M. D. and Peretti, C. (2014). Radiant floor cooling coupled with dehumidification systems in residential buildings: A simulation-based analysis. *Energy Conversion and Management*. 85**,** 254-263.

Zhang, X., Zhao, X., Smith, S., Xu, J. and Yu, X. (2012). Review of R&D progress and practical application of the solar photovoltaic/thermal (PV/T) technologies. *Renewable and Sustainable Energy Reviews*. 16(1)**,** 599-617.

Zhao, K., Liu, X.-H. and Jiang, Y. (2016). Application of radiant floor cooling in large space buildings – A review. *Renewable and Sustainable Energy Reviews*. 55**,** 1083-1096.

Zhao, K., Liu, X. H. and Jiang, Y. (2013). Application of radiant floor cooling in a large open space building with high-intensity solar radiation. *Energy and Buildings*. 66**,** 246-257.

Zhao., K., Liu., X.-H. and Jiang, Y. (2014). On-site measured performance of a radiant floor cooling/heating system in Xi'an Xianyang International Airport. *Solar Energy*. 108(274-286).

Zhao., K., Liu., X.-H. and Jiang, Y. (2015). Cooling capacity prediction of radiant floors in large spaces of an airport. *Solar Energy*. 113**,** 221-235.

Zheng., Z., Zhao., J., Guo., H., Yang., L., Yu., X. and Fang, W. (2012). Character Segmentation System Based on C# Design and Implementation. *2012 International Workshop on Information and Electronics Engineering (IWIEE).* Procedia Engineering.

Ziviani, D., Beyene, A. and Venturini, M. (2014). Design, Analysis and Optimization of a Micro-CHP System Based on Organic Rankine Cycle for Ultralow Grade Thermal Energy Recovery. *Journal of Energy Resources Technology*. 136(1)**,** 011602.

APPENDICES A – I

APPENDIX A

KUALA LUMPUR – SUBANG STATION METEOROLOGY AND SOLAR ENERGY DATA

NASA Surface meteorology and Solar Energy: Monthly Averaged Data						
Dates	(month/day/year): 01/01/2000 through 06/30/2005					
Location	Latitude 3.1 Longitude 101.6					
Elevation (m)	Average for one degree Lat./Lon Region = 151 Site = 22					
Climate zone	1 (reference Briggs et al, http://www.energycodes.gov)					
Inc Rad	Average Insolation Incident on a Horizontal Surface (kWh/m^2/day)					
T_{air}.av	Average Air Temperature at 10 m above the Surface of the Earth (ºC)					
T_{air}.min	Minimum Air Temperature at 10 m above the Surface of the Earth (ºC)					
T_{air}.max	Maximum Air Temperature at 10 m Above the Surface of the Earth (ºC)					
RH:	Average Relative Humidity (%)					
Year	**Inc Rad (kWh.m^2/day)**	**T_{air}.min (ºC)**	**T_{air}.av (ºC)**	**T_{air}.max (ºC)**	**T_{Earth}. Ave (ºC)**	**RH (%)**
Jan-00	4.809	21.324	24.282	27.293	24.983	81.277
Feb-00	5.390	21.829	25.027	28.423	25.903	76.393
Mar-00	5.255	22.497	25.307	28.257	26.163	80.699
Apr-00	5.269	23.201	25.784	28.497	26.632	81.696
May-00	5.240	23.362	26.013	28.972	26.693	81.072
Jun-00	4.480	22.871	25.535	28.286	26.186	81.208
Jul-00	4.995	22.568	25.3212	28.252	25.949	80.995
Aug-00	5.021	22.599	25.142	27.999	25.954	81.524
Sep-00	4.657	23.094	25.521	28.099	26.641	81.444
Oct-00	4.879	23.523	25.973	28.782	26.948	79.327
Nov-00	3.732	23.807	25.714	27.832	26.748	82.973
Dec-00	4.335	23.494	25.518	27.789	26.361	82.899
Jan-01	4.333	22.860	25.052	27.578	25.838	83.248
Feb-01	5.233	22.608	25.238	28.188	25.949	79.352
Mar-01	5.694	22.89	25.41	28.01	26.393	80.386
Apr-01	5.043	23.325	25.581	27.806	26.745	84.869
May-01	5.254	23.28	25.655	27.932	26.637	85.367
Jun-01	4.861	22.860	25.385	27.989	26.167	83.103
Jul-01	4.999	22.736	25.153	27.605	25.840	82.686
Aug-01	4.973	23.205	25.657	28.350	26.491	82.681
Sep-01	5.127	23.027	25.375	27.571	26.531	82.767
Oct-01	4.608	23.472	25.717	27.966	26.822	82.297
Nov-01	4.088	23.372	25.357	27.458	26.324	82.936
Dec-01	3.943	22.787	25.035	27.300	25.861	81.148
Jan-02	5.338	22.452	25.571	28.842	26.763	69.892
Feb-02	5.444	23.088	26.758	30.390	28.582	59.022
Mar-02	5.764	23.527	26.793	30.177	28.702	67.749
Apr-02	5.304	23.441	26.26	29.133	27.602	76.836
May-02	5.324	23.342	26.002	28.710	26.831	81.816
Jun-02	5.137	22.787	25.506	28.162	26.345	82.063
Jul-02	4.906	22.754	25.205	27.663	25.917	83.071
Aug-02	4.823	22.481	25.177	28.038	26.002	80.228
Sep-02	4.830	22.39	25.298	28.153	26.536	79.811
Oct-02	5.241	77.475	25.735	28.452	27.166	80.050
Nov-02	4.479	23.35	25.853	28.647	27.230	78.509
Dec-02	4.721	23.289	25.759	28.398	27.013	78.368
Jan-03	4.216	22.806	25.788	28.946	27.347	70.095
Feb-03	5.282	23.097	26.478	29.758	28.405	64.649
Mar-03	5.719	23.296	26.543	29.853	28.229	69.218
Apr-03	5.180	23.291	26.248	29.551	27.562	75.925

May-03	5.087	23.601	26.6671	30.12	27.625	75.424
Jun-03	4.835	22.479	25.455	28.426	26.573	77.678
Jul-03	4.592	22.737	25.754	29.123	26.920	75.337
Aug-03	4.873	22.787	25.370	28.153	26.383	80.104
Sep-03	4.486	22.647	25.297	27.945	26.622	79.712
Oct-03	4.510	23.172	25.819	28.745	27.131	76.669
Nov-03	4.334	23.509	25.987	28.821	27.509	76.624
Dec-03	3.827	23.432	26.309	29.478	28.174	66.728
Jan-04	5.345	23.981	27.436	30.979	30.127	57.632
Feb-04	5.338	23.872	27.564	31.662	30.006	57.156
Mar-04	5.462	24.211	27.519	31.091	29.775	72.132
Apr-04	5.293	24.567	28.131	31.979	30.404	62.458
May-04	5.346	24.403	28.197	31.698	30.211	59.925
Jun-04	4.7563	22.552	26.309	30.069	27.636	68.495
Jul-04	4.599	22.613	26.019	29.45	27.786	69.562
Aug-04	5.322	22.419	25.556	28.821	27.093	74.610
Sep-04	5.082	22.851	25.959	29.027	27.941	71.673
Oct-04	5.025	23.403	26.539	29.793	28.917	68.167
Nov-04	4.539	24.423	27.414	30.476	30.382	62.612
Dec-04	3.775	24.324	27.397	30.591	30.353	58.124
Jan-05	5.435	23.69	27.421	30.807	30.296	53.760
Feb-05	5.823	24.016	27.363	30.433	29.977	58.869
Mar-05	5.759	23.886	27.163	30.420	29.287	65.451
Apr-05	5.600	23.096	25.951	28.957	27.164	79.654
May-05	4.977	23.128	25.891	28.800	26.904	80.82
Jun-05	4.935	22.951	25.812	28.863	26.454	78.897

APPENDIX B

CALCULATED THERMODYNAMIC PROPERIES OF WORKING FLUIDS

B1: Calculated working fluid thermodynamic properties based on NH_3 mass concentration (0.3–0.7)

Stage	Temperature (ºC)	Pressure (bar)	h (KJ/Kg)	Internal Energy (kJ/kg)	S (KJ/Kg-K)	V (m^3/kg)
1	70	16	1724.60	1574.6	5.8939	0.0937
2	40	10	1671.30	1532.7	5.9383	0.1386
3	25	10	460.82	1498.1	1.8804	0.1286
4	-19	2	256.23	255.93	6.3604	0.00151
5	5	2	1638.50	1506.5	6.5689	0.6599
6	25	4	2.9890	2.5400	0.6657	0.00112
			1.703	1.2458	6.3548	0.00114
			5.7853	5.3192	6.3548	0.00116
			15.595	15.245	6.3548	0.00119
			31.789	31.303	6.3548	0.00121
			54.032	53.527	6.3548	0.00110
			198.96	261.69	6.3548	0.0552
			336.56	313.46	1.9135	0.0760
			593.23	546.73	2.7738	0.1324
7	25 *(NH_3:H_2O) (0.3 – 0.7)*	16	3.9385	2.2558	0.6648	0.00112
			2.6358	0.9218	1.8784	0.00114
			6.7009	4.9539	1.8784	0.00116
			16.619	14.836	1.8784	0.00119
			32.67	30.849	1.8784	0.00121
			54.891	53.026	1.8784	0.00110
			83.073	81.161	1.8784	0.00127
			116.81	114.85	1.1419	0.00131
			155.57	153.55	1.2425	0.00134
8	38 *(NH_3:H_2O) 0.3 – 0.7)*	16	60.774	59.074	0.8514	0.00113
			60.321	58.587	2.0849	0.00115
			65.348	63.578	2.0849	0.00118
			76.226	74.418	2.0849	0.00120
			93.14	91.291	2.0849	0.0012
			116.07	114.17	2.0849	0.00126
			144.78	142.83	2.0849	0.00129
			178.89	176.89	1.3457	0.00133
			217.90	215.84	1.4471	0.00138
9	70	16	294.35	292.71	0.9542	0.00102
10	35	16	148.07	146.46	0.5046	0.00101
11	35	4	146.99	146.58	0.5050	0.0010

B2: Calculated working fluid thermodynamic properties at turbine inlet pressure (12 – 15bar)

Stage	Temperature (°C)	Pressure (bar)	h (KJ/Kg)	Internal Energy (kJ/kg)	S (KJ/Kg-K)	V (m^3/kg)
1	70	12 – 21	1742.8	1588.1	6.0748	0.129
			1738.3	1584.8	6.0259	0.118
			1733.8	1581.5	5.9797	0.109
			1729.2	1578.1	5.9358	0.101
			1724.6	1574.6	5.8939	0.094
			1719.8	1571.1	5.8537	0.0875
			1715.00	1567.50	5.8149	0.0819
			1710.1	1563.9	5.7775	0.0769
			1705.1	1560.1	5.7411	0.0725
			1699.9	1556.3	5.7057	0.0684
2	40	10	1671.3	1532.7	5.9383	0.139
3	25	10	460.82	1498.1	1.8804	0.0016
4	-19	2	256.23	255.93	6.3604	0.0015
5	5	2	1638.5	1506.5	6.5689	0.659
6	25	4	54.032	53.527	6.3548	0.0011
7	25	12 – 21	12.000	16.374	14.947	0.822
			16.455	14.910	0.8219	0.00119
			16.537	14.873	0.8218	0.00119
			16.619	14.836	0.8217	0.00119
			16.700	14.799	0.8215	0.00119
			16.782	14.762	0.8214	0.00119
			16.864	14.725	0.8213	0.00119
			16.945	14.688	0.8212	0.00119
			17.027	14.651	0.8211	0.00119
			17.109	14.614	0.8209	0.00119
8	38	12 – 21	75.989	74.542	1.0178	0.00121
			76.068	74.501	1.0176	0.00121
			76.147	74.459	1.0175	0.00121
			76.226	74.418	1.0174	0.00121
			76.305	74.376	1.0172	0.00121
			76.384	74.335	1.0171	0.00121
			76.463	74.294	1.0170	0.00121
			76.542	74.252	1.0168	0.00121
			76.621	74.211	1.0167	0.00121
			76.700	74.170	1.0166	0.00120
9	70	12 – 21	294.02	292.79	0.9544	0.00102
			294.10	292.77	0.9544	0.00102
			294.18	292.75	0.9543	0.00102
			294.27	292.73	0.9543	0.00102
			294.35	292.71	0.9542	0.00102
			294.43	292.69	0.9541	0.00102
			294.51	292.67	0.9541	0.00102
			294.59	292.65	0.9540	0.00102
			294.68	292.63	0.9539	0.00102
			294.76	292.61	0.9539	0.00102
10	35	12 – 21	147.71	146.50	0.5047	0.00101
			147.80	146.49	0.5046	0.00101
			147.89	146.48	0.5046	0.00101
			147.98	146.47	0.5046	0.00101
			148.07	146.46	0.5046	0.00101
			148.16	146.45	0.5045	0.001001
			148.25	146.44	0.5045	0.001001
			148.34	146.43	0.5045	0.001001
			148.43	146.42	0.5044	0.001001
			148.52	146.40	0.5044	0.001001
11	35	4	146.99	146.58	0.5049	0.001006

B3: Calculated working fluid thermodynamic properties at 60 ºC – 120 ºC

Stage	Temperature (^{0}C)	Pressure (bar)	h (KJ/Kg)	Internal Energy (kJ/kg)	S (KJ/Kg-K)	V (m^3/kg)
1	60 – 120	16	1695	1551.8	5.8066	0.0895
			1710	1563.4	5.8511	0.0916
			1724.6	1574.6	5.8939	0.0937
			1738.8	1585.7	5.9352	0.0957
			1752.8	1596.5	5.9751	0.0977
			1766.6	1607.1	6.0139	0.0997
			1780.2	1617.6	6.0516	0.1016
			1793.7	1628	6.0883	0.1035
			1807	1638.3	6.1242	0.1054
			1820.1	1648.6	6.1593	0.1072
			1833.2	1658.7	6.1937	0.1091
			1846.2	1668.8	6.2274	0.1109
			1859.1	1678.9	6.2605	0.1127
2	40	10	1671.3	1532.7	5.9383	0.1386
3	25	10	460.82	1498.1	1.8804	0.0016
4	-19	2	256.23	255.93	6.3604	0.00151
5	5	2	1638.5	1485.2	6.5689	0.6599
6	25	4	54.032	53.527	0.9658	0.00110
7	25	16	4.0248	2.2301	0.6647	0.00112
8	38	16	60.858	59.044	0.8513	0.00113
9	60 – 120	16	252.42	250.90	0.8305	0.00102
			273.34	271.81	0.8928	0.00102
			294.27	292.73	0.9543	0.00102
			315.21	313.67	0.9543	0.00102
			336.17	334.63	1.0746	0.00103
			357.15	355.6	0.9543	0.00103
			378.15	376.59	1.1802	0.00103
			399.17	397.61	1.2493	0.00104
			420.22	418.65	1.3061	0.00104
			441.29	439.72	1.3622	0.00105
			462.4	460.83	1.4177	0.00105
			483.55	481.96	1.4725	0.00106
			504.73	503.14	1.5267	0.00106
10	35	16	148.07	146.46	0.5046	0.00101
11	35	4	146.99	146.58	0.5049	0.00101

APPENDIX C

C# SOLUTION ALGORITHM AND CALCULATION IMPLEMENTATION

C1: Flowchat fot the proposed System Capacity Model Calculation in C#

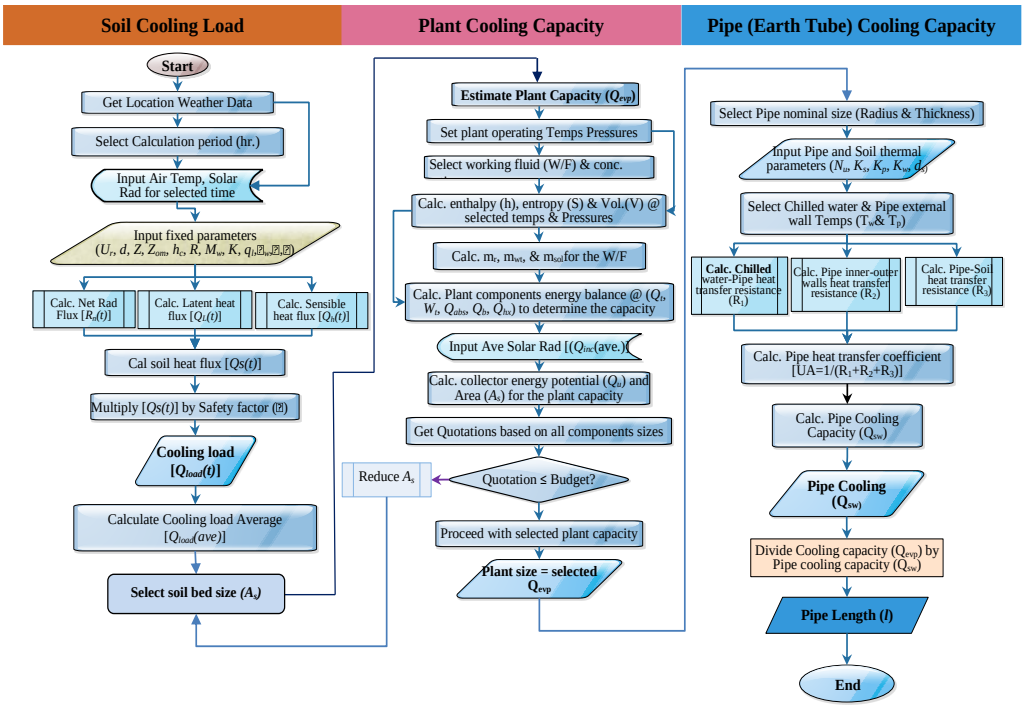

C2: Calculation Algorithm in C#

```
#region Pcc model instance
 public PlantCoolingCapacityModel Pcc { get; private set; }
 #endregion

 #region Compute Parameters
 public ICommand ComputeParameters { get; private set; }

 public bool CanComputeParameters =>
              !Pcc.IsComputed && _Q_inc_Ave != 0 && Pcc.Q_evp != 0 && Pcc.T_r != 0
           && _load_h_instance.LoadedValues != null && Pcc.X_NH3 != 0 && Pcc.n_g != 0 && Pcc.n_t
!= 0
           && Pcc.n_sp != 0 && Pcc.P_6 != 0 && Pcc.P_7 != 0 && Pcc.V_7 != 0 && Pcc.k_c != 0;

 public void ComputeParametersVal() {
    lock (Pcc) {
       Thread thread = new Thread(() => {
```

```
            Pcc.Cal_m_r(Pcc.Q_evp, Pcc.h[4].Value, Pcc.h[2].Value);
            Pcc.Cal_Q_t(Pcc.m[0].Value, Pcc.h[0].Value, Pcc.h[1].Value);
            Pcc.Cal_W_t(Pcc.Q_t, Pcc.n_t, Pcc.n_g);
            Pcc.Cal_Q_c(Pcc.m[1].Value, Pcc.h[1].Value, Pcc.h[2].Value);
            Pcc.Cal_CR(Pcc.X_NH3);
            Pcc.Cal_m_sol(Pcc.CR, Pcc.m_r);
            Pcc.Cal_m_wt(Pcc.m_sol, Pcc.m_r);
            Pcc.Cal_Q_abs(Pcc.m[4].Value, Pcc.h[4].Value, Pcc.m[10].Value, Pcc.h[10].Value,
Pcc.m[5].Value, Pcc.h[5].Value);
            Pcc.Cal_W_sp(Pcc.m_sol, Pcc.V_7, Pcc.P_7, Pcc.P_6, Pcc.n_sp);
            Pcc.Cal_Q_hx(Pcc.m[6].Value, Pcc.h[6].Value, Pcc.m[8].Value, Pcc.h[8].Value, Pcc.m[7].Value,
Pcc.h[7].Value, Pcc.m[9].Value, Pcc.h[9].Value);
            Pcc.Cal_Q_b(Pcc.m[0].Value, Pcc.h[0].Value, Pcc.m[8].Value, Pcc.h[8].Value, Pcc.m[7].Value,
Pcc.h[7].Value);
            Pcc.Cal_Q_u(Pcc.Q_b, Pcc.k_c);
            Pcc.Cal_A_c(Pcc.Q_u, _Q_inc_Ave);

            Pcc.IsComputed = true;
        });

        thread.IsBackground = true;
        thread.Start();
    }
 }
```

C3: Calculation Implementation Codes in C#

```
public void Cal_A_c(double l_Q_u, double l_Q_inc_avg) {
    _A_c = l_Q_u / (l_Q_inc_avg * 0.001);

    _A_c = Math.Round(_A_c, DECIMALPLACES);
    OnOutputPropertyChanged(this, nameof(A_c));
}
public void Cal_Q_u(double l_Q_b, double l_k_c) {
    _Q_u = l_Q_b / l_k_c;

    _Q_u = Math.Round(_Q_u, DECIMALPLACES);
    OnOutputPropertyChanged(this, nameof(Q_u));
}
public void Cal_Q_b(double l_m1, double l_h1, double l_m9, double l_h9, double l_m_8, double l_h_8) {
    _Q_b = (l_m1 * l_h1) + (l_m9 * l_h9) - (l_m_8 * l_h_8);

    _Q_b = Math.Round(_Q_b, DECIMALPLACES);
    OnOutputPropertyChanged(this, nameof(Q_b));
}
public void Cal_Q_hx(double l_m7, double l_h7, double l_m9, double l_h9, double l_m8, double l_h8,
double l_m10, double l_h10) {
    _Q_hx = ((l_m7 * l_h7) + (l_m9 * l_h9)) - ((l_m8 * l_h8) + (l_m10 * l_h10));

    _Q_hx = Math.Round(_Q_hx, DECIMALPLACES);
    OnOutputPropertyChanged(this, nameof(Q_hx));
}
public void Cal_W_sp(double l_m_sol, double l_V7, double l_P7, double l_P6, double l_n_sp) {
    _W_sp = (l_m_sol * l_V7 * ((l_P7 - l_P6) * 100)) / l_n_sp;

    _W_sp = Math.Round(_W_sp, DECIMALPLACES);
    OnOutputPropertyChanged(this, nameof(W_sp));
}
public void Cal_Q_abs(double l_m5, double l_h5, double l_m11, double l_h11, double l_m6, double l_h6) {
    _Q_abs = (l_m5 * l_h5) + (l_m11 * l_h11) - (l_m6 * l_h6);

    _Q_abs = Math.Round(_Q_abs, DECIMALPLACES);
    OnOutputPropertyChanged(this, nameof(Q_abs));
}
```

```
public void Cal_m_wt(double l_m_sol, double l_m_r) {
    _m_wt = (l_m_sol - l_m_r);
    _m_wt = Math.Round(_m_wt, DECIMALPLACES);

    _m[8].Value = _m[9].Value = _m[10].Value = _m_wt;
    OnOutputPropertyChanged(this, nameof(m_wt));
}
public void Cal_m_sol(double l_CR, double l_m_r) {
    _m_sol = (l_CR * l_m_r);
    _m_sol = Math.Round(_m_sol, DECIMALPLACES);

    _m[5].Value = _m[6].Value = _m[7].Value = _m_sol;
    OnOutputPropertyChanged(this, nameof(m_sol));
}
public void Cal_CR(double l_X_NH3) {
    _CR = 1 / l_X_NH3;

    _CR = Math.Round(_CR, DECIMALPLACES);
    OnOutputPropertyChanged(this, nameof(CR));
}
public void Cal_Q_c(double l_m2, double l_h2, double l_h3) {
    _Q_c = l_m2 * (l_h2 - l_h3);

    _Q_c = Math.Round(_Q_c, DECIMALPLACES);
    OnOutputPropertyChanged(this, nameof(Q_c));
}
public void Cal_W_t(double l_Q_t, double l_n_t, double l_n_g) {
    _W_t = l_Q_t * l_n_t * l_n_g;

    _W_t = Math.Round(_W_t, DECIMALPLACES);
    OnOutputPropertyChanged(this, nameof(W_t));
}
public void Cal_Q_t(double l_m1, double l_h1, double l_h2) {
    _Q_t = l_m1 * (l_h1 - l_h2);

    _Q_t = Math.Round(_Q_t, DECIMALPLACES);
    OnOutputPropertyChanged(this, nameof(Q_t));
}
public void Cal_m_r(double l_Q_evp, double l_h5, double l_h3) {
    _m_r = (l_Q_evp / (l_h5 - l_h3));
    _m_r = Math.Round(_m_r, DECIMALPLACES);

    _m[0].Value = _m[1].Value = _m[2].Value = _m[3].Value = _m[4].Value = _m_r;
    OnOutputPropertyChanged(this, nameof(m_r));
}
public bool Compare_Budget_Quotation(double l_budget, double l_quotation) {
    return (l_quotation <= l_budget);
}
```

APPENDIX D

EXPERIMENTAL SET-UPS

NI and LabVIEW Installations for Data Logging

NI Panel Testing and Configurations

Chilled Water Tanks, Cooled Soil bed, and Controlled Soil Bed

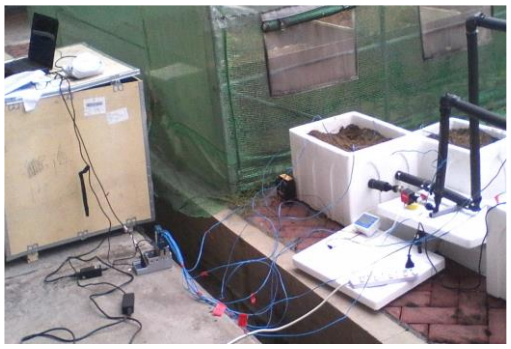

Soil Data logging to Computer through NI Data Logger

Absorption Chiller Operating Data Logging to Computer through NI Logger

APPENDIX E

SOIL COOLING TEMPERATURE PROFILE

Flow rate = 0.004kg/sec

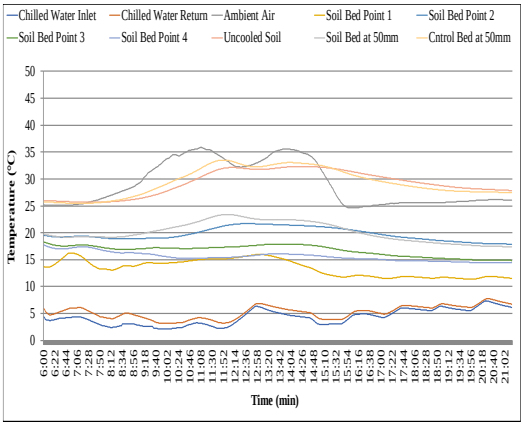

Flow rate = 0.006kg/sec

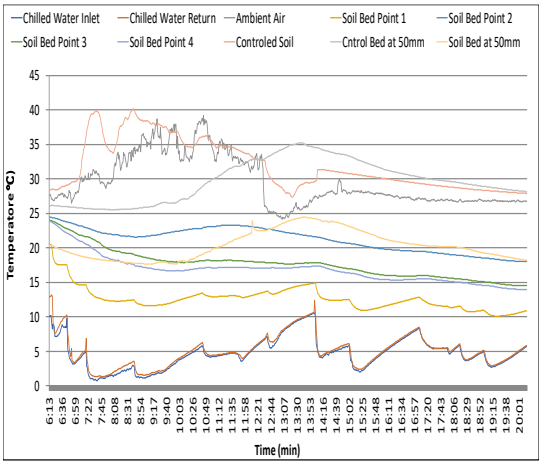

Flow rate = 0.008kg/sec

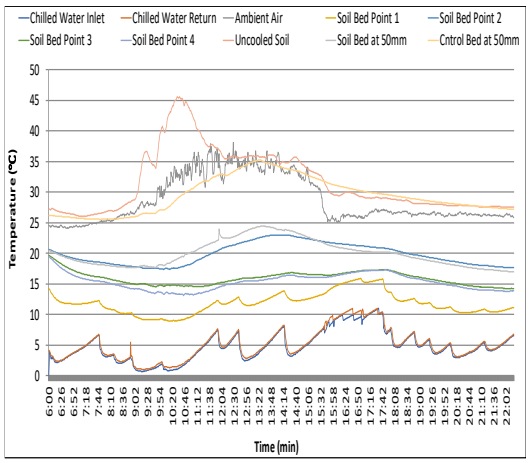

Flow rate = 0.01kg/sec

APPENDIX F

ABSORPTION CHILLER'S PERFORMANCE

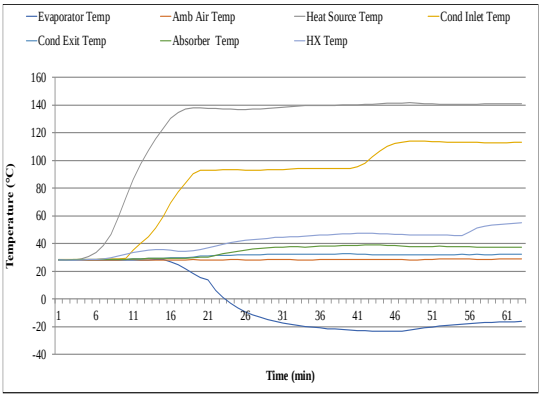

Chiller's Performance (1st Run)

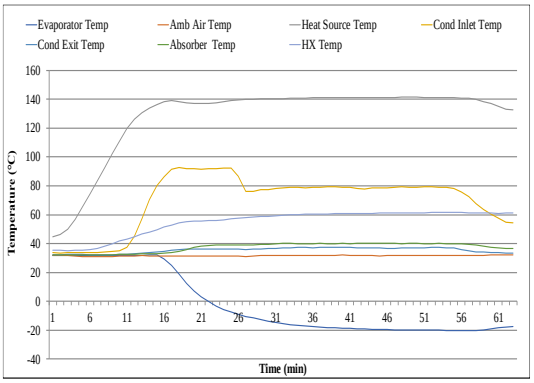

Chiller's Performance (2nd Run)

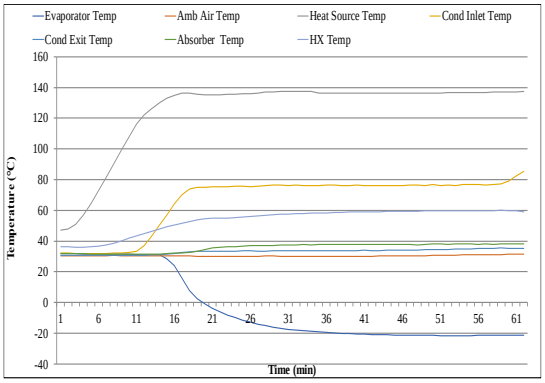

Chiller's Performance (3rd Run)

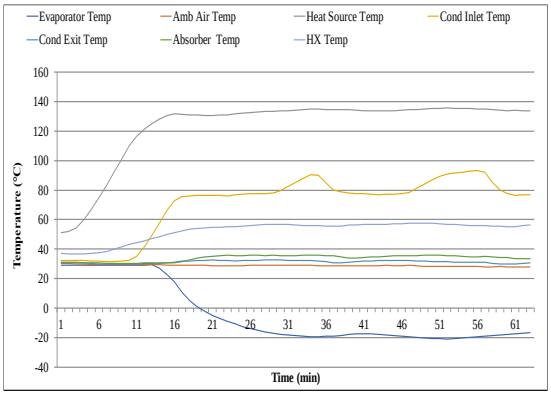

Chiller's Performance (4th Run)

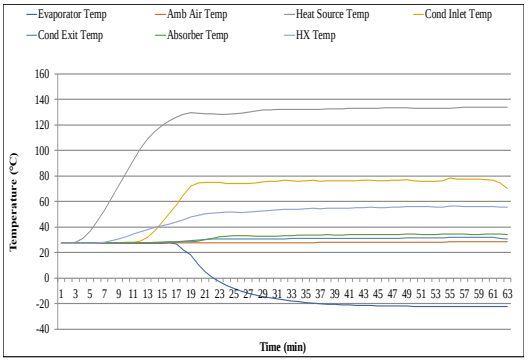

Chiller's Performance (5th Run)

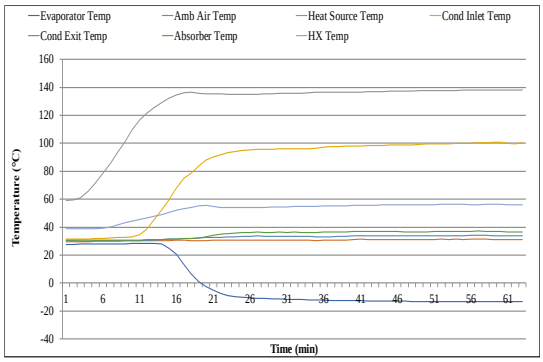

Chiller's Performance (6th Run)

APPENDIX G

PARAMETRIC ANALYSIS AND OPTIMIZATION

G1: Soil Cooling Analysis

G1-1: Soil Temperature Responses to Influencing Factors (chilled water flow rates and temperatures, and ambient air temperatures)

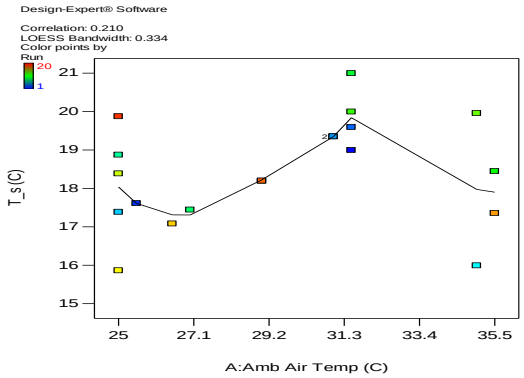

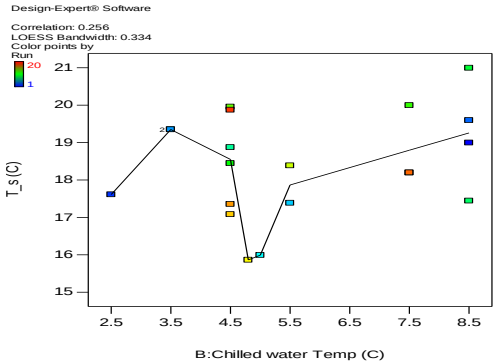

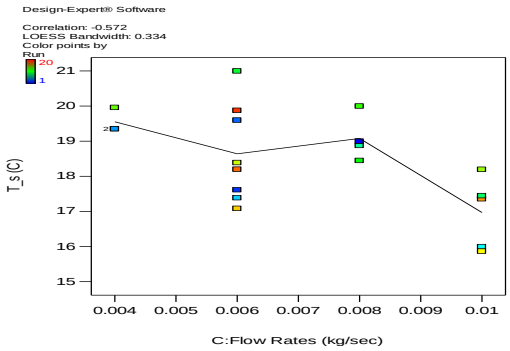

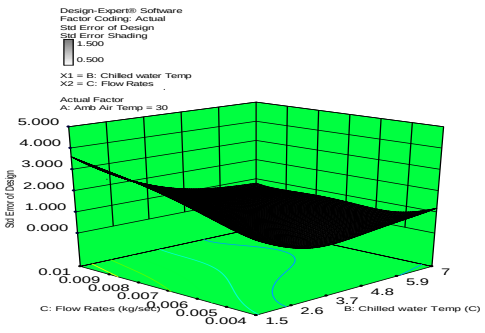

G1-3: Model Analysis and Equation

Analysis of variance table [Partial sum of square					
Source	**Sum of Squares**	**Mean Square**	**F Value**	**p-value Prob > F**	
Model	20.17	6.72	7.09	0.0030	significant
A-Amb Air Temp	*1.53*	*1.53*	*1.61*	*0.2224*	
B-Chilled water Temp	*6.52*	*6.52*	*6.87*	*0.0185*	
C-Flow Rates	*16.62*	*16.62*	*17.51*	*0.0007*	
Residual	15.19	0.95			
Lack of Fit	*13.71*	*1.05*	*2.14*	*0.2903*	*not significant*
Pure Error	*1.48*	*0.49*			
Cor Total	35.36				

$$T_s = 17.777 + 0.073\ (A) + 0.318(B) - 466.69(C)$$

G1-4: Model Diagnostics and Graph

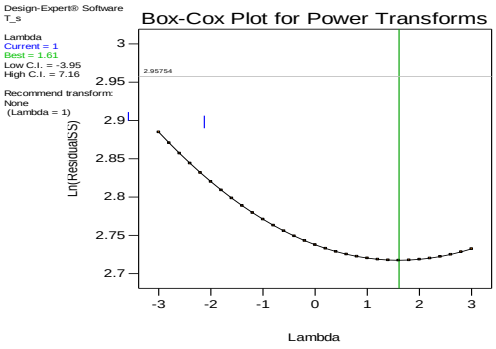

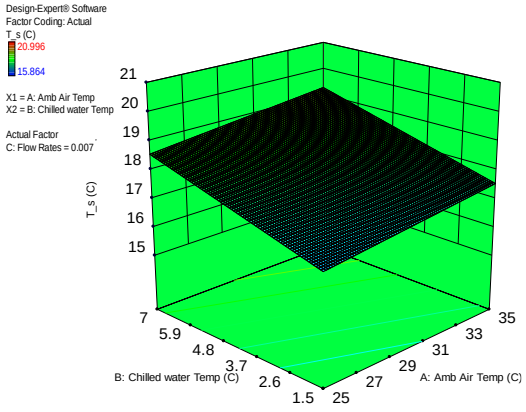

G2: Combined Plant Analysis

G2-1: Plant Performance Responses ($W_{\_t}$, $W_{\_sp}$, $Q_{\_loss}$, $COP_{\_cooling}$, $ORC_{\_eff}$, and $COP_{\_overall}$) to influencing factors (W/F temperatures, Boiler pressure, and W/F concentration ratio)

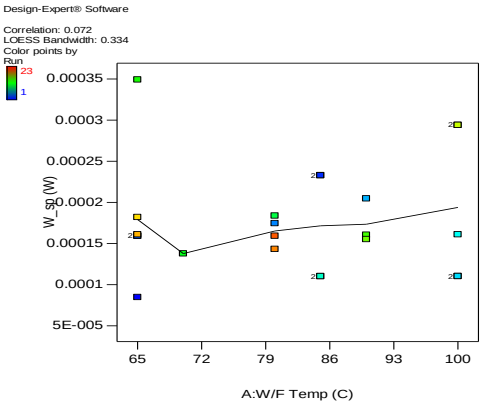

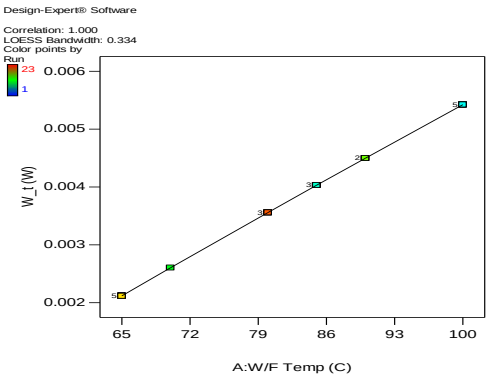

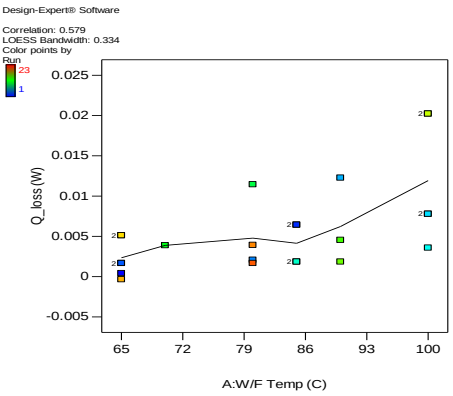

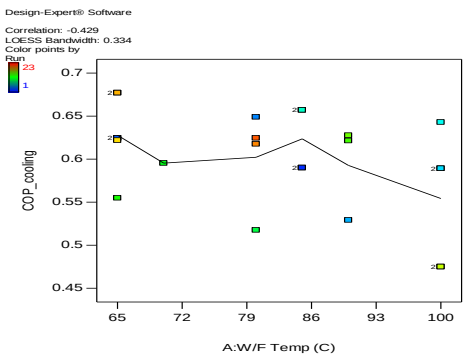

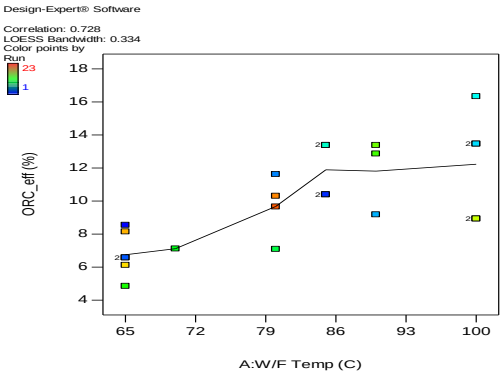
Design-Expert® Software
Correlation: 0.728
LOESS Bandwidth: 0.334
Color points by
Run
23
1
ORC_eff (%)
A:W/F Temp (C)

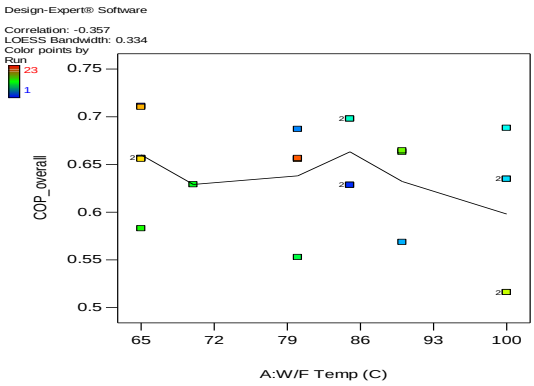
Design-Expert® Software
Correlation: -0.357
LOESS Bandwidth: 0.334
Color points by
Run
23
1
COP_overall
A:W/F Temp (C)

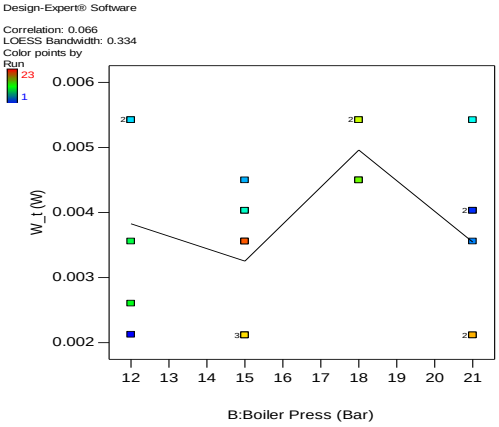
Design-Expert® Software
Correlation: 0.066
LOESS Bandwidth: 0.334
Color points by
Run
23
1
W_t (W)
B:Boiler Press (Bar)

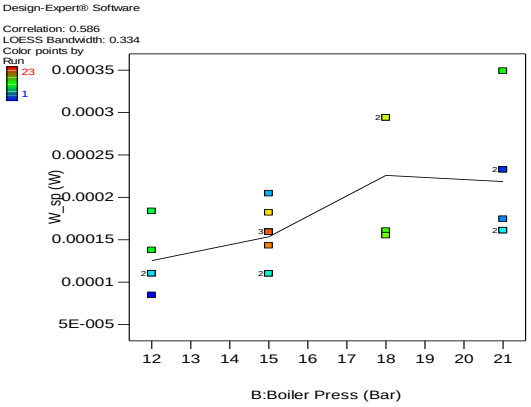
Design-Expert® Software
Correlation: 0.586
LOESS Bandwidth: 0.334
Color points by
Run
23
1
W_sp (W)
B:Boiler Press (Bar)

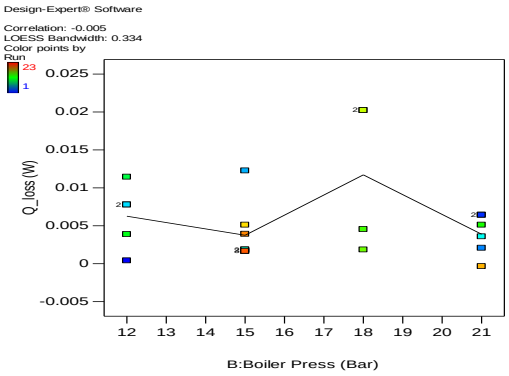
Design-Expert® Software
Correlation: -0.005
LOESS Bandwidth: 0.334
Color points by
Run
23
1
Q_loss (W)
B:Boiler Press (Bar)

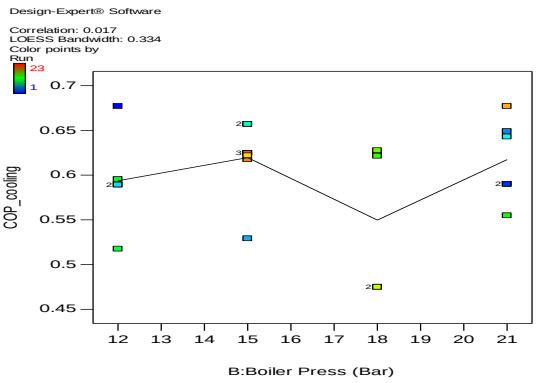
Design-Expert® Software
Correlation: 0.017
LOESS Bandwidth: 0.334
Color points by
Run
23
1
COP_cooling
B:Boiler Press (Bar)

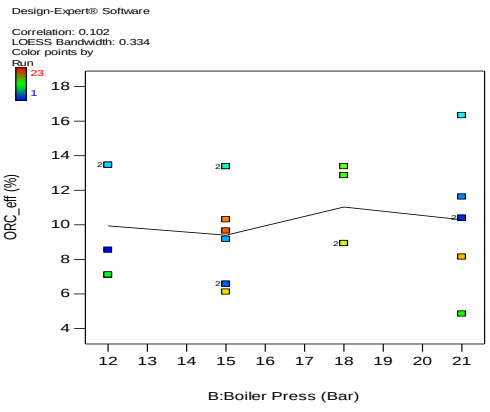
Design-Expert® Software
Correlation: 0.102
LOESS Bandwidth: 0.334
Color points by
Run
23
1
ORC_eff (%)
B:Boiler Press (Bar)

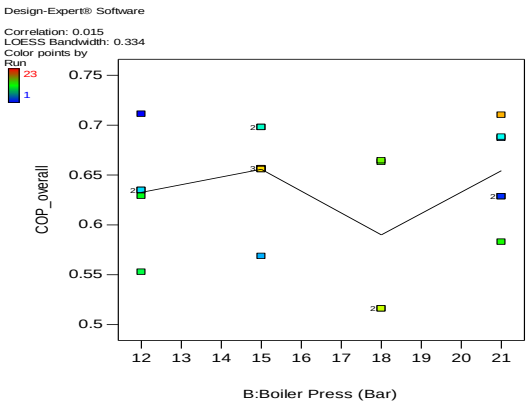
Design-Expert® Software
Correlation: 0.015
LOESS Bandwidth: 0.334
Color points by
Run
23
1
COP_overall
B:Boiler Press (Bar)

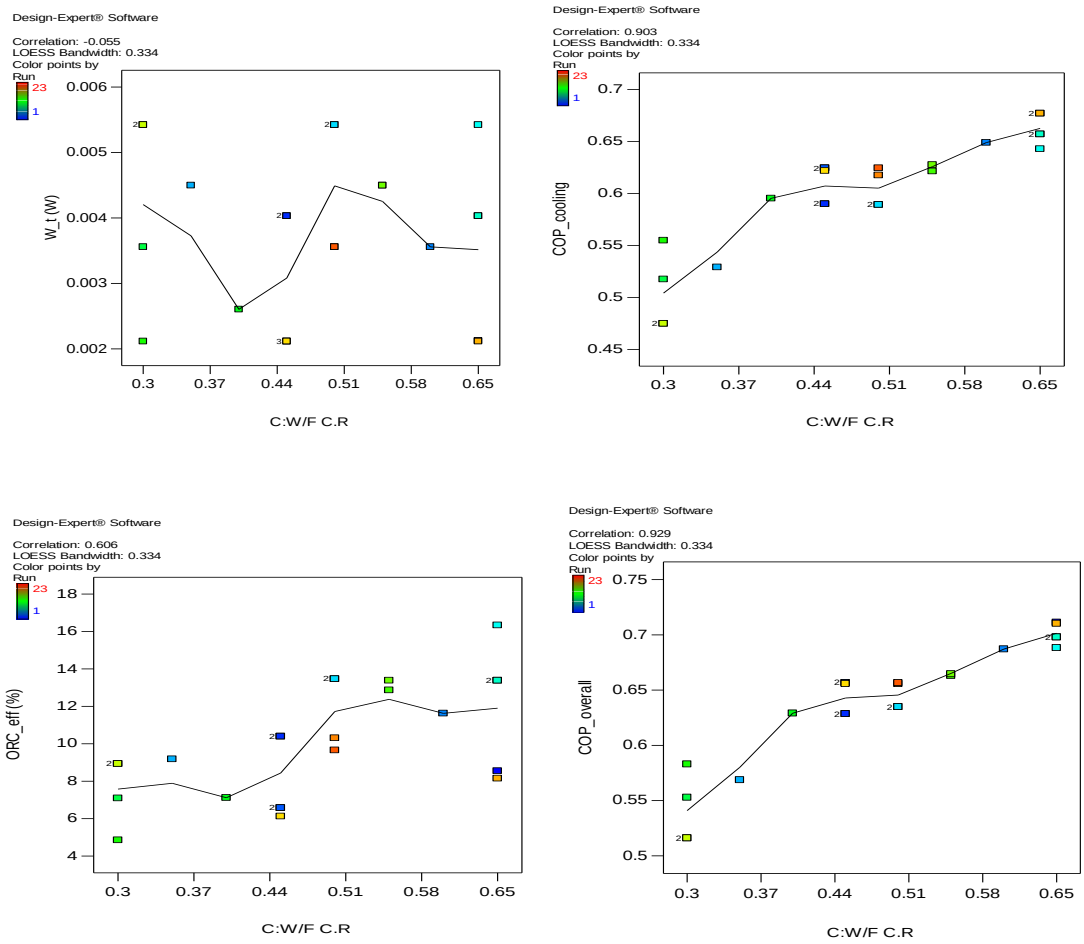

G2-3: **Analyses and Equations**

A. R1 (W_t)

ANOVA for Response Surface Quadratic model					
Source	**Sum of Squares**	**Mean Square**	**F Value**	**p-value Prob > F**	
Model	3.344E-005	3.716E-006	2.205E+007	< 0.0001	significance
A-W/F Temp	3.180E-005	3.180E-005	1.887E+008	< 0.0001	
B-Boiler Press	6.815E-012	6.815E-012	40.45	< 0.0001	
C-W/F C.R	6.179E-012	6.179E-012	36.67	< 0.0001	
AB	2.724E-011	2.724E-011	161.69	< 0.0001	
AC	1.043E-011	1.043E-011	61.89	< 0.0001	
BC	2.561E-011	2.561E-011	151.98	< 0.0001	
A^2	2.800E-009	2.800E-009	16618.54	< 0.0001	
B^2	3.911E-011	3.911E-011	232.09	< 0.0001	
C^2	2.367E-013	2.367E-013	1.40	0.2571	
Residual	2.190E-012	1.685E-013			
Lack of Fit	9.780E-013	1.956E-013	1.29	0.3557	not significant
Pure Error	1.212E-012	1.516E-013			
Cor Total	3.344E-005				

$$W_t = -4.525 \times 10^{-3} + 1.080 \times 10^{-4}(A) - 6.276 \times 10^{-6}(B) + 7.830 \times 10^{-5}(C) + 2.587 \times 10^{-8}(AB) - 4.430 \times 10^{-7}(AC) - 2.723 \times 10^{-6}(BC) - 8.369 \times 10^{-8}(A^2) + 1.595 \times 10^{-7}(B^2) + 8.046 \times 10^{-6}(C^2)$$

B. R2 ($W_{\_sp}$)

ANOVA for Response Surface Quadratic model					
Source	**Sum of Squares**	**Mean Square**	**F Value**	**p-value**	
Model	9.460E-008	1.051E-008	190.57	< 0.0001	significance
A-W/F Temp	1.479E-011	1.479E-011	0.27	0.6133	
B-Boiler Press	3.581E-008	3.581E-008	649.24	< 0.0001	
C-W/F C.R	5.039E-008	5.039E-008	913.69	< 0.0001	
AB	3.595E-011	3.595E-011	0.65	0.4340	
AC	2.036E-011	2.036E-011	0.37	0.5540	
BC	2.263E-009	2.263E-009	41.03	< 0.0001	
A^2	1.304E-010	1.304E-010	2.36	0.1481	
B^2	1.020E-010	1.020E-010	1.85	0.1969	
C^2	2.130E-009	2.130E-009	38.61	< 0.0001	
Residual	7.170E-010	5.515E-011			
Lack of Fit	2.306E-010	4.612E-011	0.76	0.6035	not significant
Pure Error	4.864E-010	6.080E-011			
Cor. Total	9.531E-008				

$$W_{sp} = 1.702 \times 10^{-4} - 2.848 \times 10^{-6}(A) + 3.563 \times 10^{-5}(B) - 7.567 \times 10^{-4}(C) - 2.972 \times 10^{-8}(AB) + 6.189 \times 10^{-7}(AC) - 2.56 \times 10^{-5}(BC) + 1.806 \times 10^{-8}(A^2) - 2.576 \times 10^{-7}(B^2) + 7.631 \times 10^{-4}(C^2)$$

C. R3 ($Q_{\_loss}$)

ANOVA for Response Surface Quadratic model					
Source	**Sum of Squares**	**Mean Square**	**F Value**	**p-value**	
Model	6.711E-004	7.457E-005	46.86	< 0.0001	significant
A-W/F Temp	1.857E-004	1.857E-004	116.72	< 0.0001	
B-Boiler Press	9.496E-009	9.496E-009	5.968E-003	0.9396	
C-W/F C.R	3.184E-004	3.184E-004	200.09	< 0.0001	
AB	1.865E-006	1.865E-006	1.17	0.2987	
AC	4.224E-005	4.224E-005	26.54	0.0002	
BC	1.150E-007	1.150E-007	0.072	0.7923	
A^2	3.808E-006	3.808E-006	2.39	0.1459	
B^2	2.890E-007	2.890E-007	0.18	0.6769	
C^2	1.595E-005	1.595E-005	10.02	0.0074	
Residual	2.069E-005	1.591E-006			
Lack of Fit	6.576E-006	1.315E-006	0.75	0.6112	not significant
Pure Error	1.411E-005	1.764E-006			
Cor Total	6.918E-004				

$$Q_{loss} = 8.901 \times 10^{-3} + 3.081 \times 10^{-5}(A) - 1.863 \times 10^{-4}(B) - 0.02432(C) + 6.769 \times 10^{-6}(AB) - 8.915 \times 10^{-4}(AC) + 1.825 \times 10^{-4}(BC) + 3.081 \times 10^{-6}(A^2) - 1.371 \times 10^{-5}(B^2) + 0.06605(C^2)$$

D. R4 ($COP_{\_cooling}$)

ANOVA for Response Surface Quadratic model					
Source	**Sum of Squares**	**Mean Square**	**F Value**	**p-value**	
Model	0.072	7.992E-003	1559.41	< 0.0001	significant
A-W/F Temp	9.113E-003	9.113E-003	1778.03	< 0.0001	
B-Boiler Press	8.608E-008	8.608E-008	0.017	0.8989	
C-W/F C.R	0.054	0.054	10483.18	< 0.0001	
AB	3.465E-007	3.465E-007	0.068	0.7989	
AC	7.309E-004	7.309E-004	142.60	< 0.0001	
BC	2.340E-006	2.340E-006	0.46	0.5111	
A^2	6.611E-008	6.611E-008	0.013	0.9113	
B^2	8.486E-007	8.486E-007	0.17	0.6907	

C^2	1.383E-003	1.383E-003	269.81	< 0.0001	
Residual	6.663E-005	5.125E-006			
Lack of Fit	1.847E-005	3.694E-006	0.61	0.6937	not significant
Pure Error	4.816E-005	6.020E-006			
Cor Total	0.072				

$$COP_{cooling} = 0.53197 - 3.379 \times 10^{-3}(A) + 1.426 \times 10^{-3}(B) + 0.709(C) - 2.918 \times 10^{-6}(AB) + 3.708 \times 10^{-3}(AC) - 8.232 \times 10^{-4}(BC) + 4.066 \times 10^{-7}(A^2) - 2.349 \times 10^{-5}(B^2) - 0.61498(C^2)$$

E. R5 ($ORC_{\_eff}$)

ANOVA for Response Surface Quadratic model					
Source	**Sum of Squares**	**Mean Square**	**F Value**	**p-value**	
Model	199.24	22.14	359.87	< 0.0001	significant
A-W/F Temp	111.77	111.77	1816.91	< 0.0001	
B-Boiler Press	1.124E-003	1.124E-003	0.018	0.8945	
C-W/F C.R	75.82	75.82	1232.57	< 0.0001	
AB	0.028	0.028	0.46	0.5104	
AC	5.58	5.58	90.76	< 0.0001	
BC	0.040	0.040	0.66	0.4327	
A^2	1.16	1.16	18.80	0.0008	
B^2	0.060	0.060	0.98	0.3414	
C^2	0.19	0.19	3.01	0.1065	
Residual	0.80	0.062			
Lack of Fit	0.32	0.063	1.05	0.4501	not significant
Pure Error	0.48	0.060			
Cor Total	200.04				

$$ORC_{eff} = -10.228 + +0.290(A) - 0.226(B) - 2.529(C) + 8.321 \times 10^{-4}(AB) + 0.3241(AC) - 0.108(BC) - 1.70110^{-3}(A^2) + 6.246 \times 10^{-3}(B^2) - 7.1142(C^2)$$

F. R6 ($COP_{\_overall}$)

ANOVA for Response Surface Quadratic model					
Source	**Sum of Squares**	**Mean Square**	**F Value**	**p-value**	
Model	0.072	7.996E-003	579.26	< 0.0001	significant
A-W/F Temp	6.013E-003	6.013E-003	435.62	< 0.0001	
B-Boiler Press	1.071E-005	1.071E-005	0.78	0.3945	
C-W/F C.R	0.057	0.057	4157.66	< 0.0001	
AB	2.262E-005	2.262E-005	1.64	0.2229	
AC	4.825E-004	4.825E-004	34.95	< 0.0001	
BC	2.078E-005	2.078E-005	1.51	0.2416	
A^2	9.449E-006	9.449E-006	0.68	0.4229	
B^2	3.366E-005	3.366E-005	2.44	0.1424	
C^2	1.774E-003	1.774E-003	128.52	< 0.0001	
Residual	1.794E-004	1.380E-005			
Lack of Fit	8.702E-005	1.740E-005	1.51	0.2885	not significant
Pure Error	9.243E-005	1.155E-005			
Cor Total	0.072				

$$COP_{overall} = 0.5955 - 3.921 \times 10^{-3}(A) - 5.879 \times 10^{-3}(B) + 0.885(C) + 2.358 \times 10^{-5}(AB) + 3.013 \times 10^{-3}(AC) - 2.453 \times 10^{-3}(BC) + 4.862 \times 10^{-6}(A^2) + 1.480 \times 10^{-4}(B^2) - 0.696(C^2)$$

G2-3: Diagnostics and Model Graphs

A. R1 (W_{t})

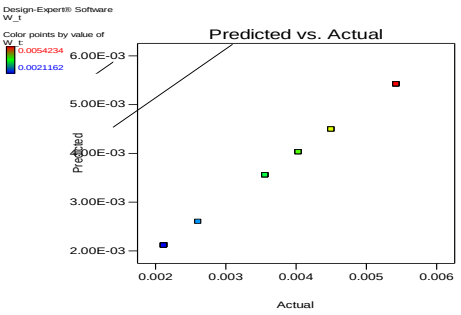

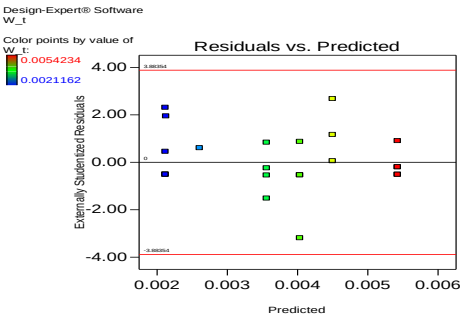

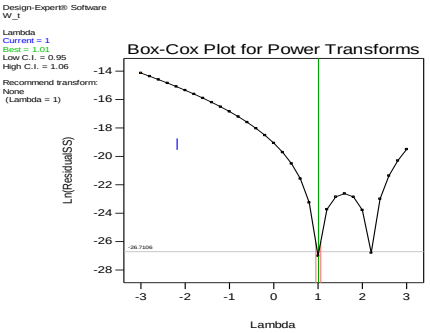

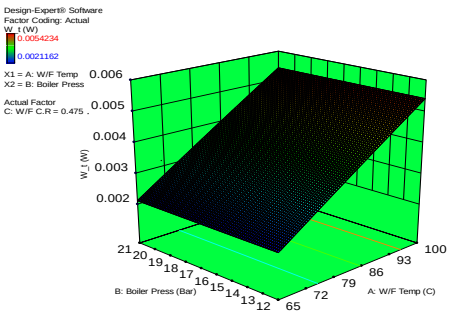

B. R2 (W_{sp})

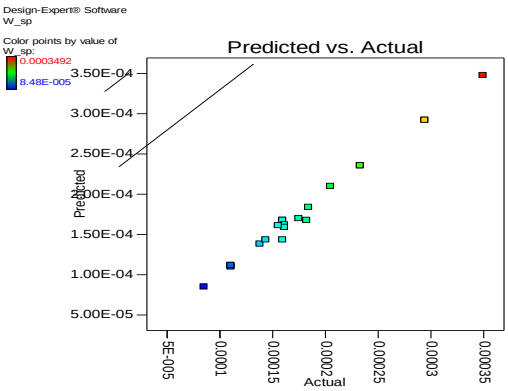

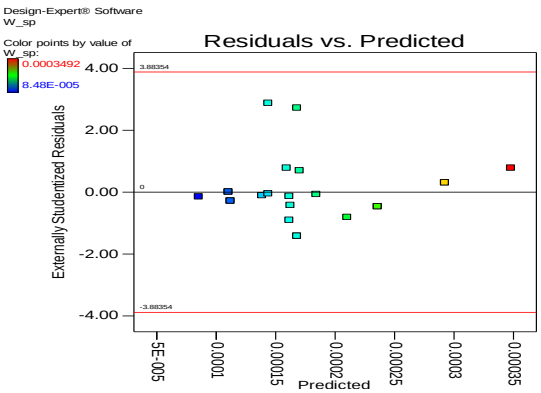

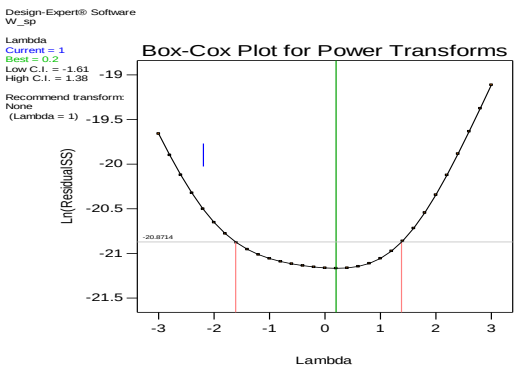

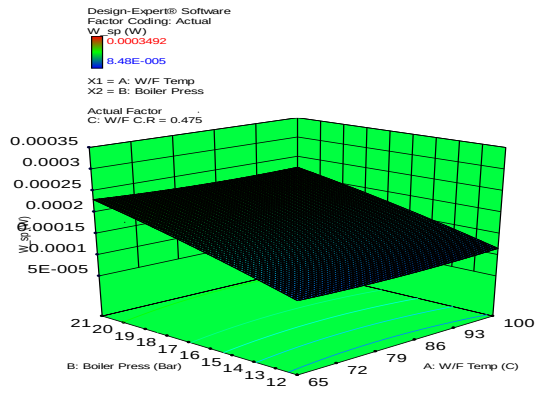

C. R3 (Q_{loss})

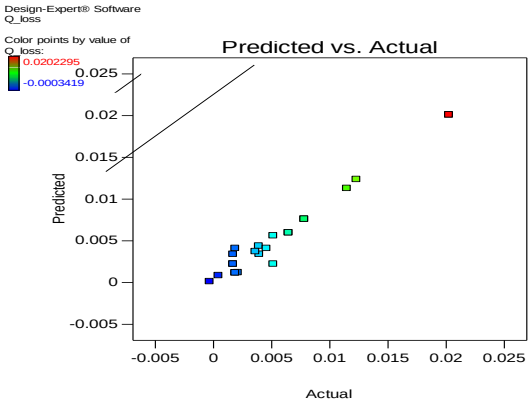

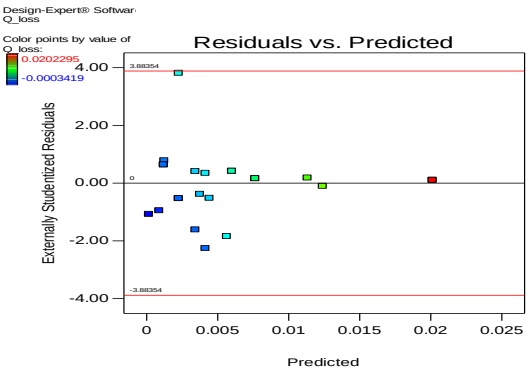

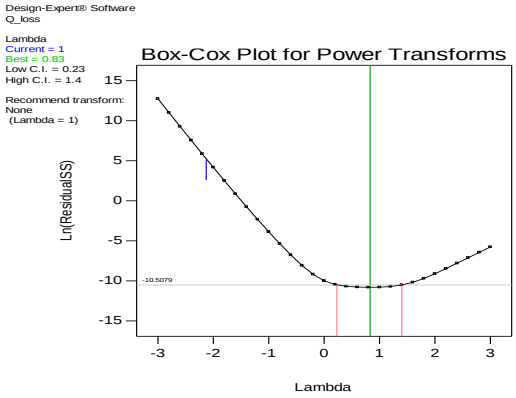

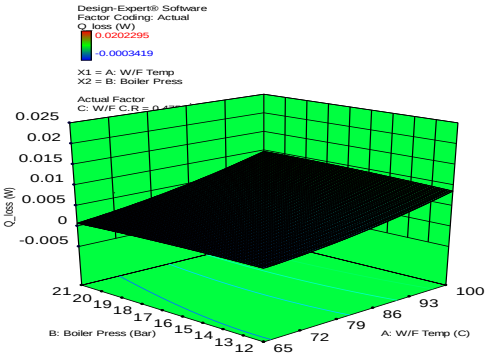

D. R4 ($COP_{cooling}$)

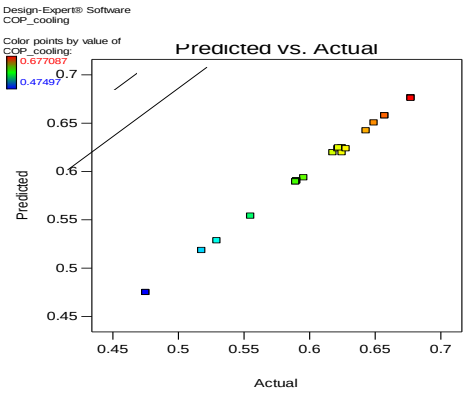

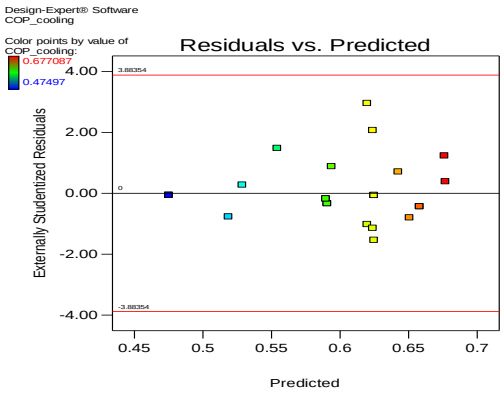

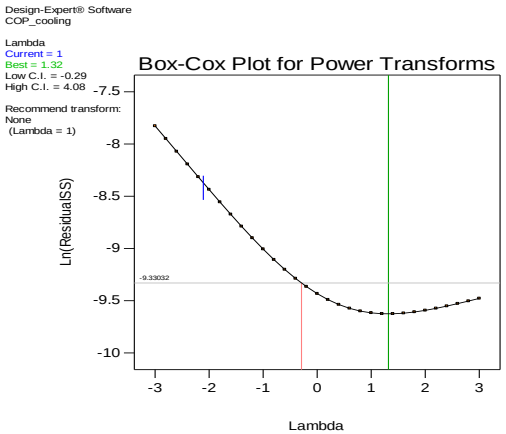

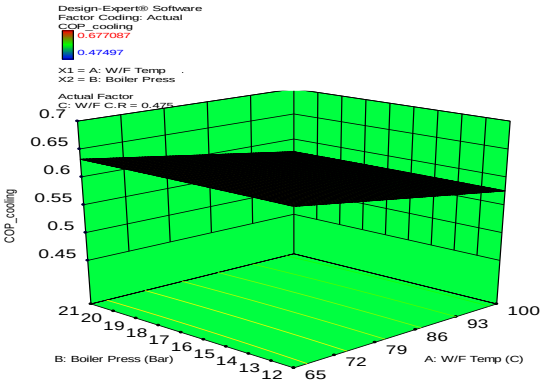

E. R5 (ORC_{eff})

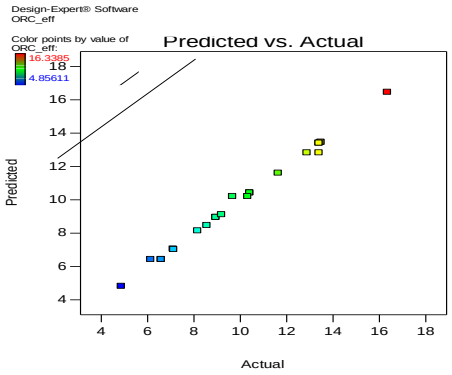

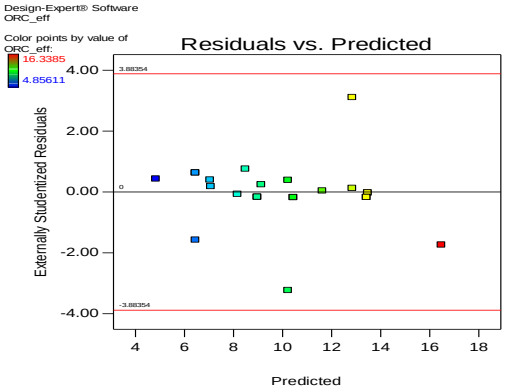

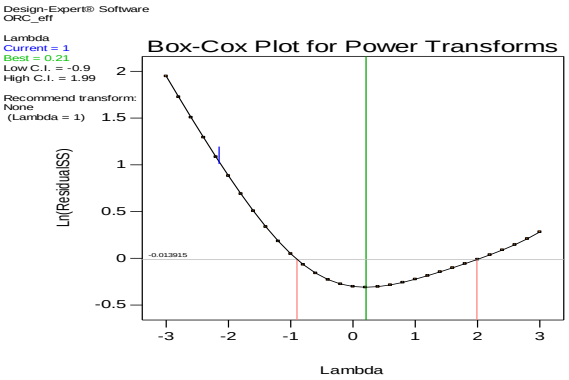

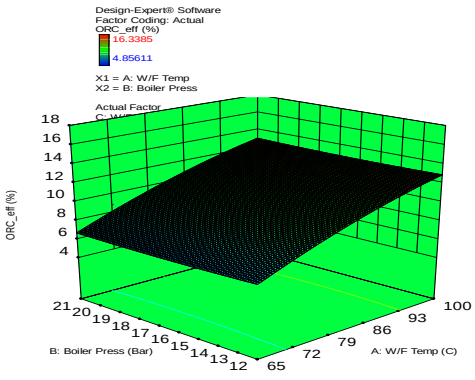

F. R6 ($COP\_{overall}$)

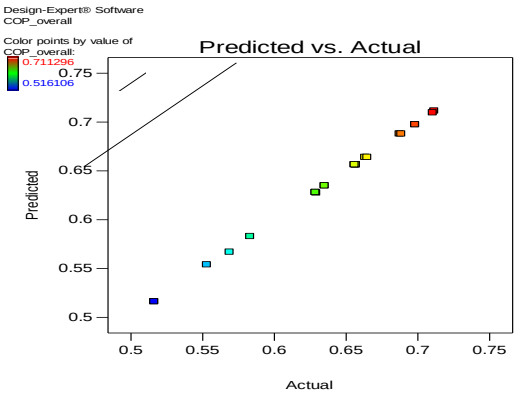

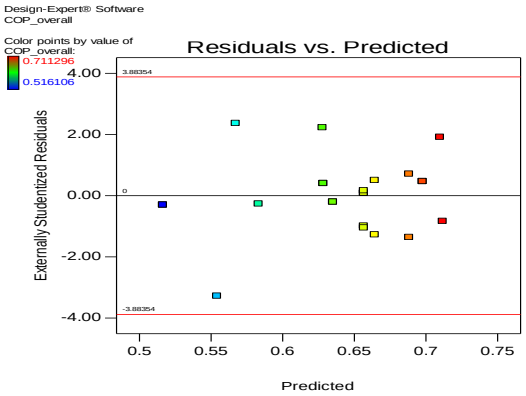

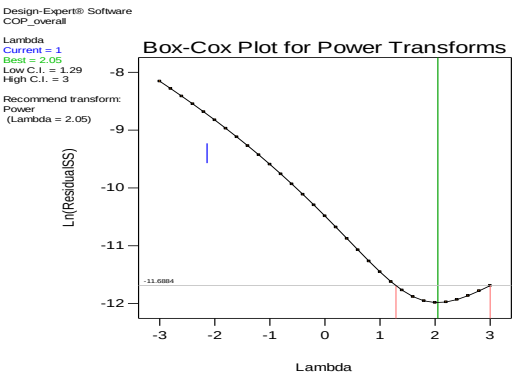

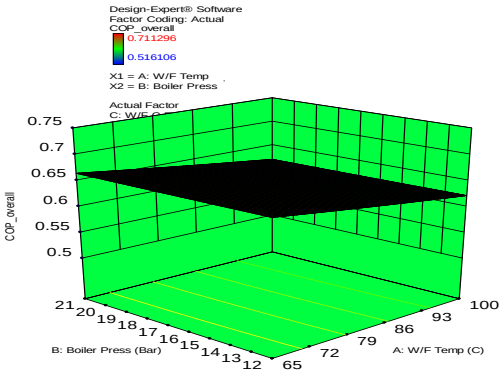

APPENDIX H

PROJECT INFORMATION ON RETScreen

H1: Project Information and Specifications

1. Proposed case (0.05kW Capacity)				
i. **Base load cooling system**				
	Technology	Absorption		
	Fuel type	User-defined fuel		
	Fuel rate	RM /kJ	0.000	
	Capacity	kW	0.05	104.7 %
	COP- seasonal		0.65	
	Cooling delivered	MWh	0.44	60.5 %
ii. **Base load power system**				
	Technology	Solar thermal power		
	Power capacity	kW	0.0045	13.5 %
	Model			
	Capacity factor	%	20.0 %	
	Electricity delivered to load	MWh	0.0026	5.7 %
	Electricity exported to grid	MWh	0	
iii. **Operating strategy - base load power system**				
	Electricity rate - base case	RM /MWh	218.00	
	Fuel rate - proposed case power system	RM /MWh	0.00	
	Electricity export rate	RM /MWh	218.00	
	Electricity rate - proposed case	RM /MWh	218.00	
iv. **Proposed case system characteristics**				
Power		**Unit**	**Estimate**	**%**
	Base load power system			
	Technology		Solar thermal power	
	Operating strategy		Full power capacity output	
	Capacity	kW	0	13.5 %
	Electricity delivered to load	MWh	0	5.7 %
	Electricity exported to grid	MWh	0	
Cooling				
	Base load cooling system			
	Technology		Absorption	
	Fuel type		User-defined fuel	
	Capacity	kW	0	104.7 %
	Cooling delivered	MWh	0	60.5 %
2. Proposed case (1.76 kW Capacity)				
i. **Base load cooling system**				
	Technology	Absorption		
	Fuel type	User-defined fuel		
	Fuel rate	MYR/kJ		
	Capacity	kW	1.76	87.5 %
	COP- seasonal		0.60	
	Cooling delivered	MWh	15	50.6 %
ii. **Base load power system**				
	Technology	Solar thermal power		
	Power capacity	kW	0.142	11.2 %
	Capacity factor	%	20.0 %	
	Electricity delivered to load	MWh	0	7.1 %
	Electricity exported to grid	MWh	0	
iii. **Operating strategy - base load power system**				

	Electricity rate - base case	RM /MWh	218.00	
	Fuel rate - proposed case power system	RM /MWh	0.00	
	Electricity export rate	RM /MWh	218.00	
	Electricity rate - proposed case	RM /MWh	218.00	
	iv. **Proposed case system characteristics**			
Power		**Unit**	**Estimate**	**%**
	Base load power system			
	Technology		Solar thermal power	
	Operating strategy		Full power capacity output	
	Capacity	kW	0.142	11.2 %
	Electricity delivered to load	MWh		7.1 %
	Electricity exported to grid	MWh	0	
Cooling				
	Base load cooling system			
	Technology		Absorption	
	Fuel type		User-defined fuel	
	Capacity	kW	2	87.5 %
	Cooling delivered	MWh	15	50.6 %
	3. Proposed case (3.5 kW Capacity)			
	i. **Base load cooling system**			
	Technology	Absorption		
	Fuel type	User-defined fuel		
	Fuel rate	RM /kJ		
	Capacity	kW	3.5	79.1 %
	COP - seasonal		0.65	
	Cooling delivered	MWh	31	45.8 %
	ii. **Base load power system**			
	Technology	Solar thermal power		
	Power capacity	kW	0.283	13.1 %
	Capacity factor	%	20.0 %	
	Electricity delivered to load	MWh		11.6 %
	Electricity exported to grid	MWh	0	
	iii. **Operating strategy - base load power system**			
	Electricity rate - base case	RM /MWh	218.00	
	Fuel rate - proposed case power system	RM /MWh	0.00	
	Electricity export rate	RM /MWh	218.00	
	Electricity rate - proposed case	RM /MWh	218.00	
	iv. **Proposed case system characteristics**			
Power		**Unit**	**Estimate**	**%**
	Base load power system			
	Technology		Solar thermal power	
	Operating strategy		Full power capacity output	
	Capacity	kW	0.283	13.1 %
	Electricity delivered to load	MWh	0	11.6 %
	Electricity exported to grid	MWh	0	
Cooling				
	Base load cooling system			
	Technology		Absorption	
	Fuel type		User-defined fuel	
	Capacity	kW	4	79.1 %
	Cooling delivered	MWh	31	45.8 %
	4. Proposed case (7.0 kW Capacity)			
	i. Base load cooling system			
	Technology	Absorption		
	Fuel type	User-defined fuel (Solar)		
	Fuel rate	RM /kJ		
	Capacity	kW	7.0	79.1 %
	COP - seasonal		0.65	
	Cooling delivered	MWh	61	45.8 %
	ii. **Base load power system**			
	Technology	Solar thermal power		
	Power capacity	kW	0.565	14.8 %
	Capacity factor	%	20.0 %	
	Electricity delivered to load	MWh	1	12.0 %

	Electricity exported to grid	MWh	0	
	iii. Operating strategy - base load power system			
	Electricity rate - base case	RM /MWh	218.00	
	Fuel rate - proposed case power system	RM /MWh	0.00	
	Electricity export rate	RM /MWh	218.00	
	Electricity rate - proposed case	RM /MWh	218.00	
	iv. Proposed case system characteristics			
Power		**Unit**	**Estimate**	**%**
	Base load power system			
	Technology		Solar thermal power	
	Operating strategy		Full power capacity output	
	Capacity	kW	0.565	14.8 %
	Electricity delivered to load	MWh	1	12.0 %
	Electricity exported to grid	MWh	0	
Cooling				
	Base load cooling system			
	Technology		Absorption	
	Fuel type		User-defined fuel	
	Capacity	kW	7	79.1 %
	Cooling delivered	MWh	61	45.8 %

H2: Proposed System Characteristics

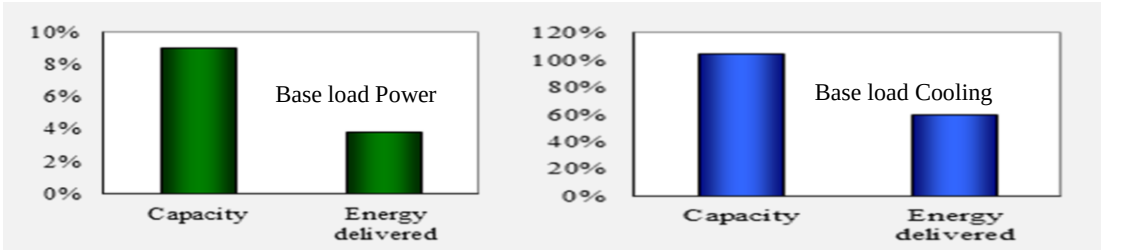

0.05 kW Capacity

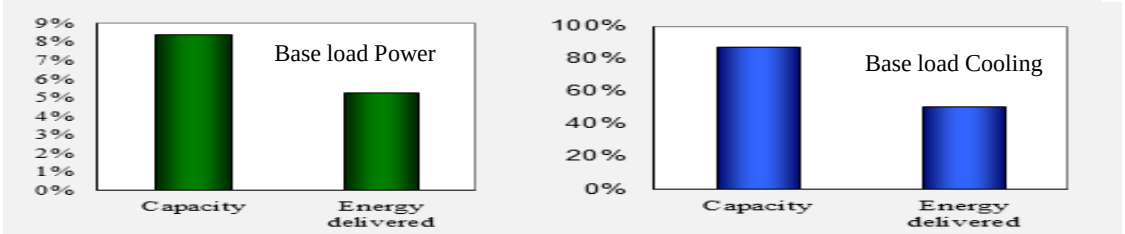

1.76 kW Capacity

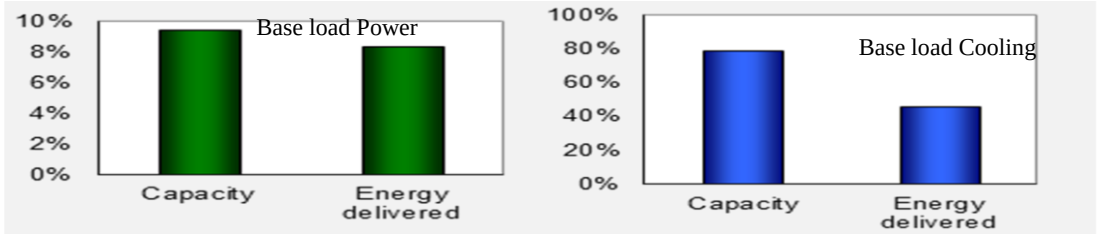

3.5 kW Capacity

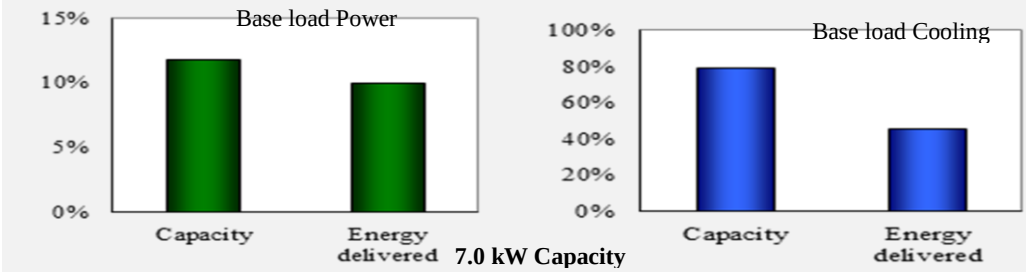

7.0 kW Capacity

H3: Financial Analysis

(1) 0.05 kW Capacity		
i. Initial costs		RM
Engineering & Development	18.2 %	6,500
Power system	37.8 %	13,500
Cooling system	35.0 %	12,500
Balance of system & misc.	9.0 %	3,200
Total initial costs	100.0 %	35,700
ii. **Annual costs and debt payments**		
O&M		68.6
Fuel cost - proposed case		0
Total annual costs		68.6
iii. **Annual savings and income**		
Fuel cost - base case		101
Electricity export income		-0.0038
GHG reduction income - 0 yrs		0
Total annual savings and income		102.68
iv. Electricity export income		
Electricity exported to grid	MWh	0
Electricity export rate	RM /MWh	218.0
Electricity export income	RM	0
Electricity export escalation rate	%	5
v. GHG reduction income		
Net GHG reduction	tCO_2/yr	0
Net GHG reduction - 20 yrs	tCO_2	7
GHG reduction income	RM	0
vi. Other Income		
Vegetable sale	Kg	0.675
Rate	RM /kg	2.5
Total income	RM	2
Duration	yr	20
Escalation rate	%	2.5 %
vii. **Financial parameters**		
Fuel cost escalation rate	%	2.5 %
Inflation rate	%	2.5 %
Discount rate	%	5.0 %
Project life	yr	20
Effective income tax rate	%	0
viii.Financial viability		
Pre-tax IRR - equity	%	-0.227 %
Pre-tax IRR - assets	%	-0.227 %
After-tax IRR - equity	%	-0.227 %
After-tax IRR - assets	%	-0.227 %
Simple payback	yr	846.40
Equity payback	yr	> project
Net Present Value (NPV)	RM	-32,147.83
Annual life cycle savings	RM /yr	-4,143
Benefit-Cost (B-C) ratio		0.02
Debt service coverage		No debt
Energy production cost	RM /MWh	
GHG reduction cost	RM /tCO_2	12,256
(2) 1.76 kW Capacity		
i. Initial costs		RM
Engineering & Development	13.2 %	6,500
Power system	29.3 %	14,500
Cooling system	45.6 %	22,500
Balance of system & misc.	11.9 %	5,850
Total initial costs	100.0 %	49,350
ii. Annual costs and debt payments		
O&M		372
Fuel cost - proposed case		0
Total annual costs		371.6
iii. Annual savings and income		

Fuel cost - base case		3,531
Electricity export income		0.0051
GHG reduction income - 0 yrs		0
Total annual savings and income		**3,591.76**
iv. **Electricity export income**		
Electricity exported to grid	MWh	0
Electricity export rate	RM /MWh	218.00
Electricity export income	RM	0
Electricity export escalation rate	%	5
v. **GHG reduction income**		
Net GHG reduction	tCO2/yr	12
Net GHG reduction - 20 yrs	tCO_2	236
GHG reduction income	RM	0
vi. **Other income**		
Vegetable sales	Kg	24.3
Rate	RM /kg	2.5
Total income	RM	60.75
Duration	yr	20
Escalation rate	%	2.5 %
vii. **Financial parameters**		
Fuel cost escalation rate	%	2.5 %
Inflation rate	%	2.5 %
Discount rate	%	5.0 %
Project life	yr	20
Effective income tax rate	%	0
viii.**Financial viability**		
Pre-tax IRR - equity	%	5.0 %
Pre-tax IRR - assets	%	5.0 %
After-tax IRR - equity	%	5.0 %
After-tax IRR - assets	%	5.0 %
Simple payback	yr	15.3
Equity payback	yr	12.38
Net Present Value (NPV)	RM	-1229.57
Annual life cycle savings	RM /yr	1337
Benefit-Cost (B-C) ratio		1.34
Debt service coverage		No debt
Energy production cost	RM /MWh	
GHG reduction cost	RM /tCO2	(113)
(3) 3.5 kW Capacity		
i. Initial costs		RM
Engineering and Development	10.2 %	6,500
Power system	32.3 %	20,500
Cooling system	39.4 %	25,000
Balance of system & misc.	18.1 %	11,525
Total initial costs	100.0 %	63,525
ii. Annual costs and debt payments		
O&M		568.2
Fuel cost - proposed case		0
Total annual costs		568.2
iii. Annual savings and income		
Fuel cost - base case		7,018
Electricity export income		0.019
GHG reduction income - 0 yrs		0
Customer premium income (rebate)		0
Total annual savings and income		7,139
iv. Electricity export income		
Electricity exported to grid	MWh	0
Electricity export rate	RM /MWh	218.00
Electricity export income	RM	0
Electricity export escalation rate	%	5
v. GHG reduction income		
Net GHG reduction	tCO2/yr	23
Net GHG reduction - 20 yrs	tCO_2	468
Net GHG reduction - 0 yrs	tCO_2	0

vi. Other income		
Vegetable Sales	Kg	48.6
Rate	RM /kg	2.5
Total	RM	122
Duration	yr	20
Escalation rate	%	2.5 %
vii. Financial parameters		
Fuel cost escalation rate	%	2.5 %
Inflation rate	%	2.5 %
Discount rate	%	5.0 %
Project life	yr	20
Effective income tax rate	%	0
viii.Financial viability		
Pre-tax IRR - equity	%	10 %
Pre-tax IRR - assets	%	10 %
Simple payback	yr	9.7
Equity payback	yr	7.93
Net Present Value (NPV)	RM	32,902.98
Annual life cycle savings	RM /yr	5,645
Benefit-Cost (B-C) ratio		2.11
Debt service coverage		No debt
Energy production cost	RM /MWh	
GHG reduction cost	RM/tCO_2	(241)
(4) 7 kW Capacity		
i. Initial costs		RM
Engineering & Development	6.7 %	6,500
Power system	25.6 %	25,000
Cooling system	50.2 %	49,000
Balance of system & misc.	17.6 %	17,150
Total initial costs	100.0 %	97,650
ii. Annual costs and debt payments		
O&M		873.9
Fuel cost - proposed case		0
Total annual costs		**873.9**
iii. Annual savings and income		
Fuel cost - base case		13,897
Electricity export income		0
GHG reduction income - 0 yrs		0
Total annual savings and income		14,141
iv. **Electricity export income**		
Electricity exported to grid	MWh	0
Electricity export rate	RM /MWh	218.00
Electricity export income	RM	0.051
Electricity export escalation rate	%	
v. **GHG reduction income**		
Net GHG reduction	tCO_2/yr	46
Net GHG reduction - 20 yrs	tCO_2	927
GHG reduction credit rate	RM/tCO_2	
GHG reduction income	RM	0
vi. **Other income**		
Vegetables	kg	97.2
Rate	RM/kg	2.5
Total	RM	243
Duration	yr	20
Escalation rate	%	2.5 %
vii. Financial parameters		
Fuel cost escalation rate	%	2.5 %
Inflation rate	%	2.5 %
Discount rate	%	10.0 %
Project life	yr	20
Effective income tax rate	%	0
viii.Financial viability		
Pre-tax IRR - equity	%	14.0 %
Pre-tax IRR - assets	%	14.0 %

Simple payback	yr	7.4
Equity payback	yr	5.95
Net Present Value (NPV)	RM	30,607.39
Annual life cycle savings	RM/yr	8,592
Benefit-Cost (B-C) ratio	-	1.75
Debt service coverage		No debt
Energy production cost	RM/MWh	
GHG reduction cost	RM/tCO2	(185)

H4: Emission Analysis

(1) 0.05 kW Capacity						
i. Base case electricity system (Baseline)						
Country - region		Fuel type	GHG emission factor			
Malaysia		All types	0.727 tCO_2/MWh			
Baseline changes during project life				Change in GHG emission factor	%	-10.0 %
ii. Base case system GHG summary (Baseline)						
	Fuel mix	CO2 emission factor	CH4 emission factor	Fuel consumption	GHG emission factor	GHG emission
Fuel type	%	kg/GJ	kg/GJ	MWh	tCO_2/MWh	tCO_2
Electricity	100.0%			0	0.727	0.3
Total	100.0%			0	0.727	0.3
iii. Proposed case system GHG summary (Combined cooling & power project)						
	Fuel mix	CO_2 emission factor	CH4 emission factor	Fuel consumption	GHG emission factor	GHG emission
Fuel type	%	kg/GJ	kg/GJ	MWh	tCO_2/MWh	tCO_2
User-defined fuel (Solar)	10.0%			1	0.000	0.0
Total	10.0%			1	0.000	0.0
iv. GHG emission reduction summary						
	Years of occurrence	Base case GHG emission	Proposed case GHG emission	Gross annual GHG emission reduction	GHG credits transaction fee	Net annual GHG emission reduction
Combined cooling & power project	yr	tCO_2	tCO_2	tCO_2	%	tCO_2
	1 to -1	0.3	0.0	0.3		0.3
5. Net annual GHG emission reduction	0.3 tCO_2 Equivalent to 0.7 barrels of crude oil not consumed					
(2) 1.76 kW Capacity						
i. Base case electricity system (Baseline)						
Country - region		Fuel type	GHG emission factor			
Malaysia		All types	0.727 tCO_2/MWh			
Baseline changes during project life				Change in GHG emission factor		-10.0 %
ii. Base case system GHG summary (Baseline)						
	Fuel mix	CO2 emission factor	CH4 emission factor	Fuel consumption	GHG emission factor	GHG emission
Fuel type	%	kg/GJ	kg/GJ	MWh	tCO_2/MWh	tCO_2
Electricity	100.0 %			16	0.727	11.8
Total	100.0 %			16	0.727	11.8
iii. Proposed case system GHG summary (Combined cooling & power project)						

		Fuel mix	CO_2 emission factor	CH_4 emission factor	Fuel consumption	GHG emission factor	GHG emission
	Fuel type	%	kg/GJ	kg/GJ	MWh	tCO_2/MWh	tCO_2
	User-defined fuel (Solar)	100 %			28	0.000	0.0
	Total	100.0 %			28	0.000	0.0
iv. GHG emission reduction summary							
		Years of occurrence	Base case GHG emission	Proposed case GHG emission	Gross annual GHG emission reduction	GHG credits transaction fee	Net annual GHG emission reduction
Combined cooling & power project		yr	tCO_2	tCO_2	tCO_2	%	tCO_2
		1 to -1	11.8	0.0	11.8		11.8
v. Net annual GHG emission reduction				11.8 tCO_2, equivalent to 27.4 Barrels of crude oil not consumed			
(3) 3.5 kW Capacity							
i. Base case electricity system (Baseline)							
	Country - region		Fuel type	GHG emission factor			
	Malaysia		All types	0.727 tCO_2/MWh			
	Baseline changes during project life				Change in GHG emission factor		-10.0%
ii. Base case system GHG summary (Baseline)							
		Fuel mix	CO2 emission factor	CH4 emission factor	Fuel consumption	GHG emission factor	GHG emission
	Fuel type	%	kg/GJ	kg/GJ	MWh	tCO_2/MWh	tCO_2
	Electricity	100.0 %			32	0.727	23.4
	Total	100.0 %			32	0.727	23.4
iii. Proposed case system GHG summary (Combined cooling & power project)							
		Fuel mix	CO_2 emission factor	CH4 emission factor	Fuel consumption	GHG emission factor	GHG emission
	Fuel type	%	kg/GJ	kg/GJ	MWh	tCO_2/MWh	tCO_2
	User-defined fuel (Solar)	100 %			47	0.000	0.0
	Total	100.0 %			48	0.000	0.0
iv. GHG emission reduction summary							
		Years of occurrence	Base case GHG emission	Proposed case GHG emission	Gross annual GHG emission reduction	GHG credits transaction fee	Net annual GHG emission reduction
Combined cooling & power project		yr	tCO_2	tCO_2	tCO_2	%	tCO_2
		1 to -1	23.4	0.0	23.4		23.4
v. Net annual GHG emission reduction				23.4tCO_2 Equivalent to 54.4 Barrels of crude oil not consumed			
(4) 7.0 kW Capacity							
i. Base case electricity system (Baseline)							
	Country - region		Fuel type	GHG emission factor			
	Malaysia		All types	0.727 tCO_2/MWh			
	Baseline changes during project life				Change in GHG emission factor	%	-10.0 %
ii. Base case system GHG summary (Baseline)							

		Fuel mix	CO_2 emission factor	CH4 emission factor	Fuel consumption	GHG emission factor	GHG emission
	Fuel type	%	kg/GJ	kg/GJ	MWh	tCO_2/MWh	tCO_2
	Electricity	100.0 %			64	0.727	46.4
	Total	100.0 %			64	0.727	46.4
iii. Proposed case system GHG summary (Combined cooling & power project)							
		Fuel mix	CO_2 emission factor	CH4 emission factor	Fuel consumption	GHG emission factor	GHG emission
	Fuel type	%	kg/GJ	kg/GJ	MWh	tCO_2/MWh	tCO_2
	User-defined fuel (solar)	100 %			95	0.000	0.0
	Total	100.0 %			95	0.000	0.0
iv. GHG emission reduction summary							
		Years of occurrence	Base case GHG emission	Proposed case GHG emission	Gross annual GHG emission reduction	GHG credits transaction fee	Net annual GHG emission reduction
Combined cooling & power project		yr	tCO_2	tCO_2	tCO_2	%	tCO_2
		1 to -1	46.4	0.0	46.4		46.4
	Net annual GHG emission reduction			46.4 tCO_2, Equivalent to 108 Barrels of crude oil not consumed			

APPENDIX G

List of Publications

1. Techno-economic analysis of innovative solar thermal chilled water and application for agricultural soil cooling, Renewable and Sustainable Energy Reviews, 2017, vol. 73 pp. 215-224
2. The Potentials of Solar Thermal Technology for Sustainable Development in Nigeria, Int. J. of Eng. And Tech. Research, 2015, vol. 3 pp.181-186.
3. Modelling and Experimental Analysis of Solar Powered Organic Rankine and Vapour Absorption Refrigeration Chilled Water for Radiant Soil Cooling System, 5th Conference on Emerging Energy and Process Technology (CONCEPT 2016), Port Dickson, Malaysia, December 2016.
4. Analysis of Stand-alone Chilled Water Radiant Cooling of OTEC Office in UTM Malaysia with RETScreen, 4th Conference on Emerging Energy and Process Technology (CONCEPT 2016), Melaka Malaysia, December 2015.
5. Techno-Economic Analysis of Innovative Production and Application of Solar Thermal Chilled Water for Agricultural Soil Cooling (ECBA 2015), Langkawi, Malaysia, November 2015.